Chem Soc Rev

REVIEW ARTICLE

View Article Online
View Journal | View Issue

Cite this: *Chem. Soc. Rev.*, 2021, **50**, 12377

Molecular photoswitches in aqueous environments

Jana Volarić, [a] Wiktor Szymanski, [ab] Nadja A. Simeth *[ac] and Ben L. Feringa *[a]

Molecular photoswitches enable dynamic control of processes with high spatiotemporal precision, using light as external stimulus, and hence are ideal tools for different research areas spanning from chemical biology to smart materials. Photoswitches are typically organic molecules that feature extended aromatic systems to make them responsive to (visible) light. However, this renders them inherently lipophilic, while water-solubility is of crucial importance to apply photoswitchable organic molecules in biological systems, like in the rapidly emerging field of photopharmacology. Several strategies for solubilizing organic molecules in water are known, but there are not yet clear rules for applying them to photoswitchable molecules. Importantly, rendering photoswitches water-soluble has a serious impact on both their photophysical and biological properties, which must be taken into consideration when designing new systems. Altogether, these aspects pose considerable challenges for successfully applying molecular photoswitches in aqueous systems, and in particular in biologically relevant media. In this review, we focus on fully water-soluble photoswitches, such as those used in biological environments, in both *in vitro* and *in vivo* studies. We discuss the design principles and prospects for water-soluble photoswitches to inspire and enable their future applications.

Received 28th June 2021

DOI: 10.1039/d0cs00547a

rsc.li/chem-soc-rev

[a] *Centre for Systems Chemistry, Stratingh Institute for Chemistry, Faculty for Science and Engineering, University of Groningen, Nijenborgh 4, 9747 AG Groningen, The Netherlands. E-mail: b.l.feringa@rug.nl, nadja.simeth@uni-goettingen.de*
[b] *Department of Radiology, Medical Imaging Center, University of Groningen, University Medical Centre Groningen, Hanzeplein 1, 9713 GZ Groningen, The Netherlands*
[c] *Institute for Organic and Biomolecular Chemistry, University of Göttingen, Tammannstr. 2, 37077 Göttingen, Germany*

Jana Volarić

Jana Volarić was born in Zagreb, Croatia in 1992. She obtained her BSc at the University of Zagreb with Prof. Hrvoj Vančik. She did her MSc at the University of Groningen with Prof. Ben Feringa on the synthesis of dynamic bisthiourea molecular motor-based catalysts. She spent 6 months in Boston in the group of prof. Hidde Ploegh (Boston Children's Hospital, Harvard Medical School) working on site-specific labeling of influenza A virus. In 2017 Jana started her PhD under supervision of prof. Ben L. Feringa on incorporating photoswitches into biosystems in order to control biomolecular function.

Wiktor Szymanski

Wiktor Szymanski received his PhD degree from The Warsaw University of Technology, Poland, in 2008, working under the supervision of Prof. Ryszard Ostaszewski. He spent two years working on the use of biotransformations in organic chemistry with Prof. Ben L. Feringa and Prof. Dick B. Janssen at the University of Groningen. Since 2010 he has been working on the construction of photoactive protein–peptide– and DNA-bioconjugates and photopharmacology in the Feringa Labs. In 2014, he joined the Department of Radiology, University Medical Center Groningen, where he was appointed in 2019 as associate professor.

1 Introduction

Water is the solvent, reagent, and mediator of a wide range of chemical transformations, assemblies and metabolic processes in every living organism.[1,2] In order to dynamically regulate the complex, multifaceted processes taking place in aqueous media, a powerful strategy is to apply an externally triggered control element. Specifically, light is a favourable stimulus as it is not natively present in a wide range of systems (except of course the process of vision and photosynthesis) and thus, can be applied orthogonally to their function.[3–5] Moreover, it can be tuned over a wide range of wavelengths and is, especially in the visible to near-infrared (NIR) light range, harmless for most living organisms.[6–8] Finally, it can be precisely delivered, allowing for high spatiotemporal control of a process of choice.[3–5,9–11]

The photons applied externally to the chosen system need to be translated into a signal the system can respond to.[4,5] This can be achieved by choosing a suitable photoactuator as a mediator. Such mediators can be small, organic molecules that are able to interact with light, *i.e.*, organic photocleavable protecting groups (photocages) or photoswitches.[3,12–15] While photocages are photolabile protecting groups that are cleaved upon irradiation and hence, can only be activated once,[13,16,17] photoswitches can be reversibly interconverted between different (functional) isomers.[3,18] This reversible nature makes them interesting candidates for a wide range of applications, including those that take place in water, where they act as photoresponsive amphiphiles,[19–27] hydrogel constituents,[28,29] probes for chemical biology,[30–32] or bioactive agents in photopharmacology.[6,7,30,33]

Molecular photoswitches are typically organic molecules bearing extended aromatic systems to make them responsive to (visible) light.[3,12] As a consequence they are inherently lipophilic. However, to apply photoswitches in aqueous media or in particular in biological systems, they need to be sufficiently water-soluble.[34–38] While general strategies for solubilizing organic molecules, for instance in the context of medicinal chemistry, are well established,[39–41] (Section 2 of this review), a similar broad set of approaches is yet to be applied to photoswitchable molecules. Moreover, rendering photoswitches water-soluble can have a serious impact on their photophysical and biological properties,[6,7] which must be taken into consideration when designing new systems (Fig. 1). Therefore, successfully applying molecular organic photoswitches to aqueous systems is challenging.

In this review, we discuss the design principles and prospects for water-soluble photoswitches as a source of inspiration and to enable their future applications. The first part of the review focuses on general principles to solubilize organic molecules in water and is followed by a section introducing different types of organic photoswitches and the impact of polar protic solvents on their properties. In the second part, we highlight selected illustrative examples of different types of photoswitches and their implementation in aqueous environment to underline the importance and impact of water-solubility on the desired application. As water is the universal solvent of life, the challenge of insufficient water-solubility of organic molecules is usually faced in a bio-inspired, biological, or medicinal context, and most strategies to overcome solubility issues are derived from this research area. Naturally, the applications and examples discussed in this review are coming from these fields. Consequently, photoswitches which are designed to be intentionally amphiphilic or lipophilic to form (supramolecular) (self-) assemblies, nano-, and microstructures in aqueous environment,[21,42–45] or (hydro)gels,[46–51] do not face the same obstacles as the ones intended to be fully water-soluble and hence, lie outside the scope of this review and we refer the reader to our recent overview.[21]

2 General aspects of the solubility of organic molecules in water and solubilizing strategies

Before discussing strategies used to solubilize organic molecules in water, we describe the definition of water-solubility,

Nadja A. Simeth

Nadja A. Simeth pursued her doctorate studies with Burkhard König at the University of Regensburg and defended her thesis in summer 2018 with summa cum laude. She then joined the group of Ben L. Feringa at the University of Groningen as a postdoc supported by a Feodor-Lynen Fellowship of the Humboldt Foundation. In autumn 2021, she was appointed as assistant professor at the University of Göttingen. She is interested in the design of smart drugs, biochemical probes and labels, as well as photoresponsive supramolecular architectures and biohybrid systems.

Ben L. Feringa

Ben L. Feringa obtained his PhD degree in 1978 at the University of Groningen in the Netherlands under the guidance of Prof. Hans Wynberg. After working as a research scientist at Shell he was appointed full professor at the University of Groningen in 1988 and named the distinguished Jacobus H. van't Hoff Professor of Molecular Sciences in 2004. He was elected foreign honorary member of the American Academy of Arts and Sciences and member of the Royal Netherlands Academy of Sciences. His research interests include stereochemistry, organic synthesis, asymmetric catalysis, molecular switches and motors, photopharmacology, self-assembly and nanosystems.

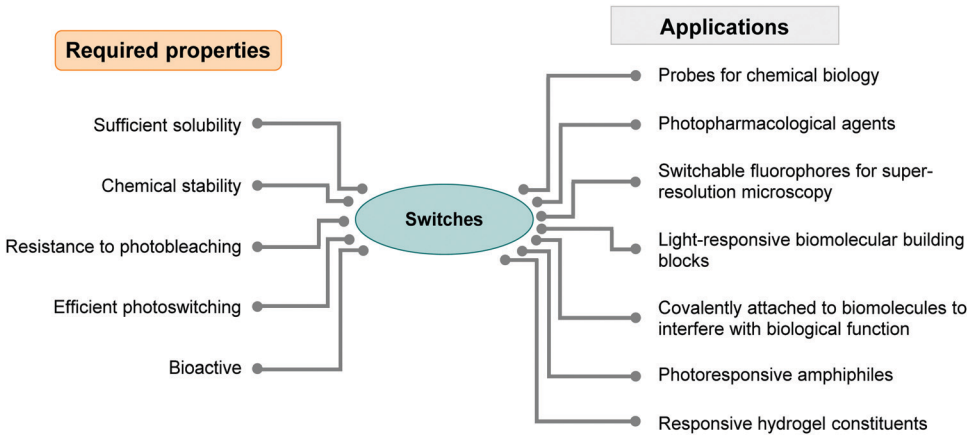

Fig. 1 Diagram summarizing the required properties of photoswitches needed for successful applications in water.

parameters that affect it and are used to predict it, as well as methods to determine the aqueous solubility of a compound of interest.

2.1 Aqueous solubility

2.1.1 Definition and general terms. Dissolving molecules in aqueous solutions is of great importance and a critical parameter for biological applications, drug discovery and material design.[52,53] Water-solubility in quantitative terms is described by amount of water (in mL) that needs to be added to the solute to dissolve it (*cf.* Table 1) at a given temperature and/or pressure.[54]

For a molecule to dissolve, it first needs to be removed from the solid form by breaking the intermolecular interactions holding the solid together (see Fig. 2). This applies to both the solids being in an amorphous and in a crystalline form. However, the more stable the (crystal) structure or lattice is, the more energy is needed to detach an individual molecule from it. The molecule is simultaneously forming stabilizing bonds with the surrounding medium. The energy released upon this so-called dissolution process in water is called hydration energy and the rate at which the solvation is proceeding is called dissolution rate, with both values being specific for each compound.[55]

In a thermodynamically stable saturated solution, the solid in its most stable crystalline form (characterized by its highest possible melting point) is in equilibrium with the dissolved species. This type of solubility is called the thermodynamic or equilibrium solubility.[39,41] Since solubility depends on the

Table 1 Overview of degree of solubility according to the US Pharmacopeia[54]

Descriptive term	Approximate volume of solvent per mass of solute (mL g^{-1})
Very soluble	<1
Freely soluble	1–10
Soluble	10–30
Sparingly soluble	30–100
Slightly soluble	100–1000
Very slightly soluble	1000–10 000
Practically insoluble	>10 000

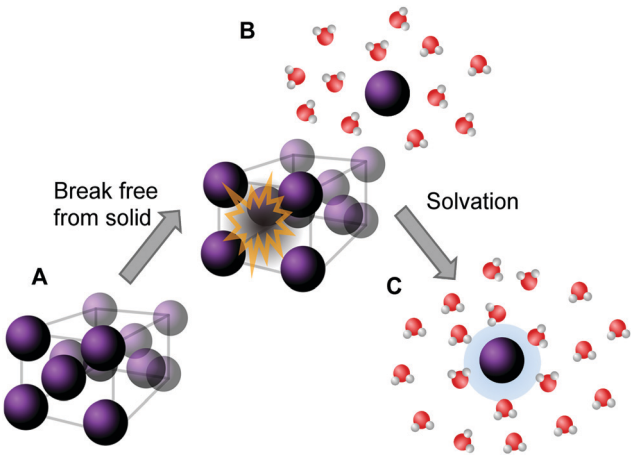

Fig. 2 Descriptive representation of the dissolution process of a crystalline solid in water. Energy is needed to first remove the molecule from its crystal structure [from (A) to (B)] and subsequently the molecule is solvated by water. Once solvated, the molecule forms stabilizing interactions with water (C), represented by the blue halo, which results in a release of energy. (Figure adapted with permission from ref. 56. Copyright 2006, Elsevier.)

solid form of the compound, it is possible to dissolve larger amounts of material by modifying the solid state of the compound into an amorphous or a less stable crystal structure *via* crystal engineering (taking advantage of polymorphism) (see Fig. 3A and B).[57] This can be achieved, for instance, by dissolving the molecule into an organic solvent, often DMSO, and then diluting it into an aqueous solution until precipitation, or the "cloud point", is reached.[39] The type of solubility achieved in this way is called the kinetic (a.k.a. dynamic or apparent) solubility (Fig. 3D), and is higher than the thermodynamic one (Fig. 3C). However, the solid will eventually assume its most stable form and possibly crystallize from solution, which is particularly problematic in biological applications.[41] Thermodynamic and kinetic solubility are general terms for both ionizable and non-ionic compounds. Additionally, the intrinsic solubility of ionizable compounds can be determined at the pH where the species is uncharged.[58]

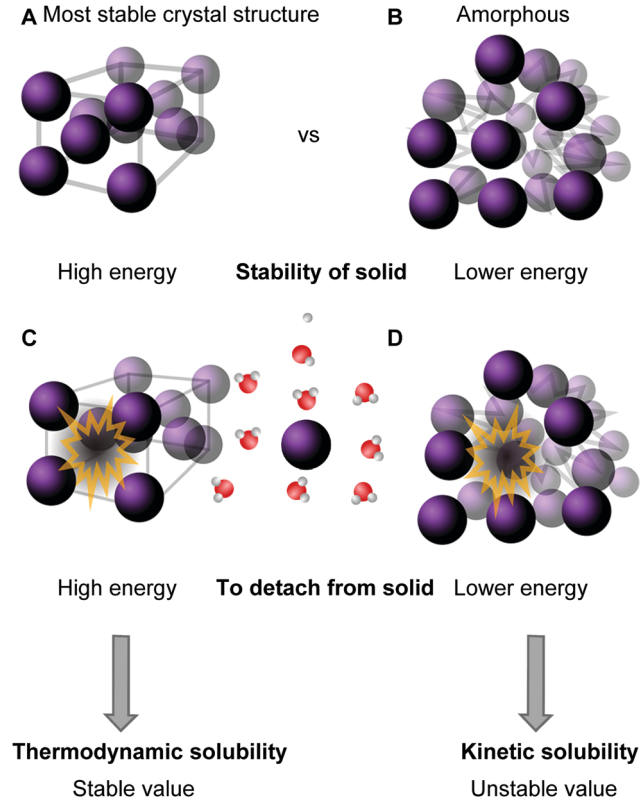

Fig. 3 Descriptive representation of solubility types: the compound is either in its most stable crystalline solid form (A) or in a less stable, amorphous, form (B). High amount of energy is needed to remove the molecule from the stable solid (C), while a lower amount of energy is needed to remove it from the less stable amorphous form (D, see ref. 60).

In the context of thermodynamics, the first step in dissolving a compound in water requires energy input to remove the molecule from the solid lattice (Fig. 2A–B). The energy released in the subsequent step, *i.e.*, solvation (Fig. 2B–C), often compensates for the first process through the formation of favorable interactions of the dissolved molecule with water. However, depending on the nature of the compound, in some examples the solvation energy is lower than the energy required for the detachment, therefore making the overall dissolving process endothermic. In the instances when the overall process is slightly endothermic, the general entropy increase, caused by the disorder increase upon solubilizing a compound, becomes relevant and ultimately drives the process. Moreover, for general aspects regarding solubility, solvent parameters and solutions, see chapter 3 of ref. 59.

Due to the numerous parameters affecting water-solubility, there is no single model which would provide a general formula to predict the solubility of a given molecule, posing a challenge for computational studies.[60–62] The most commonly applied model is the general solubility equation (GSE), reported by Yalkowski.[63,64] The GSE correlates the stability of the crystal, reflected by its melting point, and the lipophilicity of the compound described by the octanol/water partition coefficient:

$$\log S_w = -0.01(T_{mp} - 25\ ^\circ\mathrm{C}) - \log P + 0.50 \qquad (1)$$

where S_w is the molar solubility of an organic non-electrolyte in water, T_{mp} is the melting point and P is the octanol–water partition coefficient of the molecule.[63] Specifically, $\log P$ describes how well the molecule interacts with water and represents the contribution of hydration to solubility. The melting point, on the other hand, describes the stabilizing intermolecular interactions within the crystalline form of the compound.[39] While $\log P$ is used to describe non-ionic molecules, for ionizable ones $\log D$ is applied. Here, D is the water/octanol distribution coefficient that considers a sum of the concentration of all species of the compound, both dissociated and non-disassociated, in each phase, at a given pH:

$$D = \frac{\sum c_o}{\sum c_w} \qquad (2)$$

where c_o is the concentration of a given specific species in octanol and c_w is the concentration of a given species in water. Also, the propensity to form stabilizing interactions with water, such as hydrogen bonding,[39] halogen bonding,[65] electrostatic interactions,[66] polar π interaction[67] and van der Waals interactions,[68] differs between charged and non-charged compounds. Specifically, ionic compounds interact by coulombic interactions and their dissolution benefits from the high dielectric constant of water (ε = 80 at 20 °C),[69] which reduces the coulombic forces within ionic molecules and stabilizes the ions in the aqueous solution.[70]

2.1.2 Determining solubility. The Organization for Economic Co-operation and Development (OECD) guidelines describe two classical methods to determine the solubility of a compound of interest in water.[71] The shake-flask method is used for compounds with a solubility above 0.01 g L^{-1}. Specifically, the solid is stirred in water, for 24–48 h at elevated temperature, and then cooled to the measurement temperature, typically at 20 ± 0.05 °C, to finally remove the remaining solids *via* filtration. The second method, the column elution method, is used for less soluble compounds (<0.01 g L^{-1}). Here, an inert support material column is coated with excess of the compound of interest and rinsed with a recirculating amount of solvent. The change of compound concentration in water is tracked until it stabilizes thus reaching equilibrium. At equilibrium, the mass concentration of the solute in the eluent is the water-solubility of the tested compound. For both methods, the concentration of the compound in water is determined by an analytical method specific for the molecule, such as titration, voltammetry, photometry, and others.

2.1.3 A note on the impact of water-solubility of organic molecules for biological applications. Water-solubility is a central topic in the biological applications of organic molecules and critical in drug design. Interestingly, drug-like molecules require, besides sufficient water-solubility, also a certain amount of lipophilicity, for instance, to ensure membrane permeability or binding to the target site.[72] These requirements, more specifically for oral drug administration, can be approximated by the empirical "Lipinski rule of 5"[72,73] and are categorized by the Biopharmaceutics Classification System (BCS).[74]

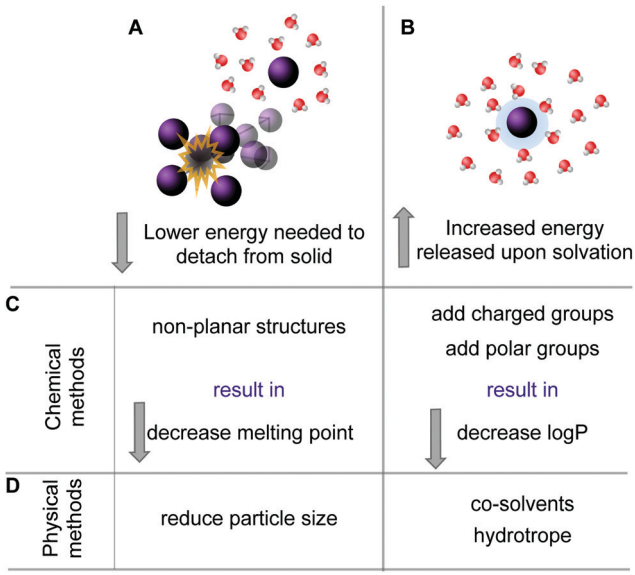

Fig. 4 Two possible processes can be influenced to increase solubility of a specific compound. One involves lowering the energy needed to remove a molecule from its solid (A). The second approach is to increase the energy that is released upon solvation (B). The chemical methods (C) to decrease the melting point thus lowering the energy needed for (A) are, *e.g.*, by designing non-planar structures and by addition of charged or polar solubilizing groups increases the stabilizing interactions with the solvent. The physical methods (D) to increase solubility involve reduction of particle size thus creating a larger surface or by adding co-solvents or hydrotropes (see also ref. 60).

2.2 General strategies to dissolve organic molecules in water

Many organic molecules are lipophilic structures that require modifications to successfully dissolve in water. The most common chemical approach is to attach additional moieties, such as charged or polar units, which increase the molecule's water-solubility.[39] Furthermore, if the molecule is an acid or a base, the simplest solubilization approach is to form a salt.[75] In addition, non-planar molecules often exhibit increased water-solubility when compared to their rigid flat isosteres.[41] Next to the chemical approaches, there is a plethora of physical methods available to improve solubility such as application of co-solvents, formulation of hydrotropes, particle size reduction and different delivery systems, such as liposomes or micelles.[55,76,77] A schematic representation of the various methods is given in Fig. 4.

In the following sections, we provide a brief overview of different strategies which have been employed to solubilize organic molecules in water using illustrative examples. Several of those solubilization strategies have also been used for photoswitches and will be discussed in Section 4. Nevertheless, some solubilization strategies are underrepresented, or have even never been applied to photoswitchable systems.

2.2.1 Solubilizing groups. Addition of a solubilizing group to the target compound increases the overall hydrophilicity of the molecule and is reflected in a lowered log *P* value.[39] Such solubilizing moieties include charged and non-charged groups and are described below.

Charged groups. Some common charged groups used to achieve water-solubility are phosphates, phosphonates, sulfonates, and ammonium groups. A crucial aspect of the solubility of ionic molecules is the effect of the counter ion, which is often overlooked. This was, for example, shown for the anthraquinone sulfonate displayed in Fig. 5A and is used in redox flow batteries.[78] Specifically, the disulfonate **2.1a** (Fig. 5A) had the highest solubility in water followed by disulfonated **2.1c** and monosulfonated **2.1b** with similar values. Furthermore, for all three compounds (**2.1a–c**) the Mg^{2+} salts exhibited the highest solubility and the Ba^{2+} salts the lowest. This phenomenon is explained by the high lattice energies of the barium and calcium salts, compared to the magnesium salt, which lead to lower water-solubility. Next to the counter-ion, the location of the solubilizing group in the molecule can also play an important role, as seen for the disulfonate anions **2.1a** and **2.1c**. In particular, **2.1c** showed more complex interactions with the cation in the crystal structure, which increases the lattice energy and lowers solubility.

Amine moieties with different substituents can be used to solubilize organic molecules in water as their pK_bs cause them to be protonated under physiological conditions.[39] For example, the benzylic site of the Akt-kinase inhibitor **2.2** was modified with an additional amine moiety (Fig. 5B).[79] The pyrrolidine group (**2.2b**) increased the solubility 10-fold with the nitrogen being protonated at neutral pH (ammonium p$K_a \approx 10$).

Non-ionic groups. In many cases, it is not necessary to attach a charged moiety to increase the water-solubility and it is sufficient to introduce an additional electronegative atom, such as oxygen or nitrogen, into the scaffold to increase the dipole moment of the whole molecule and hence, its propensity to interact with water (Fig. 6A and B, **2.3** and **2.4**). Moreover, these heteroatoms often constitute additional hydrogen bond donors/acceptors to interact with solvent and further increase solubility.[39,80] This was, for example, shown in the development of cytokine-mediated STAT1 signal transduction inhibitor **2.3** (Fig. 6A). By replacing the naphthalene (**2.3a**) with a quinoline moiety (**2.3b**), the solubility increased drastically, namely by 1400-fold.[80] Also in **2.4**, the introduction of an electronegative atom, here a fluorine, increased the solubility of the compound by lowering the melting point and decreasing log *P* (Fig. 6B).[39,81]

Other uncharged polar groups have been applied to increase aqueous solubility of organic compounds, such as polyethylene glycol (PEG) chains[82,83] or the oxetanyl sulfoxide moiety (**2.5**, Fig. 6C).[84]

2.2.2 Salt-formation. Instead of incorporating an additional solubilizing moiety, molecules that are inherently acidic or basic can be turned into their respective salts to increase their kinetic aqueous solubility. Salts are often much more soluble than their acidic or basic precursors due to higher dissolution rates in the water diffusion layer around the ionic solid (see Section 2.1.1, Fig. 4).[75] This was for example shown for diclofenac **2.6** (Fig. 7).[85] Both the intrinsic and the kinetic solubility were determined for the acid **2.6a** and its sodium salt **2.6b**. While the intrinsic solubility of the salt was virtually the same as the one of the acid, the corresponding kinetic solubilities differed significantly, favoring the salt.

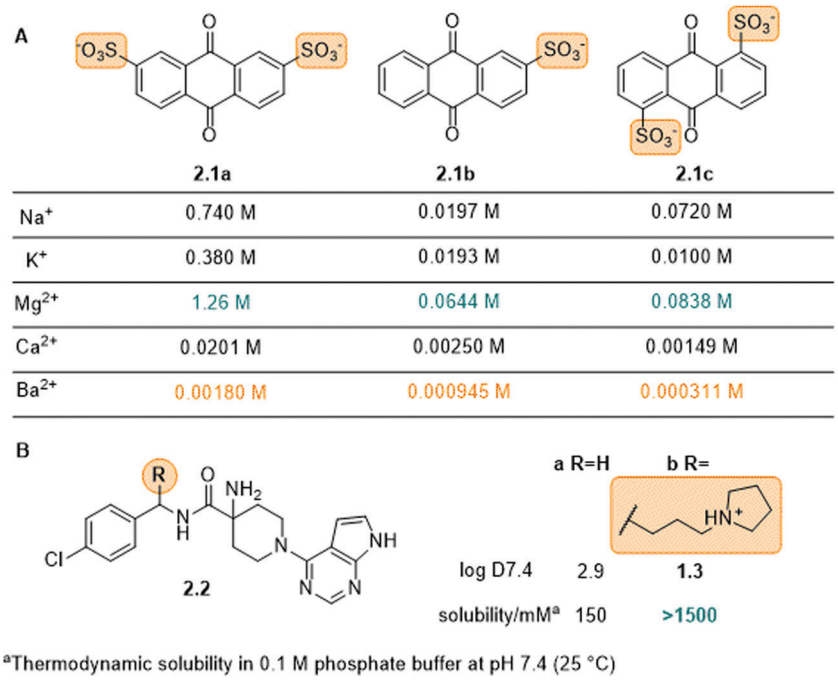

	2.1a	2.1b	2.1c
Na^+	0.740 M	0.0197 M	0.0720 M
K^+	0.380 M	0.0193 M	0.0100 M
Mg^{2+}	1.26 M	0.0644 M	0.0838 M
Ca^{2+}	0.0201 M	0.00250 M	0.00149 M
Ba^{2+}	0.00180 M	0.000945 M	0.000311 M

[a]Thermodynamic solubility in 0.1 M phosphate buffer at pH 7.4 (25 °C)

Fig. 5 The use of charged groups to increase water solubility. (A) Sulfonated anthraquinones and the solubility of the corresponding ion pairs in water at room temperature, (B) Akt-kinase inhibitors **2.2** with amine solubilizing group, their respective log *D* value and solubility in 0.1 M phosphate buffer at pH 7.4 at 25 °C.

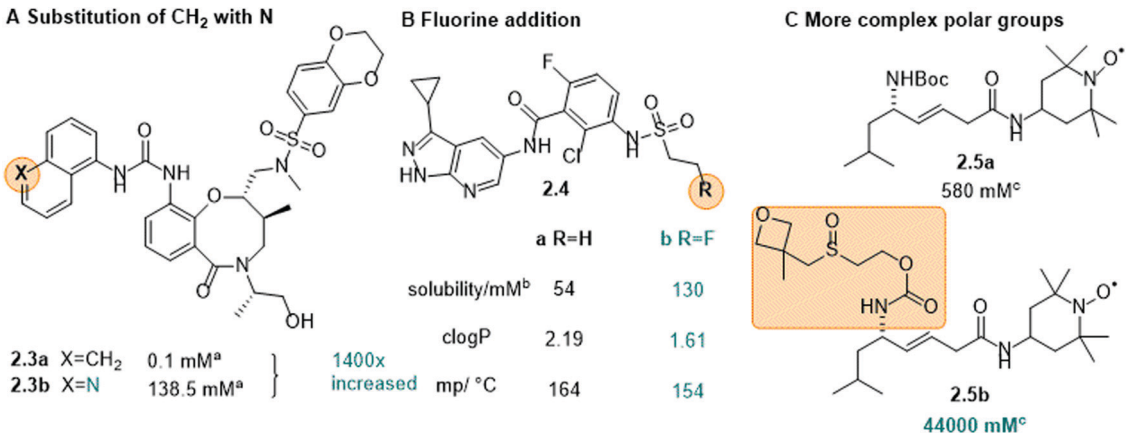

[a] Solubility measured in a phosphate buffered saline solution (pH 7.4)
[b] Solubility measured in phosphate buffer (pH 6.5)
[c] Solubility measured in water at rt

Fig. 6 Examples of using non-ionic groups to enhance solubility (A) substitution of the naphthalene moiety (**2.3a**) of the STAT1 signal transduction inhibitor **2.3** with a quinoline moiety (**2.3b**) significantly increased the solubility, (B) the addition of a fluorine atom to **2.4** and its effect on solubility, clog *P* (calculated log *P*) and the melting point, (C) the oxetanyl sulfoxide group caused a 76-fold increase in solubility of **2.5**.

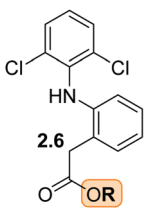

	a R=H	b R=Na^+
kinetic solubility/ mg/mL	12	40
intrinsic solubility/ mg/mL	1	1.1

Fig. 7 The difference in water-solubility, both kinetic and intrinsic, of the carboxylic acid and sodium salt form of diclofenac **2.6**.

2.2.3 Disruption of planarity and symmetry. Non-planar shape of molecules makes it more difficult for them to assemble within the crystal lattice and thus disrupting planarity lowers the melting point and results in elevated water-solubility. This phenomenon was employed in the design of different systems, where the loss of aromaticity,[39,86] introduction of a twisted ring[87] or the increase of a dihedral angle of the biaryl system increased the solubility.[88,89] It was demonstrated for **2.7** (Fig. 8A), due to the addition of an *ortho* methyl group,[88] and for the

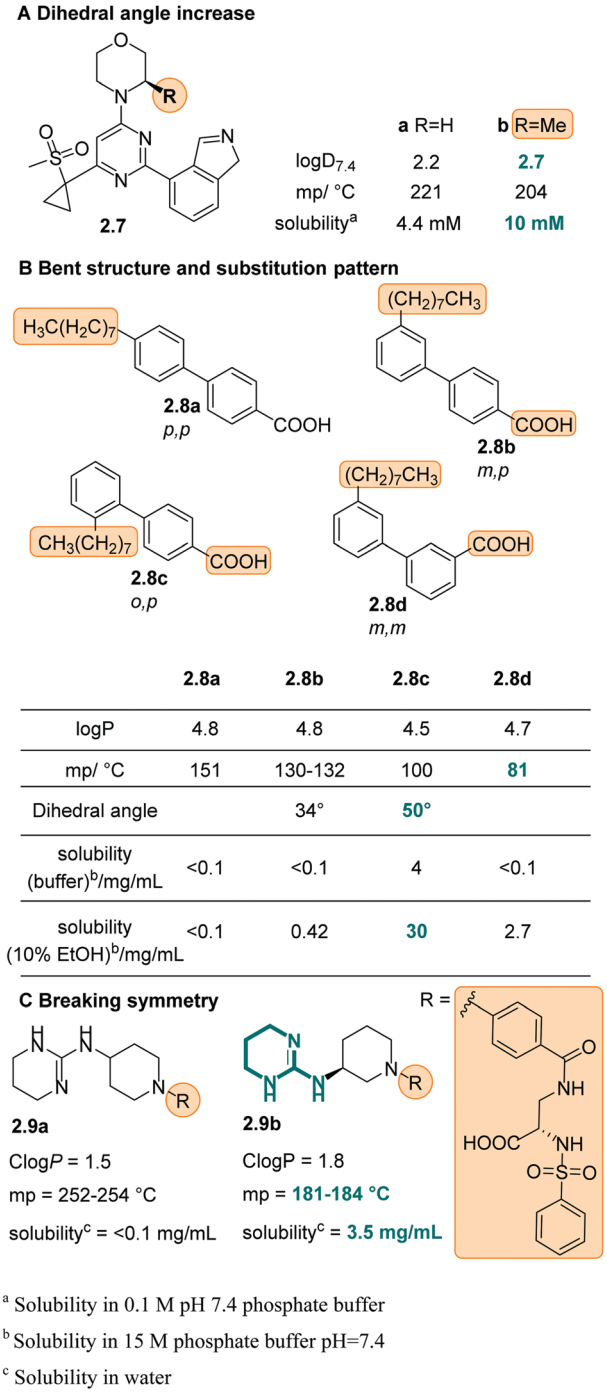

	2.8a	2.8b	2.8c	2.8d
logP	4.8	4.8	4.5	4.7
mp/ °C	151	130-132	100	81
Dihedral angle		34°	50°	
solubility (buffer)[b]/mg/mL	<0.1	<0.1	4	<0.1
solubility (10% EtOH)[b]/mg/mL	<0.1	0.42	30	2.7

[a] Solubility in 0.1 M pH 7.4 phosphate buffer

[b] Solubility in 15 M phosphate buffer pH=7.4

[c] Solubility in water

Fig. 8 Increased dihedral angle of **2.7** (A) upon addition of a methyl group, as well as the *ortho* substituents in **2.8b and c** (B) cause a decrease of melting point and increased solubility in water. (C) Introduction of a stereocenter in **2.9**, thus breaking the symmetry of the compound, significantly lowered the melting point and caused increased solubility in water.

different derivatives in **2.8**, in particular those with *ortho*, *para* (**2.8b and c**) and *meta*, *meta* (**2.8d**) substitution patterns (Fig. 8B).[89] Specifically, the non-linear molecular structure (**2.8b,d**) resulted in lower melting points compared to the original design **2.8a**.[89] Furthermore, improved solubility is a well-known phenomenon for compounds featuring branched alkyl chains compared to linear ones.[90,91] Additionally, symmetry breaking of molecules affects the entropy of melting as reported by a statistical study by Yalkowsky.[92] For instance, introduction of a stereocenter in compound **2.9** did not significantly affect the log *P*, however it drastically lowered the melting point thus indicating a significantly less stable crystal lattice and better solubility in water (Fig. 8C)[39,93,94] (see chapter 3 in ref. 60).

2.2.4 Physical methods. Next to chemical modifications, different physical methods can be applied to improve the solubility of organic molecules in water. Addition of different organic water-miscible co-solvents, such as DMSO, acetonitrile, propylene glycol, glycerin, ethanol, *etc.*, is frequently applied (see Section 2.1.1 and Fig. 4) The organic co-solvent surrounds the poorly soluble molecule and hence partially solubilizes the compound reducing interfacial tension with water.[76]

The increase of ionic strength is commonly used in the "salting out" approach, where large concentrations of salt in aqueous solution force (organic) compounds with lower solubility to precipitate out of solution. The opposite effect, namely "salting in", can be achieved by addition of so-called hydrotropes.[95–98] Hydrotropes are ionic organic salts which are added to a poorly water-soluble compound to increase its aqueous solubility in diverse ways, for instance, by forming micellar-like structures.[98] This approach is frequently used to formulate pharmaceuticals,[98] however, in many cases the amount of the hydrotropic salt needed can reach high levels and cause toxicity.[55]

Other physical solubilization methods include, particle size reduction by mechanical micronization[99] to increase the surface of the compound, nanoionisation,[55] dispersion in carriers, such as micelles,[55,76] or complexation in cyclodextrins.[100]

2.2.5 Prodrug strategy. While addition of solubilizing groups to a target molecule ensures water-solubility, it can interfere with the activity of biologically active compounds due to the increase in size and polarity. Therefore, prodrugs that have additional solubilizing moieties that are cleaved off *in vivo*, are often used in pharmacological applications.[40] The solubilizing groups described in the Section 2.2.1, such as phosphates (**2.10**, Fig. 9A),[101] PEG chains (**2.11**, Fig. 9B),[102] amino acids (**2.12**, Fig. 9C),[103] or sugar moieties[104] are used and linked *via* ester, amine, carbamate, carbonate, ether, imine and other (enzymatically) cleavable linkers to the actual drug.[105]

3 Molecular photoswitches

3.1 General definition of photoswitches and introduction of terminology describing their function and properties

A molecular photoswitch is a molecule which can be interconverted between two or more (stable) states by light.[3] This photochemical isomerization is accompanied by structural and electronic changes and leads to usually well-defined differences in the UV-Vis absorption spectra of the isomeric states, rendering them photochromic. Most of these molecules show positive photochromism, with the photochemically generated species exhibiting an absorption maximum λ_{max}(metastable)

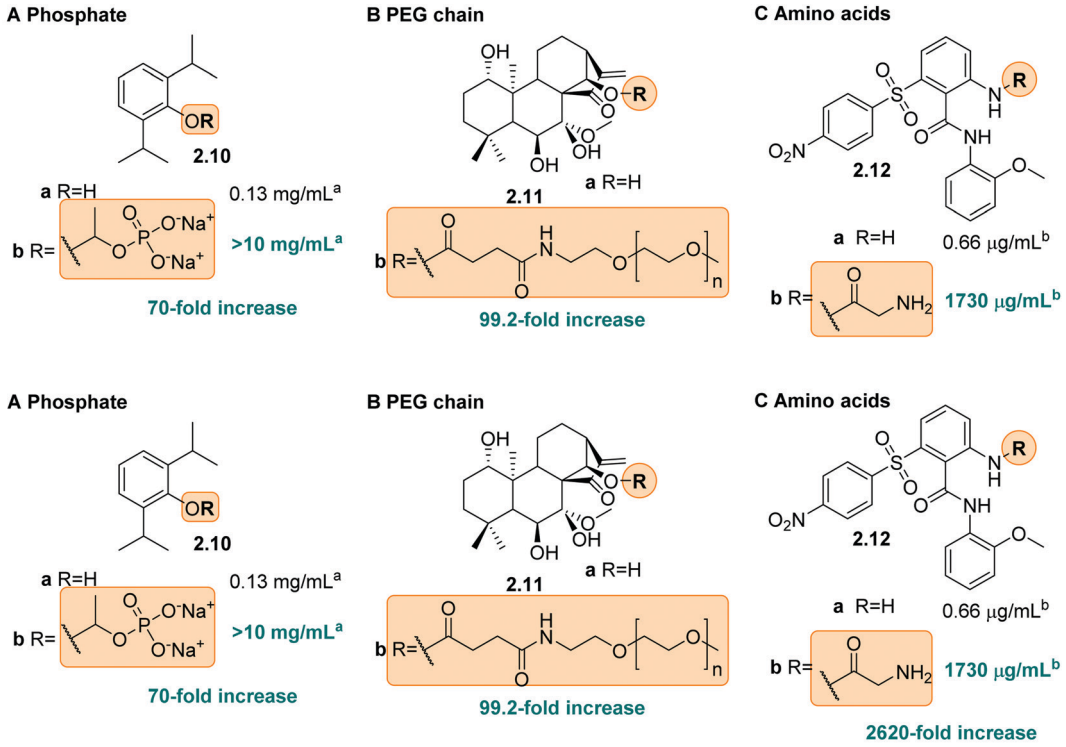

[a] Solubility in Tris buffer at room temperature, pH=7.4

[b] Solubility in water.

Fig. 9 Illustrative examples of prodrugs containing solubilizing groups: phosphate (A), PEG chains (B) and amino acid moiety (C) and their respective effect on solubility in water.

bathochromically shifted with respect to λ_{max}(stable).[106] If the initial photoisomer experiences a decolourization (bleaching) upon photoisomerization, with λ_{max}(stable) > λ_{max}(metastable), the compound shows negative or inverse photochromism.[106] Specifically, pronounced band separation facilitates selective switching between the photoisomers with light of different colours. Generally, photoswitching is a reversible, non-destructive process. However, the performance can be lost over several switching cycles due to side-reactions, typically photo degradation, irreversible cyclization, dimerization, *etc.* and can be described by the cyclability Z_{50} (the number of cycles in which the absorbance is reduced to 50% of the initial one).[106]

The extent of the isomerization process is characterized by a series of different parameters. The photostationary state (PSS) describes the dynamic equilibrium between two or more photoisomers under irradiation with light of a certain wavelength. At the PSS, depending on the system, the photoisomers will be present in a certain ratio, which we will refer to as photostationary state distribution (PSD; N.B., there is as of yet no consistency in the literature regarding this term). The photoisomerization quantum yield (QY) Φ quantifies the number of molecules of product formed per number of photons absorbed and hence, is an indication on how efficient the switch undergoes a photoisomerization process.[107] Practically, fast photoisomerization processes are observed when both Φ and the molar attenuation coefficient, $\varepsilon(\lambda)$ are high at the wavelength of excitation.[107]

Upon irradiation, the chromophore enters an excited state from where multiple relaxation pathways can take place, as shown in Fig. 10A, among them most importantly isomerization to the metastable isomer (Fig. 10B). The thermodynamically stable photoswitch is promoted into the first or second singlet excited state, then vibrationally relaxes, and eventually funnels through a region where a conical intersection resides, back to the ground state of another isomer, thereby undergoing an isomerization (Fig. 10B and C). The newly formed photoisomer is higher in energy than the original one and hence, it is metastable and isomerizes back to the stable state in a first order process with rate constant k. For convenience, this process is further characterized by a thermal lifetime τ (defined as $1/k$) or a half-life $t_{1/2}$ (describing the time in which 50% of the molecules in the metastable state isomerize back to their thermodynamically stable form) (Fig. 10D). If the thermal activation barrier between the metastable and the stable isomer is relatively low, a significant amount of thermal back isomerization is observed at ambient conditions, rendering the photoswitch a T-type one.[12,106] In the case of higher thermal activation barriers, the two photoisomers are considered bi-stable and isomerization is practically triggered exclusively using photochemical processes (P-type photoswitch).[12,106,108]

In terms of application, the experimentalist ideally chooses a specific photoswitch for a certain purpose, most often based on the type of properties that are altered upon photoisomerization,

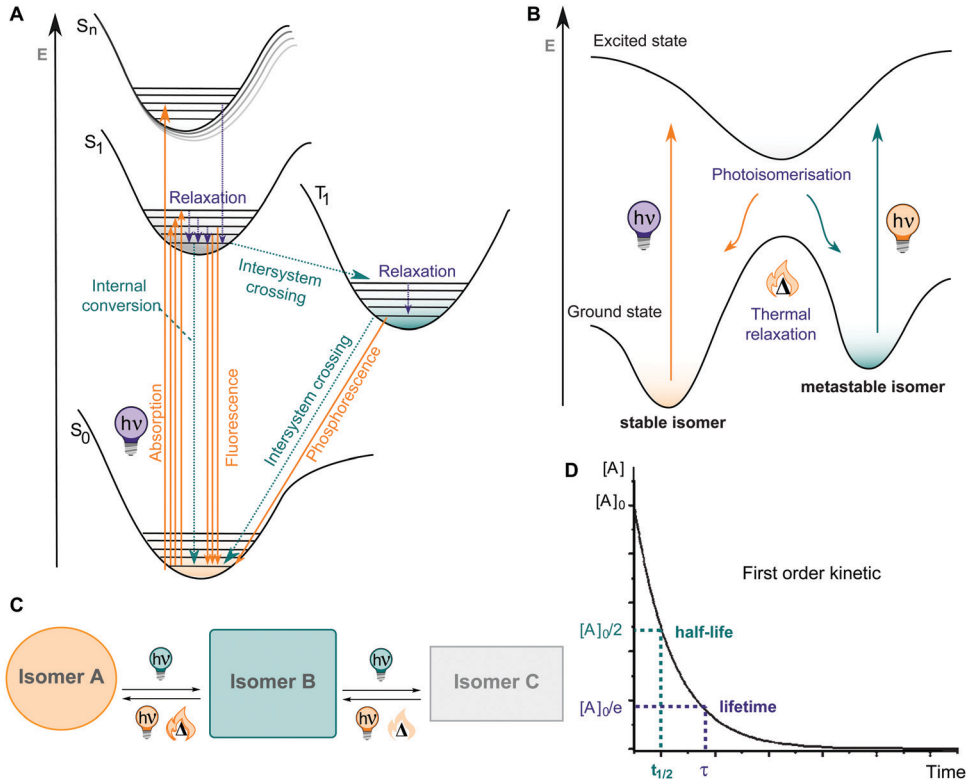

Fig. 10 (A) The Jablonski diagram highlighting the key photophysical processes possible from excited state of a photoswitch (photochemical processes are described in C); (B) schematic representation of potential energy surfaces during isomerization of a photoswitch; (C) general scheme depicting isomerization of a photoswitch upon light irradiation. Most photoswitches reversibly isomerize from A to B with application of light and heat, while in some instances isomer B can further react to form a third isomer C; (D) graph (concentration of A *vs.* time) depicting the first order kinetics of photoswitching with highlighted half-life and lifetime values.

and then incorporates the switch into the system of choice. However, in practice, this is not as straightforward, since the system's own characteristics will influence the properties of the switch. This delicate interplay is particularly challenging when embedding a photoswitchable molecule into a functional system in an aqueous environment. Consequently, in this section, we will introduce various kinds of photoswitches, organized according to their predominant photoisomerization mechanism, and discuss the influence of polar protic solvents, and especially that of water, on the photophysical and photochemical properties of the switch.

3.2 Photoswitches relying on the isomerization about double-bonds

Suitably substituted double bonds X=Y can be isomerized between an *E* and a *Z* form by light. They are frequently used as photoswitchable core motifs, as they are relatively small and hence, easy to incorporate into a larger molecule while introducing only small structural changes. Moreover, their effect can be easily predicted in each system due to their large geometrical changes accompanied by photoisomerization. These X=Y functions are often decorated with arene moieties, or in conjugation with such, to extend the π-system of the double bond and to make them responsive to light typically between 300 and 400 nm. Depending on the nature of X, Y and the substituents on the double bond, the absorption spectrum of the switch can be tuned up to the visible and near-infrared (NIR) region of the electromagnetic spectrum (*vide infra*). In the following, we will discuss various types of photoswitches, which isomerize about a C=C, C=N, or N=N double bond, highlighting both frequently used and more niche structures and the effect of polar protic solvents on their characteristics. An overview of various classes of photoswitches is displayed in Fig. 11.

3.2.1 (Stiff) stilbene. Stilbenes are molecules with the general formula Ar–CH=CH–Ar. They exist in a thermodynamically stable *E* and a photochemically generated *Z* form (*cf.* Fig. 12).[109] The *E* isomer is, depending on its substituents, quasi-planar and has its absorption maximum at *ca.* 290 nm with a strong vibrionic coupling.[110] Irradiation at the absorption maximum promotes the *E* isomer, *via* a π–π* transition, into its excited state, from which it relaxes to the *Z* form with high photoisomerization QYs ($\Phi^{E\rightarrow Z}$ is 0.40–0.60 for most (stiff) stilbene derivatives in apolar solvents).[111] The *Z* isomer can be accumulated with PSDs around 6 : 4 = *Z* : *E* in cyclohexane at the PSS^{313nm}.[112] The absorption spectrum of the *Z* form is bathochromically shifted and smoothened with respect to the *E* isomer. It exhibits a twisted, helical conformation and is considered to be the metastable isomer. In contrast to other photoswitches isomerizing about double bonds, like azobenzene or hydrazones (*vide infra*), the metastable isomer in (stiff) stilbenes is in most cases thermodynamically stable at ambient conditions and can

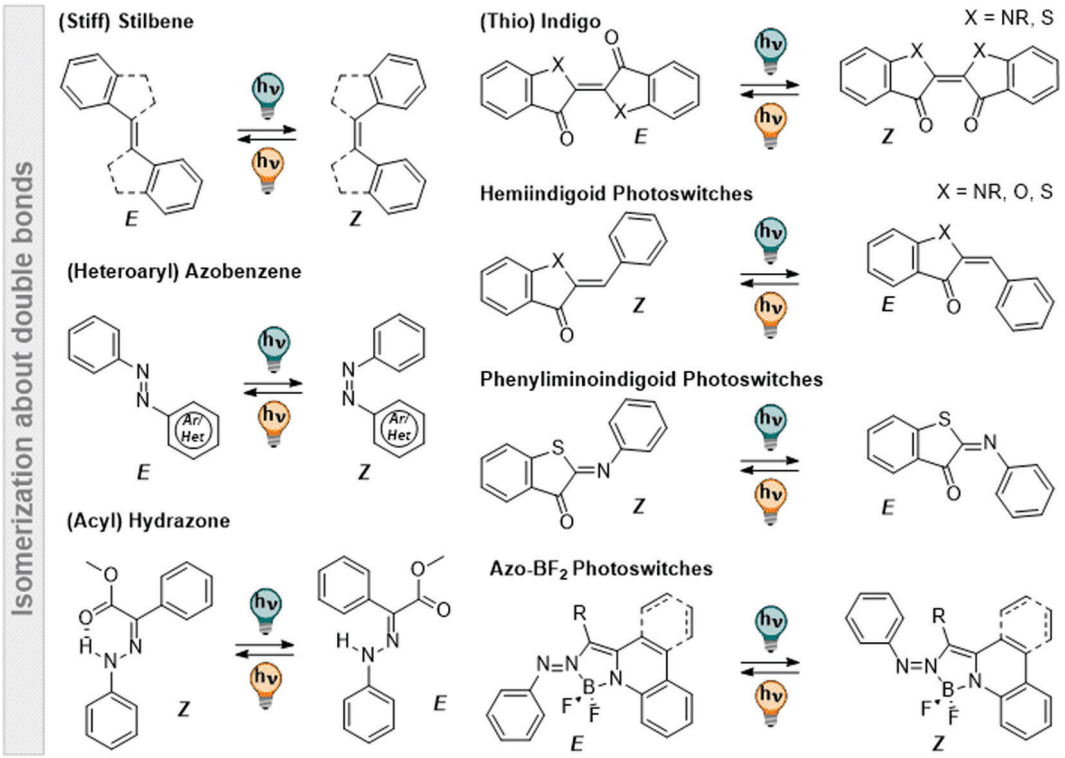

Fig. 11 Overview of various photoswitches based on double-bond isomerization (C═C, N═N, and C═N) that are discussed in Section 3.2.

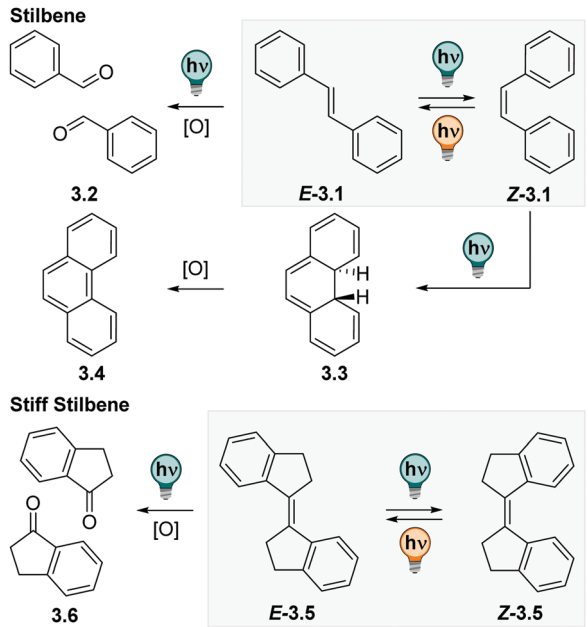

Fig. 12 Photochemical side-reactions of stilbenes. Top: *E*–*Z* photoisomerization of stilbene and the competing photo-oxidation and electrocyclic ring-closure reaction followed by irreversible oxidation. Bottom: *E*–*Z* photoisomerization in 1,1′-bis-indanyliden (stiff stilbene) and the competing photo-oxidation.

be isolated by simple column chromatography.[109] Irradiation of the *Z* stilbene induces photochemical $Z \rightarrow E$ isomerization with $\Phi^{E \rightarrow Z}$ between 0.3–0.45.[111]

The (photo)chemistry of 1,1′-bis-indanylidens (stiff stilbenes) is analogous, yet more simplified, compared to parent stilbenes as the phenyl twisting is hindered.[112,113] Originally, stiff stilbenes have been frequently used as a model system to study the parent stilbene molecule. Stiff stilbenes turned out to be photochemically more robust than stilbene itself.[109,111] While the *Z* isomer of the parent stilbenes can undergo an electrocyclic ring-closure reaction to dihydrophenanthrene, which is then irreversibly oxidized to phenanthrene and hence lost for *E*–*Z* photoisomerization (*cf.* Fig. 12), this pathway is not accessible for stiff stilbenes.[111,114] However, photo-induced oxidation reactions are observed for some derivatives under prolonged irradiation times (*cf.* Fig. 12).[115,116] As a consequence, many studies are performed under inert atmosphere.[110,112,117,118] This allows for *E*–*Z* photoisomerization that can be repeated over several cycles showing low fatigue independent from the solvent,[117,119–122] but might be a limitation in practical applications. The absorption maximum of stiff stilbenes is between 320 and 340 nm, depending on the ring-size[110] and can be shifted up to *ca.* 360 nm with suitable substituents.[123–126] As in parent stilbenes, both photoisomers of stiff stilbenes are fluorescent with low fluorescent QYs and have been subject of a large number of theoretical and photophysical studies, however, mainly in apolar solvents.[110,112,127–130] Moreover, the *E*–*Z* isomerization rate in stilbene is solvent dependent in both directions and, by trend, lower in solvents of higher viscosity or lower polarity. More importantly, it is affected by substituents, especially by those creating a dipole moment or push–pull systems.[111]

In last two decades, the stiff stilbene photoswitches are employed as the core motifs in molecular rotary motors (*vide infra*) and in a range of emerging applications,[109] such as in photo-responsive supramolecular architectures,[117,121,131,132] host–guest systems,[119,120,122,133–135] catalysis,[136] and in the context of mechanochemistry.[137–140] Their properties are investigated in a wide range of solvents like chloroform,[133] DCM,[134] benzene,[132] DMSO,[120,122] MeCN,[119] and MeOH.[123] However, only few studies have focused on the properties of (stiff) stilbenes in water or aqueous buffers, as the 1,1′-bis-indanyliden is inherently insoluble in aqueous media.[125] This is underlined by a study showing that addition of water to a solution of 5,5′,6,6′-tetrafluoro stiff stilbene in THF led to aggregation of the chromophore, which could be monitored by aggregation-induced fluorescence resulting in an increase of fluorescence QY by three orders of magnitude.[125] However, recently, a few stiff stilbene derivatives were equipped with solubilizing groups and characterized in DMSO–water mixtures, buffer solutions and even *in vivo*.[116,141–143] The compounds were reversibly switchable over several cycles,[141] however, photo-induced oxidation was observed in some cases (*cf.* Fig. 12).[116] Alternatively, heteroaromatic stilbene derivatives attracted very recently attention as alternative for classical stilbenes or azobenzenes in biological context. Specifically, styrylbenzothiazole showed promising properties in buffer and in cell studies.[144]

In summary, (stiff) stilbenes demonstrated their potential as water-soluble photoswitches in pioneering studies, but were to the best of our knowledge never part of a systematic study in this context. Hence, further investigations are required to reliably predict the effect of aqueous media on all photochemical properties of (stiff) stilbenes.

3.2.2 Molecular rotary motors based on stiff stilbene. Molecular rotary motors represent a sub-class of stiff stilbene photoswitches and are characterized by their thermal helix inversion (THI) process being directed by a stereogenic element (*cf.* Fig. 13).[3,145] The photochemical behaviour of the compounds is very similar to the parent (stiff) stilbene, but it proceeds in general with lower photoisomerization QYs.[109] Irradiation with light induces a photochemical torsion about the central double bond, resulting in an unstable photoproduct due to steric hindrance of suitably attached substituents (*cf.* Fig. 13). The chiral group facilitates the THI occurring preferably in one over the other direction and hence, results in a molecule with the potential to undergo continuous rotary motion.[146] Over the past decades, several molecular rotary motors have been developed and implemented in a vast number of applications and were the subject of several recent reviews.[147–151]

The unfunctionalized motor molecules are very lipophilic and cannot be brought into an aqueous environment, unless dissolved in micelles.[152] However, after introduction of suitable substituents, the compounds can be investigated in water and buffer (as in the example shown in Fig. 13).[152–154] So far, there is only one study focusing on the photochemical and photophysical properties of fully water-soluble molecular motors.[152] Upon irradiation with light of a suitable wavelength (*ca.* 310 nm for first generation motors and 365 nm for second generation motors),

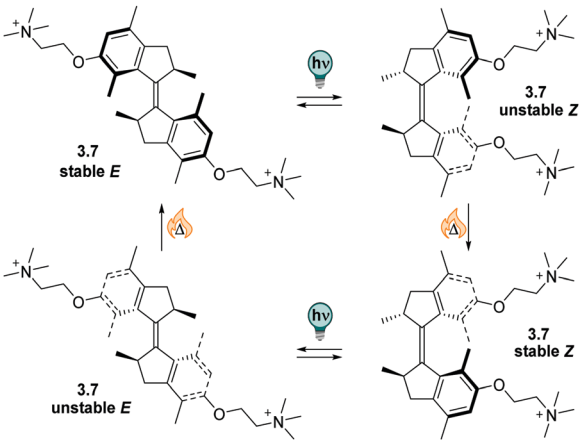

Fig. 13 A stiff stilbene-based first generation Feringa molecular motor was equipped with alkylammonium group to promote water-solubility. The unidirectional rotation of the motor relies on photochemical *E*–*Z* isomerization (irradiation with 312 nm light) and thermal helix inversion (THI, here, five days at ambient temperature in water).[152]

water-soluble molecular motors can be photoisomerized in aqueous media showing high PSDs and only little fatigue, similarly to their performance in organic solvents.[152,153] However, in a systematic study on a second-generation molecular motor, the THI was found to be strongly solvent-dependent.[155] In particular, in alkane solvents, the $t_{1/2}$ of the THI increased with increasing chain length. More polar solvents of the same size also gave longer half-lives, as did alcohols with increasing chain lengths.[155] A similar molecular motor dissolved in micelles in water showed a shorter half-life than in short alkanes, while the analogous motor functionalized with water-soluble groups gave a 10-times longer half-live of the metastable state when dissolved in buffer.[152]

In conclusion, molecular motors can be readily applied in aqueous environment and have been demonstrated to serve as fully water-soluble switches at low concentrations.[152] Similar as (stiff) stilbenes, they are insufficiently studied in water and more research is needed to realize their full potential.

3.2.3 (Heteroaryl)azobenzene. (Heteroaryl)azobenzenes are compounds of the general formula Ar–N=N–Ar, where Ar can be an aryl ring or a heteroaryl unit.[156–158] They became frequently used photoswitches and can be found in a diverse range of applications due to their small size, reliable photochemical behaviour, and the versatility of methods available to synthesize and functionalize them.[156–160] As a result, (heteroaryl)azobenzenes are quite well understood and were the subject of extensive fundamental studies. Like with the previously described stilbenes, the large geometrical change that azobenzenes undergo upon double bond isomerization significantly alters their chemical and photochemical properties.[3,156–158] In comparison to stilbene, the absorption maximum of its diazo analogue is bathochromically shifted to around 330 nm in parent azobenzene.[111,158] This allows operating the system with UV-A instead of UV-B light, which is less harmful and enables more selective addressability with respect to other chromophores present in the system.[156–158] Hence, it became a popular approach to turn any stilbene-based system into

the corresponding azo-analogue, a design principle termed azologization particularly in the context of photopharmacology.[9]

Classical azobenzenes exist in a thermodynamically stable *E* form, which is planar and apolar, and undergo *E* → *Z* isomerization after irradiation with light of a suitable wavelength (Fig. 14). The photochemically generated, metastable *Z* form has a helical conformation and a dipole moment of around 3D and can be converted back into the *E* form upon irradiation or in a first-order thermal process.[156–158] The higher polarity of the *Z* isomer influences the solubility of the unsubstituted azobenzene in polar (protic) solvents, such as water. While the *E* isomer has more propensity towards π-interactions with other azobenzene molecules due to its flat conformation, the *Z* isomer is less able to interact in the same way with other extended arenes.[156,161] Furthermore, its strong dipole moment enables the molecules to interact better with a polar environment and they show higher intrinsic solubility (Fig. 14). Specifically, a study measuring the solubility of the *E* and *Z* forms of several azobenzene derivatives showed that the *Z* isomer is 6–40 times more soluble in water than the *E* isomer. This behaviour is also seen for semi fluorinated azobenzenes and peptide conjugates.[161] The different preferences in intermolecular interactions between the two photoisomers have been employed in the construction and the dynamic control of nanoarchitectures,[162,163] amphiphiles,[19,20] and photopharmacological agents.[164]

Heteroaryl azoswitches do not show this behavior to the same extent, as also the *E* isomer is polarized even in unsubstituted derivatives due to the presence of the heteroatom(s).[157,158] As in classical azobenzenes, the *E* form is planar and the *Z* is twisted, adopting either a helical conformation in the case of 6-membered rings, and a T-shaped one if a 5-membered heteroaryl ring is directly attached to the diazo bond.[157,158,165] Moreover, the photophysical properties are influenced by the presence of the hetero atoms, rendering azoswitches based on pyridine,[166–170] indole,[171–174] indazole,[175] purine,[176,177] pyrimidine,[178,179] pyrrole,[165] imidazole,[165,180–182] pyrazole,[46,165,183–188] oxazole,[189] thiazole,[180] thiophene,[190–192] *etc.*, generally responsive to light of longer wavelength. In contrast, in classical azobenzenes the UV-Vis absorption spectrum can be tuned by introducing, for instance, (push–pull) substituents in the *para* position[156,193,194] or tetra-*ortho* substituents[195–205] and thereby influencing the position of either the π–π* transition,[199,205] the n–π* transition,[195–197] or both.[156,201]

Also, in heteroaryl azobenzenes, the *E* → *Z* isomerization is triggered by light, while the back-isomerization can occur photochemically and thermally. Both homo and heteroaryl azoswitches show little-to-no fatigue over many switching cycles in different solvents.[156–158] However, the N=N double bond in parent azobenzenes carrying electron-poor substituents has been shown to be sensitive to reduction, an important parameter to be considered

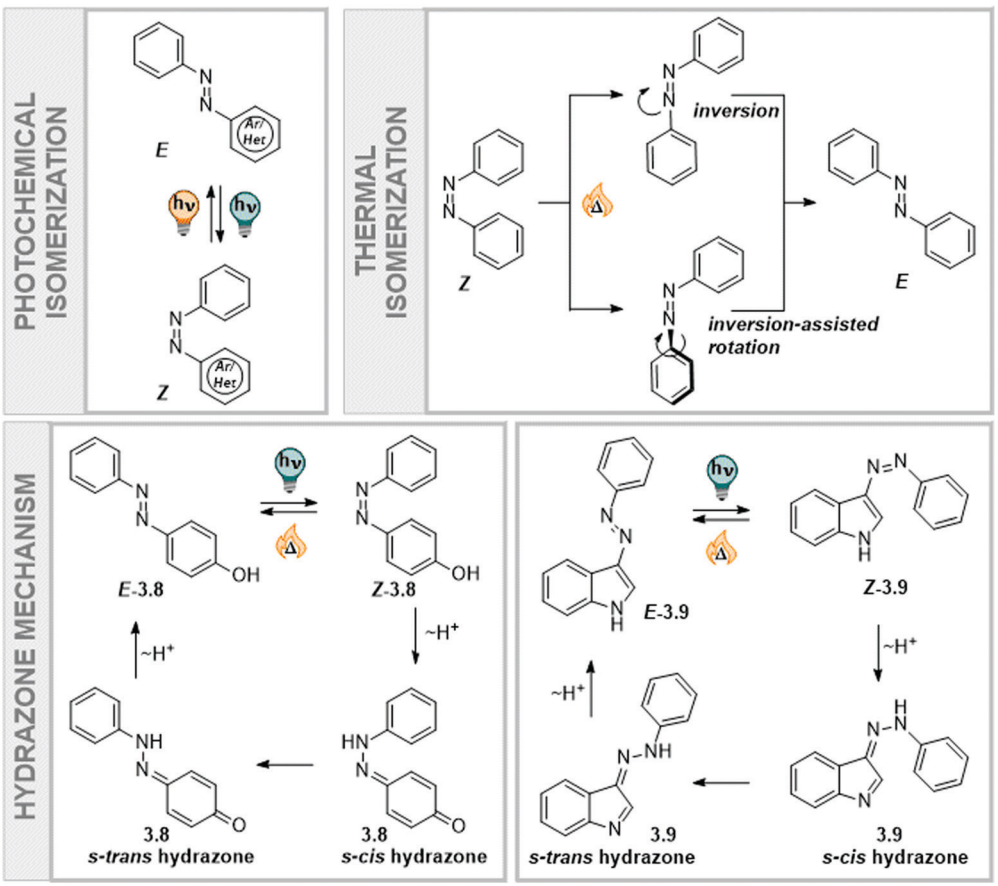

Fig. 14 Overview over photochemical and thermal isomerization pathways in azobenzenes.

during synthesis and in applications.[206,207] In the context of water-soluble photoswitches, this aspect is of greatest importance in biological systems, as the reducing agent glutathione is present in the cell.[6,30] Similar observation have also been made for some heteroaromatic analogues, like purines[177] and thiazoles,[180] while arylazopyrazoles appear to be less sensitive to these conditions.[157,185]

Moreover, the nature of the solvent has an influence on the thermal stability of the metastable form, as it stabilizes or destabilizes the transition state geometry of the reisomerization reaction. The thermal $Z \rightarrow E$ isomerization is a ground state process, and proceeds *via* an inversion transition state, an inversion-assisted rotation transition state, or follows a mechanism with a hydrazone intermediate (Fig. 14). The pathway the switch eventually employs depends on the type of the azoswitch, its substitution pattern, and the solvent in which the isomerization proceeds, and has been a subject of several studies with both homo and heteroaryl azobenzenes.[156–158] In general, push–pull substituted azobenzenes isomerize thermally *via* the faster inversion-assisted rotation transition state pathway, yielding shorter lifetimes. In polar solvents, the push–pull effect is more prominent than in apolar systems, significantly affecting the thermal lifetimes of azobenzenes isomerizing *via* this pathway, when moving to aqueous environment.[156,194] In contrast, azo-switches isomerizing *via* an inversion transition state show longer lifetimes in polar solvents.[208] Moreover, azobenzenes bearing a –OH, –SH, or –NHR as part of the heteroarene or as a substituent, have access to an alternative thermal relaxation pathway in polar protic solvents. The acidic proton can be tautomerized onto the N=N double bond of the azo-function to result in a single bond between the nitrogens about which one of the former aryl ring can easily rotate to eventually result in the energetically more stable *E* isomer (Fig. 14), which leads to extremely shortened lifetimes.[171–173] Proton transfer in the hydrazone mechanism is solvent-assisted and hence, favoured in protic or aqueous media, if the energy gained by accessing this pathway compensates for the loss of aromaticity.[172] However, recent computational and experimental work on NH-containing hetero azoswitches shows that potentially acidic moieties only at specific positions will result in shorter lifetimes in water or other protic media. If the "breaking" of aromaticity is not compensated by the low-energy single bond rotation of the hydrazone formed, the switches will isomerize *via* inversion or rotation. Consequently, they show stable *Z* isomers in polar protic solvents, such as alcohols, water, buffer or even cell medium.[172,183] The same behaviour was shown earlier for substituted parent azobenzenes, comparing the thermal half-lives of the *Z* isomers of 2-, 3-, and 4-hydroxyazobenzene.[209] While the *Z* isomers of *ortho*- and *para*-OH azobenzene rapidly isomerized through tautomerism back to the thermodynamically favoured *E* form, the *meta*-substituted analogue behaved like the parent azobenzene.[209]

Not only the rate constant of the thermal $Z \rightarrow E$ reaction is affected when moving into aqueous environment, but also the photoisomerization QYs are solvent-dependent. For parent azobenzene, $\Phi^{E\rightarrow Z}$ is higher in alcohols and water than in apolar solvents if the isomerization is triggered *via* the $S_1(n–\pi^*)$ and $S_2(\pi–\pi^*)$, while $\Phi^{Z\rightarrow E}$ $(n–\pi^*)$ is in general lower.[156] However, this trend in behaviour can change with different substituent patters and scaffolds.[156–158] As studying the fundamental properties of the switch used is often out of the scope in application studies, a comprehensive overview is missing. This makes it not trivial to predict the properties of a photoactuator when moving between different solvent systems. Specifically, using an azobenzene, which was thoroughly studied in a non-polar solvent, in an aqueous environment will not necessarily result in the same behaviour. As apolar solvents are frequently used to study azo-switches, this gap of understanding hampers the rational design of water-soluble azobenzenes.

3.2.4 Diazocines. Diazocines are cyclic analogues of parent azobenzenes, exhibiting positive photochromism in the visible range of the electromagnetic spectrum.[210–214] The strain generated by the 8-membered ring causes an inversion in relative stability of the two photoisomers of azobenzene. In diazocines, the *Z* isomer is the thermally stable form, and the *E* isomer is the metastable one.[210] Exchanging an azobenzene scaffold for a diazocine poses a way to invert the properties of a given system and gives access to additional tunability.[215,216] Moreover, in diazocines, the absorption bands associated with the $S_0 \rightarrow S_1$ transition are well-separated, giving rise to azobenzenes that can be switched bidirectionally with visible light with high quantum yields.[210]

The strain that the *E* isomer experiences results in $t_{1/2}$ of a few hours in the original CH_2–CH_2-bridged diazocines.[210] More recently, CH_2–X bridged diazocines were investigated, with X being O, S, or NR (R = Me, Et, H, Ac, *cf.* Fig. 15), and were found to feature bathochromically shifted UV-Vis absorption spectra, ranging up to the NIR.[211,217] The thermal half-life in CH_2–O derivatives in in the seconds range, while CH_2–S analogous are thermally stable over a few days.[211] Also, the influence of different substituents[218] and solvents on the switching properties has been investigated.[211,219] A recent study showed that, when moving from MeCN to pure water as a solvent, the absorption spectra of both photoisomers are affected with λ_{max} shifting by 10–20 nm in opposite directions, thereby decreasing the band separation. While $t_{1/2}$ is in some cases more than doubled in aqueous medium, the PSDs are increasingly lower with higher amounts of water added to MeCN. In the investigated series, the CH_2–NAc stood out as its properties were relatively independent from the solvents and the compounds was well-soluble in pure water (up to 1.27 mM at ambient temperature).[219]

3.2.5 (Thio) indigo. Similarly to many other photoswitches, indigo and thioindigo had been well-characterized as dyes several decades ago and their photochromism was observed

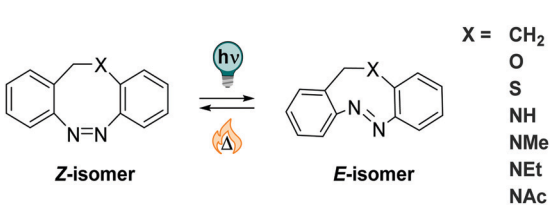

Fig. 15 Thermally stable *Z* and photochemically generated *E* isomer in diazocines with various substituents X in the bridging unit tuning their properties.

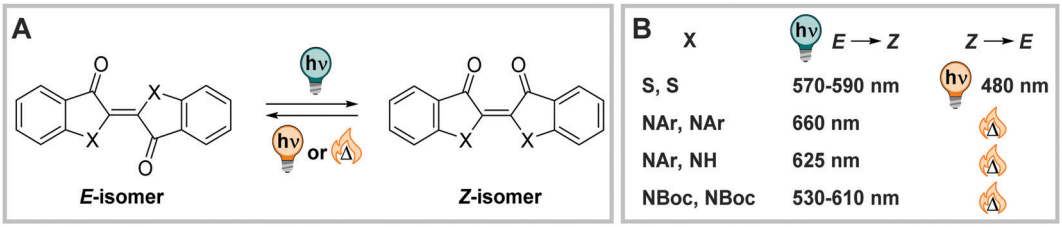

Fig. 16 (Photo)switching in indigo photoswitches. (A) Thermally stable *E* and metastable *Z* isomer in (thio)indigo derivatives. (B) Different photochemical and thermodynamic properties of (thio)indigo switches depending on the substituent X.

already in the middle of the last century.[220–222] The parent indigo dye (Fig. 16) is particularly photostable due to an efficient deexcitation pathway *via* an excited state proton transfer from the indole-NH onto the carbonyl moiety and consequently, cannot undergo *E*–*Z* isomerization.[223–225] However, when alkylated,[226] acetylated[227–229] or arylated[230,231] on the indole nitrogen, indigos become efficient photoswitches: irradiation of the thermally stable *E* isomer with orange-to-red light results in formation of the metastable *Z* form, and is accompanied by a hypsochromic shift of the absorption maximum (negative photochromism).[230]

Both photoisomers are luminescent, the *E* weaker than the *Z*, and fluorescence QYs are significantly lower than in thioindigo, while photoisomerization QYs were comparable (*vide infra*).[228] The *Z* isomers are often short-lived and could only be studied with pump–probe experiments.[226,228] On the contrary, bis-Boc and (di-)arylated indigos showed prolonged thermal lifetimes of the photochemically generated *Z*-indigo, with $t_{1/2}$ = 1–400 min (in MeCN at ambient temperature) in di-arylated and up to a few days in bis-Boc derivatives, depending on the substituents and solvent used. The half-life can be tuned by altering the substituent pattern and could be rationalized in a Hammett analysis for both compound groups.[227,230] Alternatively, the thermal $Z \rightarrow E$ isomerization rate can be tuned by varying amounts of water in mono-arylated indigo. In particular, adding increasing amounts of water to a THF solution of a mono-arylated derivative deceases $t_{1/2}$ from 1000 s to only 5 s, while the thermal half-life of the corresponding bis-arylated indigo derivate stays unaltered.[231] In bis-Boc functionalized compounds, the half-life is significantly shortened in MeCN/water mixtures, compared to toluene or pure MeCN. Also, the QYs are lower in the presence of water for the $E \rightarrow Z$ but higher for the $Z \rightarrow E$ photo isomerization.[227]

Thioindigo (Fig. 16) is the sulphur-analogue of parent indigo and was studied in various contexts, for instance in semiconducting films,[232] taking advantage of its redox switching[233] and modulation of electro-optical properties.[234] For this reason its (photophysical) characteristics and substitution effects were the subject of several experimental and theoretical studies.[232,234–236] The negative photochromism[237] of thioindigo was observed already around 80 years ago.[221,238,239] The molecule could be switched in both direction with visible light showing good PSDs and QYs ($PSD^{E\rightarrow Z}$ = 63%*Z*, $PSD^{Z\rightarrow E}$ = 74%*E* for 6,6′-di-isopropoxythioindigo in epoxy resin; $\Phi^{E\rightarrow Z}$ = 0.20, $\Phi^{Z\rightarrow E}$ = 0.38 for 6,6′-di-isopropoxythioindigo in toluene).[240] A limiting factor for the study of thioindigos is their "very low solubility in almost all conventional organic solvents and polymers"[240] for which reason suitably substituted derivatives are usually applied.[233,234,240] In this manner, it was recently possible to study the photochromic behaviour of these compounds in aqueous media.[241,242] The compounds could be solubilized and investigated in water and buffer, however, addition of 20% MeCN was needed to aid solubilization and 1% TFA stabilized the *Z* isomer.[241] Alternatively, buffer/acetone mixtures were used.[242] Reversible photoswitching could be maintained and did not show any fatigue over several cycles. QYs in both directions were lower in pure water than with co-solvent ($\Phi^{Z\rightarrow E}$ = 0.05 and $\Phi^{E\rightarrow Z}$ = 0.19, and $\Phi^{Z\rightarrow E}$ = 0.21 and $\Phi^{E\rightarrow Z}$ = 0.41 with 80% MeCN in water), which was attributed to an aggregation tendency of the dye in the absence of organic (co)solvent.[241] This observation agrees with the general solvent and concentration dependency of both QY and fluorescence observed in various thioindigo derivatives[241,243] and is also in line with the thermal isomerization kinetics, which have a close-to-sigmoidal behaviour in pure water and a (normal) exponential one in 80% MeCN in water. The apparent half-life was around 120 min in both solvent (mixtures) at ambient temperature.[241] By adding phenol substituents at suitable positions, the *Z* isomer could be further stabilized, and negligible thermal $Z \rightarrow E$ isomerization was observed over the course of several hours. However, very high amounts of co-solvent were needed to solubilize the molecules.[242]

In summary, both indigo and thioindigo derivatives can be reversibly photoisomerized in the presence of water and show robust and stable photoswitching properties with medium to good PSDs and QYs. Both scaffolds are very lipophilic, tend to aggregate in water and have to be solubilized with suitable substituents and sufficient amounts of co-solvents. The photophysical and (photo)chemical properties of both molecules are influenced by the presence of water, which results in many cases in higher thermal $Z \rightarrow E$ isomerization rates, lower QYs and lower PSDs.

3.2.6 Hemi(thio)indigo and aurone. Hemi(thio)indigo (H(T)I) formally consist of half a (thio)indigo and half a stilbene fragment and features a central C=C double bond as photoactive motif (Fig. 17).[220] Also, from a photophysical perspective, HI and HTI show a compromise of the UV-Vis properties of their parent photoswitches, having their absorption maximum usually around 450 nm, while parent stilbene shows λ_{max} around 290 nm and (thio)indigo between 550 nm and 650 nm (*vide supra*).[230,241,244] The absorption maximum of the metastable *Z* isomer is typically

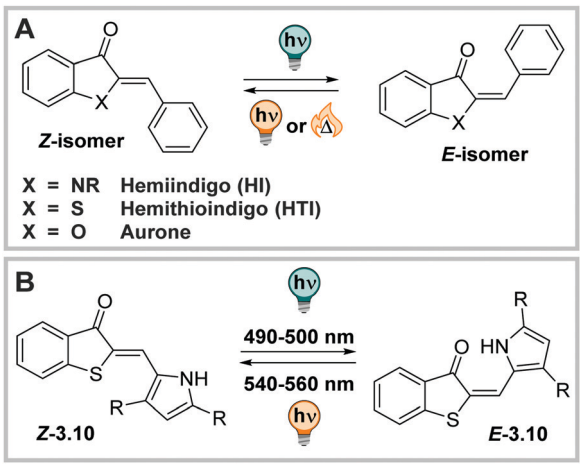

Fig. 17 (A) Chemical structures of hemiindigo (HI), hemithioindigo (HTI), and aurone. (B) Photochemical *E*–*Z* isomerization of HTI **3.10**.

bathochromically shifted with respect to the *E* and hence, their photochromic behaviour is closer to stilbene than to (thio)-indigo, which shows negative photochromism.[230,237,244] Both HI and HTI can be photoswitched in both directions using visible light.[220,245]

HI has its absorption maximum around 450 nm in the thermodynamically stable *Z* configuration,[246] and it can be shifted up to *ca.* 530 nm by careful substituent choice and taking advantage of the solvent effects.[220] The molecule exhibits good band separation and irradiation with blue lights results in formation of the metastable *E* isomer, which has λ_{max} between 510 nm and 590 nm.[245] HI shows little fatigue over many switching cycles,[220] has moderate QYs ($\Phi^{Z\rightarrow E}$ = 0.16–0.23 and $\Phi^{E\rightarrow Z}$ = 0.02–0.11, depending on the derivative), high PSDs (>80%) for the $Z \rightarrow E$ in and shows close to quantitative conversion for the $E \rightarrow Z$ photoisomerization, independent from the solvent (studied in toluene, THF, and DMSO),[245] in strong contrast to the HTI family which shows strong solvent dependency in photoswitching (*vide infra*).[247–249] The thermal half-life of the metastable *E* isomer is in the range of several years at ambient conditions in various solvents. However, when the indolic nitrogen bears substituents other than H, the two photoisomers in HI, *Z* and *E*, become energetically very similar. Experimentally, heating the pure (photochemically generated) isomers results in a mixture of *E* and *Z* forms independent of the initial configuration.[245,250] Also, this property is in strong contrast to most photoswitches isomerizing about double bonds, even comparing to the closely related HTI, aurone, or ITI (*vide infra*).[220,251,252] Also, HI could be switched reversibly in mixtures of water and organic solvents (water/DMSO 9 : 1 or water/THF 8 : 2, with a drop of TEA to increase the switching performance) and showed good to very good photochromic properties.[245] However, the authors noted that solubility at higher concentrations was an issue and more detailed analysis, *e.g.* by NMR spectroscopy, could not be performed. By attaching more efficiently solubilizing substituents,[253–255] several HI derivatives could be investigated in pure water with no or little amounts of organic co-solvents (2% (v/v) EtOH or 10% (v/v) DMSO). The $PSD^{Z\rightarrow E}$ was around 80%*E* and back-isomerization was close to quantitative. The photoisomerization QYs were lower than in organic solvents or aqueous solutions with higher contents of cosolvent ($\Phi^{Z\rightarrow E}$ *ca.* 0.03 and $\Phi^{E\rightarrow Z}$ *ca.* 0.002).[253] The *E* isomers were stable in solution and showed thermal lifetimes in the range of several days for many derivatives at ambient temperature. While low band separation and suppressed fluorescence was observed in water,[253,255] isomer-specific binding to biomolecules could reinstall the emissive properties reversibly.[255,256]

HTI can be photoisomerized in various solvents with high PSDs in both directions (>80% photochemical generated isomer) in methanol as well as DCM. The thermal half-life $t_{1/2}$ of the metastable *E* isomer is *ca.* 140 h in DCM and around 20 h in MeOH.[257] HTIs show very fast *E*–*Z* photoisomerization kinetics as single compounds or when attached to macromolecules[244,248] and the isomerization mechanism, solvent and substituent effects were studied in detail.[258] Decoration with suitable substituents can accelerate the light-induced isomerization even more. When the thioindigo fragment is used as acceptor and the stilbene fragment, functionalized with electron-donating substituents in *ortho* and *para*-position, is used as a donor moiety, the photoisomerization occurs in the low ps-range. The photoisomerization QYs were strongly depended on the substituents with $\Phi^{Z\rightarrow E}$ = 0.14–0.23 and $\Phi^{E\rightarrow Z}$ = 0.05–0.33 in DCM.[247] Moreover, HTI is fluorescent in aprotic solvents, but the fluorescence can be quenched by protic solvents as shown for some derivatives.[246] Replacing the phenyl moiety with aryl-extended pyrroles results in an improved band separation and leads to quantitative photoisomerization in both directions (in DCM, see Fig. 17). H-Bonding of the pyrrole *N*H to the carbonyl moiety leads to a significant bathochromic shift of the compounds in both photoisomers.[259] For instance, a bis-*para*-methoxy-phenyl substituted pyrrole moiety facilitated $Z \rightarrow E$ photoconversion with red light, yielding 80% of the *E* isomer (623 nm light to trigger photoisomerization in DCM).[259,260] Also, a functionalized HTI, modified with multiple methoxy and hydroxy groups which contribute to a non-planar structure, could be investigated in the presence of water. Thereby, the $PSD^{Z\rightarrow E}$ in 75% DMSO in PBS buffer contained 65% *E*, while at the $PSS^{E\rightarrow Z}$ 97% *Z* was formed. Photoswitching was stable over several cycles and the metastable *E* form had a half-life of *ca.* 30 min at 37 °C in the DMSO-buffer mixture. The same compounds could also be photoisomerized *in cellulo*, however, this conclusion was made on the basis of altered biological activity and not derived from photophysical measurements.[261] In a follow-up study, *para*-hydroxyphenyl moieties lead to very short thermal lifetimes of less than 1 min in DMSO and in the milli-second range in protic media,[262] an effect often observed in azobenzenes, where it is attributed to a tautomerization mechanism that can, however, not occur in an analogous manner in unsubstituted HTI (*vide supra*).[172,263] Several different HTI derivatives have successfully been employed as unnatural amino acids[244] and were tested *in cellulo*.[264]

Moreover, HTIs were used to build more machine-like systems with several HTI units to generate complex motion,[265,266] in information processing,[267] or to function as photoresponsive receptors.[268,269] The scaffold was further functionalized to

construct unidirectional molecular motors,[270–276] which behaviour is highly solvent-dependent[249] and influenced by the presence of water.[277]

Aurones (Fig. 17) are synthetic and natural compounds belonging to the flavonoid family,[278–280] mainly studied as highly tuneable fluorescent dyes[251,281,282] and regarding their intrinsic biological activity.[278,283,284] Alongside these studies, their photoswitching properties were investigated in chloroform and toluene. $Z \rightarrow E$ isomerization could be triggered with 400 nm light and was accompanied by formation of a bathochromically shifted band that was attributed to the metastable E isomer ($PSD^{Z\rightarrow E}$ = 55–60%E). Consequently, they show similar photochromic behaviour as the structurally related hemi(thio)indigos.[285,286] The half-life of the metastable isomer was around 40 min.[286] $E \rightarrow Z$ isomerization was induced through irradiation with 480 nm in $CHCl_3$ to regenerate >95% of the Z isomer. Also, the fluorescence intensities in chloroform depended on the photoisomer present, with the E isomer (measured at the PSS, not isolated) showing weaker intensities.[285] While the fluorescence, used to visualize cells, was recorded in Tris buffer in the presence of serum albumin and salmon sperm DNA,[285] the photochromic properties of these compounds have to the best of our knowledge only been so far studied in organic solvents[285,286] and in polymer films,[251] but not in aqueous environment.

3.2.7 Aryliminoindigoid photoswitches: iminothioindoxyl. The photochromic properties of iminothioindoxyl (ITI, Fig. 18) were only recently reported.[252] The molecule formally consists of half thioindigo and half azobenzene. The photochromic unit is the central C=N double bond, which makes ITI more polar than the C=C-containing analogue, HTI. As other indigoid photoswitches ((thio)indigo, HI, HTI and aurone),[254] ITI is an all-visible photoswitch. It undergoes photochemical $Z \rightarrow E$ isomerization when irradiated with blue light (455 nm, $PSD^{Z\rightarrow E}$ *ca.* 65% E).[252] The process is accompanied by pronounced photochromism with the absorption maximum of the newly formed isomer being *ca.* 100 nm shifted compared to the thermodynamically favoured one. The metastable E isomer can be switched back photochemically by irradiation with orange light (595 nm) or relaxes thermally with lifetimes in the millisecond range *via* inversion about the C=N nitrogen.[252] Addition of acid lead to protonation of the C=N bond and enforced an altered isomerization pathway simultaneously prolonging the thermal half-life of the switch to the second–minute range.[287] The photochemical process in the neutral ITI can be triggered in a wide range of solvents, was also observed in buffer (1.7–6.7% DMSO for solubilization, depending on the substituents), and remained unaltered in the presence of the cellular reducing-agent glutathione.[252]

3.2.8 (Acyl)hydrazone. (Acyl)hydrazones are multi-stimuli responsive switches with the general C=N–N motif.[288–290] Isomerization about the C=N double bond can be triggered by pH,[291–295] metal ions[296–298] or light.[288,299] Their multi-responsive nature, together with their isomer-dependent emission properties, make (acyl)hydrazones interesting candidates for constructing more complex systems combing acid/base chemistry, metal-ion binding and photochemical processes as triggers.[288,300–305] Thereby, the thermodynamically stable isomer in acyl (**3.11** in Fig. 19) and phenylhydrazones (**3.12–14** in Fig. 19) can have an E or Z absolute configuration, depending on the substituents.[299] Photoirradiation induces E–Z isomerization to the metastable isomer, which in acylhydrazones quickly isomerizes back to the thermally stable form (**3.11** in Fig. 19).[288] However, if a suitable H-bond acceptor, such as a pyridine (**3.12**), or a carbonyl group (**3.13**), or both (**3.14**), are stabilizing the metastable isomer through H-bonding to the hydrazone hydrogen,[306,307] bi-stable (photo)-switches with very long thermal lifetimes (up to a few thousand years)[308] in various solvents and the solid state can be obtained.[308–311] Moreover, hydrazone-based photoswitches

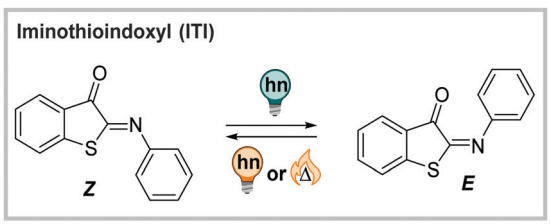

Fig. 18 Thermally stable Z and metastable E isomer of Iminothioindoxyl (ITI).

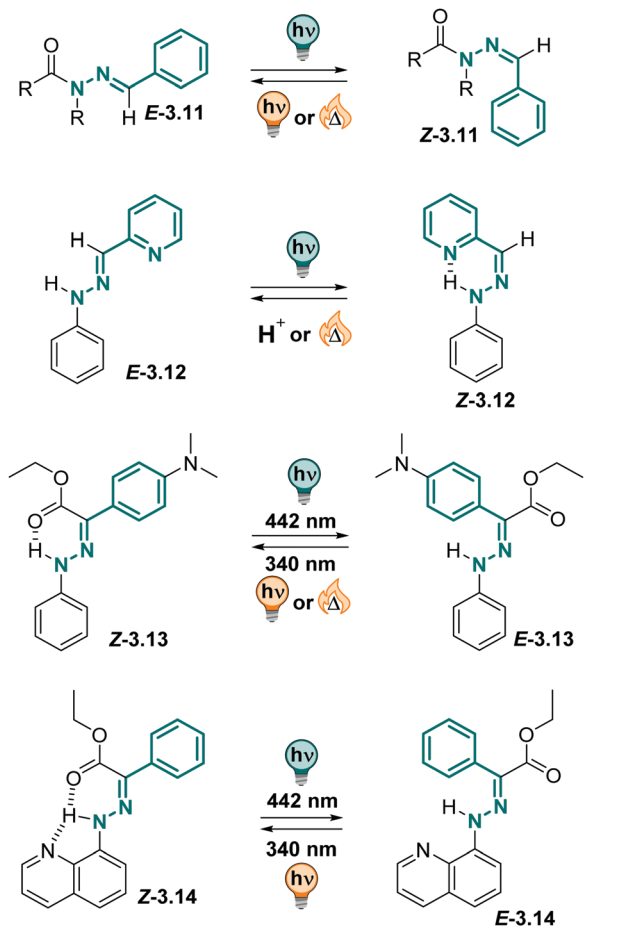

Fig. 19 Overview of various (acyl)hydrazone derivatives and their photochemically and thermodynamic properties.

show good to excellent PSDs[311,312] and fatigue resistance.[311–313] Attachment of different substituents,[311,312,314] as well as introduction of strain[314,315] can tune the properties of the (acyl)-hydrazones further and results in strongly bathochromically shifted[311,312,314] switches, giving access to a broad variety of thermal lifetimes of the metastable isomer.[315]

Recently, compound **3.13** attracted attention, as it could be switched efficiently between both photoisomers with light, it showed strongly switchable fluorescence properties and could be excited both in 1- and 2-photon absorption processes.[305,316,317] The metastable *E* isomer was stable over many years in toluene ($t_{1/2}$ = 75 years). Importantly, the photochemical behaviour could be translated into the solid state and was also observed in different aqueous media.[305,317] As in toluene and the solid state, the compound showed negative photochromism in the aqueous environment (λ_{max} = 395 nm in the *Z* to 343 nm in the *E*) and good to excellent PSDs. The photoisomerization QYs were somewhat lower in serum than in toluene ($\Phi^{Z\rightarrow E}$ = 0.19 instead of 0.32, $\Phi^{E\rightarrow Z}$ = 0.07 instead of 0.15) while the fluorescence QY of the *Z* form slightly increased (Φ^{F} = 0.035 instead of 0.007). The metastable *E* isomer showed good thermal stability, however, the exact thermal lifetime could not be assigned accurately in serum. The authors pointed out that they observed hydrolysis of the ester functional group at elevated temperatures which were required to study the thermal isomerization kinetics.[305]

Also, arylhydrazones can be used in stimuli-responsive crystals,[318] are tuneable regarding their isomerization kinetics[319] and can be employed in functional supramolecular systems.[304,320,321] Similarly to phenylhydrazones, they could be successfully switched in water and buffer solutions, maintaining good photochemical properties.[295,304,321,322] Hence, both acyl and phenylhydrazone switches can be readily employed in aqueous environment.[305,322]

3.2.9 Azo-BF_2. Phenylhydrazones (*vide supra*) can be used to synthesize BF_2-coordinated azo compounds (Fig. 20).[299,323] They can be isomerized between a thermodynamically stable *E* and a metastable *Z* isomer, like in azobenzenes. However, binding of the azo function to the BF_2 group, which acts as Lewis acid, leads to a reconfiguration of the electronic structure. Hence, visible light can be used for both forward and back-isomerization *via* a $\pi_{n-b}\pi^*$ transition.[323,324] Azo-BF_2 switches show negative photochromism, like the hydrazone switches they are derived from, and have good to excellent PSDs and very high photoisomerization QYs ($PSD^{E\rightarrow Z}$ = 97%*Z*, $PSD^{Z\rightarrow E}$ = 80%*E*, $\Phi^{E\rightarrow Z}$ = 0.48, $\Phi^{Z\rightarrow E}$ = 0.67 in DCM). The half-life in the *Z* form was around 12.5 h in deoxygenated and 0.5 h in regular DCM, an observation that is still under investigation.[323] Extending the π-aromatic system leads to a bathochromic shift[325,326] and tuning with substituents[324] results in compounds that can be addressed with NIR light, while still maintaining their (photo)chemical properties to a large extent. Moreover, the *para*-amino substituted compounds can be photoisomerized in the presence of water (MeCN–PBS buffer 1 : 1 mixture) showing no fatigue after several switching cycles. However, the authors observed hydrolysis to the starting hydrazone when the compounds were kept in the solvent mixture for a few hours,[324] potentially limiting the range of applications in aqueous environment.

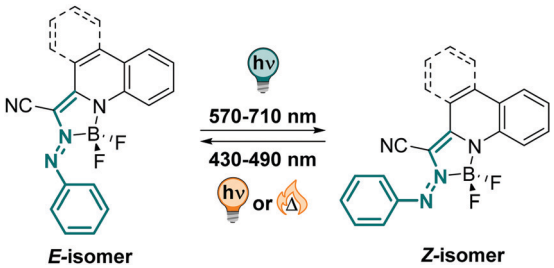

Fig. 20 Thermodynamically stable *E* and metastable *Z*-isomer of an azo-BF_2 switch.

3.3 Isomerization based on photochemical cyclization reactions

A large group of photoswitches is based on light-induced electrocyclizations, which are pericyclic reactions and involve the formation or cleavage for a chemical bond (Fig. 21).[3] They follow the Woodward–Hoffmann rules and can occur thermally, but usually require high temperatures (>100 °C), or proceed photochemically. Hence, the stereochemical outcome is determined by torquoselectivity, and the photochemically formed bond can typically only be opened by a light-stimulus and is thermally very stable. In the context of photoswitches, the 3,3′-electrocyclic ring-closure or opening reaction is the most frequently observed, and it constitutes the key process in

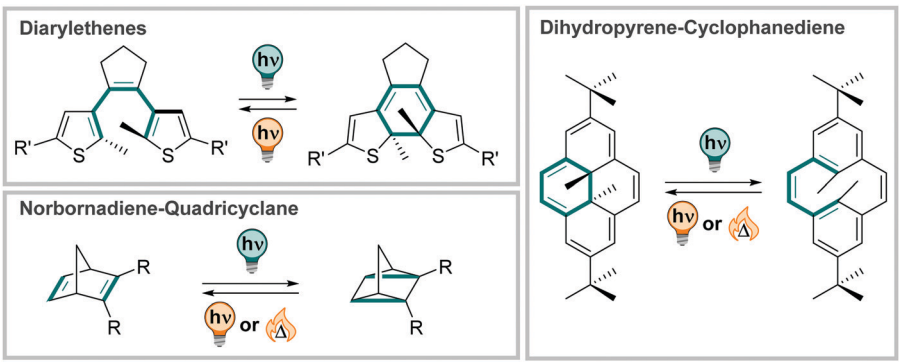

Fig. 21 Overview of molecules discussed in Section 3.3.

diarylethenes, fulgides, fulgimides, and spiropyrans, *etc.*[3,327–330] In this section, we only discuss molecules that relay purely on electrocyclization (see Fig. 21), while compounds isomerizing in mixed mechanisms are subject of the next section.

3.3.1 Diarylethenes. Diarylethenes (DAEs) are ethene groups substituted with two (hetero)aryl moieties to assemble a hexatriene system that can undergo a photochemical 6π-electrocyclisation reaction.[328,331] DAEs are a prevalent group of photoswitches, they exhibit a large structural diversity, and are widely used in numerous applications. The ethene moiety is usually bridged or substituted with sterically demanding substituents to avoid a competing *E–Z* isomerization around the double bond (as in stilbenes, *vide supra*), rendering DAEs purely operational through photochemical ring-closing/opening reactions (Fig. 22A).[328,331] This C=C bond is often part of a (perfluorinated) cyclopentadiene ring,[332] but can also be fused to more complex structures, like maleimide (*vide infra*),[333–335] imidazole,[336] thiazole,[332] phenanthroline,[337] benzoquinone (*vide infra*),[338,339] *etc.* to tune the properties of the switch or enable additional function.[333,340–342] The aryl rings are often (benzo)thiophenes, resulting in dithienylethenes (DTEs),[3,328,331] as switching between the open and the closed form gives the best compromise between the loss of aromaticity and the gain in stabilization upon cyclization to result in bi-stable photoswitches. Furthermore, also other (hetero)aromatic systems such as pyridine,[343,344] benzene,[328] naphthalene,[345] indole,[333] (benzo)furan,[328,331,344] pyrrole,[328] oxazole,[346] imidazole,[347] and thiazole,[340,348] *etc.*, have been employed.

Upon irradiation of DAEs with UV light, a ring-closure reaction takes place. The flexible, less coloured open isomer is converted into the more rigid closed (*C*) form (Fig. 22B). The *C* form is strongly coloured due to the extended π-system.[328,331] The absorption maximum in the visible range is between *ca.* 450 and 700 nm.[349] The reverse ring-opening reaction can be triggered with a suitable source of visible light and usually proceeds quantitatively, as the resulting open form is not absorbing in the visible-range.[328,331] The conrotatory ring-closure reaction makes a thermal ring-opening forbidden according to the Woodward–Hoffman rules, and results in thermally bi-stable photoswitches for many derivatives based on 5-membered heterocycles.[350] On the other hand, benzene[328] or pyridine-substituted[343,344] diarylethenes feature thermally labile closed forms, as the difference in aromaticity between the *O* and *C* form in the 6-membered ring-systems is too large.[328] This instability of the closed isomer overcomes the Woodward–Hoffmann rules and results in metastable *C* forms.[350] Similarly, DTEs with electron-donating substituents show thermally induced $C \rightarrow O$ interconversion at elevated temperatures (illustrative examples are displayed in Fig. 22B).[350]

The properties of DTEs, such as QYs,[351,353,354] PSDs,[353] and wavelength of irradiation for *O–C* photo-interconversion[355,356] were subject of extensive study and optimization. The characteristics and the efficiency of the *O–C* interconversion strongly depends on structural properties, such as the type of bridging moiety,[333,335,338,357] the nature of the (hetero)aromatic ring or the substituents of the aryl rings[358,359] or at the reactive carbon,[354,360] and the influence of the used solvent.[357] While the QY of the closing reaction $\Phi^{O\rightarrow C}$ is between 0.21 and 0.59 for differently substituted perfluoro cyclopentene bridged derivatives in *n*-hexane,[331] and QYs up to 1.0 were measured for

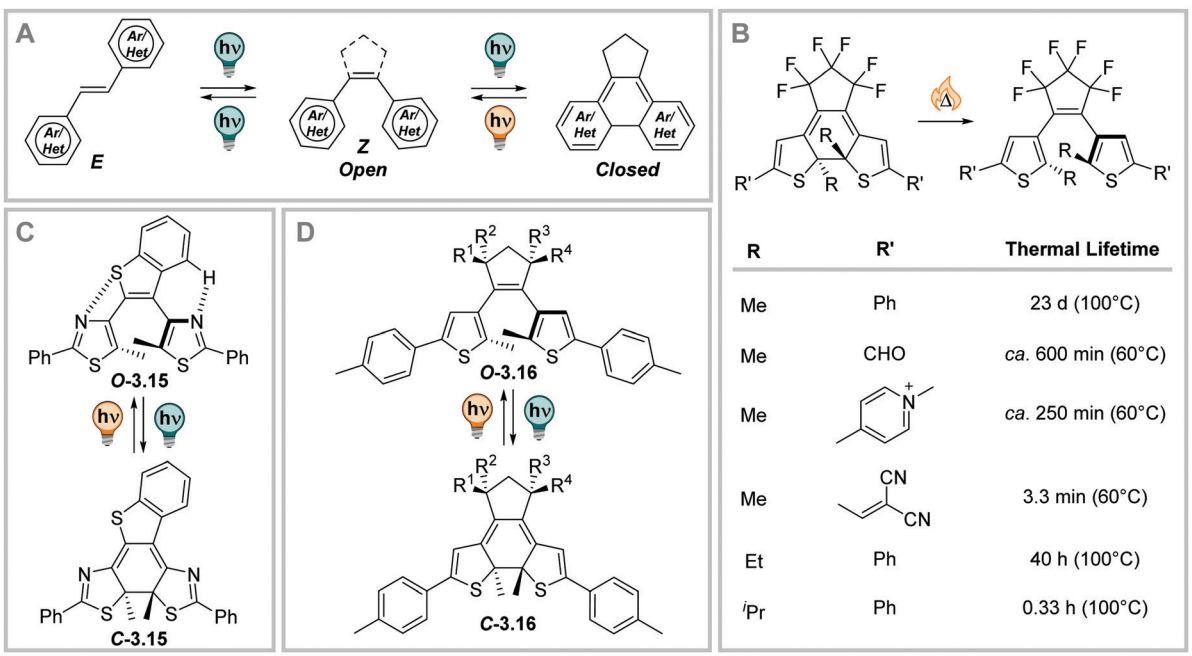

R	R'	Thermal Lifetime
Me	Ph	23 d (100°C)
Me	CHO	*ca.* 600 min (60°C)
Me		*ca.* 250 min (60°C)
Me		3.3 min (60°C)
Et	Ph	40 h (100°C)
^{i}Pr	Ph	0.33 h (100°C)

Fig. 22 (Photo)switching in diarylethenes (DAEs). (A) Schematic representation of different photochemical mechanisms accessible to DAEs.[328,331] (B) The influence of different substituents R on the thermal lifetime of the closed isomer.[331,350] (C) DAE **3.15** shows close to quantitative photoisomerization quantum yields.[351,352] (D) DTE **3.16** show close to quantitative PSDs in both directions and high, solvent independent ring-closure quantum yields.[353]

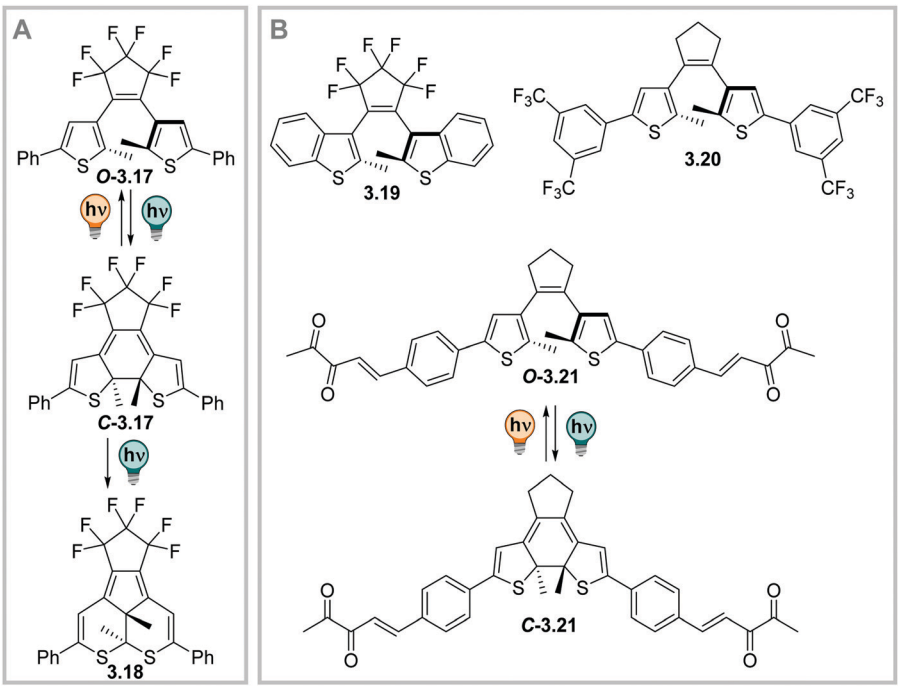

Fig. 23 Tuning the photochemical stability of DAEs. (A) Photochemical side-product formation upon prolonged irradiation times with UV-light.[331] (B) Scaffolds that prevent side-product formation: benzothiophene-based DAEs, *e.g.* **3.19**,[331] DTEs with electron-poor substituents such as **3.20**,[367] and DTEs isomerizing upon excitation of an intramolecular triplet sensitizer like **3.21**.[356]

more optimized derivatives (Fig. 22C) in *n*-hexane[351,352] and in the solid state,[361] the QY for this reaction is generally lower in polar solvents (*vide infra*).[351,357] QYs of the inverse reaction are, by trend, lower than the ones of the closing reaction of the same molecules, namely 0.03–0.47 in *n*-hexane,[331,351] however, they can be tuned through introduction of substituents other than methyl in the 2-position of the heteroaryl ring, resulting in the $C \rightarrow O$ process becoming the more efficient one.[354] On the other hand, sterically demanding substituent at this position influences the thermal lifetime of the closed form. The sterical strain makes it less stable and leads to thermal instability of the *C*-isomer (*vide supra*, Fig. 22B).[362] Also, the $PSD^{O \rightarrow C}$ strongly varies with different structural properties ranging between low[344] to almost quantitative.[353]

Moreover, many derivatives of DAEs generally show a very high fatigue resistance over many switching cycles, *i.e.* large Z_{50} values.[328,331,363] However, in thiophene-based diarylethenes, a photochemical by-product formation from the singlet excited state, which is competing with the $O \rightarrow C$ reaction, can take place, limiting its performance (Fig. 23A). This reaction is irreversible and hence, build-up of this component featuring a five-membered central ring can be observed after prolonged irradiation times with UV-light or repeated switching cycles (Fig. 23A).[331,363] The fatigue resistance can be improved, for instance, by introducing steric hindrance (Fig. 23B),[363–366] by attaching electron withdrawing substituents to the aryl-moieties (Fig. 23B),[367–369] or by (intra- or inter-) molecular triplet sensitization (Fig. 23B).[356,360]

DAEs with (perfluorinated) cyclopentadiene bridges can be switched reversibly over several cycles in the solid state[331,361] and in a wide range of solvents, including water,[358] aqueous buffer, and[349,370] in living cells.[371] However, by changing the bridging moiety to electron-acceptor moieties such as maleimide,[333] maleic anhydride,[357] or benzoquinone,[338] the $O \rightarrow C$ reaction is suppressed in polar solvents and hence, cannot proceed in water and water/co-solvent mixtures (Fig. 24)[333] Here, the predominantly occurring photochemical process is the population of a twisted intramolecular charge transfer (TICT) state.[357,372] Thereby, the heteroaryl rings, such as (benzo)thiophene[335,338,357,372] and indole,[333] serve as donor and the bridging group functions as acceptor.

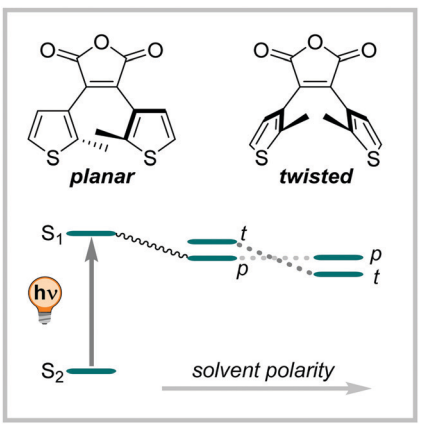

Fig. 24 Schematic representation of the population of a twisted intramolecular charge transfer (TICT) state depending on the solvent polarity. After excitation to the S_1 the compound relaxes preferably into a state where the thiophene rings have a planar (p) or twisted (t) conformation, depending on the solvent polarity.[357]

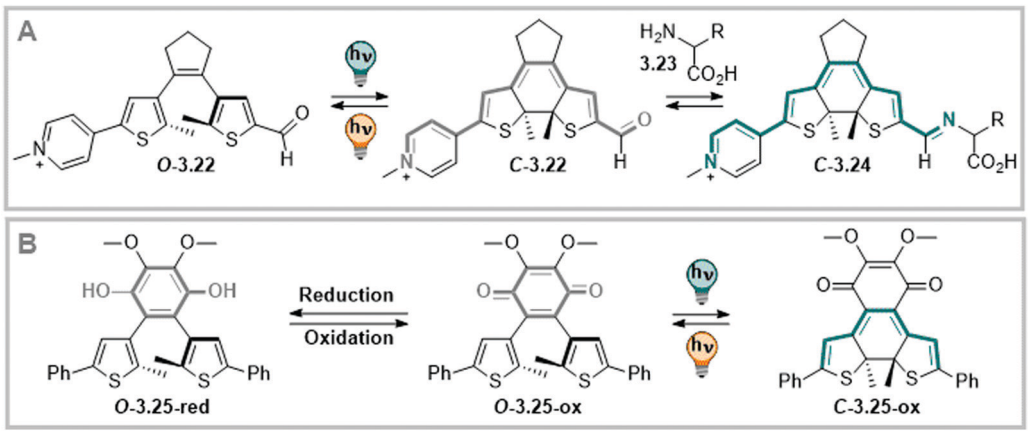

Fig. 25 Photoswitching electronic properties in DTEs. (A) Switching between electronically insulated and connected isomers, where the closed form is able to serve as catalyst after imine formation.[375] (B) A photoswitchable redox cofactor bearing a benzoquinone bridging unit that can be toggled between an oxidative (open) and non-oxidative form (closed).[338]

This state is increasingly favoured with increasing polarity of the solvent and is mirrored by a decrease of $\Phi^{O\rightarrow C}$ in the same compound (0.13 in hexane and 0.003 in MeCN, respectively).[357] On the other hand, the inverse $C \rightarrow O$ reaction can proceed in polar solvents quantitatively[333,335,338,357] resulting in a visible-light responsive one-way switchable system with negative photochromism.[333,335,338]

While photoswitches based on double-bond isomerization are often used by taking advantage of the geometrical changes between the photoisomers, switches isomerizing *via* an electrocyclic reaction can be used to construct systems providing both steric and electronic modulation. In the more flexible open form, the two aryl groups are orientated perpendicular to the ethene bridge. However, in the closed form, the conjugation in the π-system extends throughout the whole backbone of the switch (Fig. 25A). This altered π-conjugation is, on the one hand, responsible for the colour of the *C* isomer, and on the other hand allows for electronic communication between the two sides of the molecule.[373,374] In this way, a photoswitchable pyridoxal 5′-phosphate mimic was constructed (Fig. 25A).[375] Only in the closed form, the aldehyde function is conjugated to the pyridinium ring and hence becomes electrophilic enough for imine formation and catalysis. Both photoisomerization and catalysis were fully compatible with aqueous media (water : EtOH, 1 : 1). Alternatively, the DAE scaffold can be merged with an electronically active molecule, such as benzoquinone, and used as a multi-stimuli responsive switch or as photoswitchable oxidant (Fig. 25B).[338,339] Here, the *C* isomer incorporates a part of the benzoquinone electrons in the conjugated backbone and hence, shifts its redox potential in a photo-dependent manner. The closed form is not available in redox reactions but can be activated by light and serve as oxidant with, for instance, Hantzsch ester or in isolated mitochondria demonstrating the compatibility of the concept with an aqueous environment. While the difference redox properties of the two isomers stayed intact, the *O* form could not be ring-closed in the same solvent due to the presence of a TICT (*vide supra*) and somewhat limits this system.[338]

Another interesting feature in DAEs is that some derivatives exhibit switchable fluorescence, rendering them interesting candidates for molecular logic and smart materials.[365,376] Moreover, switchable fluorescence can be employed for super-resolution *in vivo* imaging (see Section 4.3.3).[358,371] Alternatively, DAEs can be used to construct systems for (internal) fluorescence quenching *via* FRET in one but not the other photoisomer when covalently linked to a suitable fluorophore.[377]

3.3.2 Dimethyldihydropyrene. The dimethyldihydropyrene–cyclophanediene (DHP–CPD, Fig. 26) photochromic couple is a family member of the aforementioned DAEs (Section 3.2.1).

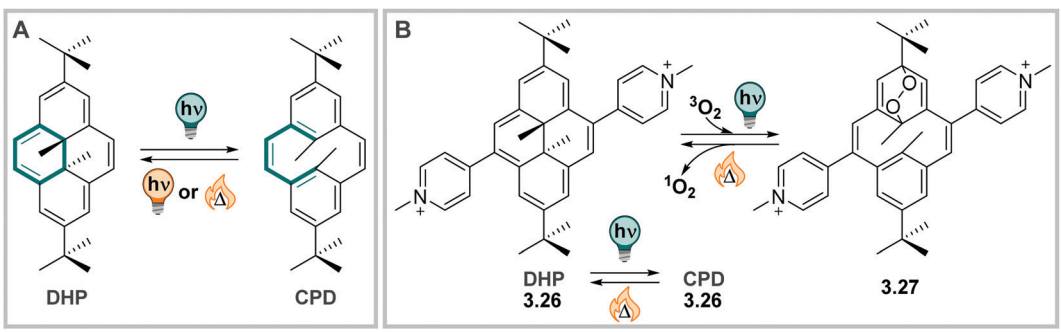

Fig. 26 The dihydropyrene/cyclophanediene photochromic couple. (A) (Photo)switching between the two isomers. (B) Photoswitching in the presence of oxygen can lead to endoperoxide derivative **3.27**, which then thermally releases $^1O_2$.

However, their photochemical behavior strongly deviates from typical DAEs and hence, these switches are discussed here separately. The planar, highly conjugated DHP form features 14 delocalized π-electrons that give the molecule an absorption profile in the visible-NIR range of the electromagnetic spectrum.[378] The two central methyl groups prevent irreversible oxidation of the core, analogous to the ones in DAEs. Upon irradiation with visible light, the meta-stable ring-open isomer CPD is formed, which is accompanied by a decolorization, rending DHP a T-type photoswitch with negative photochromism. The properties of the system are strongly solvent-dependent. Both the QY $\Phi^{C\rightarrow O}$ (from 0.28 in *n*-heptane to 0.07 in DMSO) and the thermal stability of the metastable CPD decrease with increasing polarity of the solvent. The thermal $t_{1/2}$ of DHP is up to one day in apolar solvents and decreases significantly to *ca.* 30 min in DMSO. On the other hand, λ_{max} is bathochromically shifted in more polar solvents and tails up to 835 nm in DMSO/water (8 : 2).[379] The absorption spectrum of the DHP–CPD system can be further tuned by attaching substituents to the ethene bridge,[380,381] the aryl moieties,[381] by replacing the methyl groups by other functional groups,[382] or by extending the conjugated π-system of the backbone.[383] Specifically, attaching donor–acceptor substituents in conjugation over the whole switch structure leads to absorption bands tailing to 900 nm.[381]

Moreover, irradiation under air generates an endoperoxide derivative, that thermally releases $^1O_2$ while simultaneously forming the starting material without any degradation. This opens possibilities for the construction of multi-functional photoactuators and photodynamic therapy (PDT) agents.[378] The switch has also been reported in the context of switchable redox properties,[383] cooperative switching events in a homodimer,[384] as light-responsive ligand in metalorganic complexes,[385] and as ligand in biological systems (see Section 4.1).[386] The last of these examples demonstrates the possibility to reversible switch between DHP and CPD under assay conditions, indicating the compatibility of the photoswitch with aqueous media. However, a study on a more diverse set of structural derivatives is required to correlate its properties with, for instance, the related DAEs and to understand the full potential and limitations of the DHP–CPD couple in various solvents.

3.3.3 Miscellaneous: norbornadiene. There are several additional photoswitches that employ electrocyclic reactions for their light-induced isomerization.[3,108] However, many of them were not yet, or hardly, considered for studies in aqueous environments, as the previously discussed CHP-CPD couple (Section 3.3.2.). This could be because they are intrinsically insoluble in water and would require elaborate substituent design to become hydrophilic. However, photoswitches isomerizing *via* similar mechanisms can be readily switched in aqueous media. Here, we use norbornadiene as an example to discuss these aspects.

The thermally stable norbornadiene is a T-type photoswitch that undergoes a photochemical [2+2] cyclization reaction upon irradiation with light, showing negative photochromism (Fig. 27).[108] The formed quadricyclane absorption is strongly hypsochromically shifted compared to the starting material.[387–389] The isomerization can be reverted photochemically,[390] thermally, or (electro)-chemically,[391–393] for instance by adding a metal catalyst[394,395]

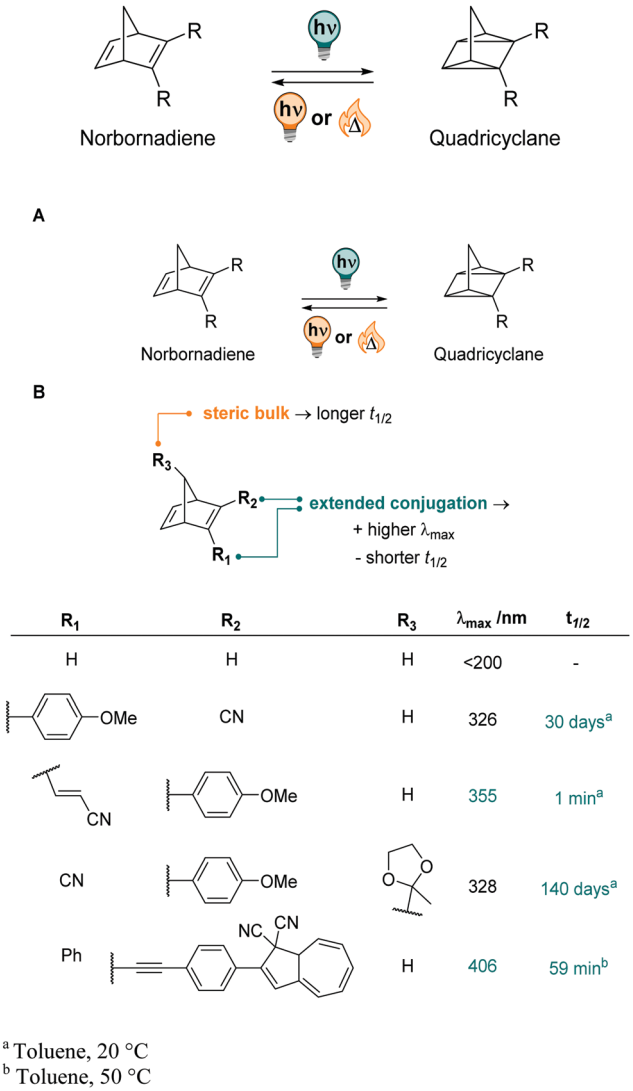

R_1	R_2	R_3	λ_{max} /nm	$t_{1/2}$
H	H	H	<200	-
	CN	H	326	30 days[a]
		H	355	1 min[a]
CN			328	140 days[a]
Ph		H	406	59 min[b]

[a] Toluene, 20 °C
[b] Toluene, 50 °C

Fig. 27 (A) The norbornadiene/quadricyclane photochromic couple, (B) the effect of substituents on the photochemical properties, including the position of the absorption band and the half-life of the metastable quadricyclane.

or acid,[396] and (photo)switching is very robust over many cycles.[388,397,398] Norbornadiene and quadricyclane are similar in size and volume and therefore do not offer many possibilities for applications where the photoswitch should induce large geometrical changes in a system.[387] However, the photochemically generated quadricyclane is a small, light molecule and consists out of five highly strained rings, making the metastable isomer highly energetic and thus an excellent candidate for (solar) thermal energy storage that can be used in films or on surfaces.[388,397,399–403] By attaching different substituents R (Fig. 27B), the absorption profile of norbornadiene can be tuned up to the green region of the visible spectrum.[389,404–406] The thermal lifetime of quadricyclane strongly depends on the substituents and the solvent or matrix.[398,402,405,406] Most studies naturally focus on characterizing the compounds' properties in film or toluene, however, photoisomerization was also reported

in MeCN, revealing lower QYs $\Phi^{NB\rightarrow QC}$ (0.03 instead of 0.28) than in toluene, but longer thermal lifetimes ($t_{1/2}$ = 29 h instead of 18 h) for the same compound.[407] To the best of our knowledge, the compound's photochromism was never studied in aqueous environment and the acid-sensitivity[396] of the quadricyclane as well as small geometrical changes upon isomerization[387] limit its potential applications.

3.4 Mixed mechanisms

In this section, we highlight photoswitches based on electrocyclic ring-closing and opening reactions, which undergo additional (photo)chemical isomerization processes. This typically results in a more complex isomerization mechanisms, involving multiple steps and several intermediates that often cannot be studied independently. An overview of the photoactuators discussed is displayed in Fig. 28.

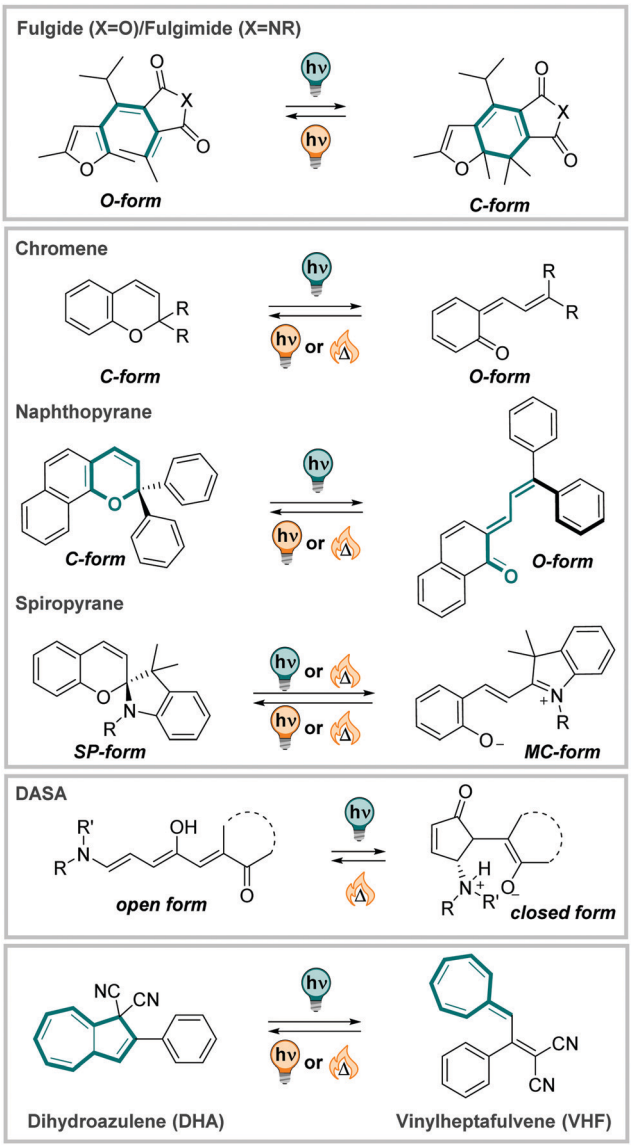

Fig. 28 Overview of the molecules discussed in Section 3.4: fulgides, fulgimides, chromenes, naphthopyrans, spiropyrans, DASAs, and dihydroazolenes.

3.4.1 Fulgides and fulgimides. Similarly to DAEs, fulgides and fulgimides have a central 6π-electron system as the photochromic motif. Their electronic structure renders their UV-Vis absorption bands bathochromically shifted compared to the structurally comparable diarylmaleimides (DAMs).[408] Irradiation with light of a suitable wavelength facilitates a conrotatory electrocyclization reaction, resulting in the corresponding closed isomer (Fig. 29). In contrast to DAEs, fulgides and fulgimides contain only one (hetero)aromatic moiety, such as benzene,[409] (benzo)furan,[410–412] thiophene,[410,413,414] thiazole,[410] oxazole,[413] pyrazole,[410] pyrrole[413] and indole.[408,415,416] The second ring-structure is either a succinic anhydride (when Y═O, Fig. 29) to build a fulgide, or a succinimide (when Y═NR, Fig. 29) and is then called fulgimide.[410]

Two exocyclic double-bonds assemble the full molecule, condensing it to the heteroaromatic substructure.[410] Thereby, the R-substituent in the bridging part has a crucial role. Both, fulgides and fulgimides were synthesized with a large variety of R-groups in the bridge. For instance, R═Me,[408,412] ^{i}Pr,[408,412] CF_3,[412,417] ^{t}Bu,[412] COOH,[416,417] have been employed. While smaller substituents allow for reversible *E*–*Z* isomerization of the ring-open isomers, the larger substituents, like ^{i}Pr, or cyclic variations, do not.[408,418] Consequently, the ring-open isomers can be separated and the isometrically pure *E* can be used to photoswitch exclusively *via* an electrocyclic mechanism.[418] Fulgides with smaller substituents, such as R═Me, undergo reversible *E*–*Z* isomerization under irradiation with the same wavelength of light (Fig. 29) as the one used for the ring-closure reaction, because the UV-Vis spectra of both *E* and *Z* form are significantly overlapping.[412] However, the electrocyclic reaction still performs well, as it is irreversible under the same conditions and hence, functions as a photochemical sink.[370] The ring-closing reaction in fulgides proceeds with varying quantum yields, determined to be $\Phi^{E\rightarrow C}$ = 0.12–0.54 for different (benzo)-furans in apolar solvents, and significantly lower for indolyl fulgides ($\Phi^{E\rightarrow C}$ = 0.04–0.07).[412,414] Moreover, QY and PSD values are strongly dependent on different substituents and sensitive to both steric and electronic aspects and hence, various structural

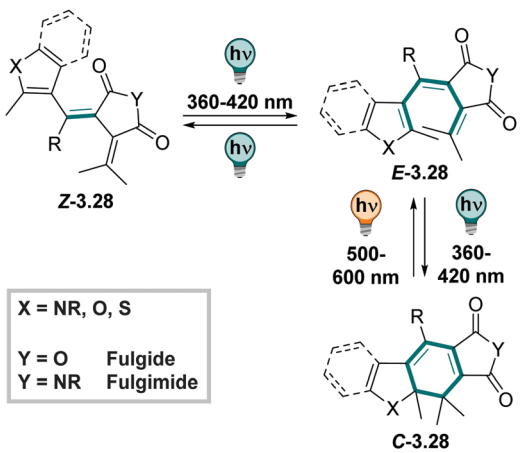

Fig. 29 General switching of fulgides and fulgimides and the various isomers involved.

modifications were explored.[412,418] In contrast, moving from a fulgide to the corresponding fulgimide leaves the photochemical properties mainly unaltered.[412] However, the spectra are bathochromically shifted compared to the corresponding fulgides.[412,419] The closed isomer is strongly coloured due to its large π-system, conjugated throughout several ring-structures and hence, it absorbs in the visible range around 450 nm to 550 nm in fulgides and up to around 600 nm in fulgimides.[408,410,412,413] Both switches are thermally very stable and show no significant decolouration reaction after several days at 50 °C in solution.[410] However, the *C* form benzene-based fulgides is thermally labile due to the higher degree of aromaticity of the benzene scaffold.[409]

Irradiation of the *C* isomer with visible light leads to quantitative bleaching and electrocyclic ring-opening, and results in complete conversion to the *E* isomer.[412] The reaction in general proceeds in (benzo)furan-based fulgides less efficiently than in indolyl fulgides.[412] As for the closure reaction, the efficiency of the $C \rightarrow E$ interconversion is strongly substituent-dependent with quantum yields $\Phi^{C\rightarrow E}$ = 0.05–0.42 for isomerization under irradiation with visible light.[412,414] Photoisomerization can be repeated several times in various solvents, in polymer films and the solid state in both directions without formation of side-products, and is very robust.[409–411,414] Moreover, many fulgides and fulgimides show fluorescence,[408,420] which can vary between the two photoisomers.[416,421,422] Fulgides and fulgimides are used in a wide range of applications, for instance, as switchable polymer films,[413,420] on surfaces,[423] and in biological applications.[370,411]

Fulgides and fulgimides are less lipophilic than the structurally related DAEs and exhibit the rather polar succinyl moiety. Hence, they are generally better soluble in polar organic media and water than many DAE representatives, without the need for any further functionalization. To spontaneously dissolve in pure water, though, further solubilizing groups need to be attached.[408,410,416,417] While in DAMs the closing reaction is suppressed by a TICT in polar (protic) media, such as water (*vide supra*), fulgides and fulgimides can be reversibly photoisomerized in solvent–water mixtures (aqueous ethanol (1 : 1))[410] and aqueous buffer.[370,408,411,416] Both the thermal stability remains unaltered[408,410] and the photochemical properties stay intact and were subject of detailed mechanistic studies.[416] Quantum yields ($\Phi^{O\rightarrow C}$ = 0.16 or 0.17 and $\Phi^{C\rightarrow E}$ = 0.10 or 0.15 in DMSO and HEPES buffer, respectively, for the same benzofuranyl fulgimide)[370] as well as the $PSD^{O\rightarrow C}$ are similar in buffer compared to polar organic solvents like DMSO (36%*C* in DMSO *vs.* 35%*C* in HEPES buffer, 31%*C* in DMSO *vs.* 32%*C* in phosphate buffer, and 66%*C vs.* 73%*C* in 30% DMSO in phosphate buffer of the respectively same fulgimide).[370,408] On the other hand, the photochemical ring-opening reaction proceeds quantitatively, independent from the used solvent, as only the closed isomer is absorbing in the visible region and can hence be addressed selectively.[370,408,410,411] However, fulgides undergo hydrolysis in alkaline solutions, while fulgimides are stable under the same conditions over days.[410] Also, in fulgimides having a CF_3 attached to the bridging moiety, it was demonstrated that this functional group can hydrolyse to the corresponding COOH under slightly basic conditions (phosphate buffer, pH 7.4, Fig. 30A).[417] On the other hand, fulgimides bearing a carboxylic acid group at the same position can be switched reversibly in the same buffer (**3.30** in Fig. 30B)[416,417] but showed some sensitivity to acidic conditions. There, the molecules lose the COOH function to result in the non-photochromic H-bridged derivative ***C*-3.31** (Fig. 30A).[417]

3.4.2 Chromene, naphthopyrane, spiropyrane and spiroxacine. Chromenes have a central hexatriene moiety with oxygen as one heteroatom and can consequently undergo a 6π-electrocyclic reaction, (Fig. 31) similarly to DAEs (*vide supra*), fulgi(mi)des (*vide supra*), DHPs (*vide supra*), and dihydroazulenes (*vide infra*).[108,424] The energetically lowest transition is around 320 nm for the parent closed compound and can be tuned by attaching different substitutions[108,424,425] or introduction of other heteroatoms to the scaffold.[108] Irradiation with UV light leads to C–O bond cleavage and rapid formation of the strongly coloured open (O) form, which interconverts between different isomers (cisoid-trans (TC) and transoid-trans (TT), Fig. 31).[108,426–428] The open form is thermally metastable and quickly converts back to the closed isomer. This property makes the chromene scaffold attractive for the development of photochromic ophthalmic lenses.[108] Chromenes themselves were not

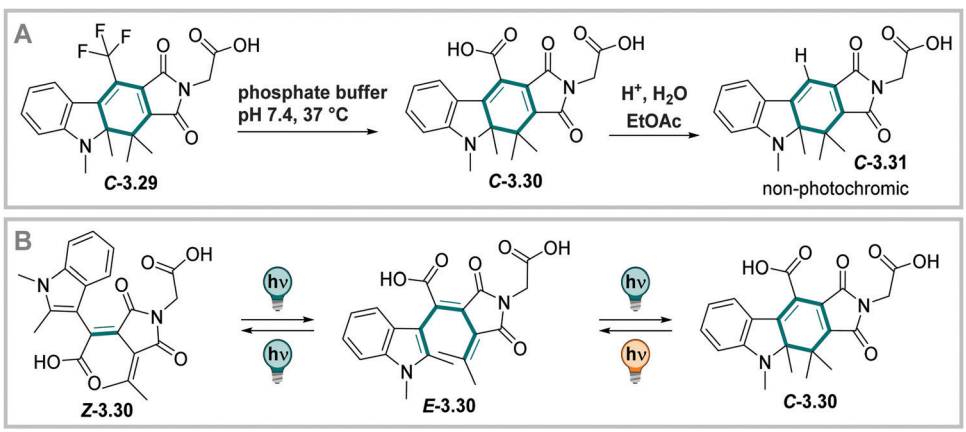

Fig. 30 Stability of differently functionalized fulgimides. (A) Hydrolysis of a CF_3-substitutent in the bridging unit under slightly basic conditions and subsequent loss of CO_2H upon acid conditions. (B) Photoswitching of fulgimide **3.30** with CO_2H group in the bridge.

extensively investigated in aqueous environment, however, they are the photochromic core structure in naphthopyrane, spiropyrane, and spiroxacine (*vide infra*), which are well-studied in various solvents.

Naphthopyrans are benzo-extended chromenes showing similar photochromic properties as the parent compound (Fig. 31).[108,426,427] The larger π-system induces a bathochromic shift of the absorption spectrum and makes the compound responsive to visible light.[429] Additional substituents or scaffold hopping to heteroarenes allows further tuning of the UV-Vis absorption properties.[430–433] Similarly to chromene, the open form of naphthopyran exists as several isomers, which can be converted into each another photochemically and thermally. Attachment of substituents or bridging between the pyran ring and the naphthalenic core by a fused alkyl chain can assist to direct the equilibrium between the isomers towards one species. However, this is usually synthetically laborious and compromises other properties, such as the lifetime of the open forms.[430] Depending on the substituents, the decolorization reaction occurs in microseconds to a few hours.[430,431,433,434] Attachment of suitable functional groups, like the positively charged *N*-alkylated picolinium, makes naphthopyrans soluble in buffer in the presence of small amounts of organic co-solvent (*e.g.* 5% DMSO).[427] It was shown that photoisomerization can be triggered in the aqueous media[427,429] and shows very good fatigue resistance over several cycles.[429]

Spiropyrans (Fig. 32), *i.e.*, pyrans exhibiting a spiro-junction in α-position next to the oxygen, were originally reported as thermochromic compounds.[329] However, only after their photochromism was reported in a derivative consisting of an indoline and a chromene moiety, which are condensed *via* a spiro-bond and oriented perpendicular to each other, the class of molecules attracted more attention. Since then, this structure is associated with the term spiropyran in the context of (photo)-responsive molecules, a terminology which we will follow in the subsequent discussion. Spiropyran can be reversibly interconverted into its merocyanine form in a ground state or excited state process.[329,435] Their isomerization can be triggered with a whole range of stimuli, including heat, pH, electrons, and light, and hence, makes them prominent candidates for a large variety of applications.[329] Upon irradiation with UV-light, the chromene moiety of the ring-closed spiropyran (SP) opens in a 6π electrocyclic ring-opening reaction (*vide supra*) to give the[436–441] ring-open merocyanine (MC) form.[329,442] The central double-bond of the system undergoes further *E–Z* isomerization upon irradiation with the same light source, and its configuration can be separately controlled only if the phenolic oxygen is protonated or alkylated (*vide infra*).[439,443] In this isomer, the indoline nitrogen is in conjugation to the pyran oxygen. Hence, the ring-open merocyanine form can exists in a neutral and a zwitterionic form (*cf.* Fig. 32). For thermochromic spiropyrans, it was reported that the electron-withdrawing (EWG, often $-NO_2$) substituents in *para*-position to the pyran oxygen stabilize the zwitterionic form (*cf.* Fig. 32), while an electron-donating substituent (EDG) promotes the neutral merocyanine form.[329] This electronic property is the key to the multi-responsive nature of the switch, making it the subject of many studies as was reviewed in detail elsewhere.[329,442] The MC form is strongly coloured and has an absorption maximum in the visible range around 500–600 nm,[439,440,444,445] shows solvatochromism,[329] and was extensively studied also from a theoretical point of view.[446,447] Heating or irradiation with a suitable light source result in the isomerization back the SP form, which is the thermally more stable one in most organic solvents (in contrast to aqueous media, *vide infra*).[448,449] The QYs of both photochemical reactions are highly solvent- and substituent-dependent.[329] For instance, QYs for the ring-opening range from 0.11 in MeCN up to 0.83 in methylcyclohexane for *para*-NO_2 SP. The reversible (photo)isomerization can be repeated over several cycles without showing significant fatigue in a wide range of solvents.[329,450]

An interesting aspect in the SP-MC photochromic couple is its sensitivity towards acids: the charged MC can not only serve as complexation site (Lewis base) for metal ions,[451] but also as

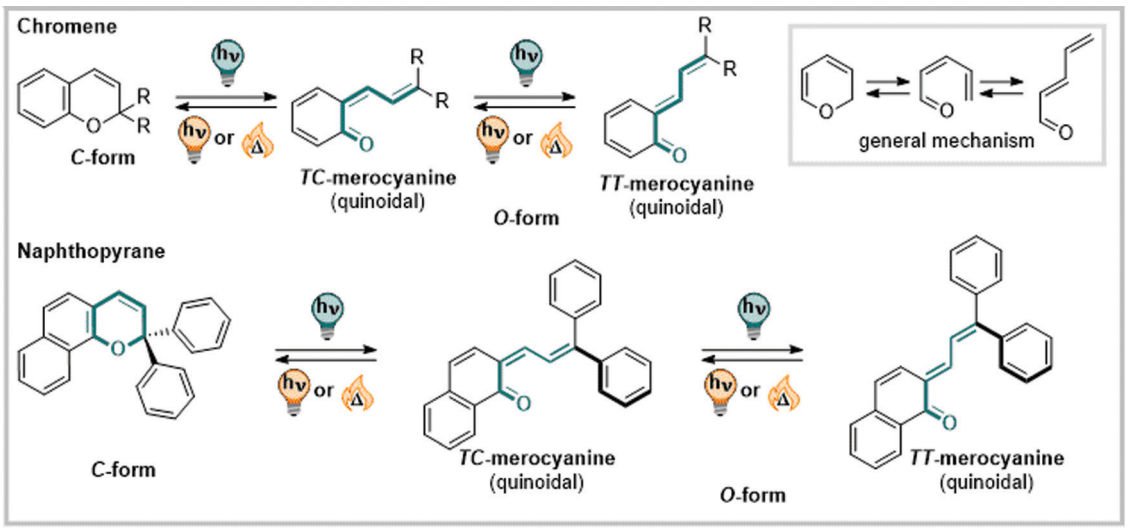

Fig. 31 General photoswitching mechanism in chromene and naphthopyran.

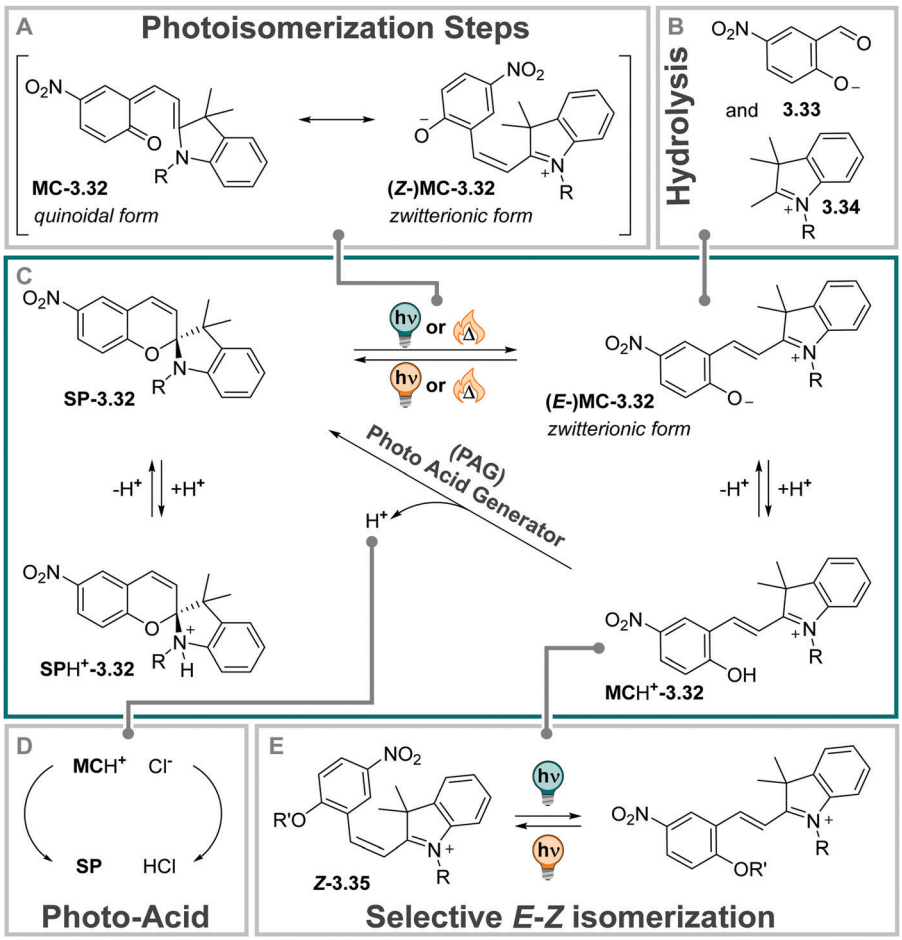

Fig. 32 Overview of various characteristics in the spiropyran/merocyanine photochromic couple, using a representative structure (**3.32** and **3.35**) bearing an NO_2 substituents in *para*-position to the pyran oxygen. Central box (C): **SP-3.32** can be photoisomerized *via* the *Z*-MC intermediate displayed its two resonance structures in (A) into the corresponding MC-**3.32**, which is sensitive to hydrolysis (B). Both the SP and the MC form can be protonated, with the open isomer being the weaker acid making the system a photo acid generator (PAG) upon ring-closure (D). The MC-form can undergo selective *E*–*Z* photoisomerization when the phenolic oxygen is protonated or alkylated (E).

Brønsted base.[448,452,453] The phenolic oxygen can be protonated at lower pH to result in $\mathbf{MCH^+}$, exhibiting pK_a-values between 3.7 and 4.4 depending on the substituent in the *para* position on the corresponding indoline moiety. Specifically, EWGs in *para*-position to the phenolic oxygen lower the pK_a by stabilization of the zwitterionic structure (for instance, $-NO_2$ in Fig. 32).[448] Protonation leads to a significant energetic stabilization of the open form, to such an extent that the spiropyran can be interconverted quantitatively to the MC form by protonation, resulting in acidochromism.[440] The characteristics depend, for instance, on substituents, solvents properties and interaction with other (macro)molecules.[440,454] Protonated $\mathbf{MCH^+}$ shows negative photochromism upon irradiation with visible light.[455] The corresponding closed form $\mathbf{SPH^+}$ has pK_a-values between 0.4 and 1.6,[448] *i.e.* it is more acidic than the merocyanine form and hence, the SP-MC pair can serve as a photo-acid-generator (PAG) in the right environment.[303,456] The anionic pyran oxygen does not only play an important role in metal complexation and as a base, but is also crucially involved in the hydrolytic stability of the photoswitch. The attack of water as a nucleophile on the ene-iminium cation has been shown to promote hydrolysis into the corresponding Fischer base and aldehyde, and is mediated by the negatively charged oxygen (Fig. 32).[445,448,457] Hence, the kinetics of merocyanine hydrolysis is substituent (=stabilization of neutral and zwitterionic form) and pH dependent: at neutral pH, water can hydrolyse the MC, while in basic pH the OH^- serves as nucleophile. At the same time, MCH^+ is relatively stable towards hydrolysis.[448] Another interesting feature of the protonated MC is that it can undergo selective, reversible *E*–*Z* isomerization upon irradiation with different light-sources, a process that can classically not be studied isolated from the SP-MC interconversion (Fig. 32).[439] Similarly, the *E*–*Z* isomerization can be accessed when ring-closure is blocked by a photo-labile protecting group on the phenolic oxygen (Fig. 32).[443]

SP is frequently used in aqueous environment, like buffer,[437,445,450,458–461] or in cells[462] as a photo-acid generator (PAG) or classical photoswitch. Irradiation with UV-light results in photochemical formation of the MC form ($PSD^{C\rightarrow O}$ = 38–85%*MC* and $\Phi^{C\rightarrow O}$ = 0.01–0.08 in aqueous solution or buffer).[437,445,459,461]

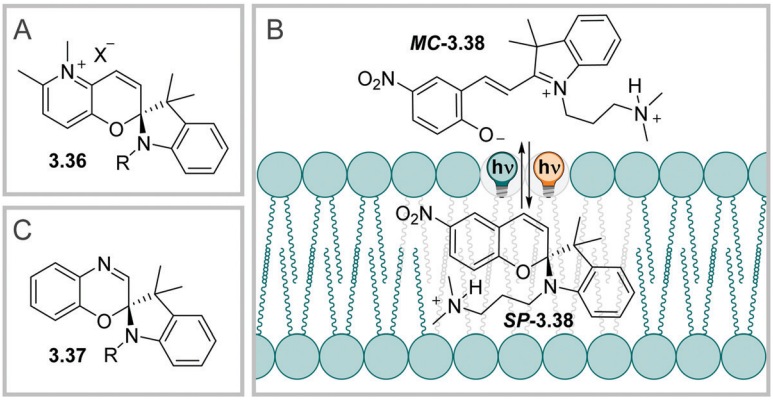

Fig. 33 Chemical structure of a Py-SP (A) and spirooxacine (C). (B) Photoisomerization of **3.38**, with **SP-3.38** being more hydrophobic than **MC-3.38**, allowing it to diffuse through lipid bilayers.

In contrast to organic solvents, where the thermal equilibrium is completely on the side of the SP form, the rates for the thermal equilibration in both directions are very similar in water due to the highly polar nature the solvent that stabilizes the zwitterionic MC form.[448,449,459,463] Thermal equilibration ($t_{1/2}$ = 1–6 h) results in the formation of 33–80% MC.[445,459,461,462] In many examples, the rate of the competing hydrolysis reaction of the MC form is usually 2–10 times lower.[445,459] The isomerization kinetics can be modulated, for instance, by introduction of suitable substituents. In this manner, an *ortho*-COOH derivative showed thermal SP-MC equilibration in one minute while the corresponding *para*-NO_2 compound required *ca.* two hours. The hydrolysis rates stayed the same for both compounds in the applied buffer ($t_{1/2}$ = 4 h).[445] Irradiation with visible light allows to quantitatively access the closed isomer with $\Phi^{O\rightarrow C}$ 0.005–0.1, comparable to that in organic solvents.[459,462]

Spiropyrans can be functionalized at positions other than the indoline nitrogen to enhance solubility or introduce further functional groups. For instance, introduction of a pyridine, or pyridinium scaffold (Py-SP-Me, see **3.36** in Fig. 33) leads to highly polar compounds and enhances the water-solubility of both isomers.[437,458,460] The scaffold can be robustly reversibly photoisomerizated (PSD$^{C\rightarrow O}$ 26%*MC*, PSD$^{O\rightarrow C}$ 100%*SP*, $\Phi^{C\rightarrow O}$ 0.033, $\Phi^{O\rightarrow C}$ *ca.* 0.2 in PBS buffer).[437,458] Moreover, Py-SPs are relatively stable towards hydrolysis and can be stored in aqueous solution for several weeks and for a few days in cell extract, which can be of advantage for biological studies involving spiropyrans for longer periods of time.[458,460] Moreover, they have been used as PAGs, analogous to SP.[464]

Spiropyrans found many applications, *e.g.*, as photocontrolled binders to biomolecules, often DNA,[435,459,461] in high-resolution imaging,[465] and in fluorescence[466,467] or conductance switching.[468–470] A key feature is the interconversion between a charged and a neutral species, which has great impact on the solubility of the compound in different media. For instance, it was shown that the neutral spiropyran **3.38** is better soluble in uncharged liposomes than its zwitterionic merocyanine form (Fig. 33).[444] Moreover, the neutral spiropyran can enter living cells passing the membrane and can be switched inside.[462,471]

While many studies focus on substituent effect on the core, also the central C=C bond of the hexatriene systems can be modified. In spirooxazine **3.37**, the C=C is replaced by a C=N bond (Fig. 33)[3] which results in a molecule exhibiting an absorption profile that is bathochromically shifted with respect to parents SP.[472,473] Upon irradiation with UVA-light, up to *ca.* 50% MC can be accumulated in DMF.[472] The isomerization process is more efficient than in SP as no triplet states are involved.[472] The quantum yields associated with this process are highly solvent dependent and reach from $\Phi^{C\rightarrow O}$ = 0.25 (MeOH) to 0.71 (toluene) for the same molecule. Also, the rates of the thermal back-reaction strongly depend on the solvent and are faster in polar (protic) than apolar media, spanning from a few hundred milliseconds to tens of seconds.[473,474] The thermal rates are significantly slower in polymer films[475] or gels.[476] Alternatively, the open form can be stabilized by metal complexation.[477] Most derivatives can be reversibly isomerized over several cycles without showing fatigue.[473,476]

3.4.3 Donor–acceptor Stenhouse adducts. The photochromism of donor–acceptor Stenhouse adducts (DASAs) was first described in 2014 and thus, DASAs a rather young class of photoswitches.[478] Nevertheless, they were studied extensively over the past years in theory[479–484] and experiment,[483–491] and first applications show tremendous opportunities for future developments.[490,491] The molecules belonging to this class consist of a donor moiety, a triene bridge with an oxygen on C_2, and an acceptor moiety (Fig. 34). Typically, the acceptor moiety is Meldrum's acid or 1,3-dimethyl barbituric acid in 1st[478] and 2nd[492] generation DASAs, and was replaced by strongly electron withdrawing carbon acids in the 3rd generation.[493] The donor moiety is a dialkylamine in generation 1 DASAs[478] and secondary anilines, including functionalized indolines, in the 2nd and 3rd generation (Fig. 34).[480,492,493] The main transition band of the push–pull substituted triene is the π–π* transition and lies between 450 and 700 nm, depending on the substituents and the solvent.[490,491] Apolar solvents induce a bathochromic shift, while in polar-protic solvents λ_{max} is hypsochromically shifted.[491,494] Also, the type of donor moiety influences the position of the absorption maximum strongly. Dialkylamine-based DASAs exhibit their

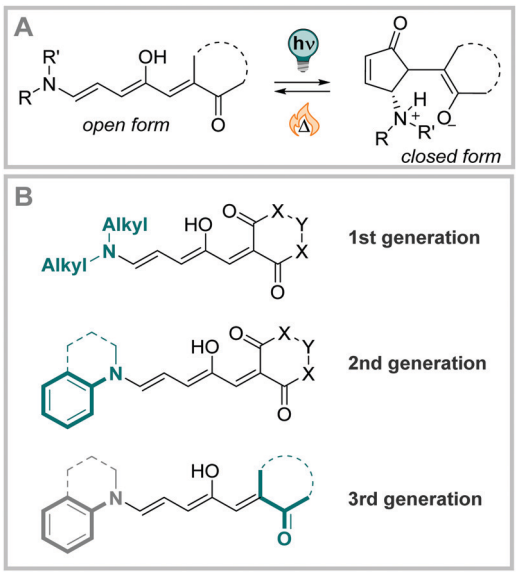

Fig. 34 Overview of the (photo)isomerization in DASA (A) and general structures of generation 1, 2, and 3 derivatives (B).

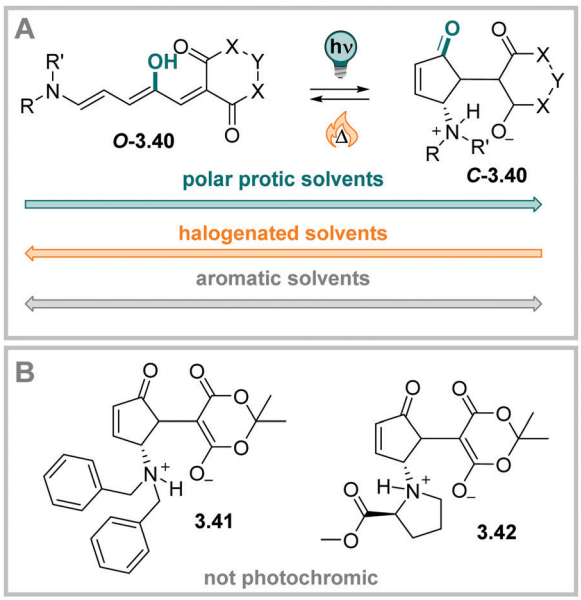

Fig. 36 Stable isomers of DASA. (A) Solvent-dependent thermal equilibrium between the open and the closed isomer in DASA. (B) Non-photochromic derivatives.[495]

maximum around 500 nm, while DASAs bearing (cyclic) anilines absorb up to 700 nm, hence, reaching the NIR region of the electromagnetic spectrum. This red-shift is particularly pronounced in derivatives bearing electron-donating substituents in *ortho* or *para* positions on the aromatic donor.[489,494,495]

DASAs are characterized by strong inverse photochromism, with the less coloured, cyclic form hardly showing any absorbance above 300 nm. Upon irradiation of the open form, the π–π* transition of the push–pull substituted triene rapidly bleaches, and new transition bands attributed to the formation of the cyclic form arise.[491] The open triene form is a strongly coloured, hydrophobic, extended structure. On the other hand, the closed form is colourless, hydrophilic, and significantly more compact.[478,495] Both the band separation of the two photoisomers, as well as the wavelength of irradiation in the UV-B and C region of the electromagnetic spectrum, made photochemical back-isomerization so far not practical, rendering DASAs efficiently T-type switches for any applications.[491] The photochemically induced isomerization mechanism involves multiple steps and intermediates and was thoroughly studied in recent years.[483,484,486,487,496] A simplified picture is given in Fig. 35. Irradiation induces photochemical $Z \rightarrow E$ isomerization of $C_2{=}C_3$ (A → A′, Fig. 35).[483,484] Thereby, the hydroxy group facilities a pre-selection of this double bond by steric interactions and by influencing its bond length.[487] The C=C isomerization is followed by a rotation around the C_3–C_4 bond (A′ → A″, Fig. 35), a thermal ring-closure reaction (A″ → B′, Fig. 35), and a concluding H^+ transfer onto the donor or acceptor moiety, respectively (B′ → B, Fig. 35).[483,484] The hydroxy group on C_2 is also crucially involved in the cyclization step, as non-hydroxy DASAs only showed unselective *E*–*Z* isomerization of several double bonds but no productive cyclization reaction.[487] Different solvents influence the overall behaviour strongly (see Fig. 36A), but the actinic step is only slightly perturbated and the same key intermediate (A′) is generated, indicating that the thermal step is the overall rate-limiting one.[486]

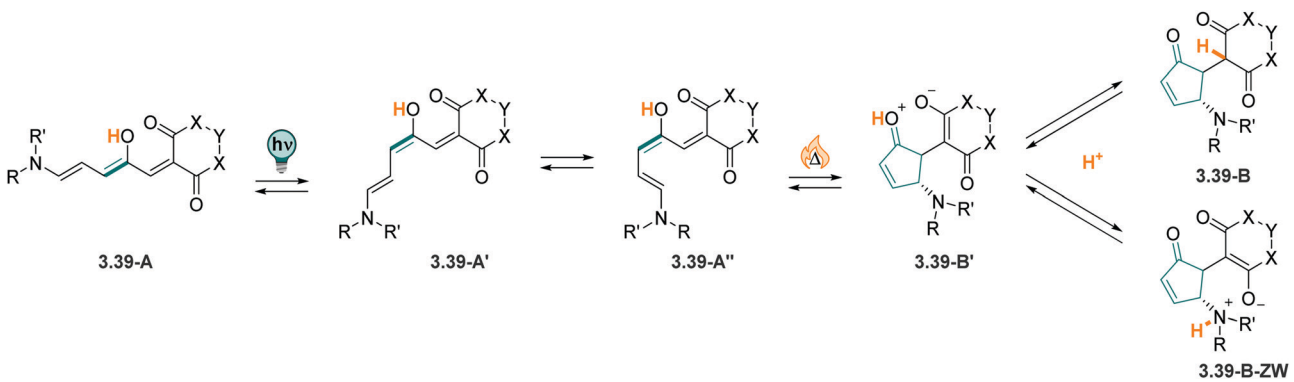

Fig. 35 Simplified (photo)isomerization mechanism of DASA photoswitches.

The closed form is thermally metastable and goes back to the open triene in the range of minutes to a few hours.[497] The thermal lifetimes are strongly solvent-dependent. Generation 1 DASAs exist almost exclusively in their linear form in solution.[478,495,497] In contrast, substituted anilines in 2nd generation DASAs exist to a substantial amount in their cyclic form at the thermodynamic equilibrium,[497] a characteristic which was further studied and improved in 3rd generation DASA photoswitches.[493]

Moreover, both QYs and thermal isomerization rates in DASAs are concentration depended. The $\Phi^{L\rightarrow C}$ decreases from *ca.* 20% to around 3% at 1000 times higher concentrations, while the thermal isomerization rate becomes *ca.* three times faster.[498] Further studies showed that the effects of the solution-state dielectric and intermolecular interactions on the degree of charge separation could provide a rationalization for this behaviour. The stronger the zwitterionic character of the respective open and closed isomers, the more pronounced are the concentration effects.[494,499]

Some first generation DASA derivatives, such as **3.41** and **3.42** in Fig. 36B, could not be photoisomerized in any of the media studied so far. The origin of this behaviour is still under investigation.[495] Furthermore, DASAs bearing a dialkylamine donor moiety switch reversibly mainly in aromatic apolar solvents,[478,497] the secondary aniline, present in generation 2 and 3 DASAs, allows for switching in a wider range of solvents, including THF,[492,493] dioxane,[497] halogenated solvents[489,492,493,497] and, MeCN,[492,493,497] and in polymer matrices.[500–502]

In strong contrast, in polar protic solvents such as methanol and water, the cyclic, hydrophilic form is energetically more stable than the linear isomer and does not isomerize to the linear state.[491] Also, on magnetic nanoparticles, the formation of the cyclic form is irreversible.[503] Different strategies have been explored to stabilize the linear form in polar protic solvents, including the addition of molecular receptors,[504] or peptides,[505] which could so far only slow down the cyclization reaction in the dark. A better stabilization of the linear isomer is realized in the presence of a Pd^{II}-based molecular vessel.[506] The open form can even be spontaneously generated in aqueous media, but the photochemically induced ring-formation was suppressed inside the cavity.[506] However, reversibility in water and PBS buffer was observed when the DASA photoswitch was part of a micelle-forming homo-polymer.[507]

The pronounced changes in their geometry and polarity make DASAs interesting candidates for a wide range of applications.[490,491] For instance, they have already been used in responsive polymers,[501,502,508] on surfaces,[509,510] to photocontrol wettability,[500,511] in sensing and,[512,513] for dynamic, self-regulating flows.[514] Furthermore, DASAs are responsive to multiple stimuli[505,512,513] which allows to further tailor their switching behavior. However, their uncontrolled behavior in water currently limits their application in this medium.

3.4.4 Dihydroazulene. Dihydroazulene (DHA) has an absorption maximum in the UV-region of the spectrum (*ca.* 360 nm for **DH** in MeCN) and undergoes a photochromic 10π-electrocyclic ring-opening reaction. The corresponding ring-open isomer has a zwitterionic resonance structure (Fig. 37) and is strongly colored.[108] The thermal lifetime of the metastable vinylheptafulvene (VHF) depends on substituents and medium it is embedded in and is usually in the minute to hours range.[515–517] The compound was not yet used in aqueous systems, but in liquid crystals,[518] polymer films,[519] in macrocycles,[520] rotaxanes,[521] for solar energy storage,[522,523] or to photocontrol emission properties.[515] Moreover, the DHA/VHF couple can be combined with further photochromic units to assemble multi-stage switches[404,524–527] or with electrochemically active unit to achieve photoswitchable redox properties.[516,528]

4 Illustrative examples of photoswitches in aqueous media

As described in Section 2, various strategies have been applied to solubilize organic molecules in water. Next to the effect of aqueous media on the photochemical properties of the photoswitch and the thermal lifetime of the metastable form (see Section 3), chemical stability in water and in biological environment also plays an important role. For instance, some azobenzenes are stable in the presence of biological antioxidants, such as glutathione,[529–531] while others are susceptible to reduction. They thus lose their functionality and form potentially toxic side products like diarylhydrazines and anilines.[532] Furthermore, enzymes naturally present in living organisms, particularly azidoreductases that are active in hypoxic cancerous tissue with low oxygen levels, can also reduce azobenzenes.[533] Especially, the *Z* isomer of azobenzene was found to be more prone to reduction than the less polarized *E* form.[534] Instability towards reduction can be circumvented by attaching different substituents to the azobenzene core[200] or by heteroaryl design resulting in many systems that are stable under physiological conditions in timeframes required for their application.[6,11,200,535–537] However, the introduction of different solubilizing moieties often has consequences for biological activity and uptake, such as selective accumulation in different sub-cellular

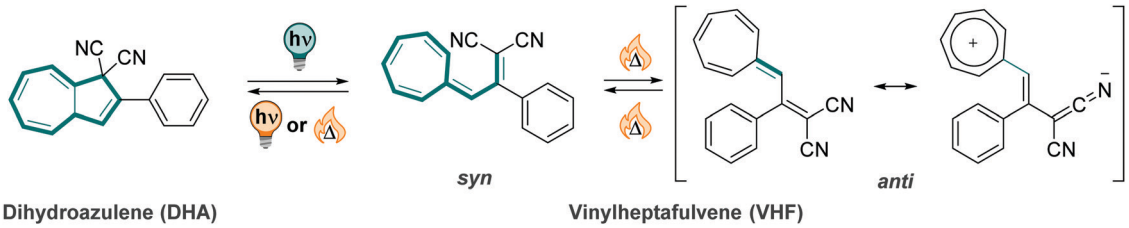

Fig. 37 General mechanism of the (photo)isomerization in the dihydroazulene/vinylheptafulvene photochromic couple.

compartments[538–540] or even hindered cellular uptake of freely dissolved molecules.[541,542]

Keeping all the aforementioned limitations in mind, in this section we will discuss different solubilization approaches applied to photoswitches in aqueous media.

4.1 Small molecules that act as ligands in biological systems

In biomedical research and the pharmaceutical world, small molecule actuators are extensively applied to regulate biological processes.[543–546] In this way, a wide range of biomolecules, such as proteins,[547–549] DNA and RNA,[550] as well as oligosaccharides,[551–553] can be targeted. Small molecules are usually applied remotely and reach the actual target site by diffusion. Consequently, the local concentration at the target site is often low, unless the molecule exhibits specific uptake (like phosphonate into mitochondria)[538] or an explicit delivery technique, for instance using liposomes, is used.[554] However, increasing the overall concentration of the bioactive molecule would affect not only the target site but also others. Eventually, side effects, as often observed in cancer therapy, or accumulation in the environment, which is one of the causes for growing multi-resistance in bacteria, often outweigh the beneficial effects of drug-therapy.

For these reasons, the use of an external stimulus, such as light, to enable local and temporal control of bioactivity, became a very promising approach in recent years.[7] Still spatiotemporal control is limited by diffusion of the light-responsive molecule. Thus, systems which can only be turned on once, such as those employing photocleavable protecting groups (photocages), are not ideal for many applications.[7] In contrast, molecular photoswitches can be reversibly activated specifically at the target site and deactivated to protect the surroundings.[30] Depending on the nature of the photoswitch, the deactivation process can be achieved by light or thermally (auto-inactivation, see Section 3 for different types of photoswitches). In this section, we discuss different solubilization approaches of photoswitchable molecules used as small molecular actuators in biological systems and highlight selected examples illustrating how to control biological function.

4.1.1 Introduction of charged moieties to molecular photoswitches. As seen in Section 2, the most straightforward approach to increase the solubility of an organic molecule in water is to attach a charged group to its structure. This can be a permanently charged moiety, for instance, a pyridinium salt, or acidic or basic functionalities, that become protonated or deprotonated under physiological conditions. Frequently used are tertiary ammonium groups, carboxylic acid, sulfonates, phosphates, and phosphonates.

In some cases, however, the charged unit affects the properties of the compound beyond just providing the required solubility. For instance, it can simultaneously enable binding to the target or interfere with cellular uptake. On the one hand, a positively charged group can increase the adherence of the molecule to cellular membranes, which are negatively charged on the headgroups of lipids, thus increasing the cellular uptake.[555] However, charged moieties can also hinder the internalization pathway by diffusion through the lipid bilayer due to insufficient lipophilicity of the compound.[556] These contradicting effects, improved adherence and decreased diffusion through the membrane, illustrate the importance of a balanced design of drug-like molecules.

Except for diffusion and passive uptake, some compounds are actively uptaken by protein transporters and receptors.[557] Here, the charged moiety can either be a part of the transporter/receptor substrate or it does not interfere with the uptake process. Hence, introduction of a charged group to enhance aqueous solubility might seem straightforward, however, it often is accompanied by consequences for several other key parameters that need to be taken into consideration.[541,557]

In the following sections, we discuss frequently used charged groups in photoswitchable biologically active ligands.

4.1.1.1 Ammonium ion. The most explored moieties used for solubilizing photoswitches with a charged group are the protonated tri-alkyl amine or a tetra-alkyl-ammonium groups. Both are positively charged in aqueous media at a pH < 9[558,559] and consequently, provide good aqueous solubility. Moreover, the (permanently) charged moieties can serve as binding groups towards different biomolecules. They can, for instance, act as an inhibitor of voltage gated channels,[560,561] which are involved in communication between cells, in transport, and self-defense mechanisms.[562] In this context, such compounds were used to photocontrol, for example, insulin release[563] and to block channels in neuronal tissue.[215,561,564,565] In another example, photoswitches carrying ammonium groups were used to restore vision in degenerated photoreceptor layers of mice. In particular, two azobenzenes, one with a diethylammonium group (**4.1a**, Fig. 38A) and one with a permanently positively charged triethylammonium group (**4.1b**, Fig. 38A), were investigated for this purpose.[566] The charged photoswitches blocked ion channels in neuronal ganglions in their *E* form (Fig. 38C), while after $E \rightarrow Z$ photoisomerization with 480 nm light the molecules were sterically too hindered to be accommodated by the channel and hence, activate it (Fig. 38C). Both **4.1a** and **4.1b** are well soluble in water, however, they target different cell types in the retina[566] due to distinct internalization mechanisms. The presence of receptors in certain cell types leads to active uptake of the permanently charged **4.1b**[566] while non-permanently charged **4.1a** is mainly passively uptaken.[566] This observation indicated that introduction of a permanent or non-permanent charge not only renders the molecules water-soluble, but also has consequences for their activity as well as their uptake. To further investigate this, similar photoswitches were designed to test the effect of one or multiple charges on their ability to inhibit voltage-gated potassium channels.[567] Interestingly, **4.2b** possessing two permanent charges (Fig. 38B) exhibited no activity on cells due to poor uptake and impaired diffusion through the cellular wall. On the other hand, **4.2a**, possessing only a single positive charge, could be taken up and successfully bind to its target. These examples clearly show that designing a photoswitch with permanently charged tri-alkylammonium groups brings water-solubility, however, the molecules need to be able to reach their specific target and therefore, should be carefully designed on a per-case basis.

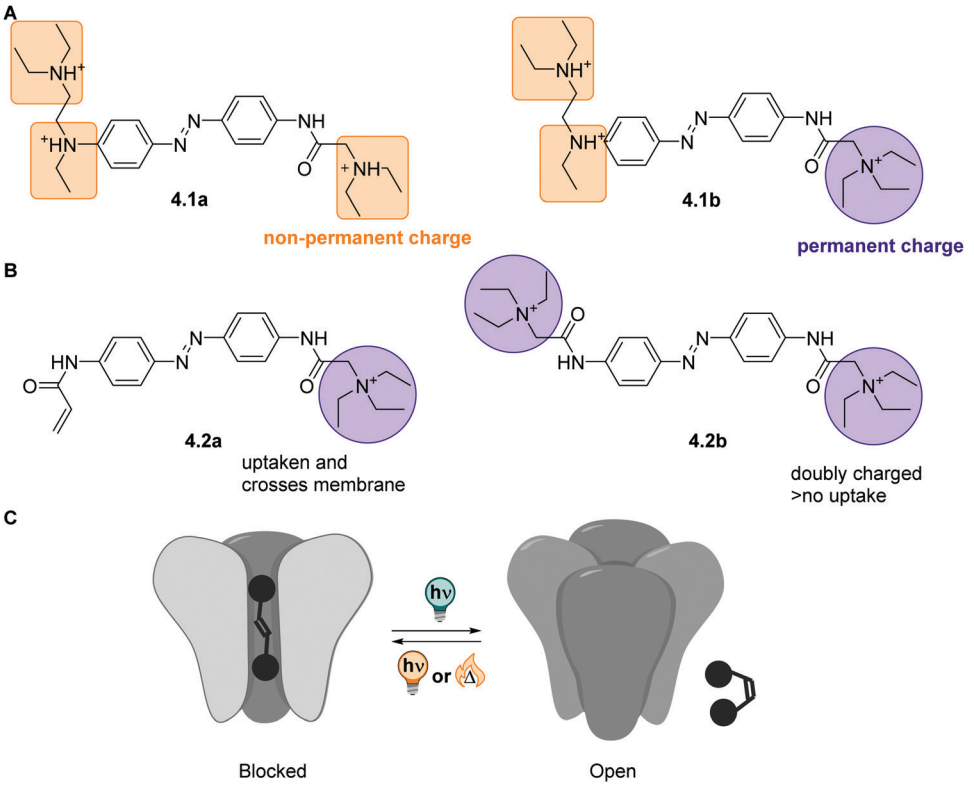

Fig. 38 Azobenzene photoswitches furnished with permanently charged (A and B) (**4.1b**, **4.2a**, **4.2b**) ammonium groups or with non-permanently charged alkylamines (**4.1a** and **4.1b**). (C) The charged elongated *E* isomer can easily fit into the channel cavity thus blocking it, while the *Z* isomer does not fit into the cavity leaving the channel open.

Moreover, positively charged nitrogen units are frequently used to bind to RNA[568,569] and DNA,[461,568–573] by interacting with the negatively charged phosphate backbone. For instance, trimethylammonium and aminomethaniminium groups have been applied to both interact with DNA and solubilize spiropyrans (Fig. 39A and B).[461,568–570] Spiropyrans **4.3a** and **4.3b** were used as photoswitchable DNA intercalators (Fig. 39). The closed spiropyran (SP) isomer, having a non-charged and non-planar core structure, is not suitable for DNA binding, despite bearing a permanent charge at the substituent. On the other hand, the merocyanine (MC) form is aromatic and planar, which is favorable for DNA intercalation. Protonation of the phenol group in slightly acidic environment, such as often found in in cancerous cells,[574,575] additionally improved binding to negatively charged DNA.[576]

To further explore the design, two molecules containing a positively charged amidine group, known to bind to DNA,[576–578] were investigated (compounds **4.4a** and **4.4b**).[459] Switches **4.4a** and **4.4b** (Fig. 39) were carefully designed to match the assay conditions suitable for DNA binding studies, where at pH 5–9 at room temperature the thermal equilibrium is reached within 5h (20 : 80 = SP : MC for **4.4a**) or 1h (85 : 15 = SP : MC for **4.4b**).[459,579] It was found that MCH^+ binds 35 times (**4.4a**) or 66 times (**4.4b**) stronger to DNA compared to their corresponding unprotonated MC forms. While **4.4a** MC, **4.4b** MC and **4.4b** MCH^+ intercalate DNA, **4.4a** MC showed a less specific binding mode.[459]

Besides spiropyrans, also suitably substituted azobenzenes can be used as visible-light responsive DNA modulators. The visible light-responsive tetra-*ortho* fluoro azobenzene motif was functionalized taking inspiration of the DNA minor groove binder netropsin and was used to target nucleosomal DNA (Fig. 39D, **4.5a** and **4.5b**).[580] Upon irradiation with 520 nm light in DMSO, relatively high PSDs were reached (70 : 30 = *Z* : *E* for **4.5a**, 73 : 27 = *Z* : *E* for **4.5b**) and by irradiation with 405 nm light the PSDs were 7 : 93 = *Z* : *E* (**4.5a**) and 3 : 97 = *Z* : *E* (**4.5b**), respectively, in DMSO. Most importantly, the *Z*-**4.5a** isomer showed good thermal stability (after 9 h 77 : 23 = *Z* : *E*) in Tris buffer with 2–5% DMSO. Furthermore, the *E* isomer **4.5a** was successfully bound to nucleosomes while the *Z* isomer did not.

4.1.1.2 Other nitrogen salts. Similar to ammonium groups, pyridinium moieties often increase water-solubility, while also enhancing the affinity to DNA. In this context, both azobenzene[581] and DTE-based[582] switches were used to develop light-responsive DNA binders. In particular, pyridinium-functionalized photoswitches, selectively binding to G-quadruplex DNA, attracted considerable attention in the last years.[116,349,583–587] G-quadruplexes are four stranded secondary structures of guanine-rich DNA that form stacked tetrads and are involved in a plethora of biological processes, ranging from transcription, replication, genome stability to cancer growth.[588] In this context, azobenzenes with a permanently charged methylated piperidine, pyridine or morpholine group on each end were synthesized

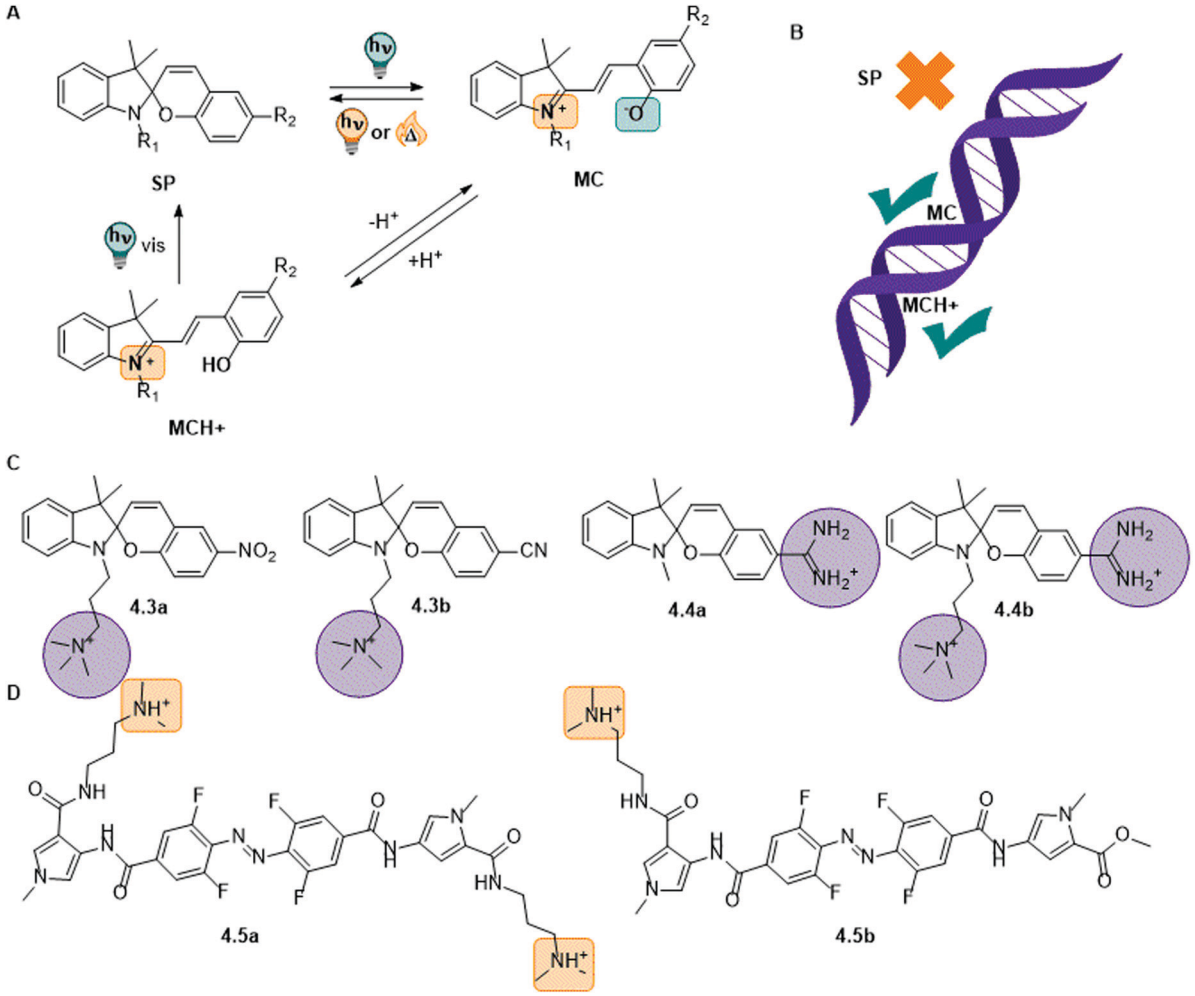

Fig. 39 (A) The spiropyran photoswitch **SP** undergoes a ring opening reaction upon irradiation with light thus forming the open zwitterionic **MC** isomer. Under acidic conditions, **MC** is protonated, forming the positively charged **MCH**$^+$ isomer which can be ring-closed upon irradiation with visible light. (B) Both charged isomers **MC** and **MCH**$^+$ bind to double stranded DNA, while the **SP** does not interact with DNA. (C) Spiropyrans **4.3a and b**, carrying a nitro and cyano groups, were further modified to carry one positive charge (**4.4a**) or two positive charges (**4.4b**) to explore the effect of additional charge on their DNA binding properties. (D) Visible light-controlled azobenzenes **4.5a**, carrying two positive charges, and azobenzene **4.5b**, carrying one positive charge, were designed to modulate DNA.

(**4.6**,**7** and **10**, Fig. 40A and C). The molecules induced formation of G quadruplexes in the *E* form, while the *Z* isomer caused dissociation. However, this effect was significantly diminished in the presence of metal cations, such as those present at physiological conditions (**4.6**, Fig. 40A.)[583,584] A similar photoswitch, stiff stilbene **4.7** (Fig. 40A) behaved analogously to azobenzene **4.6**. and induced reversible formation of G quadruplexes.[116] The *Z* isomers of stiff stilbenes are thermally more stable than *Z*-azobenzenes, which could be beneficial form certain applications. However, irradiation with 400 nm light caused refolding triggered by irreversible photo-induced oxidation and degradation of the stilbene (Fig. 40B, structures **4.7a** and **4.7b**).[116] This photochemically induced side-reaction has been reported previously[115,589] and limits the applicability of the stiff stilbene-based modulators in the long term. The stilbenes were further modified to introduce a more flexible piperazine group (**4.8**, Fig. 40C), which resulted in affinity for G4 DNA over duplex DNA facilitating toxicity towards cancer cells,[590,591] while remaining less toxic towards a non-malignant mammalian cell line.[585] In contrast, the photophysical properties of the structurally related aryl-stilbazolium ligands (**4.9**, Fig. 40C) were hampered in the presence of DNA rendering them unable to switch due to too strong binding affinity.[586]

Very recently, a DTE furnished with pyridinium moieties (structure **4.10**, Fig. 40) was reported to bind to different G4 topologies in the closed and open form. The compound was readily soluble in phosphate buffer and the switching could be reversibly performed with visible light (450 and 635 nm).[349] The two photoisomers exhibited toxicity towards cancer cells, with the closed form being two-fold more potent than the open one (IC_{50} of **4.10c** = 10 mM, **4.10o** = 23 mM). However, in a study on a very similar DTE switch containing a hexafluorocyclopentane group, it was reported that the pyridinium-DTEs are potentially toxic to eukaryotic organisms.[587] Switching was successfully performed *in vivo* in a transparent nematode organism (*Caenorhabditis elegans*) with sufficient oral uptake of both open

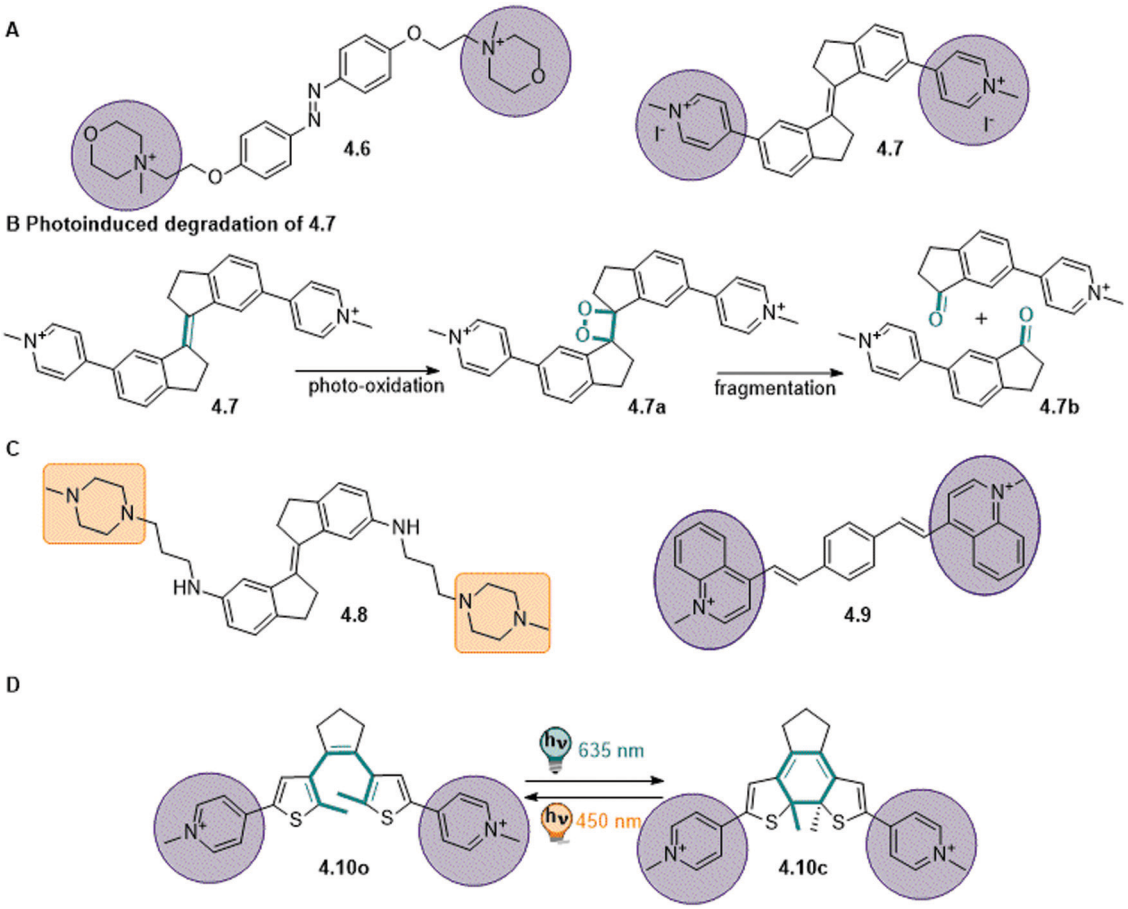

Fig. 40 Photoswitches solubilized with positively charged cyclic amines and heteroatoms containing nitrogen atom. (A) Azobenzene **4.6**, carrying two methylated morpholine moieties, and stilbene **4.7** with two pyridinium groups were used to modulate G quadruplex DNA structures. (B) Irreversible photooxidation of stilbene **4.7** into **4.7b** *via* **4.7a**. (C) Stilbene **4.8** functionalized with two piperazine groups exhibited affinity for G4 DNA over duplex DNA, facilitating toxicity towards cancer cells while the structurally related **4.9** was bound too strongly to DNA prohibiting photoswitching. (D) The photoisomerization of a DTE photoswitch carrying two pyridinium groups of which the open form **4.10o** showed higher toxicity towards cells opposed to the closed form **4.10c**.

and closed forms. The striking observation was that nematodes fed with the ring-closed form appeared to be paralyzed. Upon visible light irradiation, the paralysis was significantly less present. However, it seemed that both DTEs were toxic to the organism. Nevertheless, it must be noted that the tested concentrations were very high (up to 12 mM in 10% DMSO in phosphate buffer, pH = 7).

Another photoswitch that was functionalized with a *N*-alkylated picolinium moiety to bind to dsDNA, is chromene **4.11** (Fig. 41).[427,592] Under continuous irradiation with UV light, the two interconverting open isomers, called **4.11***TC* and **4.11***TT*, are formed. They showed the ability to intercalate to the DNA double helix, which in return electrostatically stabilized the meta-stable photoisomer.[427] When the light

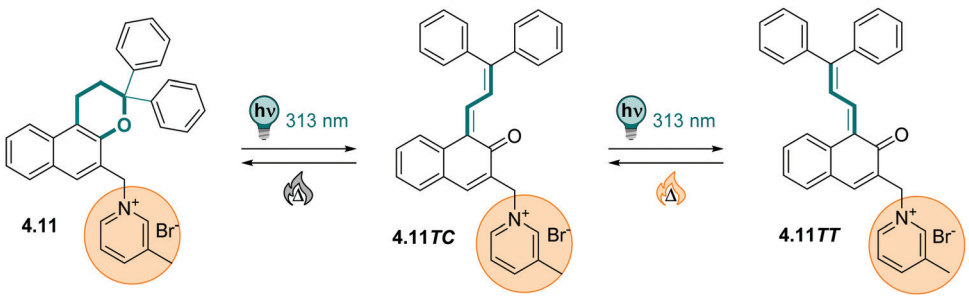

Fig. 41 The chromene photoswitch **4.11** forms the open **4.11***TC* isomer upon UV irradiation, which interconverts to the TT isomer (**4.11***TT*).

stimulus was removed, the open form undergoes ring-closure and the chromene could no longer interact with DNA. As expected, the solubility was suboptimal due to the highly aromatic nature of chromene. Upon addition of the DNA in buffer, the switch precipitated and therefore, a 5% DMSO solution had to be used for the experiments.

4.1.1.3 Sulfonate, phosphate and phosphonate. Phosphonate, phosphates, and sulfonates, as well as related functional groups, are negatively charged when dissolved in water and can be readily employed to increase water-solubility.[78] Sulfonated azobenzenes are often used as food colorants and dyes, such as carmoisine[593] or Congo Red (Fig. 42).[594] Besides their coloring properties, the molecules were also studied regarding their activity as DNA binders or as inhibitor of an HIV1 protease. However, the photochemical switching properties of the sulfonated dyes are to the best of our knowledge not reported.

On the other hand, a phosphate-containing lipid with an incorporated azobenzene unit was used as a ligand for the G-protein coupled receptor (GPCR) S1P1-5 to photocontrol pain hypersensitivity in mice.[595] Alternatively, photoswitchable ATP analogues bearing multiple phosphate groups were used to interfere with the kinesin-microtubule systems.[596] Also, in designing azobenzene-based antagonists (**4.13**, Fig. 43) of the AMPA receptor, which is involved in neuronal firing, the introduction of a phosphonate group was key for assuring solubility under physiological conditions.[597] A previously reported non-light active AMPA antagonist, NBQX, based on a quinoxalinedione moiety failed at clinical trials due to its insufficient solubility, which resulted in renal toxicity (Fig. 43).[598] Attaching a methylphosphonate group (structure **4.12**, Fig. 43) increased the solubility, and was adopted in the design of the photoswitchable analogue.[598,599]

Moreover, phosphonate and phosphate groups have been attached to DTE photoswitches to ensure both water-solubility and inhibitory activity towards a *Mycobacterium tuberculosis* (MTB)-specific enzyme.[600] Phosphoribosyl isomerase A (mtPriA), an enzyme unique to MTB species, possesses a symmetric active site with two phosphate-binding sites. Since a specific geometry and distance between both sites is crucial for competitive

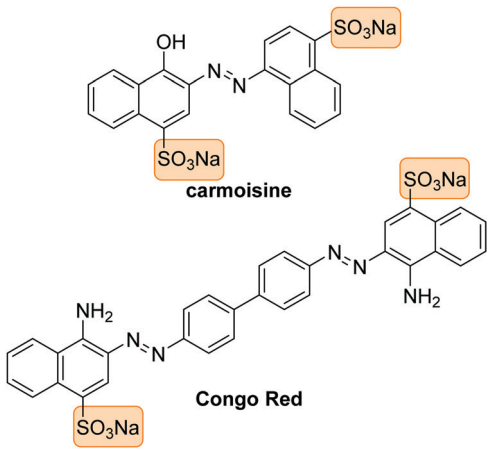

Fig. 42 Sulfonated azobenzene dyes, carmoisine and Congo red.

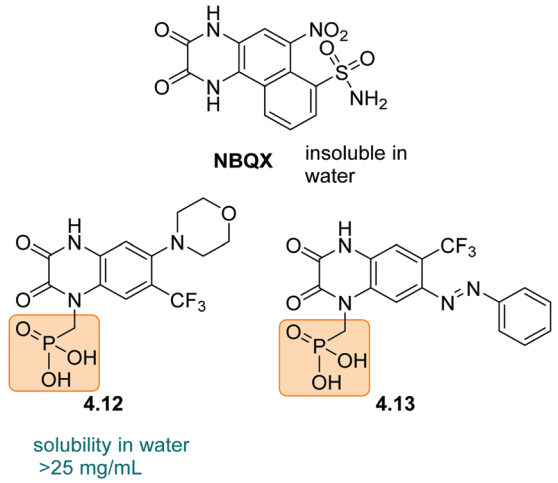

Fig. 43 Introduction of a methyphosphonate group (**4.12**) to the AMPA antagonist **NBQX** ensured water-solubility. Molecule **4.12** was modified to incorporate a light-responsive azobenzene switch (**4.13**) as photocontrolled AMPA receptor antagonist.

inhibition, mtPriA is an excellent target for photoswitchable inhibitors whose geometry and flexibility can be altered by light. Five bistable DTE switches containing phosphonate or phosphate groups at different positions were studied regarding their binding properties towards the active site of mtPriA (Fig. 44).[600] DTE **4.14m** with *meta*-phosphate groups featured the largest difference in binding constants between the open (K_i = 0.5 μM) and closed form (K_i = 4.4 μM). The same DTE switches (**4.14m**, **4.14p**, **4.15m**, **4.15p**) were applied as inhibitors for the imidazole glycerol phosphate synthase (ImGP-S) multienzyme complex and were able to reversibly interrupt the allosteric communication between the enzymes in the multienzyme complex.[601] Recently, alkyl phosphate-functionalized azobenzenes were used to control the tryptophan synthase (TS) multienzyme complex in a similar fashion. The solubility of the compounds strongly depended on the length of the alkyl-linker between the azo-function and the phosphate group. Consequently, stock-solutions for photochemistry and biochemical evaluation were prepared in pure water and the concentration was adjusted to the respective solubility. Only one derivative required the

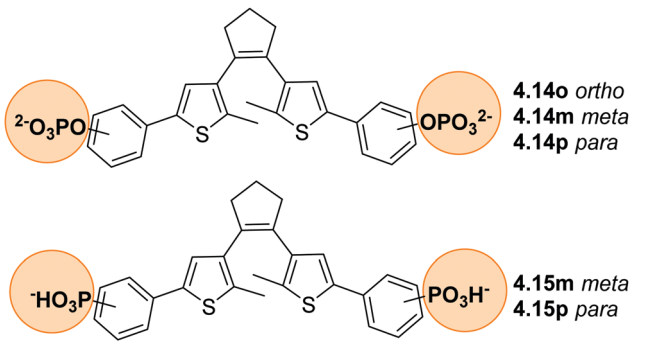

Fig. 44 DTE-base mtPriA inhibitors with phosphate and phosphonate groups on different positions of the phenyl ring.

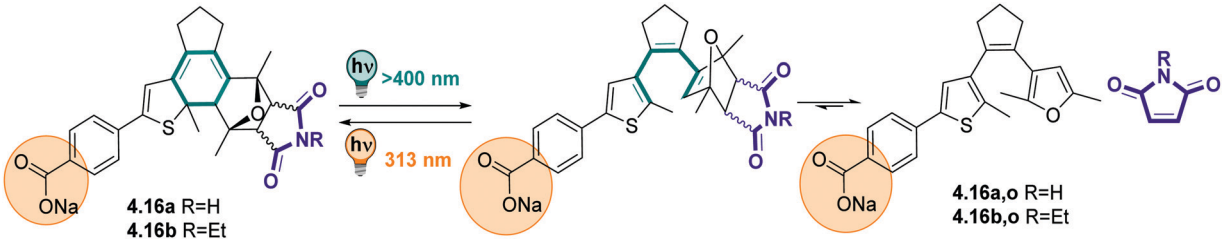

Fig. 45 The prodrug based on a DAE forms the ring-open isomer upon irradiation with 400 nm light which can undergo reverse Diels–Alder reaction releasing maleimide and the open furyl-substituted DAE.

addition of 15% DMSO to be studied by UV-Vis spectroscopy and was excluded for biological evaluation.[602]

4.1.1.4 Carboxylates. Like sulfonates, phosphonates and phosphates, also carboxylates are anionic under physiological conditions, which facilitates solubility. Accordingly, the sodium salts of two carboxylic acid functionalized DAE derivatives (**4.16a and b**, Fig. 45) were prepared to solubilize the photoswitches in buffer. While the previous examples discussed photoswitches that alter their biological activity by a photoinduced structural change, this example showcases that photoisomerization process can be linked to drug release. Maleimide, a small molecule that can modulate DNA topoisomerase II by what is supposed to be a covalent attachment to a cysteine side chain,[603] was condensed with a furyl-containing DAE in a Diels–Alder reaction.[604] Photoinduced $O \rightarrow C$ isomerization locks the bioactive molecule and no maleimide is released. The reverse Diels–Alder reaction takes place at physiological conditions and body temperature and is induced by visible light. Maleimide is slowly released (50% release in 92 h at 40 °C), generating a daily dose of 46 μM (**4.16a,o**) and 5 μM (**4.16b,o**), which corresponds to the bioactive dosage window for pharmaceutical applications.[603]

4.1.1.5 Sulfonylurea. Sulfonylurea-based drugs are often used to treat diabetes,[605] despite their relatively limited solubility in water, and are hence often solubilized using co-solvents.[606] Azobenzene sulfonylurea **4.17** with a pK_a of 4.76 readily dissolves in water at sufficiently high concentrations to be tested in biological assays when diluted from a 50 mM DMSO stock solution.[34] The acidity of **4.17** ensures its deprotonation and solubility under physiological conditions. Moreover, its anionic nature makes it unlikely that the compound would interact with DNA, due to the negatively charged phosphate backbone of the macromolecule. Furthermore, **4.17** was tested *in vivo* to photocontrol of glucose homeostasis using a mouse model.[607] In these studies, the potential toxicity of **4.17** was investigated in detail, since a previous study reported that many amino group-bearing azobenzenes are mutagenic and carcinogenic.[608] However, compound **4.17** was proven as reasonably safe, presumably due to its negatively charged character in water (Fig. 46).

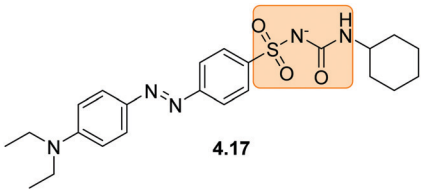

Fig. 46 The conjugate acid of azobenzene sulfonylurea **4.17** with a pK_a of 4.76 is deprotonated and thus negatively charged in aqueous solutions.

4.1.2 Introduction of non-charged polar groups to molecular photoswitches

4.1.2.1 Hydroxamic acids. Hydroxamic acids are highly polar moieties and assist water-solubility of a compound through ionic and hydrogen-bond interactions with the solvent. Moreover, they can be found as the active moiety in biologically relevant molecules.[609] In this context, classical azobenzenes **4.18a–h** (Fig. 47A) were functionalized with hydroxamic acids and studied as photoswitchable histone deacetylase (HDAC) inhibitors in cancer cell essays to develop potential therapeutics.[610] The molecules were irradiated in DMSO stock solutions and subsequently diluted into the assay buffer showing good solubility. The reported switches had varying half-lives, ranging from 4 min to over 8 h in 1% DMSO in HDAC assay buffer at room temperature, thereby offering a selection for a short-lived compound that deactivates quickly after light activation or, a more stable version which remains in its light-activated isomer for a longer time. Their stability towards photobleaching and reduction in cellular environment was demonstrated by performing multiple switching cycles in the presence of glutathione. Also, arylazopyrazoles **4.19a–c** (Fig. 47B) were designed as inhibitors of amidohydrolase, which is closely related to HDAC and present in many hospital-acquired bacteria.[611] In particular, the hydroxamic acid group interacts with the protein by forming a complex with the Zn^{2+} ion, which facilitates binding of the ligand. It additionally allows the otherwise lipophilic photoswitches to readily dissolve in phosphate buffer in the case of **4.19a** and **4.19b**, while **4.19c** could not be solubilized. The arylazopyrazole derivatives proved to exhibit excellent photophysical properties with high PSDs (from 85–90% *Z* to 93–97% *Z*). The metastable forms of switches **4.19a** and **4.19b** had relatively long half-lives of 17.8 h and 19.4 h, respectively (30 °C, phosphate buffer). Both types of azobenzene-based HDAC inhibitors show that a balanced design consisting of an ionic effector group, that also facilitates water-solubility, and an aromatic photoswitch can results in drug-like compounds holding promise for cellular studies and beyond.

4.1.2.2 PEG chain. As described in Section 2.2.1, a common approach to solubilize organic molecules in water is the attachment

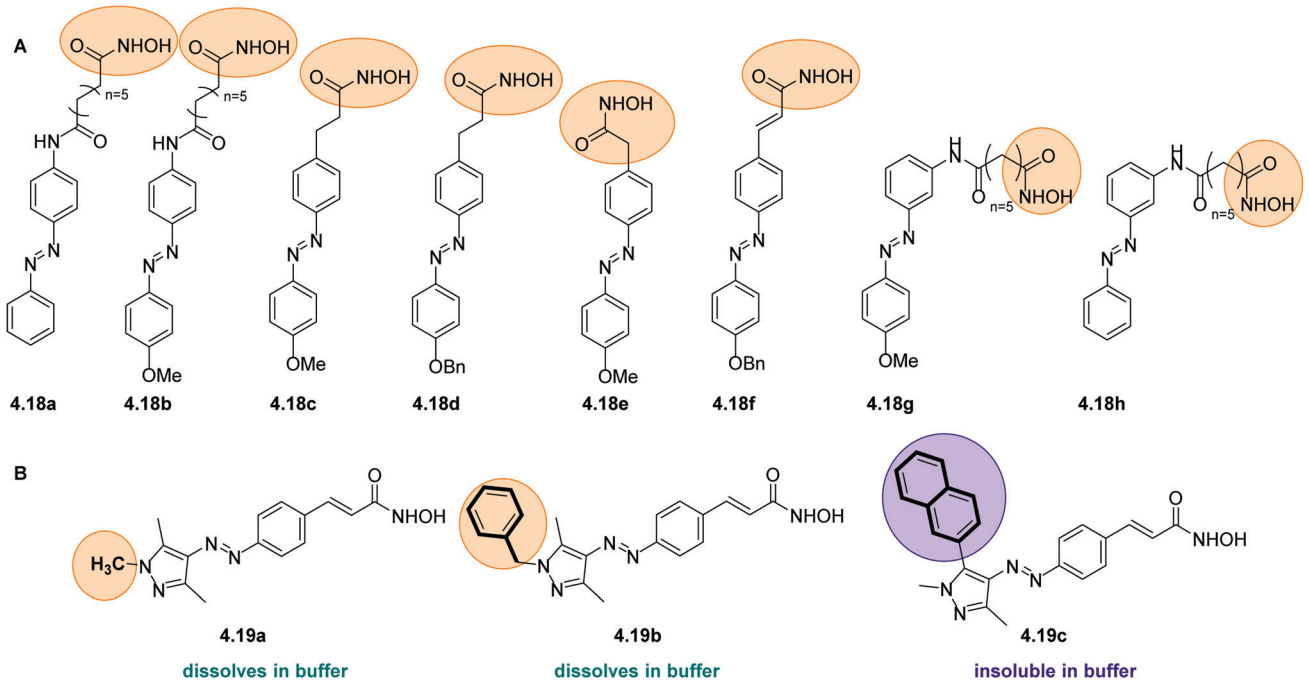

Fig. 47 (A) Selected examples of photoswitchable hydroxamic acid-based HDAC inhibitors. (B) Arylazopyrazoles carrying a hydroxamic acid moiety functionalized with different substituents and their effect on solubility.

of hydrophilic PEG chains.[102] This approach is often applied for solubilizing photoswitchable self-assembly systems.[162,612]

Dihydropyrenes are insoluble in water but could be solubilized in aqueous media by attaching PEG5-10 chains to their core. RNA aptamers, which are single stranded RNA molecules that bind to target molecules,[386,613] were optimized by iterative *in vitro* selection to differently bind to isomers of dihydropyrenes. Dihydropyrenes were chosen as aptamer ligands, since both isomers are conformationally very rigid and therefore feature distinctly different shapes.[383] Molecule **4.20c** (Fig. 48) was identified as the most promising hit and was used to photocontrol the assembly of a ribozyme,[386] a catalytically active RNA cluster.[614] Binding of the pegylated **4.20c** to the aptamer stabilized the ribozyme's catalytic site allosterically and showed a 900-fold difference in catalytic rates compared to **4.20o**.

Also, PEGylation together with attachment of a guanidium group was successfully used in the design of a complex molecular glue, a molecular structure that glues two (or more) other molecules together through strong non-covalent interactions.[615–617] Azobenzene photoswitch **4.21** was modified with multiple adherence guanidinium groups that bind to oxyanion-rich areas on the surface of the target protein *via* salt bridges (Fig. 49).[618] Additionally, the azobenzene featured a sulfonamide group on the other side, acting as an inhibitor towards a carbonic anhydrase. Azobenzene **4.21** only functioned as inhibitor in its *E* configuration, since the *Z* geometry prohibited the molecular glue from accessing the active site. In this example, both the PEG-chains and the guanidinium moieties are crucial for water-solubility. Additionally, the presence of multiple guanidiniums ensured superb cell-membrane permeability.[619] The large molecule could be reversibly photoisomerized in aqueous solution and had a half-life of 2.3 h in HEPES buffer at 37 °C.

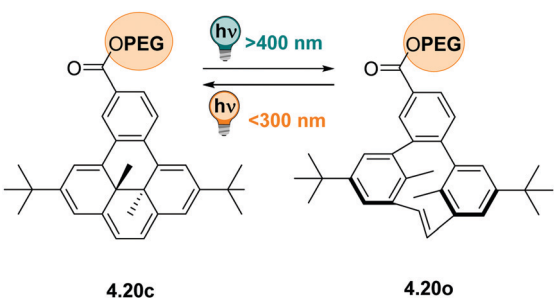

Fig. 48 The water-soluble dihydropyrene photoswitch, carrying a PEG chain, undergoes a ring opening reaction upon irradiation with visible light and the ring-closing process under UV irradiation.

4.1.3 Dipole moment, heteroatom-based rings, and scaffold hopping. Another approach to enhance the water-solubility of organic molecules is to redesign them into more polar analogs, or by using a scaffold hopping-like strategy. The latter is commonly used in medicinal chemistry and involves modifying the core structure of a known drug while attempting to keep their original activity.[620,621] In the context of photoswitches, typically, polar groups are introduced onto or into the structure of the switch or classical arenes are replaced by heteroarenes. Both approaches have been, for instance, applied extensively on azobenzenes and on DAEs switches[157] and are discussed in the following section using representative examples.

4.1.3.1 Azobenzenes and heteroaryl azobenzenes. Scaffold hopping in classical azobenzenes has been applied to achieve improved photophysical properties in water and better water-solubility.

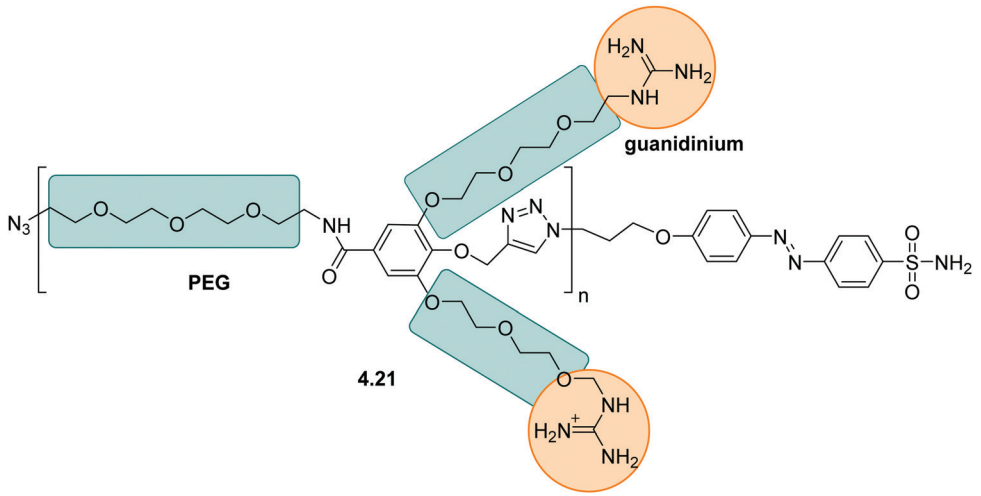

Fig. 49 Azobenzene **4.21** carries multiple PEG linkers as well as guanidinium groups which enable water-solubility as well as enable binding to the target protein *via* salt bridges.

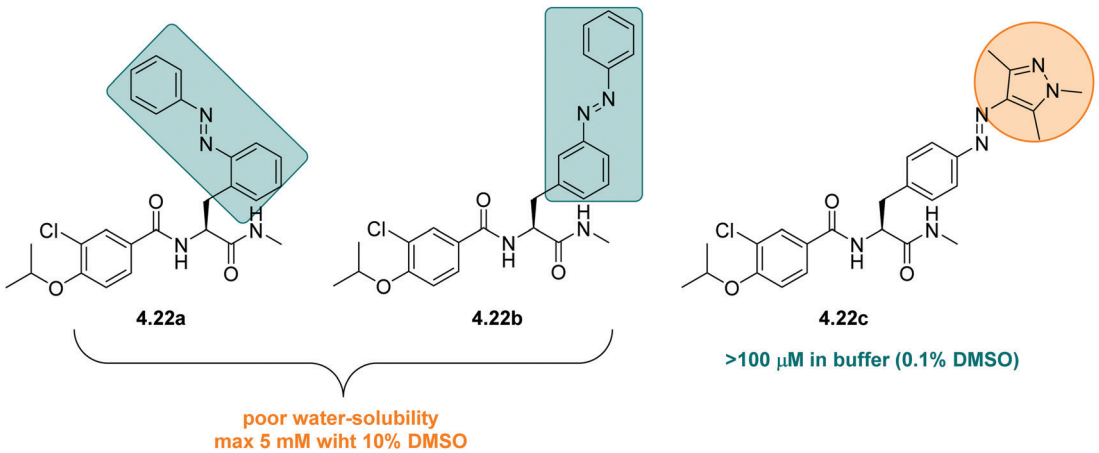

Fig. 50 Photoswitchable CENP-E inhibitors containing an azobenzene were poorly water-soluble (**4.22a and b**) while the heteroaromatic arylazopyrazole photoswitch **4.22c** exhibited much better aqueous solubility.

In one example, azo-analogues **4.22a–b** (Fig. 50A), which were designed as inhibitors of CENP-E, a protein involved in chromosome movement, were very poorly soluble under aqueous conditions. In contrast, the phenylazopyrazole photoswitch **4.22c** was much more soluble and could be tested on cells at >100 μM in buffer with 0.1% DMSO.[622] In a 1 : 1 water : acetonitrile mixture, the half-life of **4.22c** was longer than 24 h at 37 °C and the PSDs were 93%*Z* (PSS^{365nm}) and 86%*E* (PSS^{510nm}). *E*-**4.1.22c** (IC_{50} 0.29 μM) had a 10-fold higher inhibitory activity than the *Z* form (IC_{50} 2.4 μM). Therefore, cell proliferation could be inhibited or slowed down upon irradiation with green light (510 nm), forming the *E* isomer, when testing the compound on living cells (HeLa). Compounds **4.22a** and **4.22b**, based on classical azobenzenes, had to be tested *in vitro*/in the enzyme essay for inhibition of CENP-E with 10% DMSO reaching maximum concentration of only 5 μM and no difference in activity between their *E* and *Z* isomers could be observed.

Next to arylazopyrazole switches, other heteroaryl-azobenzene derivatives were also studied in biological context. One example is the azo-functionalized pyrazolopyrimidine **4.23c**, which was applied *in cellulo* to photocontrol the RET transmembrane tyrosine kinase receptor.[623] The photoswitch was investigated next to azobenzene **4.23b**, which had a *Z* form with a lifetime of only 2 min in water, and a stilbene variant **4.23a**, which irreversibly decomposed upon irradiation. Photoswitch **4.23c** had good photochemical properties in water where it achieved 87% of *Z* at the PSS^{365nm} with a sufficiently long lifetime applicable for biological studies (τ = 9.7 h. at 37 °C). This example shows how a minor change, such as an additional heteroatom in the ring or a stilbene scaffold instead of an azobenzene, can have a great impact on the photochemical properties, as well as water-solubility (as seen for **4.23**, Fig. 51) The azoswitch **4.23c** could undergo multiple photoswitching cycles without fatigue in the presence of glutathione, showing its resistance to reduction. Interestingly, the observed difference in activity of the inhibitor of the *Z* form was 3.8 (enzyme essay) and 3.2 (in cells) times higher than the thermally stable *E* isomer.

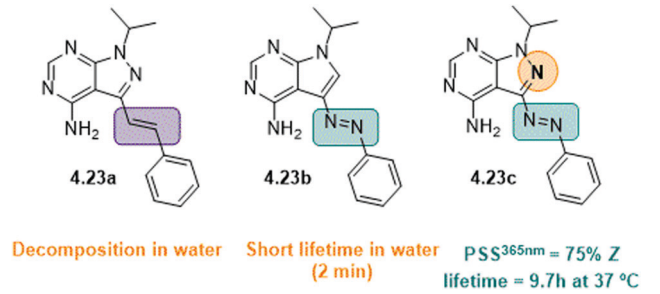

Fig. 51 Inhibitors of RET transmembrane tyrosine kinase receptor, illustrating the effect of a different switch system (stilbene **4.23a** *vs.* azobenzene **4.23c**) and an additional heteroatom (**4.23b and c**) on the (photo)chemical properties in aqueous solutions.

Like pyrazole, also pyridine motifs can contribute to water-solubility in azobenzenes. For instance, compound **4.24** has been applied to photocontrol GPCRs[624] as well as inhibitor of alpha-chymotrypsin. To study this compound sufficient aqueous solubility was crucial to achieve high-enough concentrations to determine the IC_{50} values.[35] Moreover, a set of azobenzene- and azopyridine-based sirtuin inhibitors was designed (Fig. 52). Most of the compounds of the library had the required photophysical properties in water and long thermal half-lives of the metastable *Z* isomers (>300 h).[625] However, phenyl azopyridines carrying a hydroxy or amino group (such as **4.25a** and **4.25b**) exhibited shortened half-lives due to tautomerization (see Section 3.2.3).[626,627] The respective azopyridines were consequently modified by methylation of the aniline (example **4.25d**) or introduction of methyl groups in the *ortho* positions (example **4.25c**) as attempt to increase the thermal half-lives. However, this often rendered the compounds insufficiently water-soluble and caused aggregation.[36,37] Compound **4.25e**, bearing a C7 chain, had better water-solubility which in return affected the inhibitors activity. For longer fatty-acids (such as **4.25f**), precipitation during the assay was an issue. Based on these observations, the authors concluded that in some examples the higher inhibitory activity of the *Z* form, which was found to be up to 21-times more potent than the *E* isomer, was in fact not due to its helical geometry but due to its better availability caused by higher solubility in water. This example demonstrates the complexity encountered in attempts that aim to encompass excellent water-solubility, improved bioactivity, and maintain advantageous photochemical properties.

4.1.3.2 DAE and fulgimides. Classical DAEs are highly apolar structures and, thus, are often decorated with charged groups such as carboxylate and phosphate anions to enable solubilization (*vide supra*). Alternatively, modification in the core structure or moving to the related class of fulgides or fulgimides can be considered, similar to the heteroaryl design in azobenzenes.[157] Especially in DAEs, such structural modifications are affecting the photophysical and photochemical properties significantly (for more details, see Section 3.3.1) and are discussed with illustrative examples in the following section.

In compound **4.27** (Fig. 53), the typically used central cyclopentadiene ring was replaced by a maleimide, mimicking

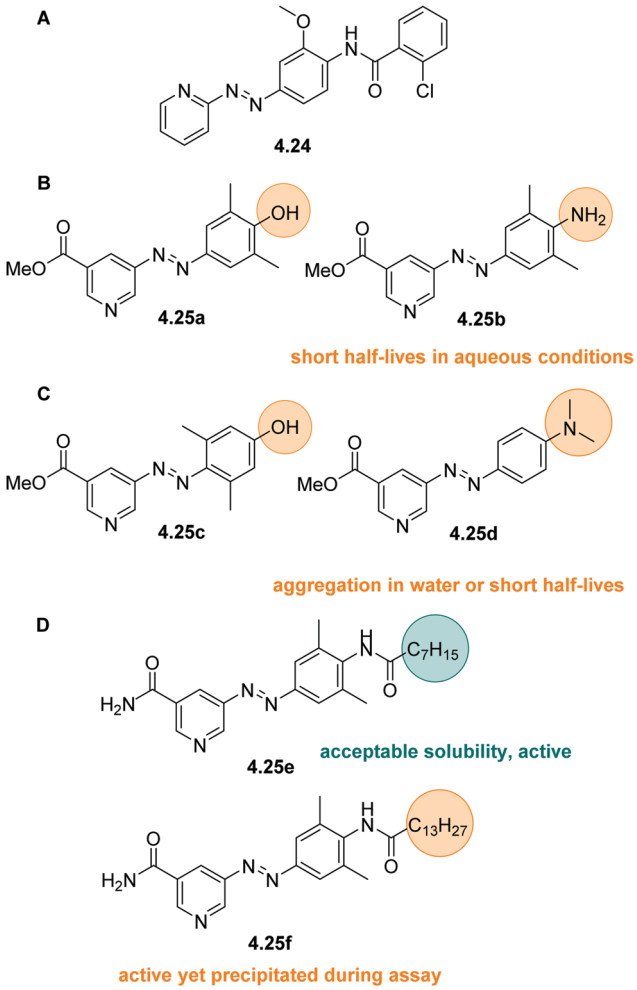

Fig. 52 Different substituents in azopyridine-based sirtuin inhibitors and their effect on their water-solubility, (photo)chemical properties and activity.

the structure of bisindoylmaleimide **4.26** (Fig. 53), a potent sirtuin inhibitor.[335] Introduction of this motif induced a bathochromic shift in the UV-profile in comparison to the cyclopentadiene-bridged analogue. The compound was tested for its inhibitory activity towards Sirt2 and exhibited a 22-fold difference in activity between the open (IC_{50} 4.2 μM) and the closed form (IC_{50} 92.3 μM), featuring a PSD of 98 : 2 = *C* : *O* under irradiation with 312 nm light in DMSO. Due to the TICT taking place, this reaction could not be induced in polar protic solvent, such as the assay buffer, and $O \rightarrow C$ photoisomerization needed to be performed in the DMSO stock solutions, highlighting another limitation that can be met when certain DTEs are used in aqueous media. However, photoinduced ring-opening was possible *in situ*.[335] Therefore, the use of the structurally related indolyl fulgimides was explored for the same target.[408] Fulgimides are more flexible and polarized and hence, in general, better soluble than DTEs in aqueous environment. Moreover, the open forms (Fig. 53, *Z*-**4.28** and *E*-**4.28**) isomerize upon 400 nm light irradiation and only the *E* form further cyclizes to the closed form *C*-**4.28**. Several derivatives were studied and showed superior

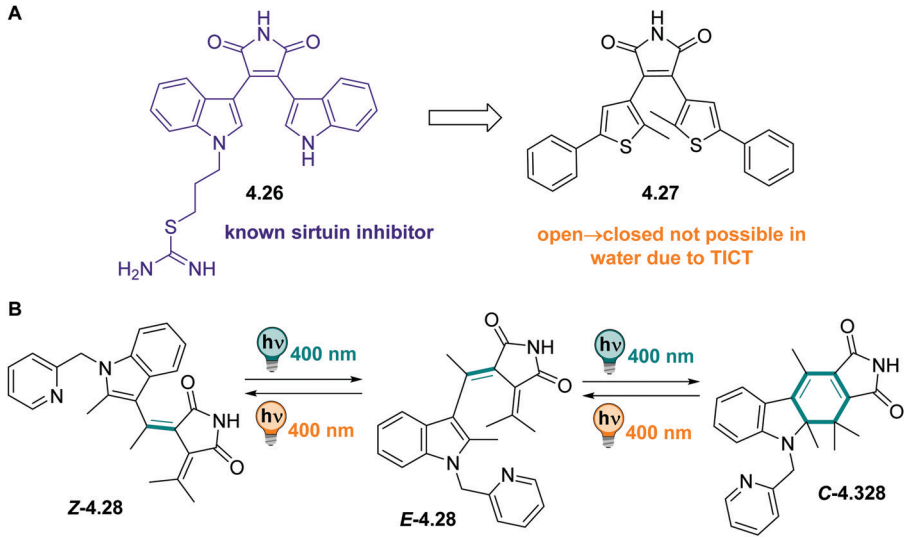

Fig. 53 (A) The potent sirtuin inhibitor **4.26** was redesigned into the photoswitchable system **4.27**. (B) Since **4.27** could not undergo ring-closing in aqueous solution, the system was further redesigned into photoswitchable fulgimides **4.28**.

photophysical and photochemical properties compared to the previously developed DTEs, such as reversible photoswitching in the assay buffer. However, **4.28** exhibited only low inhibitory activity with a 1.5-fold difference between the open form and the PSS^{400nm} sample (*ca.* 30% closed form). Similar observations were made in a later study comparing DTEs based on maleimide and fulgimides as light-controlled dopamine receptor ligands.[628] Again, the DTEs showed a larger difference in activity between the two photoisomers (11-fold compared to 4-fold) but could not be isomerized reversibly in aqueous solution. These examples showcase that optimization of photochemically properties and solubility in water by simultaneously retaining the biological potency is not trivial.

DTEs and fulgimide photoswitches were also studied together as light-controlled inhibitors of zinc dependent HDACs.[418] Avoiding donor–acceptor designs and hence, a TICT like in the examples discussed before, was the key design principle in obtaining a small library of compounds that could be addressed reversibly in polar protic solvents by light. However, some of the DTE derivatives were unstable upon irradiation, especially in aqueous solutions. DTEs **4.29a** and **4.29b** formed a byproduct upon isomerization, bearing a central five-member ring as displayed in Fig. 54 (see also Section 3.3.1).[333,629] While **4.29a** very quickly converted almost completely to the byproduct, **4.29b** had a higher fatigue resistance and could form 80% closed-ring isomer after 60 s of irradiation with only small amounts of

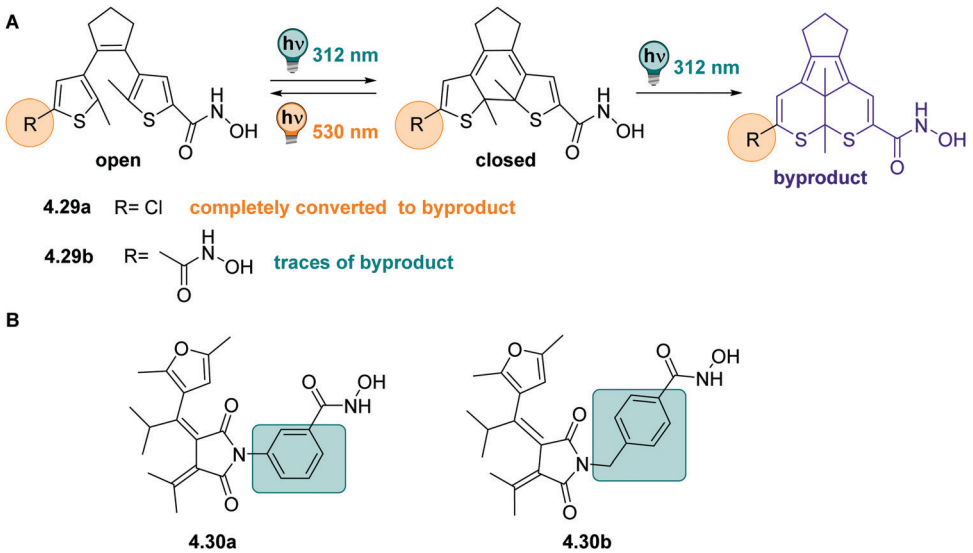

Fig. 54 Light-controlled inhibitors of zinc dependent HDACs. (A) DTE **4.29a** was unstable upon irradiation in water, quickly forming the byproduct, while DTE **4.29b** formed 80% if the closed isomer with minimal byproduct formed. (B) Fulgides **4.30a and b** showed excellent photochemical properties in water however the difference in activity was much smaller compared to the DTE switches.

byproduct formed.[418] DTE **4.29b** showed inhibition of HDAC, however, with small differences in affinity between the photoisomers. As an alternative, fulgide photoswitches were synthesized. Both fulgides **4.30a** and **4.30b** reached over 95% of the closed isomer at the PSS^{365nm} in DMSO. The properties were similar in buffer with 1% DMSO, however, minor fatigue was noticed. In enzyme activity assays, fulgimide **4.30b** showed nanomolar affinity for HDAC, but the differences in activity of the two isomers were low also for these derivatives. Again, the photochemical behavior can be adjusted by modifying the photoswitchable core, a translation to the biological potency of the compounds is however not obvious.

4.1.4 Increasing solubility by breaking planarity. In general, planar structures are less soluble than non-planar structures (see Section 2.2.3). Hence, disruption of the planarity by attaching suitable substituents or by designing bent structures can improve solubility. In the case of photoswitches, this aspect becomes particularly interesting, as the light-induced photoisomerization is in most cases accompanied by a significant structural change (*cf.* Section 3 for a more detailed overview). In this context, classical azobenzene photoswitches were studied regarding the difference in solubility between the planar *E* and the helical *Z* isomer,[630–633] in which the phenyl rings are twisted out of plane.[634] For instance, the solubility difference of the *E* and *Z* isomers was tested for azobenzenes **4.31** and **4.32**,[635] where the *Z* isomer was 20-times (**4.31**) or 1.4-times (**4.32**), respectively, more soluble in phosphate buffer then the *E* form (Fig. 55A).[636] A similar phenomenon regarding the solubility was also observed for some azopyridines discussed in Section 4.1.3 (*vide supra*).[625]

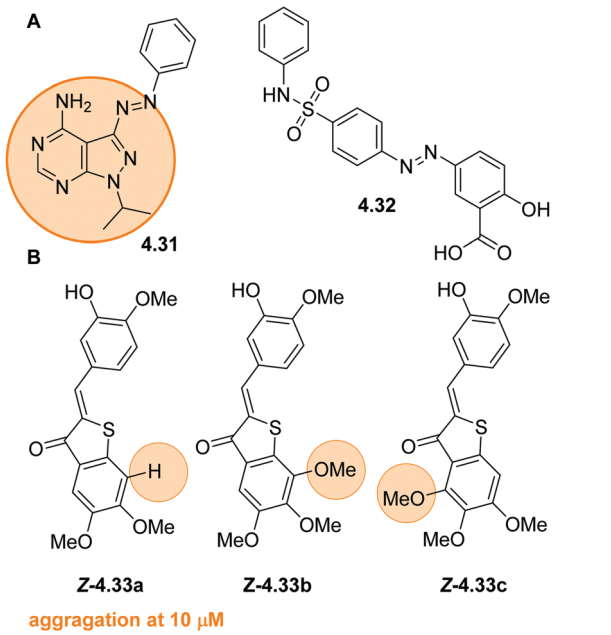

Fig. 55 Breaking planarity to increase water-solubility. (A) Azobenzene-based photoswitches where the *Z* isomer was 20-times (**4.31**) or 1.4-times (**4.32**) more soluble in phosphate buffer then the *E* form. (B) Introduction of three methoxy groups increases water-solubility and disables aggregate formation.

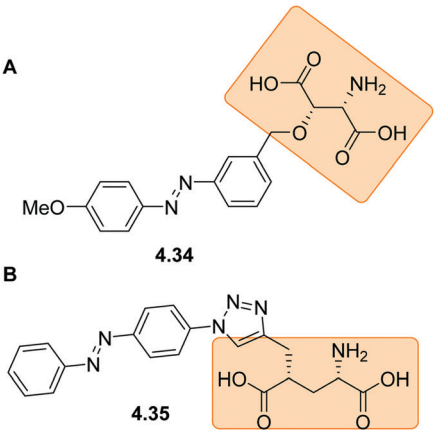

Fig. 56 Photoswitchable glutamate receptors carrying anionic amino acid moieties. Azobenzene **4.34**, featuring an aspartate moiety, could be solubilized at concentrations of 0.1 mM in phosphate buffer (A), while the glutamate azo-derivative **4.35** was poorly soluble in water and required heating and addition of DMSO in the stock solutions despite carrying a glutamate moiety (B).

The planarity in photoswitches can also be affected by attaching suitable substituents to the photoswitchable core. In this way, a library of hemithioindigo inhibitors (Fig. 55B) was designed based on a known compound colchicine.[261] While some compounds were not sufficiently water-soluble and caused aggregation and toxicity (**4.33a** aggregation at 10 μM), the tri-methoxy-substituted compounds (**4.33b** and **4.33c**) dissolved much better in water since the molecule's planarity was broken with a methoxy group sticking out of plane. In this manner, π-staking was prevented, and the water-solubility was increased.[261]

4.1.5 Solubilization by attaching bioactive ligands or substrates. Many biologically interesting targets for photopharmacology have substrates or known inhibitors that are inherently water-soluble, such as amino acids or sugar moieties. Functionalizing a molecular photoswitch with these types of ligands often enhances the water-solubility of the whole construct. For instance, azobenzenes furnished with anionic amino acids, such as aspartate[637] or glutamate,[638] were used to achieve light control over glutamate receptors. An azobenzene carrying an aspartate group (Fig. 56A, structure **4.34**) was used to inhibit the activity of archaeal aspartate transporter Glt_{Tk} where the molecule could be dissolved at concentrations of 0.1 mM in potassium phosphate buffer (50 mM, pH = 7.0).[637] Furthermore, for **4.34** *E* was 3.4 times more active than *Z* with IC_{50}s of 2.5 μM and 9.1 μM, respectively.[637] A glutamate azo-derivative, **4.35**, (Fig. 56B) was designed to photocontrol *N*-methyl-D-aspartate receptors (NMD), which play an important role in neurological function.[639] This photo-agonist was inactive in its *E* form and could be activated in milli-second precision with both one-photon (360–375 nm) and two-photon (740 nm) excitation. However, in some instances addition of only a glutamate moiety does not result in sufficient solubility, as shown for **4.35** which was poorly soluble in water and adhered to filters. Therefore, different adjustments needed to be done for each separate experiment to achieve

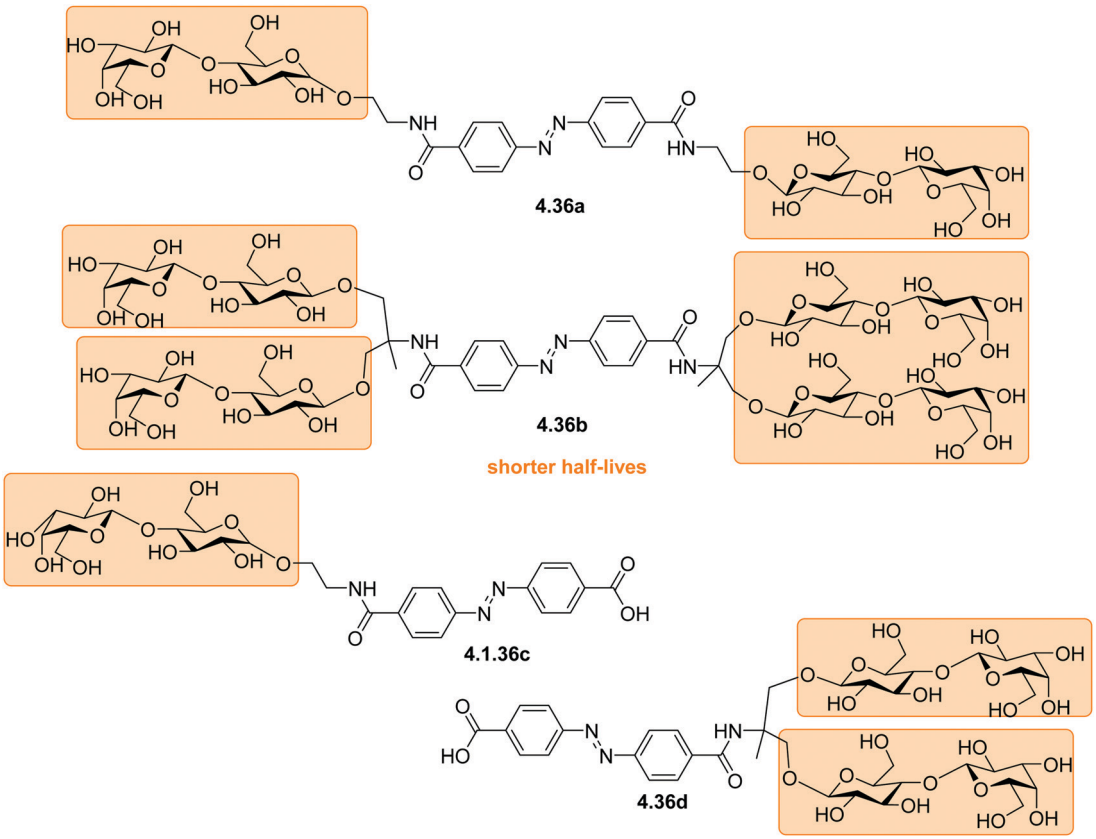

Fig. 57 Azobenzene photoswitches decorated with multipole sugar moieties with increased water-solubility.

sufficient solubility. For instance, the stock solution was prepared in DMSO before buffer addition and the buffer required heating to 40 °C.

Alternatively, sugar moieties were attached to photoswitches and lead to significant increase of their solubility in water.[640–644] Specific sugar moieties can be recognized by a selective carbohydrate-binding protein from *E. coli* called lectin.[645] In this manner, photoswitchable lectin binders were studied regarding the differences in binding affinities of the photoisomers bearing either a single or multiple sugar groups. (Fig. 57, **4.36a–d**)[640,641] Incorporation of multiple carbohydrates simultaneously increased binding to lectin and solubility in water.[641] The half-lives of the *Z* forms of these azobenzenes were longer in aqueous environment, compared to DMSO solutions.[640] As a general trend, symmetric molecules with sugar moieties on each side (**4.36a** and **4.36b**) isomerized faster than unsymmetric derivatives (**4.36c** and **4.36d**).[640] Beyond this study, azobenzene systems with incorporated sugar moieties were used to control bacterial adhesion with light,[642] inhibition of beta-galactose,[643] and as glycosphingolipids for cancer immunotherapy.[644]

Besides functionalizing photoswitches with amino acids and sugars, bioactive small molecules, such as antibiotics, were attached to light-responsive compounds. In this manner, ciprofloxacin was connected to an azobenzene and a spiropyran, and both compounds could be readily dissolved and studied in a microbial growth assay medium. (Fig. 58A, **4.37 and 4.38**).[646]

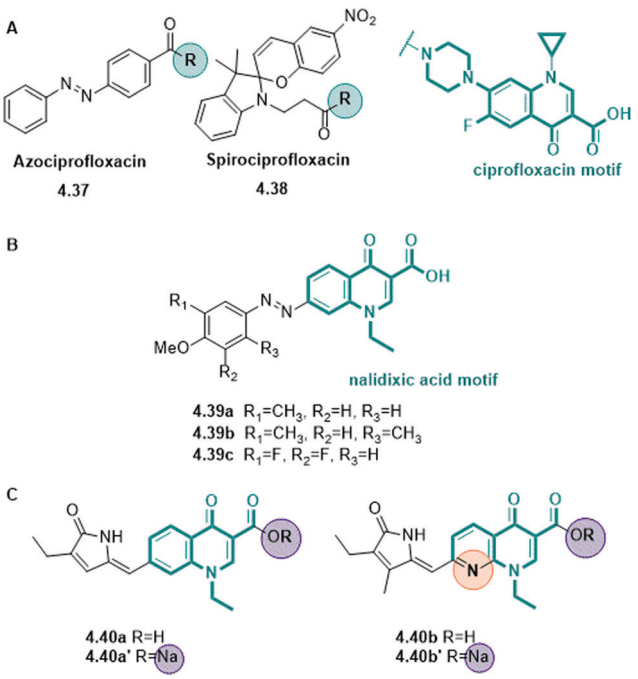

Fig. 58 Photoswitchable antibiotics. (A) Ciprofloxacin was modified to incorporate an azobenzene (**4.37**) or a spiropyran photoswitch. (**4.38**). Azobenzenes **4.39a–c** (B), hydantoin **4.40a** and phytochrome **4.40b** (C) contain the nalidixic acid motif ensuring antimicrobial activity.

The spirociprofloxacin was efficient against Gram negative *Escherichia coli*, while the azociprofloxacine showed activity on Gram-positive *Micrococcus luteus*. The azo version could be switched over multiple cycles without degradation, but the spirociprofloxacin exhibited fatigue in aqueous media, possibly caused by instability of merocyanine in water (see Section 3. Spiropyran).[445]

Alternatively, azobenzenes were structurally merged with known antibiotics,[6,7,30] such as nalidixic acid (Fig. 58B. structures **4.39a–c**)[647] The photoswitchable antibiotics were designed for the spatiotemporally control of their activity with light. Specifically, the active *Z* isomer is temporarily formed upon irradiation and then thermally relaxes back to the inactive *E* isomer within a few hours. Despite its high potency as antibacterial agents, nalidixic acid has already limited solubility in water.[648] Therefore, it comes as no surprise that the MIC value determination of the light-controlled derivatives had to be performed at low concentrations (64 μg mL^{-1}) due to solubility restrictions.[647] In another study, using photoswitchable hydantoin[649] and phytochrome,[650] it was shown that the limiting water-solubility can be improved by transforming the carboxylic acids to sodium salts (Fig. 58C, **4.40** and **4.40b**).[651]

4.1.6 Solubilizing photoswitches in protein–probe complexes. For fluorescent imaging, spatiotemporal precision and control is of great importance to image different cellular pathways, pathogens or for disease diagnosis.[652–654] Application of photoswitchable molecules that can be reversibly interconverted between one fluorescent and one non-emissive form can provide higher precision in bioimaging compared to classical fluorescence probes since the changing signal is easier to distinguish from background fluorescence.[655,656] A crucial requirement for application *in vivo* is sufficient water-solubility of the switchable fluorescent dye.[38] However, fluorescence dyes often have extended aromatic structures which render them inherently insoluble in aqueous media. A common strategy to sufficiently solubilize such compounds is by forming of a protein–probe complex. In this manner, a combined molecule consisting of a glycoprobe, fluorescent linker naphthalimide (**Naph**, visualized in the green fluorescence channel), and a spiropyran photoswitch was designed (Fig. 59, **4.41**).[657] The probe binds to human serum albumin (HSA) *via* a host–guest interaction between the dye and a hydrophobic pocket of the HSA protein,[658–660] thus preventing the aggregation of the dye. While the SP isomer does not emit fluorescence, the MC form emits in the red reference channel, when bond to the host. In this way, the probe was used as a two-channel fluorescence probe (green and red) that could be reversibly controlled by light and applied in living cells.

Very recently, a similar system was reported, where a photoresponsive probe containing **Naph** and a modified merocyanine were used for high-resolution fluorescence microscopy (see Section 4.3.4) to visualize the distribution of β-galactosidase in cells (Fig. 59, **4.42**).[661] The probe contained a galactose moiety attached directly to the phenol ring of the merocyanine group, thus preventing photoisomerization to the closed spiropyran isomer. Upon cleavage of the sugar moiety by the β-galactosidase, the red fluorescence increased due to formation of the free merocyanine. Merocyanine could then photoswitch to the fluorescence-silent spiropyran form and was used for high-resolution fluorescence microscopy. The protein–probe complex between the dye and human serum albumin (HSA) ensured solubility in water, minimal phototoxicity, and good cellular uptake.[661]

4.2 Water-soluble molecular photoswitches as biomolecular building blocks

To achieve light-controlled activity of biomolecules, molecular photoswitches have been designed as biomolecular building blocks, such as amino acids and nucleotides, and were incorporated into the backbone of biomacromolecules.[662] Several strategies can be applied and for each there are different requirements regarding water-solubility. For short peptides synthesized by solid phase peptide synthesis (SPPS) on resin, it is feasible to use organic solvents throughout the synthesis. Therefore, there are no requirements for aqueous solubility of the photoswitchable building block, as long as the final product dissolves appropriately under the required conditions. In contrast, aqueous solubility is of great importance for photoswitchable building blocks which need to be uptaken and processed by a living organism before they are incorporated into a biomolecule. Insufficient solubility can induce aggregate formation possibly resulting in toxicity.[663]

4.2.1 Amino acids

4.2.1.1 Genetic code expansion. The 20 canonical amino acids are building blocks of all living beings. Incorporation of unnatural amino acids *in vivo* offers the possibility to structurally modify proteins and to control and study their activity. Genetic code expansion is a technique that allows the integration of such unnatural building blocks by hijacking the synthetic machinery of the target organism.[664–669] Also, genetic code expansion can be applied to introduce photoresponsive building blocks into a complex protein.[670–672] It is of pivotal importance that the photoswitchable substrate is sufficiently water-soluble, non-toxic, and successfully uptaken by the organism for efficient incorporation.[673,674]

In the context of photoswitchable unnatural amino acids, to our knowledge, only azobenzene-based structures have been incorporated *via* genetic code expansion. Classical azobenzene-based amino acids were used to control DNA binding activity[670] and to explore the mechanism of an allostery model bi-enzyme complex.[671,672] Furthermore, visible light-controlled azobenzenes with tetra-*ortho* substituents have been successfully incorporated into proteins such as the green fluorescent protein (GFP)[668] and firefly luciferase[669] to reversibly control their properties.

Moreover, employing photoswitchable amino acids with an additional thiol-reactive group provides a novel approach of crosslinking peptides. After *in vivo* incorporation of the functionalized photoactuator into a protein of choice, the unnatural amino acid can react with a nearby moiety, such as a cysteine side chain, and crosslink two sides of the protein (Fig. 59). Both classical azobenzenes with a reactive anchoring group in the *meta* position (Fig. 60A, **4.43**, **4.44**)[675] and a penta-fluoro-azobenzene amino acid **4.45** (Fig. 60B)[676] were successfully incorporated into both *E. coli* and mammalian cells.

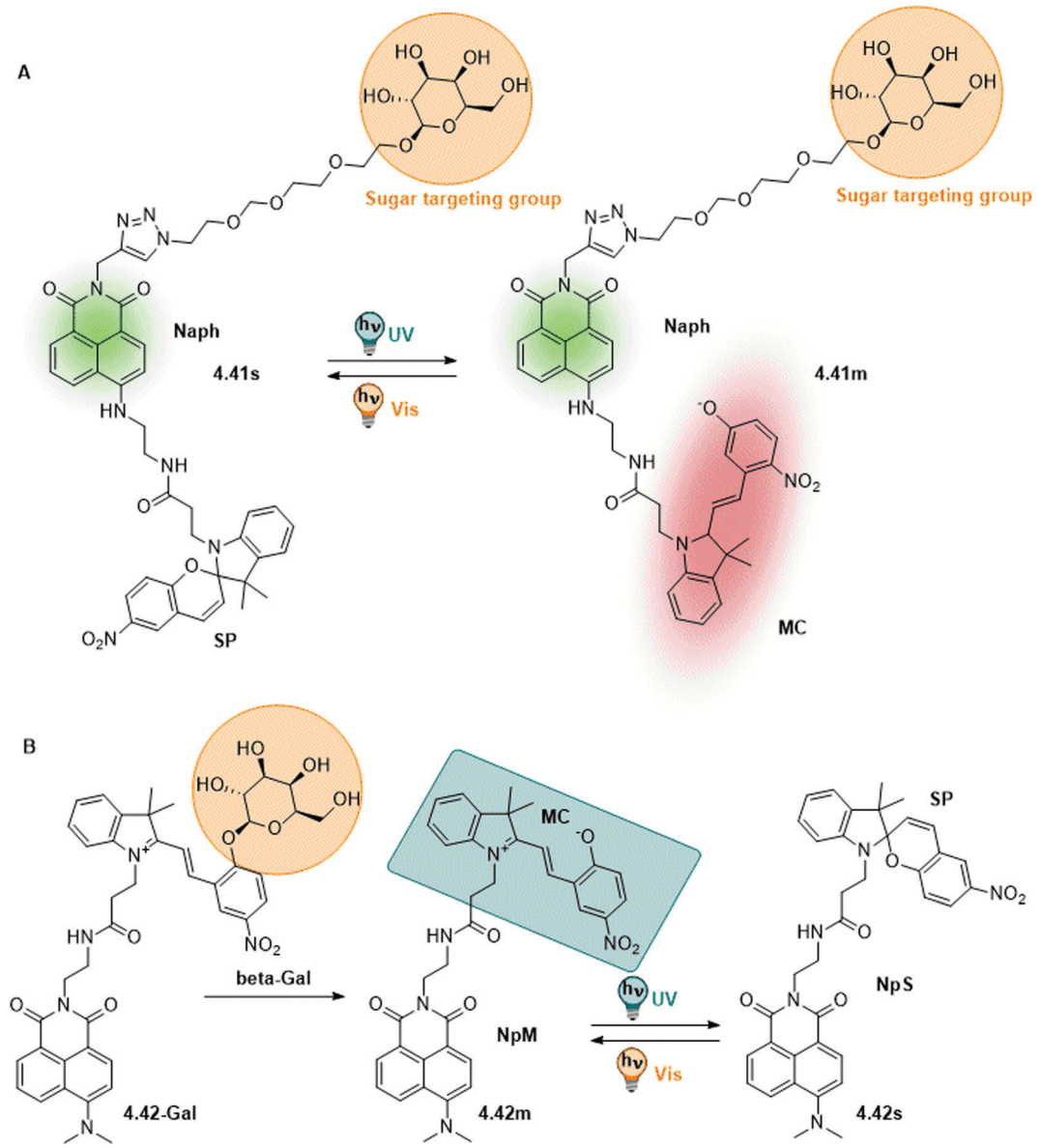

Fig. 59 (A) Spiropyran photoswitch with a fluorescent linker and a sugar targeting group. (B) Spiropyran based photoswitch carrying a fluorescent moiety and a galactose group locking it in the merocyanine form. Upon cleavage of the sugar, the photoswitch can reversibly switch from **MC** to **SP** form in water.

4.2.1.2 Solid phase peptide synthesis. Solid phase peptide and oligonucleotide synthesis have been employed to synthesize known biomolecules with unnatural moieties such as photoswitches and even molecular motors,[153] on a resin by stepwise coupling of each building block.[677–680]

Peptides with a photoswitch in the backbone. Azobenzenes with two biphenyl rings were incorporated *via* SPPS into a highly water-soluble short peptide chain to study the photochemical behavior of the construct in water (Fig. 61A, **4.46**).[681] The stability towards reduction of the incorporated azobenzene **4.46** was tested by incubation with 10 mM glutathione (GSH) as the environment in mammalian cells is highly reducing.[682] No degradation was observed, however, GSH catalyzed the $Z \rightarrow E$ isomerization of the short model peptide and significantly shortened its thermal half-life. Already 50% of the *Z* isomer relaxed to the *E* at 37 °C in 60 min, while in the absence of GSH hardly any isomerization was observed. The mechanism of this phenomenon is yet unknown, though, the authors speculated that a GSH radical or thiolate anion reversibly attacks the azo double bond thereby reducing it and allowing free rotation.[682]

While for most classical azobenzenes incorporation *via* SPPS was successful,[681,683] the visible light-responsive tetra-*ortho*-fluoro azobenzene was a more challenging substrate.[684] Both diazocine and tetra-*ortho*-fluoro azobenzene amino acids (**4.48** and **4.49**, Fig. 61) were incorporated into a peptide backbone to study protein–protein interactions. While diazocine **4.48** was compatible with SPPS, the fluorine groups of tetra-*ortho*-fluorinated

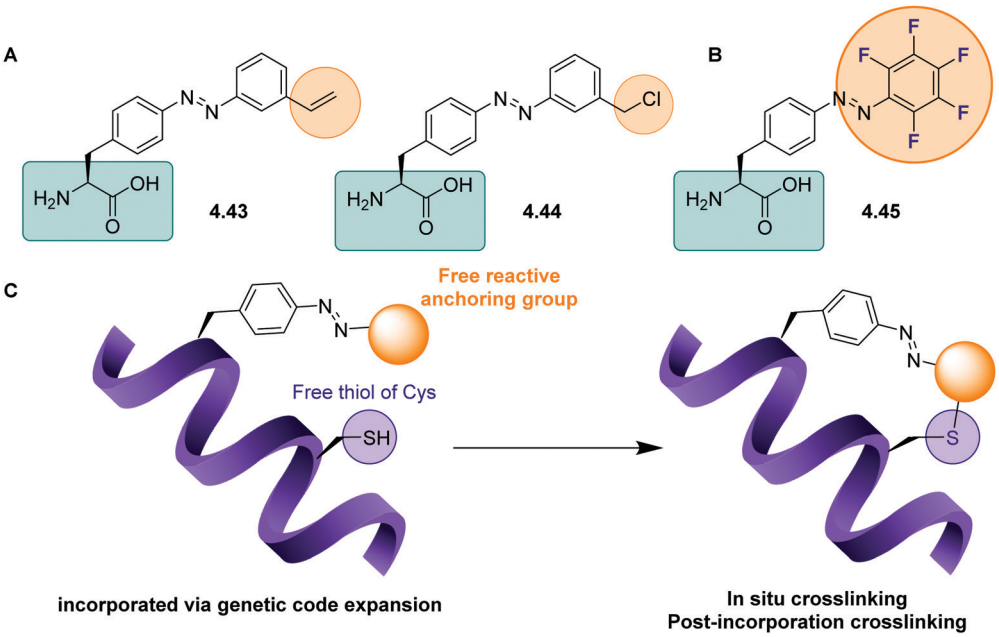

Fig. 60 Azobenzene-based amino acids with a covalent attachment point on the opposite side of the photoswitch, both controlled by UV light (A) and by visible light (B). (C) After the light responsive amino acid is incorporated into the protein, the anchoring group reacts with a free thiol moiety nearby thus crosslinking the protein.

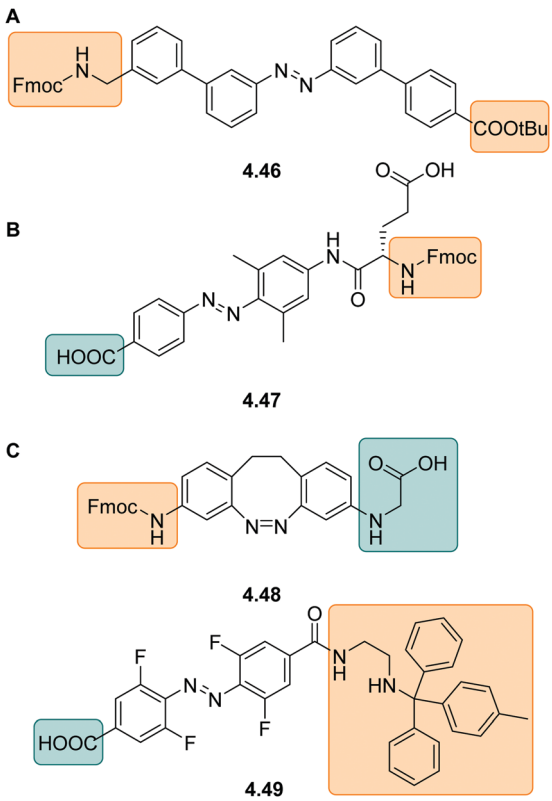

Fig. 61 Azobenzene-based amino acids for SPPS with free (amino) acid groups highlighted in green and protected ones highlighted in orange.

azobenzene core were prone to nucleophilic aromatic substitution under deprotection conditions required for Fmoc removal during SPPS procedures. Therefore, molecule **4.49** was equipped with a modified trityl group and incorporated into the peptide in solution.

Cell-penetrating peptides. For most photoswitchable short peptides synthesized by SPPS, the water-solubility enabled by the peptide chain is sufficient to use the construct in diverse applications. However, for the class of cell penetrating peptides (CPP), the delicate interplay between water-solubility, lipophilicity and polarity plays a crucial role in their activity.[685–687] CPPs are often cyclic, short peptides which are readily uptaken into cells and are further able to carry various cargo.[688,689] A major obstacle for clinical use of CPPs is that they can exhibit systemic toxicity and cause side effects due to poor selectivity and disruption of cell membranes.[690,691] For this reason, achieving activation with spatio-temporal control using light is an appealing approach. However, introduction of an aromatic, lipophilic photoswitch into the backbone of a CPP has a great influence on its cellular uptake. Hence, the modified CPP needs to compromise between solubility and lipophilicity and needs to take the impact of all isomers of a photoswitch into account.[692,693]

While in most other applications azobenzenes are frequently used, for CPPs the DTEs completely dominate the field, with only one example of a hemithioindigo analogue.[694] DTEs have proven to be the best choice due to the difference in rigidity of the two isomers which can be translated efficiently to photocontrol cellular uptake. Incorporation of a DTE into the backbone of the CPP enables formation of a hydrophobic, flexible open form that exhibits good membrane affinity. In particular, the *O*-DTE switch serves as a substitute for a β turn in the peptide sequence (Fig. 62A).[695] Upon irradiation with light and formation of the more rigid *C* isomer, the hydrophobicity

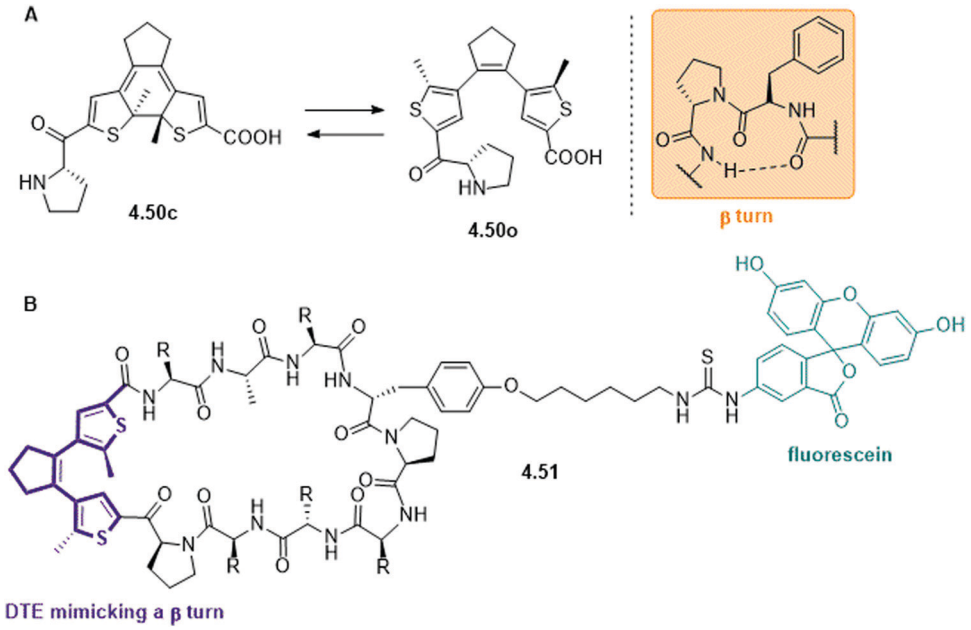

Fig. 62 The open isomer of a DTE-based amino acid was used to mimic a β-turn (A) in a cell penetrating peptide by incorporation into the cyclic peptide backbone and modified it with a fluorescein group for visualization (B). The fluorescent molecule was attached *via* a long flexible linker to not compromise the cellular permeability.

decreases and significantly deviates from the original CPP, therefore hindering cellular uptake. Additionally, the CPP was modified with fluorescein, attached *via* a long linker to minimize the effect of the large fluorescent organic molecule on permeability (Fig. 62B, **4.51**). While it was shown that CPPs can tolerate attachment of relatively large organic molecules while retaining their properties,[692] for **4.51** labeling of the peptide with the hydrophilic fluorophore decreased the cell–membrane permeability.[693] Specifically, the open isomer of DTE **4.51** had a high tendency to form aggregates which inhibited internalization.[693]

In another approach, gramicidin S (Fig. 63A), a CPP and a short cyclic peptide with strong antimicrobial properties, was used. Besides its use as an antibiotic, gramicidin S is also a potent cancer therapeutic agent. However, it exhibits systemic toxicity showing high mortality rates in mouse studies,[696,697] probably due to blood lysis.[698] To locally activate the molecule by light and potentially limit side-effects, a DTE has been incorporated into the structure of gramicidin S analogues (Fig. 63B).[699] The photoswitchable peptides **4.52** and **4.53** were studied for their antimicrobial and anticancer properties both in cells[698] and in living zebrafish embryos.[700] As **4.52** does not show significant hemolytic activity compared to other tested peptides, it suggests that hemolysis is not the major mechanism of toxicity. However, this derivative was one of the most hydrophobic ones and was poorly water-soluble, forming aggregates in aqueous solutions.[698,700] The second analogue, the gramicidin S derivative **4.53** could be further tested on an animal tumor model[701] to successfully target cancer cells in its more cytotoxic open form, while the closed form was 5.5 to 8-fold less active. In contrast to the parent compound, **4.53** was stable in blood and resistant to proteolysis *in vivo*. Moreover, introduction of light-control by the DTE minimized the toxicity *in vitro* in mice with eight times lower activity of the closed isomer. Unfortunately, in living mice, the activity of the light-responsive version **4.53** was lower than the one of parent compound (30% compared to 60–80%).[696]

4.2.2 Nucleotides. Photoswitches have been employed to modify oligonucleotides for over two decades and have found applications in chemical biology and material science. They are usually incorporated into the oligonucleotide by resin-based methodology, much as the previously described examples with peptides (see Section 4.2.1). Due to the synthetic method, water-solubility of the photoswitchable building block is not required to incorporate it into DNA or RNA. However, the highly negatively charged environment of DNA/RNA can have a significant effect on the photoresponsive capabilities of some switches, as well as their stability in aqueous solutions. An extensive review on light-controlled polynucleotides has recently been published by our group.[702] Hence, within this section only a few illustrative examples focusing on the role of water-solubility are highlighted.

Different azobenzenes have been successfully incorporated both into DNA[703,704] and RNA.[704,705] Here, the *E* isomer is able to participate in π-stacking and allows helix formation, whereas the *Z* form destabilizes the helix. Azobenzene-based nucleosides **4.54p** and **4.54m** were used to photocontrol RNA duplex formation and they readily dissolved in PBS buffer (5–7 μM, pH = 7.4) also as nucleosides up to 0.6 (**4.54p**) and 0.4 mg mL^{-1} (**4.54m**). The photochemical properties were excellent, reaching a PSD^{365nm} of 91% *Z* for **4.54p** and 88%*Z* for **4.54m** (Fig. 64)[705] and exhibiting long thermal half-lives of the *Z* isomers (97 h for **4.54p** and 113 h for **4.54m**, PBS buffer at 37 °C). However, incorporation into the RNA strands affected the thermal stability of the *Z* forms. By trend, the half-lives of the RNA-azobenzene constructs were longer than for the non-bound nucleosides (138 h for **4.54p**, 196 h and 155 h for **4.54m**, depending on the

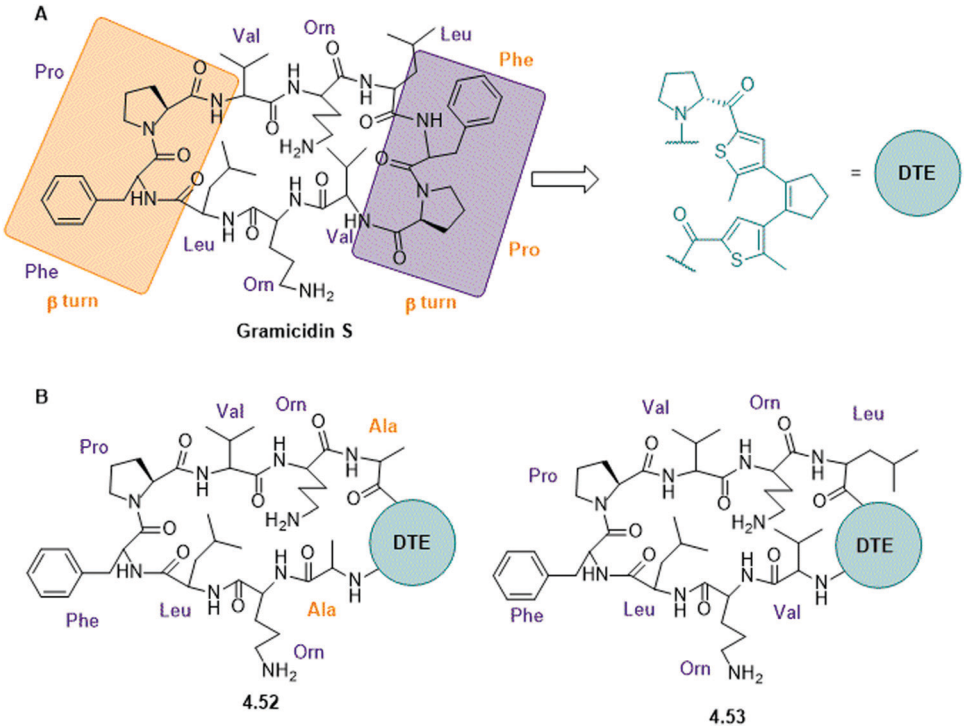

Fig. 63 (A) Gramicidin S, a cell penetrating cyclic peptide with antibiotic and anticancer properties contains two β-turns (in orange), of which one (in blue) was replaced with a photoswitchable DTE amino acid. (B) Two modified photoswitchable Gramicidin S analogues, where the amino acids shown in orange, are substituted in the original structure CPP **4.52** was the less water-soluble design due to too high hydrophobicity while **4.53** was the most successful and subsequently was tested in animal studies.

used RNA strand), except for one example, namely **4.54p**, which had a shorter thermal half-life when incorporated into RNA (86 h). This suggests that both the location and orientation of the photoswitch within the RNA strand influences the thermal relaxation rate. This finding was confirmed in a similar study, where the thermal $Z \rightarrow E$ isomerization was generally faster when the switches were incorporated into DNA compared to RNA.[704] Recently, a visible-light-controlled system has been reported, where a tetra-*ortho*-chloro azobenzene structure **4.55** was incorporated into the backbone of RNA.[706]

A photoswitchable nucleotide based on a DAE with an adenosine instead of the typical thiophene group (**4.56**, Fig. 65A) was designed to form Watson–Crick base pairs.[707] In **4.56**, very low amounts of the closed isomer could be obtained in aqueous solvents. Consequently, the design was improved by using an uracil or cytosine group instead of adenosine, as the pyrimidine-based systems could reversibly switch in aqueous environments. (Fig. 65B, **4.57-C and -U**) The photochemical properties were tested in a water/ethanol mixture (9/1) in which the compounds could be dissolved up to 300 μM. These systems showed no fatigue over several irradiation cycles (60 μM, 366 nm and visible light) and a PSD^{366nm} of 83%*C* (**4.57-U**) or 98%*C* (**4.57-C**), respectively.[708] While the closed form of **4.57-C** quickly switched to the open isomer at room temperature, **4.57-U** was stable after 60 min at 90 °C. Interestingly, after incorporation into a DNA strand the photochemical properties of **4.57-U** remained unaffected.

Spiropyrans have been widely applied as DNA intercalators (see Section 4.1), however, they are rarely being covalently attached to DNA[702,709,710] due the hydrolytic instability of many derivatives in aqueous conditions.[711] Spiropyran **4.58** (Fig. 66A) was attached to the 2′-position on a nucleotide, placing the switch in the minor groove of the DNA strand.[712] The close proximity to the DNA bases appeared to quench the triplet state involved in the photoswitching process of the spiropyran by energy or electron transfer.[712] To avoid this issue, a 6-nitrospiropyran **4.59** was designed.[450] Nucleobase analogue **4.59** was incorporated into DNA on resin and in the final construct could form up to 40% of the open merocyanine form upon irradiation. It exhibits an *S* configured C3′ as a stereogenic element providing the adequate geometry to match the helical backbone structure of DNA. As **4.59** hydrolyzed in its MC form, its analog **4.60** was synthesized to further improve the design. Its synthesis *via* the phosphoramidite route was inefficient, therefore, the reversible aldol reaction was used to substitute the aldehyde part **4.60ald** by post synthetic modification of the spiropyran while it was already attached to DNA (Fig. 66B). The surrounding DNA bases had a positive effect on the thermal stability of **MC-4.60** increasing its lifetime from a few minutes in the non-bound spiropyran unit, to more than two hours when incorporated into the oligonucleotide.[450]

4.3 Covalent attachment to biomolecules

Photoswitches have been covalently attached to different biological targets at strategically selected locations to photocontrol bioactivity and for fluorescent labeling.[634,702,713,714] For achieving photocontrol over the target biosystem, the photoresponsive molecule can: (1) act as a steric obstruction in one of is

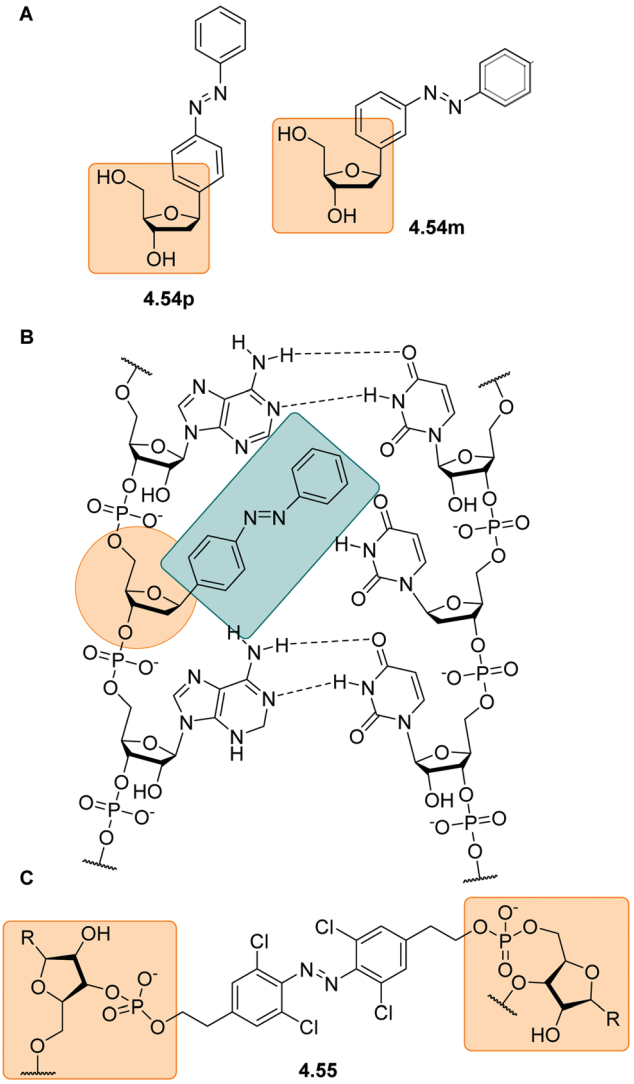

Fig. 64 (A) Azobenzene-based nucleosides **4.54p** and **4.54m** used to photocontrol RNA duplex formation and their location upon incorporation into the RNA strand (B). Visible light-responsive tetra-*ortho*-chloro substituted azobenzene **4.55** incorporated into RNA (C).

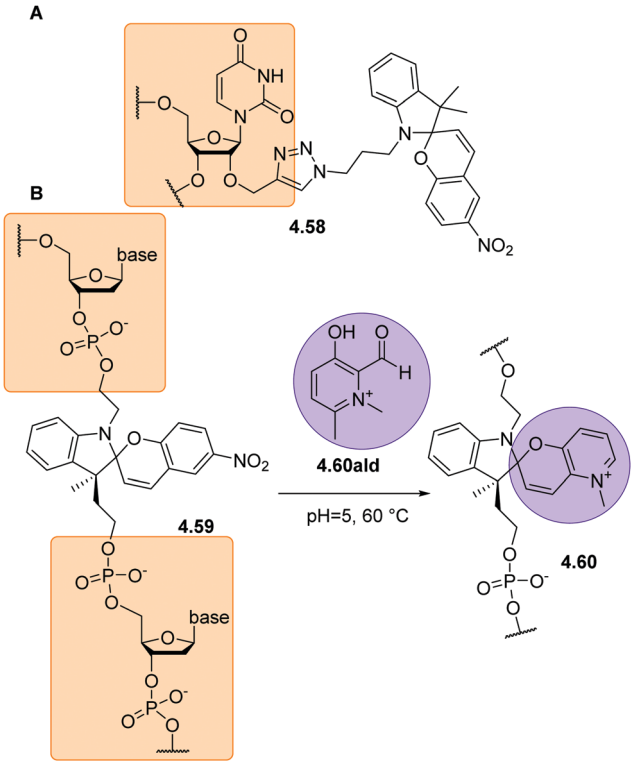

Fig. 66 (A) Spiropyran **4.58** was attached to the 2′-position on a nucleotide in the minor groove of the DNA strand, placing it too close to the DNA bases thus diminishing its photoswitching properties. The design was improved by attaching the spiropyran **4.59(B)**, which could form 40% of the open merocyanine isomer upon irradiation which was prone to hydrolysis. By utilizing the reversible aldol reaction, the aldehyde part of the photoswitch **4.59** was replaced with **4.60ald** after it was incorporated into DNA, resulting in **4.60** with improved thermal stability.

configurations; (2) have one side of the light-controlled molecule acting as a ligand, which can access the binding pocket of the biological target in only one configuration; or (3) induce a change in charge upon switching, which disturbs the activity or stability of the biological target. For some smaller systems, such as peptides obtained by solid phase peptide synthesis, the use of organic solvents to introduce modifications is often customary and it permits attachment of water-insoluble organic molecules (see Section 4.2).[662] However, larger and more complex biomolecules are more sensitive to environmental conditions.[715–718] Hence, aqueous solubility of the label becomes of key importance, as too high amounts of organic co-solvent can potentially unfold, inactivate or even destroy the target (biomacro)

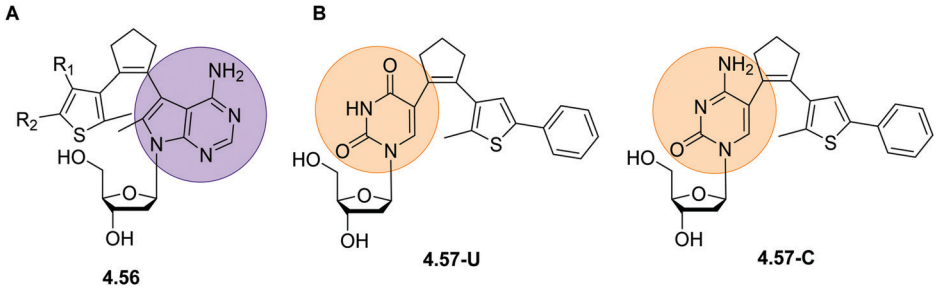

Fig. 65 Photoswitchable nucleotides with an incorporated DEA switch. DEA **4.56** (A) with an adenosine did not undergo efficient cyclization reaction in water, while the uracil (**4.57-U**) and the cytosine (**4.57-C**)-based DEA nucleotides had favorable properties in aqueous solutions.

molecule.[715,719–721] Moreover, covalent attachment of a photoswitch should not cause aggregation of the modified target. Finally, for labelling or application of the modified biomolecule *in cellulo* or *in vivo*, (partial) insolubility, aggregation and the use of organic co-solvent are not tolerated.

Over the past decades, an extensive toolbox of methods for covalent attachment of small organic molecules to various proteins, has been developed. Labeling can be performed in both random and highly specific ways, depending on the application requirements.[722,723] Typical chemical methods, which were also successfully used to attach photoswitches, are trapping of natural or artificially introduced cysteine side-chains with α-halogen-acetyl or maleimide functions,[724] reactions of lysine residues or the N-terminus of peptides with different reactive groups such as indoles or activated NHS esters,[725–727] (photo)click reactions on biomolecules pre-functionalized with an alkyne or azide unit or the Staudinger–Bertozzi ligation,[728,729] among others. Except for chemical modifications, there are various enzymatic labeling techniques available such as sequence recognition-based sortase A ligation, subtiligase that catalyzes formation of peptide bonds, or different transferases, ligases and oxidoreductases.[730–732]

Having chosen the appropriate covalent attachment strategy, a suitable location where the photoswitch will be placed has to be selected. For single covalent attachment, the site the photoswitch will be placed is of great importance because the structural change of the switch must directly interfere with the target's activity. In contrast, for crosslinkers, the general strategy to employ the switch is to reversibly disrupt and/or stabilize the secondary structure of the target protein (*vide infra*).

4.3.1 Single-point attachment. For single-point, covalent attachment, a suitable location for the introduction of the photoswitch needs to be selected, so that the geometrical and electronic changes evoked upon photoswitching can be used to interfere with the function of the target in a light-dependent manner. Such locations could be, for instance, close to a ligand-binding pocket, or at a protein–protein, or protein-membrane interface. (see Fig. 67). In the following section, we discuss different scenarios in which covalent attachment of a photoswitchable pendant was used to enable light-control over biological properties and focus the role of the pendant's solubility in biologically relevant media.

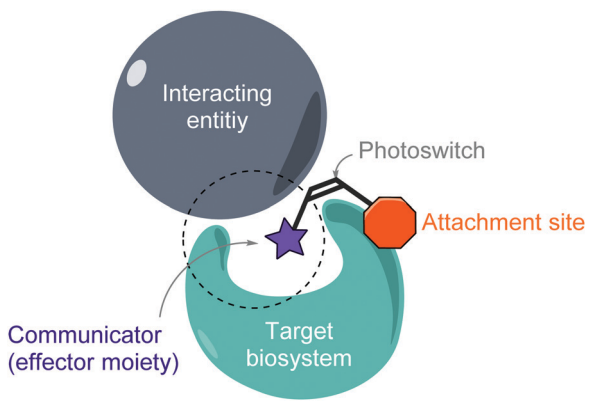

Fig. 67 Schematic representation of the role of the photoswitch when interfering with the target biosystem itself, or its interaction with another entity (neurotransmitter molecule, small biomolecule interacting, bacterial cell, *etc.*).

4.3.2 Controlling interactions between biomolecules. Covalent attachment of light-responsive organic molecules to complex biological targets is challenging, as it is requires solubility of the label in a medium where the biomolecule is stable. An illustrative example is the functionalization of a pore-forming toxin, Fragaceatoxin C (FraC). FraC is a predatory protein that lyses cells by forming perforations in the lipid bilayers, through sequential binding to the cell membrane, unfolding, and forming multimeric pores, causing leakage of cellular content (Fig. 68A).[733] Directing the cell lysing activity of FraC to specific targets, such as cancer cells, required the introduction of an external biorthogonal control element. Consequently, a molecular photoswitch was attached at strategically selected locations to employ light as external stimulus. Specifically, the azobenzene substitutes a sphingomyelin molecule which plays an important role in stabilization of the pore and hence constitutes a crucial design element.[734] However, of the four azobenzenes pendants considered in the study (Fig. 68A) only the two water-soluble molecules carrying a sulfonate (**4.61c**) and a trimethylammonium group (**4.61d**) could be successfully attached to the FraC toxin. Functionalization with uncharged azobenzenes **4.61a** and **4.61b** turned out to be not feasible at the conditions at which the protein was stable, limiting the scope of labels. The remaining two candidates were selectively attached to FraC *via* the thiol group of the genetically introduced cysteine side chains, using a chloroacetyl handle. The switch was positioned at locations crucial for binding of FraC to the lipid bilayer of the prey cell to directly interfere with the nanopore assembly in the membrane (Fig. 68A). Both FraC-azobenzene conjugates showed activity, with **4.61c** being the more active one. The photoisomerization of the bioconjugate was unrestrained and, interestingly, the thermal half-life of *Z*-**4.61c** attached to a Cys of the toxin was nine times longer than of the free **4.61c** molecule.[734,735] The label prohibited lysis activity in the *E* form presumably by blocking either the protein's insertion into the lipid bilayer or the formation of a mature pore (Fig. 68A). Upon irradiation with λ = 365 nm light, photochemical $E \rightarrow Z$ isomerization of the label was induced ($PSD^{E\rightarrow Z}$ (λ = 365 nm) = 5 : 95, DMSO). The formed *Z* isomer did no longer hinder the activity of FraC enabling successful lysis of blood as well as cancer cells selectively upon irradiation.

Alternatively, azobenzene-based pendants can be used to control cell–cell interactions. Also in this example, the water-solubility of the photoswitch-labels is crucial, since labeling takes place *in vivo*. Within a living organism, insolubility of the organic molecule can cause aggregation of the bioconjugate, exhibiting fatal toxicity for the living organism.[55,736] In this context, the surface of human cells was equipped with azide-handles by metabolic oligosaccharide engineering (Fig. 68B).[737] These handles served as an attachment point for glycosylated azobenzene **4.62** *via* its alkyne moiety, in a copper-catalyzed click-reaction.[737] (Fig. 68B).[738] Azobenzene **4.62** readily dissolved in buffer, due to the presence of the mannoside and thus allowed for the click reaction to efficiently proceed in the

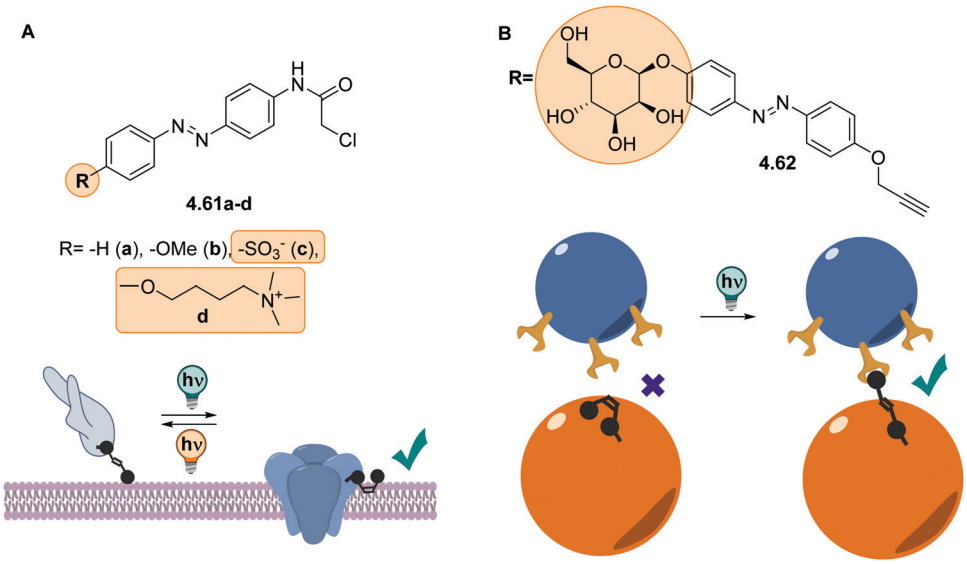

Fig. 68 (A) Azobenzene photoswitches with water-solubilizing groups (**4.61c and d**) were successfully used to photocontrol nanopore assembly of the FraC toxin. (B) Azobenzene **4.62**, carrying a mannoside group, was incorporated onto the surface of human cells; the *Z* isomer did not allow bacterial adhesion, while the elongated *E* isomer enabled it.

cell medium and for successful labeling of the living human cells. The sugar unit also carried a functional role for cell–cell interaction with *E. coli* cells *via* lectin (compound **4.62** in Fig. 68B). If the photoswitch is in its *Z* form after irradiation with UV light, the mannoside is sterically not accessible for bacteria, which in turn cannot bind to the human cell (see Fig. 68B). Upon irradiation with 488 nm light, the *E* isomer is recovered, and its straight geometry presents the sugar moiety that now points away from the human cell membrane allowing bacterial adhesion. The aim of this fundamental study was to elucidate the mechanism of cell-to-cell interactions by a light-responsive tool and to further increase the understanding of bacterial adhesion to human cells. The photophysical properties of **4.62** were only reported in DMSO, showing high PSDs ($PSD^{E\rightarrow Z}$ (λ = 365 nm) >90% *Z*) and long thermal half-lives of the metastable isomer (>30 h).[737]

4.3.3 Controlling channels and receptors. Often the addition of charged groups has dual role: functionality and water-solubility. Functionalization with charged groups can solubilize the organic compound in water, but simultaneously, the charged species can lead to selective uptake to specific cellular compartments or trigger a biological response (see also Section 4.1. non-covalent modulators).[538,539,541,542] For instance, light-controlled protein channels can be designed in such a way. Protein channels and receptors are natively present in membranes and are involved in cellular transport between cells or organelles.[562,739] In principle, their action can be controlled with non-covalently attached, light-responsive small molecules, acting on proteins and other biomolecules as discussed in Section 4.1. However, in those cases, the small molecules readily diffuse away from the binding sites making them less available, especially for rapid biological processes. Thus, it is beneficial to covalently attach the photoswitch to the target protein close to the binding pocket thereby increasing its local availability.

4.3.2.1 Photoswitchable labels generating a charge upon switching. In an illustrative example a spiropyran switch, that photoisomerizes to the charged merocyanine form was used to control the mechano-selective channel of large conductance (MscL) with light.[740] MscL is a channel protein in the bacterial membrane serving as a safety valve that opens upon increased pressure in the cell.[741] It was reported that introduction of charged groups inside the hydrophobic pore causes the channel to be permanently open.[742] Thus, attaching a spiropyran photoswitch that can be reversibly toggled between uncharged and a charged form by irradiation with light results in photo-controlled opening and closing of the channel (compound **4.63**, Fig. 69A).[740] Not only the charge repulsion forces the channel to open, but also the hydrophilicity of the cavity is enhanced, thus attracting water into the channel. Five photoswitchable labels were attached to the channel protein *via* a halo acetyl moiety connected to a cysteine side chain introduced (using genetic modification) and precisely positioned in the constriction zone of the protein channel. Sufficient solubility of the functionalized photoswitch was achieved by treating the matrix-bound MscL protein with a solution of **4.63** in water, using 20% DMSO as organic cosolvent. In this example, the presence of co-solvent was tolerated due to the stability of the protein and the labelling being performed while the MscL was bound *via* histidine tag to the Nickel column.[740,743] The **4.63**-modified MscL channel was also incorporated into liposomal vesicles for on demand light-triggered drug delivery.[743] The protein channel remained closed in the dark and upon irradiation with UV light the channel opened due to the formation of the charged merocyanine **4.63m**.

Though the use of spiropyran photoswitches as a masked charge carriers to photocontrol membrane channels is a very elegant approach, it is not frequently used. This might be due to the fact that it is responsive to multiple stimuli in addition to light, such as pH and heat (see Section 3.4.2), which makes spiropyrans less controllable than other switches, like azobenzenes.

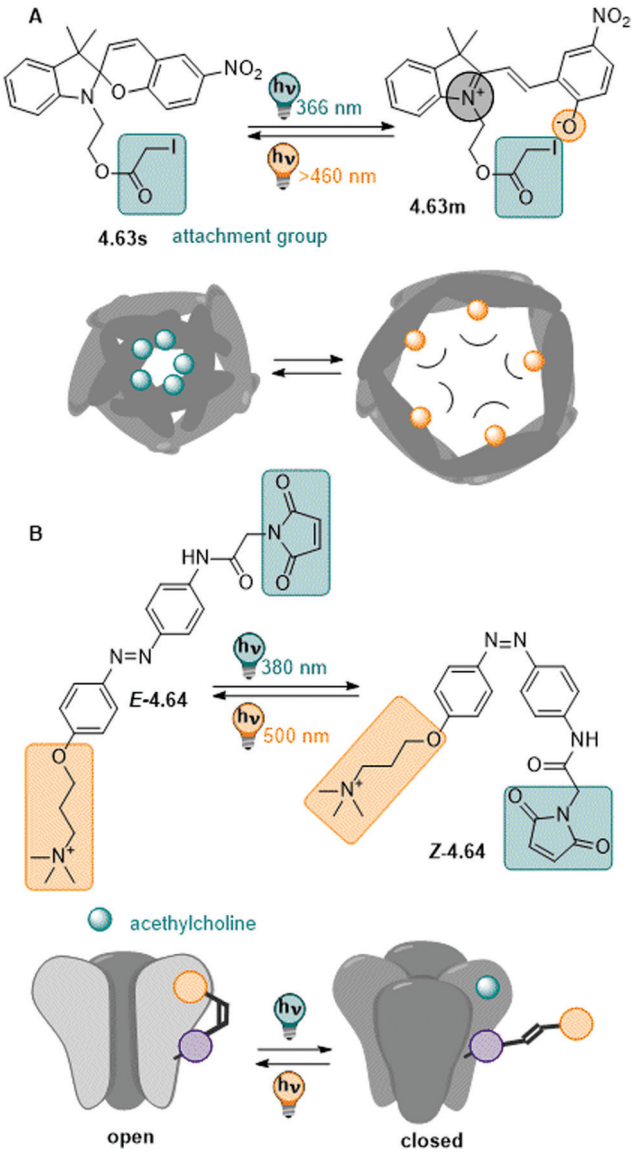

Fig. 69 (A) Five spiropyran **4.63** units covalently attached to the MscL channel. Upon photoisomerization the charged merocyanine isomers force the channel to open, while the uncharged isomer **4.63** allows the channel to remain closed. (B) Azobenzene carrying a homocholine group was attached to the ligand-gated channel nAChR in the *Z* orientation preventing the binding of the natural ligand acethylcholine and leaving the channel open. Upon irradiation with 380 nm light the *E* isomer does not block the binding site of acethylcholine resulting in closure of the channel.

However, its unique switching of polarity/charge, together with inverse photochromism in the visible range, make spiropyran a valuable photoswitchable label and control element.

4.3.2.2 Photoswitchable labels functionalized with ligands. Ligand-gated channels have been a target for covalent single-point attachment of photoswitches for decades and this methodology is now established as the most frequently used strategy when using photoswitches as covalent label.[744] The first attempt was already reported in the 1980s, where a reduced disulfide bridge was alkylated with a bromomethyl-azobenzene.[745] Since then, this strategy was further developed, employing various photoswitches decorated with different bioactive moieties, such as the positively charged tri-alkylammonium group. Especially, the cysteine thiol-maleimide reaction has been used to introduce various azobenzenes with specific binder moieties attached to the photoswitch. In this manner, light-responsive ligand-gated channels, such as the G protein-coupled dopamine receptor,[746] the gamma-aminobutyric acid (GABAa) receptor,[747] and ionotropic glutamate receptors, which feature a glutamate-modified azobenzene, have been developed.[748–753]

Another successful application in this context is the photocontrol of neuronal nicotinic acetylcholine receptors (nAChRs).[754] The nAChRs are ligand-gated channels present in the mammalian nervous system, that are presumably involved in nicotine addiction and various psychiatric disorders.[755] To regulate these channels with light, azobenzene-pendants bearing a positively charged homocholine moiety were designed (Fig. 69B, compound **4.64**).[756] Homocholine acts as agonist towards nAChRs and competes with the naturally present neurotransmitter acetylcholine, which contains a trimethylammonium group as binding motif.[757] The *E* form of the antagonist **4.64** does not occupy the binding pocket, therefore allowing the naturally present neurotransmitter acetylcholine to bind and activate nAChR.[754] Upon irradiation, the homocholine moiety of the formed *Z* isomer blocks the binding pocket, causing inhibition of nAChR. Herein, the homocholine carries a dual role, both acting as an antagonist of nAChR and as a water-solubilizing group for photoswitch **4.64**. Moreover, due to its aqueous solubility, azobenzene **4.64** could be successfully applied *in vivo* where it was incorporated into the specific reward system region of the mouse brain. Here, viral transfection was used to introduce the cysteine mutant of nAChR *in vivo*, which was subsequently labeled with **4.64**.[758]

Though compound **4.64** could be used for initial studies in mice, photoisomerization required illumination with UV light. As this is damaging for tissue and has limited penetration depth, researchers strive to find better solutions in the long-term moving to photoactuators responsive to visible and NIR.[195,215,537,759,760] A great challenge in this context is to redesign photoswitches or modify them in a suitable manner while retaining the necessary water-solubility as showcased in the following example.

A strategy to circumvent UV light, is to use near-infrared light two-photon (2p) excitation to induce $E \rightarrow Z$ isomerization.[761,762] The first reported maleimide-azobenzene-glutamate probes (**4.65**, Fig. 70A) themselves had a very limited response to two-photon excitation.[763] To improve this, a 2p absorbing antennae, namely a naphthalene or pyrene moiety, respectively, was attached (Fig. 70B), compounds **4.66a** and **4.66b**.[763] The large aromatic antennae rendered the whole assembly poorly water-soluble, impairing both the efficient attachment to the protein and the binding to the glutamate receptor.[763,764] Consequently, the antenna strategy was not perused further. Instead, an electronically asymmetric azobenzene core was designed recently, which was reported to be a more efficient 2p absorbing variant of **4.64**.[765] This structure, bearing an electron-donating group at the *para*, as well as fluoro substituents in *ortho* positions, significantly enhanced the 2p absorption

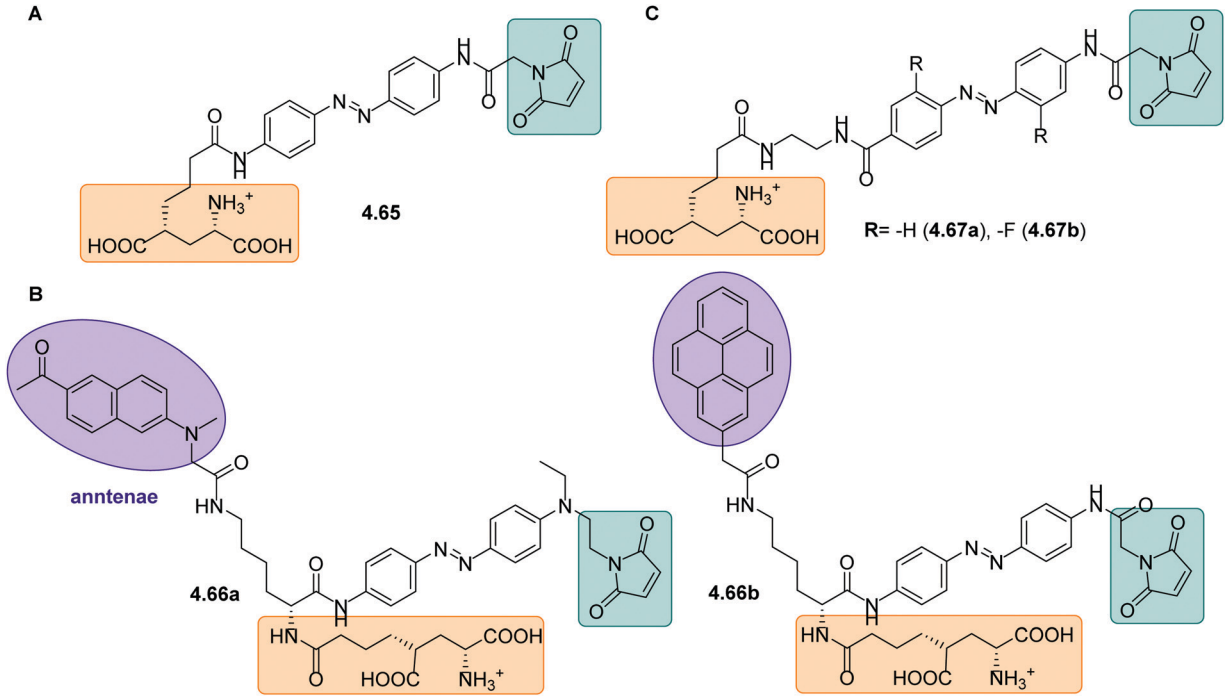

Fig. 70 The maleimide-azobenzene-glutamate probe which can undergo two-photon (2p) excitation thus enabling photoswitching with near-infrared light, **4.65**, had a limited response to two-photon excitation (A). Therefore, 2p absorbing antennae were introduced to the design by incorporating naphthalene (**4.66a**) or pyrene (**4.66b**) groups (B). However, the large aromatic antennae drastically reduced the water-solubility of the constructs leading to the design of **4.67** (C). Azobenzene **4.67b** contains an electron-donating group at the *para* position and fluoro substituents in *ortho* position which significantly enhance the 2p absorption.

(Fig. 70C, structures **4.67a** *vs.* **4.67b**). Avoiding the necessity for including insoluble aromatic antennae in their structure, these probes could be covalently attached to the receptor in sufficient yields.[765] They showed thermal isomerization half-lives of around 10 min in aqueous conditions (1% DMSO in PBS buffer). The new probes **4.67a and b** could activate the ionotropic glutamate receptor reversibly and, in contrast to the previous designs, allowed studies both in mature neurons *in vitro* as well as *in vivo* in *C. elegans* due to the enhanced water-solubility.

4.3.4 Covalent attachment to antibodies for super-resolution microscopy. The resolution limitation of conventional microscopy is caused by the diffraction limit in correlation with the wave nature of light.[766] Hence, the threshold of classical microscopes is around 250 nm resolution in the lateral or 500 nm in axial resolution, both for visible light.[766] Super-resolution microscopy techniques enable surpassing the diffraction limit by, for example, utilizing photoswitchable fluorescent molecules. This is the case in single molecule-localization microscopy (SMLM), which gives improved resolution (20–30 nm for lateral and 50–60 nm for axial resolution).[767] SMLM takes advantage of photoswitching, or blinking, of the fluorescence, and relies on acquiring a large set of images, each with low resolution of the fluorophore location, gradually leading to a high-resolution image upon signal overlay. Next to fluorescent proteins and quantum dots, organic dyes, such as cyanine (Fig. 71A, **4.68**)[768,769] and rhodamine dyes (Fig. 71B, **4.69**),[770,771] have been used as photoswitchable fluorophores. Cyanines can reversibly switch from the fluorescent (**4.68a**) to the dark state (**4.68b**) through numerous cycles in the presence of primary thiol-containing reducing agents (RA), which add to the excited state of the cyanine dye (Fig. 71A, **4.68b**).[768,769] Furthermore, functionalized rhodamine dyes reversibly alter their fluorescence between on (and off) upon switching between the open and closed forms. The fluorescent zwitterionic **4.69b** form and the colorless lactone **4.69a** are displayed in Fig. 71B as an example.[770,771]

Besides cyanines, rhodamines and spyropirans, DTE switches have been successfully applied to super-resolution spectroscopy. DTEs are known for their high thermal stability of both the open and closed-ring states, as well as for their good fatigue resistance enduring numerous switching cycles (see Section 3.3.1).[331] These properties make DTEs applicable for high-resolution fluorescence microscopy, such as reversible saturable optical linear fluorescence transitions (RESOLFT), where switchable fluorescent probes are required for consecutive activation/deactivation by short laser pulses[772–775] However, the main obstacle for using DTEs in bioimaging is their intrinsically hydrophobic core, which renders them insoluble in water. Despite various attempts to suitably functionalize DTEs, it has been challenging to obtain fully water-soluble switches.[774] Introduction of sulfonates[774] or sugar moieties[776–778] and incorporation of PEG chains proved insufficient[779] to reach this goal. While the PEGylated DTEs were soluble in water, they were unstable in aqueous media and tended to self-associate, which led to fluorescence quenching.[779,780] Furthermore, attachment of the lipophilic DTE to a protein to acquire solubility through the target does still not provide full water-solubility, and significant amounts of co-solvents

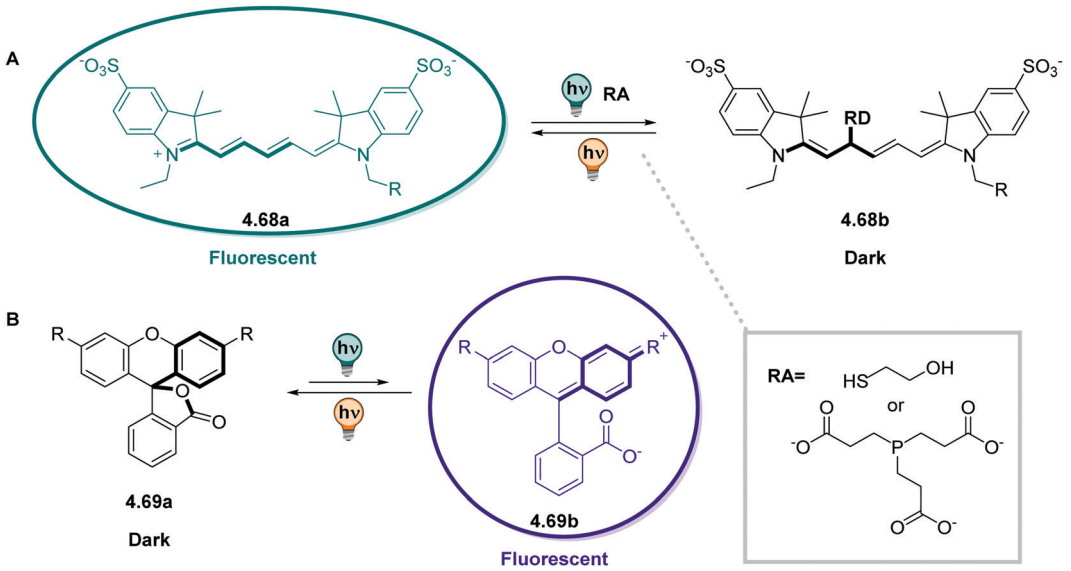

Fig. 71 Fluorescence photoswitching for super-resolution microscopy. (A) Fluorescence switching of cyanine dyes in the presence of primary thiol-based reducing agents or TCEP; (B) fluorescence switching in functionalized rhodamine dyes which undergo a reversible transition from open to closed form (and *vice versa*) from the fluorescent zwitterionic form to the dark lactone.

(30% EtOH in water) are needed as shown for fluorescence probe **4.70** (Fig. 72A).[781]

More recently, DTE derivatives containing benzothiophene dioxide groups with perfluorocyclopentene as the bridging unit were decorated with carboxylic acid moieties to enable water-solubility (Fig. 72B, **4.71** and **4.72**).[371] These compounds are highly fluorescent in the ring-closed and non-fluorescent in the ring-open isomer.[782] DTEs **4.71** and **4.72** can be dissolved in an aqueous buffer in up to micromolar concentration, without the need for the addition of cosolvent. Both switches retained their photochromic properties in water, such as reversible switching with UV and visible light over numerous cycles. However, fluorescence QYs decreased and emission lifetimes were shortened by *ca.* 20–30%, compared to those in organic media.[371] For covalent attachment to free lysine residues of a secondary antibody, one of the acid moieties on the DTE was converted to an NHS ester.[201] The most abundant antibody type, immunoglobulin G (IgG) regularly features around 16 lysine amino acids exposed to the solvent and available for modification.[783] Therefore mouse-specific secondary antibodies, which are antibodies that bind to all other antibodies produced by mice, were labeled with DTEs **4.71** and **4.72** and used in RESOLFT microscopy imaging of tubulin filaments and nucleopore complexes.[784] Even though the DTE switches could be successfully applied for RESOLFT methods, single-molecule localization microscopy (SMLM) could not yet be achieved with compounds **4.71** and **4.72**.[785] For SMLM, the 'blinking' fluorophores require a very high fluorescence QYs, high brightness, and an efficient ring-closure reaction to efficiently switch off the fluorescence. To increase the electronic push–pull character between the bridging unit and the aryl rings, electron-donating groups, *i.e. para*-methoxy substituents in the phenyl moiety (**4.73** and **4.74** in Fig. 72B), were introduced to improve the photophysical properties of the dyes. The probes were successfully attached to secondary antibodies *via* the NHS ester attachment strategy and applied to obtain clear STORM images of tubulin and vimentin structures *in cellulo*.[655] This development demonstrated how optimizing the water-solubility of a given photoswitch, together with fine-tuning its photophysical properties, lead to the rapid development of a highly efficient dye for fluorescent imaging of living cells with super-resolution microscopy.

4.3.5 Photoswitches used for two-point attachment (crosslinkers). Photoswitches used as crosslinkers have two reactive groups, one on each side of the molecule, that can form two covalent bonds with the biological target molecule.[713,786] As a photoswitch-crosslinker staples or bridges two attachment points of the same target, the conformational change of the switch upon irradiation has a tremendous impact on the three-dimensional structure of the crosslinked system. Azobenzenes largely dominate the field of photoswitchable crosslinkers, but have, to the best of our knowledge, so far only been reported for proteins and peptides.[634,786] The success of azobenzene-crosslinkers is due to their large conformational change affecting their end-to-end distance, their accessible synthesis, tunability of properties, and proper functioning in aqueous conditions. Fewer reports involve the application of DAEs to staple proteins, for instance, to photocontrol destabilization of an α helix[787] and to control protein–protein interactions *via* small peptides.[788] However, in the second study[788] the experiments were performed under argon to avoid side-product formation as the presence of oxygen caused rapid oxidative degradation of the DAE-peptide constructs.

Since the photoswitch is often attached to a comparably large water-soluble protein, in most cases the solubility of the biomolecule is enough to dissolve the construct. Thus, lipophilic crosslinkers can be used, as long as the protein can tolerate the

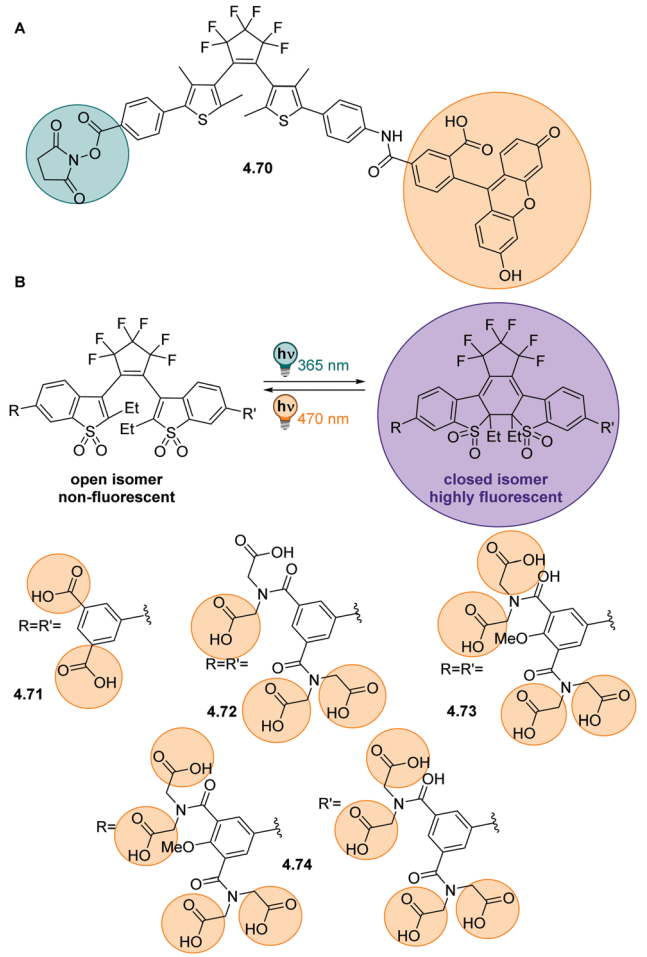

Fig. 72 DTE fluorescent probes are lipophilic molecules that require significant amounts of co-solvents during attachment to the target protein (30% EtOH in water for **4.70**). DTE derivatives containing benzothiophene dioxide groups with perfluorocyclopentene as the bridging unit were decorated with carboxylic acid moieties to enable sufficient water-solubility (B). Multiple carboxylated probes were sufficiently soluble for application in *in celullo* STORM fluorescence imaging.

required amounts of organic co-solvent.[254,789] The latter is very target-dependent and, unfortunately, not feasible for some proteins. In these cases, water-soluble photoswitches need to be applied to avoid, for instance, aggregation of the construct.

4.3.5.1 Water-insoluble switches. Hydrophobic azobenzene switches, like the frequently used **4.75** (Fig. 73A), could be attached to different model peptides and proteins, and the target itself was usually able to ensure water-solubility of the whole construct.[49,790–793] However, in other examples, such as for collagen peptides, the protein's water-solubility was not sufficient to solubilize the labelled target.[794,795] Consequently, organic co-solvents were added to achieve photocontrol of folding of the triple helical structure employing an azobenzene crosslinker carrying alkyne bridges (**4.76**, Fig. 73B).[794,795]

In another study, the reversible (de)stabilization of an α helical cell-penetrating peptide (CPP) was achieved by the simple azobenzene crosslinker **4.75a** described above. (Fig. 73A).[796] In the *E* form, the α helix was disrupted, and the internalization was prevented, while the *Z* isomer allowed the peptide to from the α helix. While in many biological applications, the aggregation of the modified protein can cause toxicity, in this work the formation of different sizes of aggregates was used to study internalization of the CPP into HeLa cells. Strikingly, the *Z* isomer formed much larger aggregates (300 nm size) compared to the *E* isomer (1.5 nm) which indicates that the internalization mechanism of the two isomers is different due to aggregate formation.[796]

The attachment of a photoswitchable crosslinker does not only affect the properties of the target molecules, but mutually influences the properties of the label (similar observations have also been made for non-covalent binders, see Section 4.2). To study the effect of the secondary protein structure on the photochemical properties of the photoswitch (Fig. 73C), azobenzene crosslinker **4.75b** was covalently attached to both a model α helix peptide (**4.77a and b**) and furnished with two glutathione moieties on both ends (**4.78**).[797] The glutathione-functionalized derivative cannot form an α helix and served as a control. The constructs were studied in aqueous conditions (20 μM in 10 mM sodium phosphate at pH 7, 25 °C) regarding both their photochemical and thermodynamic properties. The quantum yield of the $Z \rightarrow E$ isomerization of the α helix-bound azobenzene **4.77** was higher than the control **4.78** (Φ = 0.49 compared to 0.38), while the value for $E \rightarrow$ Z was similar (Φ = 0.1 compared to 0.12). Furthermore, the thermal half-lives of *Z*-azobenzenes bound to an α helix were longer than the *Z*-glutathione-azobenzene construct **4.78** ($t_{1/2}$ = 26.7 compared to 11.5 min at 25 °C), presumably due to an enforced rotational mechanism caused by the constrains of the covalently linked protein.

While in classical azobenzenes the planar *E* isomer can lead to aggregation due to π–π stacking,[798] tetra-*ortho* substituted derivatives do not show the same tendency, since the steric clash of the *ortho* substituents leads to a slightly twisted conformation in the *E* form. Moreover, they can be efficiently operated with biocompatible visible light in both directions. However, for tetra-*ortho*-methoxy substituted derivatives, the compounds were found to degrade in the presence of glutathione.[199] Diazocines, on the other hand, are stable under these conditions and also have a non-planar conformation in both isomeric forms thus preventing aggregation. Hence, they are a valid alternative to build visible-light responsive crosslinkers. Consequently, diazocine crosslinker **4.79** was recently used to staple the α helix in a Trp-cage protein, where the shorter *Z* isomer allowed formation of the Trp fold and the extended *E* isomer destabilized it.[799]

While diazocines generally reach very high PSD in organic solvents, with more than 90% of the metastable *E*, it was observed in other studies that in water the PSD values drop significantly to 16–60% depending on the derivative.[215,800] For diazocine **4.79** the PSD^{385nm} was 46 : 54 = *E* : *Z* and the half-life of the *E* form was 6.2 h (0.5 mM in 10% D_2O in water, pH = 5.5, at room temperature).

4.3.5.2 Water-soluble switches. Application of water-soluble photoswitches extended the substrate scope for photoresponsive

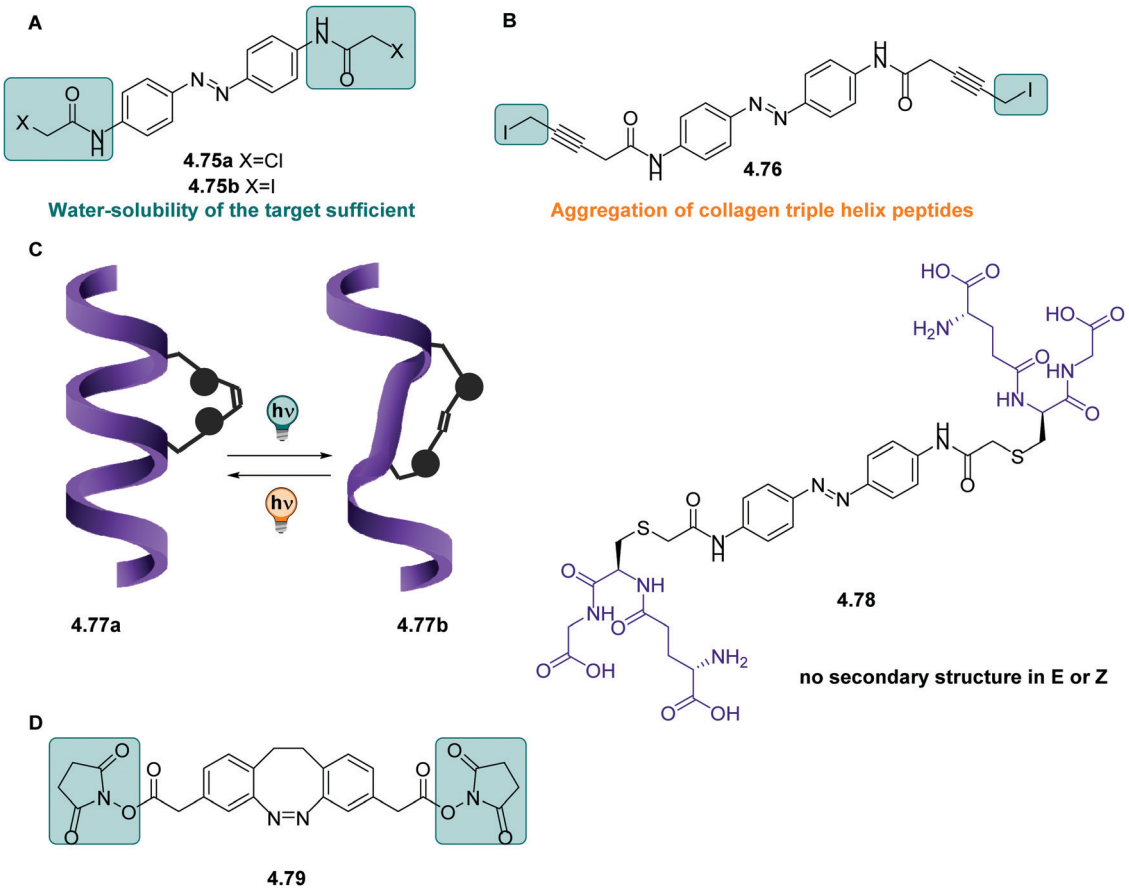

Fig. 73 While for many applications the hydrophobic azobenzene crosslinker **4.75** could be successfully applied as the target itself ensured water-solubility of the crosslinker-protein construct (A), for other examples, such as the collagen peptides with photoswitch **4.76**, the resulting crosslinked biomolecule aggregated due to insufficient aqueous solubility (B). The *Z* isomer of azobenzene **4.77** allowed retention of the secondary structure of the α helical cell-penetrating peptide upon crosslinking, while the *E* isomer disrupted the secondary structure (C). The *Z* isomer of the diazocine **4.79** allowed formation of the Trp fold, while the extended *E* isomer destabilized it.

crosslinkers by enabling the two-point labeling of sensitive targets which do not tolerate organic cosolvents.[789,801] In particular, the water-soluble sulfonated azobenzene **4.80**[802,803] (Fig. 74) has been successfully applied to crosslink numerous targets, such as peptides involved in protein–protein interactions,[804–806] transcription factors,[807] complex targets like clathrin adhesion proteins,[808] and have even been applied *in vivo* in zebrafish studies.[535] The sulfonate moieties were placed in *meta* position to the azo bond to allow for water-solubility without interfering with the photochemical properties of the azobenzene.[809] However, they have been shown to influence or even inhibit cellular uptake of the modified target.[807,810]

To crosslink over larger distances, azobenzene **4.80** has been extended with a biphenyl group (**4.81**) or alkyne linkages (**4.82**).[809,811] Both modifications increased the lipophilicity of the molecules significantly so that the azobenzenes were insoluble in water without the presence of the sulfonate groups, emphasizing key elements required for waterborne crosslinking (Fig. 74).[809,811]

To move from UV-light to visible-light responsive azobenzenes, tetra-*ortho*-methoxy azobenzene **4.83**, containing an azonium bond, was developed. Protonated azobenzenes form an intramolecular H-bond between a protonated nitrogen of the azo bond and the neighboring oxygen of the methoxy group in the *E* form more readily than in the *Z* form.[812,813]

The switch was used to crosslink fynomers, small antibody mimetics[812] and could be isomerized upon irradiation with 633 nm light while being bound to the protein. The thermal half-lives of the *Z* isomers were in the range of seconds ($t_{1/2}$ = 2–9 s) for most targets, except for one example. Here, the protein environment at the attachment site was positively charged, forcing the azobenzene to deprotonate to the neutral state and as a consequence significantly elongating the half-life (from 7.2 s to ~100 s). Hence, azonium-based azobenzenes are an interesting system in which the protein environment at the attachment location can be adjusted to modify the half-life of the switch.

Next to the sulfonate group, carbohydrate moieties have been used to ensure water-solubility. They were attached on each side of the photoswitch and carried a reactive group, such as chloroacetyl, allyl, propargyl or azide, for attachment to a target (Fig. 75, **4.84–88**).[814,815] The advantage of using glycoconjugates of azobenzenes is their biocompatibility, high water-solubility, and possibility of attaching the reactive handle at various positions onto the carbohydrate moiety.

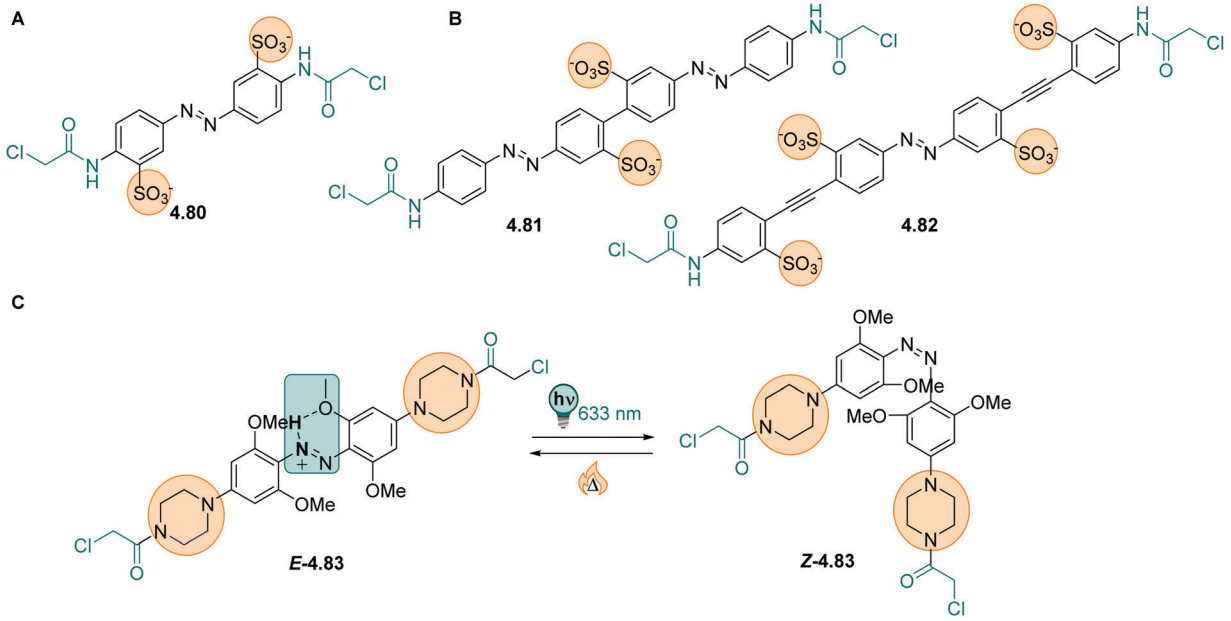

Fig. 74 Water-soluble crosslinkers. (A) Sulfonated azobenzene **4.80** has been successfully applied to crosslink numerous targets and was subsequently multiplied and elongated in designs **4.81** and **4.82** to achieve larger end-to-end distance change upon switching (B). The azonium-based azobenzene **4.83** with tetra-*ortho*-methoxy substituents can be switched with 633 nm light and has a protonated nitrogen atom which forms a stabilizing hydrogen bond with the adjacent methoxy group only in the *E* isomer.

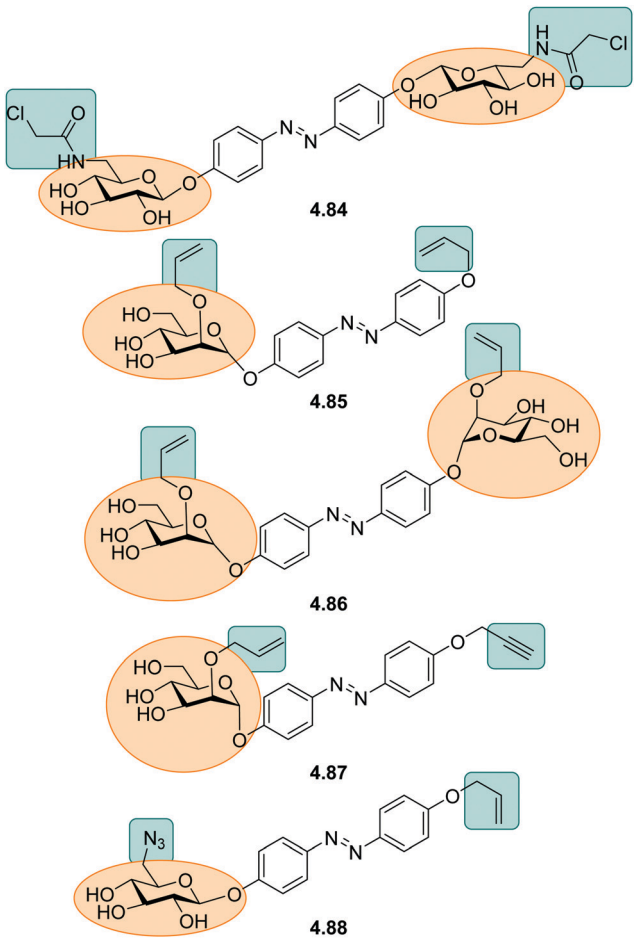

Fig. 75 Azobenzene photoswitches modified with carbohydrate moieties to ensure water-solubility. The sugar groups have one or two reactive handles at various positions for attachment to a target.

5 Conclusion

Over the past decades, light responsive molecules have taken the spotlight as a powerful tool to manipulate and interfere with numerous (bio) molecular systems and materials both in organic and aqueous media. However, photoswitches are inherently lipophilic organic molecules and thus naturally poorly soluble or insoluble water. Solubility of organic molecules in the "universal solvent of life" is of critical importance, especially for biological and medicinal applications most prominently seen in photopharmacology, as its absence can compromise bioavailability, resulting in aggregation or even toxicity.

As with other organic molecules, photoswitches can be solubilized using different approaches, the development of which is mainly driven by the pharmacological field (Section 2.2). Common solubilization approaches, including the attachment of charged and non-charged polar moieties, or the conversion of acids and bases into their respective salts (Sections 2.2.1 and 2.2.2), are also applied in the context of photoswitches. Other methods, such as distorting the planarity of flat molecules, designing unsymmetrical structures or the functionalization with a cleavable solubilizing group (prodrug strategy, see Section 4.1.2), are less frequently used to solubilize light-responsive molecules.

However, even after the photoswitch has been successfully solubilized in water, this polar protic solvent can have a tremendous effect on the photophysical and photochemical properties of the photoresponsive molecule. As described in Section 3, water often has a strong impact on the half-life of the metastable form of the photoswitch, for instance, in push–pull azobenzenes and azobenzenes bearing –SH, –OH, –NHR substituents (Section 3.2.3). Moreover, the polar protic solvent can

also hamper the reversibility of photoswitching in the case of DAEs (Section 3.3.1) and DASAs (Section 3.4.3). While azobenzenes show typically high photoswitching QYs in polar solvents, for some indigos and thioindigos the QY decrease in water (Section 3.2.5). Also, photophysical properties, such as the absorption maxima of the two photoisomers, are influenced, which leads for instance in diazocines to a reduced band separation and thus lower PSDs (Section 3.2.4). Finally, the stability of the switch itself can be decreased in water and for some compounds, like azo-BF_3 switches (Section 3.2.9) and some spiropyrans (Section 3.4.1), hydrolysis has been observed.

Nevertheless, many successful and fascinating examples of applications of photoswitches in water have been described. In Section 4.1, we discuss how different solubilization strategies

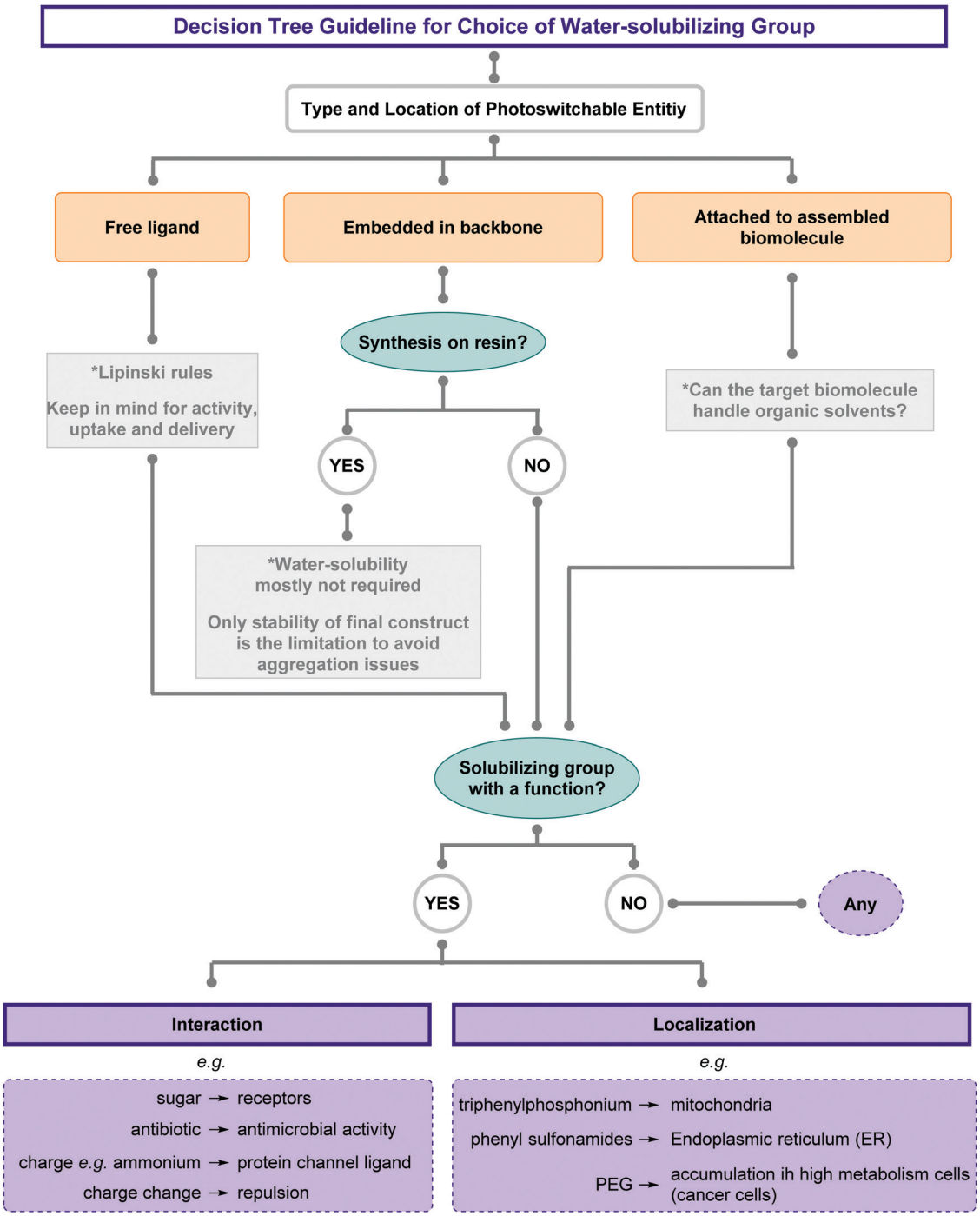

Fig. 76 Decision tree guideline for choosing the water-solubilizing group for a specific molecule based on the type and location of the photoswitchable entity (in orange). Grey boxes describe general considerations to keep in mind while designing a construct, mint-green circles ask key questions for the design and purple areas possible roles of the solubilizing group with illustrative examples.

are applied on small photoswitches acting as ligands in biological systems. Here, the attachment of solubilizing groups is most frequently used. However, the installation of a solubilizing group, both carrying a charge or not, can often have a strong effect on the localization of the bioactive molecule *in cellulo* and *in vivo*. This was, for example, extensively reported for ion channel inhibitors solubilized with ammonium groups (see Section 4.1.1). Furthermore, the photoswitchable molecule needs to be sufficiently water-soluble for achieving bioavailability, while remaining lipophilic enough to remain bioactive. At the same time, excellent photochemical properties need to be retained. This fine balance of various parameters was illustrated for cell-penetrating peptides (Section 4.1.3.1). In this case, toxicity due to aggregation was avoided upon water-solubilization of hemithioindigo inhibitors by disrupting the planarity of the molecules upon simple introduction of an additional methoxy group.

In the case of applications where the photoswitch is designed as a biomolecular building block, such as an amino acid or a nucleotide, the photoactuator is typically incorporated *via* SPPS in organic solvents. Hence, the solubility of the switch itself is less important for the attachment process, however, the final construct needs to exhibit the right solubility properties matching the characteristics of the assembled biomolecule (see Section 4.2). If, for instance, the resulting peptide is relatively small, lipophilic and large aromatic structures can cause unwanted aggregation, as seen for the cell penetrating peptides. For photoswitches incorporated into the backbone of DNA and RNA, it was observed that the vicinity of the biomolecule can hamper the photochemical properties of the integrated photoswitch. In contrast, photoswitches which are attached to a target molecule after its synthesis, or to a naturally occurring target, need to fulfil different criteria regarding to their solubility, while not affecting the native activity of the biomolecule. Specifically, the required water-solubility is dependent on the tolerance of the biomolecule towards co-solvents. The MscL channel could withstand 20% DMSO in water to label it with a spiropyran, while the nanopore-forming toxin FraC required the use of fully water-soluble azobenzenes, to only name two examples. Moreover, in a biologically more complex setting, like *in cellulo* or *in vivo*, such as needed for super-resolution fluorescence microscopy in living cells, the water-solubility of the photoswitchable fluorophore need to be extremely high as any aggregate formation results in high toxicity (Section 4.3.4).

Based on this literature overview, we summarized the available water-solubilizing strategies in Fig. 76. Herein we propose a decision tree to aid the reader in the design of the water-soluble light-responsive construct. The type and location of the photoswitchable entity requires specific considerations and leads to key decisions which further dictate the solubilizing approach. While the water-solubilizing groups can be summarized in a generalized fashion, the photoswitch selection has to be performed on a case-to-case basis, considering that many of them have not been studied in water in detail. Nevertheless, it is of crucial importance to consider the photochemical properties of the chosen photoswitch in an aqueous environment.

In summary, various aspects need to be considered to successfully apply a photoswitch in aqueous media and to establish a system that operates efficiently in water, shows hydrolytic stability, is (bio)available, retains its desired activity while preserving excellent photobistability. Furthermore, the influence of the labelled biomolecule on the photoswitch properties (*e.g.* energy transfer) and *vice versa* need to be taken into account. To tackle this complexity, both a suitable photoswitch and an appropriate solubilization strategy need to be chosen. In the examples discussed here, mostly azobenzenes and DAEs are used as photoactuators. Other classes (spiropyrans, heteroaryl azobenzenes, H(T)Is, fulgides, stilbenes) are to a lesser extent applied, while some switches (hydrazones, DHPs), have been hardly used in aqueous environment. This is often because they are in general not extensively investigated and less well understood, they are not (thoroughly) studied in polar protic or aqueous media, or there are no suitable soluble analogous yet available. Consequently, there is a strong need to rationally explore the photophysical and photochemical proprieties of a wider range of photoswitches in aqueous media. Moreover, suitable solubilizing strategies need to be found for both the underexplored switches and for the more frequently used ones. Currently, solubility problems are often overcome using cosolvents, and with that the issue of kinetic solubility. However, this can lead to aggregation and precipitation of the compound and hence, hamper the development of advanced applications, such as *in vivo* studies. Therefore, research needs more focus on the development of photoswitches showing high thermodynamic solubility in water. This can be achieved using classical approaches such as the introduction of polar or charged groups. However, more challenging solubilizing strategies need to be systematically explored and involved in the design of novel photoswitches, for example, by favouring the incorporation of 3D over 2D moieties, a current trend that has shown some promising results in drug development.[41] Also, prodrug strategies or the formation of hydrotropes could lead to major advances designing truly water-soluble photoswitches. Having these novel methods readily available together with a more detailed understanding of photoswitching in aqueous media, it will pave the way to numerous applications in the chemical biology, pharmaceutical and medicinal fields, but will also have a strong influence on other research areas, opening tremendous opportunities for surface functionalization, smart soft-materials as well as responsive and adaptive systems compatible with living systems.

Conflicts of interest

The authors declare no competing financial interest.

Acknowledgements

We thank Dr Stefano Crespi (University of Groningen) and Dr Jeffrey Buter (University of Groningen) for fruitful discussion during the preparation of this review. We gratefully acknowledge the generous support from the Humboldt Foundation (Feodor-Lynen scholarship to NAS), the Horizon 2020 Framework Program (ERC Advanced Investigator Grant No. 694345 to BLF),

the Ministry of Education, Culture and Science of the Netherlands (Gravitation Program No. 024.001.035 to BLF), and the Netherlands Organization for Scientific Research (NWO, VIDI Grant No. 723.014.001 for WS).

References

1 K. Reichardt and L. C. Timm, *Soil, Plant and Atmosphere*, Springer International Publishing, Cham, 2020, pp. 7–13.
2 A. Pohorille and L. R. Pratt, *Orig. Life Evol. Biosph.*, 2012, **42**, 405–409.
3 *Molecular Switches*, ed. B. L. Feringa and W. R. Browne, Wiley-VCH Verlag GmbH & Co. KGaA, Weinheim, Germany, 2011.
4 R. Göstl, A. Senf and S. Hecht, *Chem. Soc. Rev.*, 2014, **43**, 1982–1996.
5 P. Suppan, *Chemistry and Light*, Royal Society of Chemistry, Cambridge, 2007.
6 W. A. Velema, W. Szymanski and B. L. Feringa, *J. Am. Chem. Soc.*, 2014, **136**, 2178–2191.
7 M. M. Lerch, M. J. Hansen, G. M. van Dam, W. Szymanski, B. L. Feringa, G. M. van Dam, W. Szymanski and B. L. Feringa, *Angew. Chem., Int. Ed.*, 2016, **55**, 10978–10999.
8 A. M. Ali, G. A. Woolley, G. A. Woolley, C. Pedone, G. Colombo, L. D. D'Andrea, R. Fattorusso, G. A. Woolley and S. J. Korsmeyer, *Org. Biomol. Chem.*, 2013, **11**, 5325–5331.
9 J. Broichhagen, J. A. Frank and D. Trauner, *Acc. Chem. Res.*, 2015, **48**, 1947–1960.
10 K. Hüll, J. Morstein and D. Trauner, *Chem. Rev.*, 2018, **118**, 10710–10747.
11 M. J. Fuchter, *J. Med. Chem.*, 2020, **63**, 11436–11447.
12 K. Nakatani, J. Piard, P. Yu and R. Métivier, *Photochromic Materials: Preparation, Properties and Applications*, Wiley-VCH Verlag GmbH & Co. KGaA, Weinheim, Germany, 2016, pp. 1–45.
13 T. Slanina, P. Shrestha, E. Palao, D. Kand, J. A. Peterson, A. S. Dutton, N. Rubinstein, R. Weinstain, A. H. Winter and P. Klán, *J. Am. Chem. Soc.*, 2017, **139**, 15168–15175.
14 P. Klán, T. Šolomek, C. G. Bochet, A. Blanc, R. Givens, M. Rubina, V. Popik, A. Kostikov and J. Wirz, *Chem. Rev.*, 2013, **113**, 119–191.
15 M. J. Hansen, W. A. Velema, M. M. Lerch, W. Szymanski and B. L. Feringa, *Chem. Soc. Rev.*, 2015, **44**, 3358–3377.
16 L. Josa-Culleré and A. Llebaria, *ChemPhotoChem*, 2021, **5**, 298–316.
17 T. Slanina, *Photochemistry: Volume 45*, PI Group (UK) Ltd, Croydon, 2018, pp. 175–190.
18 A. Goulet-Hanssens, F. Eisenreich and S. Hecht, *Adv. Mater.*, 2020, **32**, 1905966.
19 S. Kaneko, K. Asakura and T. Banno, *Chem. Commun.*, 2017, **53**, 2237–2240.
20 E. Chevallier, C. Monteux, F. Lequeux and C. Tribet, *Langmuir*, 2012, **28**, 2308–2312.
21 S. Chen, R. Costil, F. K. Leung and B. L. Feringa, *Angew. Chem., Int. Ed.*, 2021, **60**, 11604–11627.
22 S. Chen, F. K.-C. Leung, M. C. A. Stuart, C. Wang and B. L. Feringa, *J. Am. Chem. Soc.*, 2020, **142**, 10163–10172.
23 P. M. Erne, P. Štacko, D. J. van Dijken, J. Chen, M. C. A. Stuart and B. L. Feringa, *Chem. Commun.*, 2016, **52**, 11697–11700.
24 D. J. van Dijken, J. Chen, M. C. A. Stuart, L. Hou and B. L. Feringa, *J. Am. Chem. Soc.*, 2016, **138**, 660–669.
25 P. M. Erne, L. S. van Bezouwen, P. Štacko, D. J. van Dijken, J. Chen, M. C. A. Stuart, E. J. Boekema and B. L. Feringa, *Angew. Chem., Int. Ed.*, 2015, **54**, 15122–15127.
26 J. T. van Herpt, J. Areephong, M. C. A. Stuart, W. R. Browne and B. L. Feringa, *Chem. – Eur. J.*, 2014, **20**, 1737–1742.
27 M. A. Schoondorp, A. J. Schouten, J. B. E. Hulshof and B. L. Feringa, *Langmuir*, 1993, **9**, 1323–1329.
28 R. Kou, T. Wang, Z. Chen, R. Zhu, H. Cai, H. Pang, S. Xuan and G. Liu, *Langmuir*, 2019, **35**, 13110–13115.
29 L. Ji, G. Ouyang and M. Liu, *Langmuir*, 2017, **33**, 12419–12426.
30 I. M. Welleman, M. W. H. Hoorens, B. L. Feringa, H. H. Boersma and W. Szymański, *Chem. Sci.*, 2020, **11**, 11672–11691.
31 C. Brieke, F. Rohrbach, A. Gottschalk, G. Mayer and A. Heckel, *Angew. Chem., Int. Ed.*, 2012, **51**, 8446–8476.
32 H.-M. Lee, D. R. Larson and D. S. Lawrence, *ACS Chem. Biol.*, 2009, **4**, 409–427.
33 K. Hüll, J. Morstein and D. Trauner, *Chem. Rev.*, 2018, **118**, 10710–10747.
34 J. Broichhagen, M. Schönberger, S. C. Cork, J. A. Frank, P. Marchetti, M. Bugliani, A. M. J. J. Shapiro, S. Trapp, G. A. Rutter, D. J. Hodson and D. Trauner, *Nat. Commun.*, 2014, **5**, 5116.
35 D. Pearson, N. Alexander and A. D. Abell, *Chem. – Eur. J.*, 2008, **14**, 7358–7365.
36 J. M. Kuiper and J. B. F. N. Engberts, *Langmuir*, 2004, **20**, 1152–1160.
37 M. Shimomura, R. Ando and T. Kunitake, *Ber. Buns. Phys. Chem.*, 1983, **87**, 1134–1143.
38 S. L. Niu, C. Massif, G. Ulrich, R. Ziessel, P.-Y. Renard and A. Romieu, *Org. Biomol. Chem.*, 2011, **9**, 66–69.
39 M. A. Walker, *Expert Opin. Drug Discovery*, 2014, **9**, 1421–1433.
40 D. Jornada, G. dos Santos Fernandes, D. Chiba, T. de Melo, J. dos Santos and M. Chung, *Molecules*, 2015, **21**, 42.
41 M. Ishikawa and Y. Hashimoto, *J. Med. Chem.*, 2011, **54**, 1539–1554.
42 D. Frath, S. Yokoyama, T. Hirose and K. Matsuda, *J. Photochem. Photobiol., C*, 2018, **34**, 29–40.
43 S. Yagai and A. Kitamura, *Chem. Soc. Rev.*, 2008, **37**, 1520.
44 Z. Ding, Y. Zhang, Y. Gao, B. Yang and S. Jiang, *Nanoscale*, 2020, **12**, 2071–2080.
45 F. Xu, L. Pfeifer, S. Crespi, F. K.-C. Leung, M. C. A. Stuart, S. J. Wezenberg and B. L. Feringa, *J. Am. Chem. Soc.*, 2021, **143**, 5990–5997.
46 G. Davidson-Rozenfeld, L. Stricker, J. Simke, M. Fadeev, M. Vázquez-González, B. J. Ravoo and I. Willner, *Polym. Chem.*, 2019, **10**, 4106–4115.
47 Y.-L. Zhao and J. F. Stoddart, *Langmuir*, 2009, **25**, 8442–8446.
48 S. Tamesue, Y. Takashima, H. Yamaguchi, S. Shinkai and A. Harada, *Angew. Chem., Int. Ed.*, 2010, **49**, 7461–7464.

49 A. Myrhammar, D. Rosik and A. E. Karlström, *Bioconjugate Chem.*, 2020, **31**, 622–630.
50 H. Yamaguchi, Y. Kobayashi, R. Kobayashi, Y. Takashima, A. Hashidzume and A. Harada, *Nat. Commun.*, 2012, **3**, 603.
51 L. Li, J. M. Scheiger and P. A. Levkin, *Adv. Mater.*, 2019, **31**, 1807333.
52 H. Birch, A. D. Redman, D. J. Letinski, D. Y. Lyon and P. Mayer, *Anal. Chim. Acta*, 2019, **1086**, 16–28.
53 S. Stegemann, F. Leveiller, D. Franchi, H. de Jong and H. Lindén, *Eur. J. Pharm. Sci.*, 2007, **31**, 249–261.
54 US Pharmacopeia, *USP 30-NF 25*, 2007.
55 F. L. O. Da Silva, M. B. D. F. Marques, K. C. Kato and G. Carneiro, *Expert Opin. Drug Discovery*, 2020, **15**, 853–864.
56 S. N. Bhattachar, L. A. Deschenes and J. A. Wesley, *Drug Discovery Today*, 2006, **11**, 1012–1018.
57 N. Blagden, M. de Matas, P. T. Gavan and P. York, *Adv. Drug Delivery Rev.*, 2007, **59**, 617–630.
58 E. Baka, J. E. A. Comer and K. Takács-Novák, *J. Pharm. Biomed. Anal.*, 2008, **46**, 335–341.
59 E. V. Anslyn and D. A. Dougherty, *Modern Physical Organic Chemistry*, University Science Books, Mill Valley, 2006.
60 A. Lusci, G. Pollastri and P. Baldi, *J. Chem. Inf. Model.*, 2013, **53**, 1563–1575.
61 G. Klopman and H. Zhu, *J. Chem. Inf. Comput. Sci.*, 2001, **41**, 439–445.
62 J. S. Delaney, *Drug Discovery Today*, 2005, **10**, 289–295.
63 T. Sanghvi, N. Jain, G. Yang and S. Yalkowsky, *QSAR Comb. Sci.*, 2003, **22**, 258–262.
64 A. Avdeef and M. Kansy, *Mol. Pharmaceutics*, 2020, **17**, 3930–3940.
65 L. Mendez, G. Henriquez, S. Sirimulla and M. Narayan, *Molecules*, 2017, **22**, 1397.
66 K. S. Sidhu, J. M. Goodfellow and J. Z. Turner, *J. Chem. Phys.*, 1999, **110**, 7943–7950.
67 H. Lee, F. Dehez, C. Chipot, H.-K. Lim and H. Kim, *J. Chem. Theory Comput.*, 2019, **15**, 1538–1545.
68 G. Graziano, *J. Phys. Chem. B*, 2001, **105**, 2632–2637.
69 *Disordered Pharmaceutical Materials*, ed. M. Descamps, Wiley-VCH Verlag GmbH & Co. KGaA, Weinheim, Germany, 2016.
70 J. E. Ricci and T. W. Davis, *J. Am. Chem. Soc.*, 1940, **62**, 407–413.
71 OECD, *Test No. 105: Water Solubility*, OECD Guidelines for the Testing of Chemicals, Section 1, OECD Publishing, Paris, 1995, DOI: 10.1787/9789264069589-en.
72 C. Lipinski and A. Hopkins, *Nature*, 2004, **432**, 855–861.
73 C. A. Lipinski, F. Lombardo, B. W. Dominy and P. J. Feeney, *Adv. Drug Delivery Rev.*, 1997, **23**, 3–25.
74 G. L. Amidon, H. Lennernäs, V. P. Shah and J. R. Crison, *Pharm. Res.*, 1995, **12**, 413–420.
75 A. T. M. Serajuddin, *Adv. Drug Delivery Rev.*, 2007, **59**, 603–616.
76 A. K. Nayak and P. P. Panigrahi, *ISRN Phys. Chem.*, 2012, **2012**, 1–5.
77 A. Fahr and X. Liu, *Expert Opin. Drug Delivery*, 2007, **4**, 403–416.
78 J. Mao, W. Ruan and Q. Chen, *J. Electrochem. Soc.*, 2020, **167**, 070522.
79 M. Addie, P. Ballard, D. Buttar, C. Crafter, G. Currie, B. R. Davies, J. Debreczeni, H. Dry, P. Dudley, R. Greenwood, P. D. Johnson, J. G. Kettle, C. Lane, G. Lamont, A. Leach, R. W. A. Luke, J. Morris, D. Ogilvie, K. Page, M. Pass, S. Pearson and L. Ruston, *J. Med. Chem.*, 2013, **56**, 2059–2073.
80 S. S. Scully, A. J. Tang, M. Lundh, C. M. Mosher, K. M. Perkins and B. K. Wagner, *J. Med. Chem.*, 2013, **56**, 4125–4129.
81 S. Wenglowsky, D. Moreno, J. Rudolph, Y. Ran, K. A. Ahrendt, A. Arrigo, B. Colson, S. L. Gloor and G. Hastings, *Bioorg. Med. Chem. Lett.*, 2012, **22**, 912–915.
82 Z. A. Parray, M. I. Hassan, F. Ahmad and A. Islam, *Polym. Test.*, 2020, **82**, 106316.
83 R. B. Greenwald, Y. H. Choe, J. McGuire and C. D. Conover, *Adv. Drug Delivery Rev.*, 2003, **55**, 217–250.
84 E. M. Skoda, J. R. Sacher, M. Z. Kazancioglu, J. Saha and P. Wipf, *ACS Med. Chem. Lett.*, 2014, **5**, 900–904.
85 A. Llinàs, J. C. Burley, K. J. Box, R. C. Glen and J. M. Goodman, *J. Med. Chem.*, 2007, **50**, 979–983.
86 F. Lovering, J. Bikker and C. Humblet, *J. Med. Chem.*, 2009, **52**, 6752–6756.
87 H. Chen, Z. Yang, C. Ding, L. Chu, Y. Zhang, K. Terry, H. Liu, Q. Shen and J. Zhou, *ACS Med. Chem. Lett.*, 2013, **4**, 180–185.
88 K. M. Foote, K. Blades, A. Cronin, S. Fillery, S. S. Guichard, L. Hassall, I. Hickson, X. Jacq, P. J. Jewsbury, T. M. McGuire, J. W. M. Nissink, R. Odedra, K. Page, P. Perkins, A. Suleman, K. Tam, P. Thommes, R. Broadhurst and C. Wood, *J. Med. Chem.*, 2013, **56**, 2125–2138.
89 M. Hiramatsu, Y. Ichikawa, S. Tomoshige, M. Makishima, A. Muranaka, M. Uchiyama, T. Yamaguchi, Y. Hashimoto and M. Ishikawa, *Chem. – Asian J.*, 2016, **11**, 2210–2217.
90 B. Laprade, T. W. Mauger and H. Petersen, *Drug Dev. Ind. Pharm.*, 1977, **3**, 73–85.
91 S. Forster, G. Buckton and A. E. Beezer, *Int. J. Pharm.*, 1991, **72**, 29–34.
92 A. Gavezzotti, *J. Chem. Soc., Perkin Trans. 2*, 1995, 1399.
93 V. V. Levterov, O. Michurin, P. O. Borysko, S. Zozulya, I. V. Sadkova, A. A. Tolmachev and P. K. Mykhailiuk, *J. Org. Chem.*, 2018, **83**, 14350–14361.
94 G. Niu, R. Zhang, J. P. C. Kwong, J. W. Y. Lam, C. Chen, J. Wang, Y. Chen, X. Feng, R. T. K. Kwok, H. H.-Y. Sung, I. D. Williams, M. R. J. Elsegood, J. Qu, C. Ma, K. S. Wong, X. Yu and B. Z. Tang, *Chem. Mater.*, 2018, **30**, 4778–4787.
95 J. O. Bockris, J. Bowler-Reed and J. A. Kitchener, *Trans. Faraday Soc.*, 1951, **47**, 184–192.
96 R. Sadeghi and F. Jahani, *J. Phys. Chem. B*, 2012, **116**, 5234–5241.
97 L. I. N. Tomé, S. P. Pinho, M. Jorge, J. R. B. Gomes and J. A. P. Coutinho, *J. Phys. Chem. B*, 2013, **117**, 6116–6128.
98 V. Dhapte and P. Mehta, *St. Petersbg. Polytech. Univ. J. Phys. Math.*, 2015, **1**, 424–435.
99 P. Khadka, J. Ro, H. Kim, I. Kim, J. T. Kim, H. Kim, J. M. Cho, G. Yun and J. Lee, *Asian J. Pharm. Sci.*, 2014, **9**, 304–316.

100 S. Rawat and S. K. Jain, *Eur. J. Pharm. Biopharm.*, 2004, **57**, 263–267.
101 H. Kumpulainen, T. Järvinen, A. Mannila, J. Leppänen, T. Nevalainen, A. Mäntylä, J. Vepsäläinen and J. Rautio, *Eur. J. Pharm. Sci.*, 2008, **34**, 110–117.
102 J. Shen, D. Zhang, Z. Zhao, L. Jia, D. Zheng, G. Liu, L. Hao, Q. Zhang, X. Tian, C. Li and H. Guo, *Int. J. Pharm.*, 2013, **456**, 80–86.
103 M. Zhou, R.-H. Luo, X.-Y. Hou, R.-R. Wang, G.-Y. Yan, H. Chen, R.-H. Zhang, J.-Y. Shi, Y.-T. Zheng, R. Li and Y.-Q. Wei, *Eur. J. Med. Chem.*, 2017, **129**, 310–324.
104 B. M. A. Sanches and E. I. Ferreira, *Int. J. Pharm.*, 2019, **568**, 118498.
105 J. Rautio, N. A. Meanwell, L. Di and M. J. Hageman, *Nat. Rev. Drug Discovery*, 2018, **17**, 559–587.
106 H. Bouas-Laurent and H. Dürr, *Pure Appl. Chem.*, 2001, **73**, 639–665.
107 S. E. Braslavsky, *Pure Appl. Chem.*, 2007, **79**, 293–465.
108 H. Dürr and H. Bouas-Laurent, *Photochromism: Molecules and Systems*, 1st edn, Elsevier Science, Amsterdam, 2003.
109 D. Villarón and S. J. Wezenberg, *Angew. Chem., Int. Ed.*, 2020, **59**, 13192–13202.
110 M. Oelgemöller, B. Brem, R. Frank, S. Schneider, D. Lenoir, N. Hertkorn, Y. Origane, P. Lemmen, J. Lex and Y. Inoue, *J. Chem. Soc., Perkin Trans. 2*, 2002, 1760–1771.
111 D. H. Waldeck, *Chem. Rev.*, 1991, **91**, 415–436.
112 M. Quick, F. Berndt, A. L. Dobryakov, I. N. Ioffe, A. A. Granovsky, C. Knie, R. Mahrwald, D. Lenoir, N. P. Ernsting and S. A. Kovalenko, *J. Phys. Chem. B*, 2014, **118**, 1389–1402.
113 W. Fuß, C. Kosmidis, W. E. Schmid and S. A. Trushin, *Angew. Chem., Int. Ed.*, 2004, **43**, 4178–4182.
114 D. C. Todd and G. R. Fleming, *J. Chem. Phys.*, 1993, **98**, 269–279.
115 R. Lechner, S. Kümmel and B. König, *Photochem. Photobiol. Sci.*, 2010, **9**, 1367–1377.
116 M. P. O'Hagan, S. Haldar, M. Duchi, T. A. A. Oliver, A. J. Mulholland, J. C. Morales and M. C. Galan, *Angew. Chem., Int. Ed.*, 2019, **58**, 4334–4338.
117 Y. Wang, Y. Tian, Y.-Z. Chen, L.-Y. Niu, L.-Z. Wu, C.-H. Tung, Q.-Z. Yang and R. Boulatov, *Chem. Commun.*, 2018, **54**, 7991–7994.
118 J.-X. Wang, L.-Y. Niu, P.-Z. Chen, Y.-Z. Chen, Q.-Z. Yang and R. Boulatov, *Chem. Commun.*, 2019, **55**, 7017–7020.
119 T. Shimasaki, S. Kato, K. Ideta, K. Goto and T. Shinmyozu, *J. Org. Chem.*, 2007, **72**, 1073–1087.
120 S. J. Wezenberg and B. L. Feringa, *Org. Lett.*, 2017, **19**, 324–327.
121 Y. Li, E. C. M. Tse, C. J. Barile, A. A. Gewirth and S. C. Zimmerman, *J. Am. Chem. Soc.*, 2015, **137**, 14059–14062.
122 J. Jong, B. L. Feringa and S. J. Wezenberg, *ChemPhysChem*, 2019, **20**, 3306–3310.
123 T.-G. Zhan, H.-H. Yin, S.-T. Zheng, W.-C. Lin, N.-L. Shen, J. Cui, L.-C. Kong, L.-J. Liu and K.-D. Zhang, *Chem. Commun.*, 2018, **54**, 9356–9359.
124 N. Zhu, X. Li, Y. Wang and X. Ma, *Dyes Pigm.*, 2016, **125**, 259–265.
125 Y.-H. Wu, K. Huang, S.-F. Chen, Y.-Z. Chen, C.-H. Tung and L.-Z. Wu, *Sci. China: Chem.*, 2019, **62**, 1194–1197.
126 C. Cao, G. Chen and Y. Wu, *Sci. China: Chem.*, 2011, **54**, 1735–1744.
127 M. de Wergifosse, A. L. Houk, A. I. Krylov and C. G. Elles, *J. Chem. Phys.*, 2017, **146**, 144305.
128 G. Hohlneicher, R. Wrzal, D. Lenoir and R. Frank, *J. Phys. Chem. A*, 1999, **103**, 8969–8975.
129 S. H. Courtney and G. R. Fleming, *J. Chem. Phys.*, 1985, **83**, 215–222.
130 J. F. Letard, R. Lapouyade and W. Rettig, *J. Am. Chem. Soc.*, 1993, **115**, 2441–2447.
131 X. Yan, J.-F. Xu, T. R. Cook, F. Huang, Q.-Z. Yang, C.-H. Tung and P. J. Stang, *Proc. Natl. Acad. Sci. U. S. A.*, 2014, **111**, 8717–8722.
132 R. Costil, S. Crespi, L. Pfeifer and B. L. Feringa, *Chem. – Eur. J.*, 2020, **26**, 7783–7787.
133 S. Lee and A. H. Flood, *J. Phys. Org. Chem.*, 2013, **26**, 79–86.
134 S. Olsson, C. Schäfer, M. Blom and A. Gogoll, *ChemPlusChem*, 2018, **83**, 1169–1178.
135 S. J. Wezenberg and B. L. Feringa, *Nat. Commun.*, 2018, **9**, 1984.
136 Z. S. Kean, S. Akbulatov, Y. Tian, R. A. Widenhoefer, R. Boulatov and S. L. Craig, *Angew. Chem., Int. Ed.*, 2014, **53**, 14508–14511.
137 T. J. Kucharski and R. Boulatov, *J. Mater. Chem.*, 2011, **21**, 8237.
138 Z. Huang, Q.-Z. Yang, D. Khvostichenko, T. J. Kucharski, J. Chen and R. Boulatov, *J. Am. Chem. Soc.*, 2009, **131**, 1407–1409.
139 S. Akbulatov, Y. Tian, Z. Huang, T. J. Kucharski, Q.-Z. Yang and R. Boulatov, *Science*, 2017, **357**, 299–303.
140 S. Akbulatov, Y. Tian and R. Boulatov, *J. Am. Chem. Soc.*, 2012, **134**, 7620–7623.
141 H. Zhu, L. Shangguan, D. Xia, J. H. Mondal and B. Shi, *Nanoscale*, 2017, **9**, 8913–8917.
142 M. P. O'Hagan, P. Peñalver, R. S. L. Gibson, J. C. Morales and M. C. Galan, *Chem. – Eur. J.*, 2020, **26**, 6224–6233.
143 K. A. Rotstan, M. M. Abdelsayed, L. F. Passalacqua, F. Chizzolini, K. Sudarshan, A. R. Chamberlin, J. Míšek and A. Luptak, *eLife*, 2020, **9**, e51737.
144 L. Gao, J. C. M. Meiring, Y. Kraus, M. Wranik, T. Weinert, S. D. Pritzl, R. Bingham, E. Ntouliou, K. I. Jansen, N. Olieric, J. Standfuss, L. C. Kapitein, T. Lohmüller, J. Ahlfeld, A. Akhmanova, M. O. Steinmetz and O. Thorn-Seshold, *Cell Chem. Biol.*, 2021, **28**, 228–241.
145 N. Koumura, R. W. J. Zijlstra, R. A. van Delden, N. Harada and B. L. Feringa, *Nature*, 1999, **401**, 152–155.
146 R. A. van Delden, M. K. J. ter Wiel, M. M. Pollard, J. Vicario, N. Koumura and B. L. Feringa, *Nature*, 2005, **437**, 1337–1340.
147 D. Roke, S. J. Wezenberg and B. L. Feringa, *Proc. Natl. Acad. Sci. U. S. A.*, 2018, **115**, 9423–9431.
148 S. Kassem, T. van Leeuwen, A. S. Lubbe, M. R. Wilson, B. L. Feringa and D. A. Leigh, *Chem. Soc. Rev.*, 2017, **46**, 2592–2621.
149 V. García-López, D. Liu and J. M. Tour, *Chem. Rev.*, 2020, **120**, 79–124.

150 M. Baroncini, S. Silvi and A. Credi, *Chem. Rev.*, 2020, **120**, 200–268.
151 J. C. M. Kistemaker, A. S. Lubbe and B. L. Feringa, *Mater. Chem. Front*, 2021, **5**, 2900–2906.
152 A. S. Lubbe, C. Böhmer, F. Tosi, W. Szymanski and B. L. Feringa, *J. Org. Chem.*, 2018, **83**, 11008–11018.
153 C. Poloni, M. C. A. Stuart, P. van der Meulen, W. Szymanski and B. L. Feringa, *Chem. Sci.*, 2015, **6**, 7311–7318.
154 A. S. Lubbe, Q. Liu, S. J. Smith, J. W. De Vries, J. C. M. M. Kistemaker, A. H. De Vries, I. Faustino, Z. Meng, W. Szymanski, A. Herrmann and B. L. Feringa, *J. Am. Chem. Soc.*, 2018, **140**, 5069–5076.
155 A. S. Lubbe, J. C. M. Kistemaker, E. J. Smits and B. L. Feringa, *Phys. Chem. Chem. Phys.*, 2016, **18**, 26725–26735.
156 H. M. D. Bandara and S. C. Burdette, *Chem. Soc. Rev.*, 2012, **41**, 1809–1825.
157 S. Crespi, N. A. Simeth and B. König, *Nat. Rev. Chem.*, 2019, **3**, 133–146.
158 N. A. Simeth and S. Crespi, (Hetero)aryl azoswitches and their application, *Photochemistry*, 2020, vol. 48, pp. 344–375.
159 E. Merino, *Chem. Soc. Rev.*, 2011, **40**, 3835–3853.
160 D. Larsen, P. M. Bjerre and S. R. Beeren, *Chem. Commun.*, 2019, **55**, 15037–15040.
161 C. Brown, S. K. K. Rastogi, S. L. L. Barrett, H. E. E. Anderson, E. Twichell, S. Gralinski, A. McDonald and W. J. J. Brittain, *J. Photochem. Photobiol., A*, 2017, **336**, 140–145.
162 J. W. Fredy, A. Méndez-Ardoy, S. Kwangmettatam, D. Bochicchio, B. Matt, M. C. A. Stuart, J. Huskens, N. Katsonis, G. M. Pavan and T. Kudernac, *Proc. Natl. Acad. Sci. U. S. A.*, 2017, **114**, 11850–11855.
163 D. Bochicchio, S. Kwangmettatam, T. Kudernac and G. M. Pavan, *ACS Nano*, 2019, **13**, 4322–4334.
164 S. K. Rastogi, Z. Zhao, S. L. Barrett, S. D. Shelton, M. Zafferani, H. E. Anderson, M. O. Blumenthal, L. R. Jones, L. Wang, X. Li, C. N. Streu, L. Du and W. J. Brittain, *Eur. J. Med. Chem.*, 2018, **143**, 1–7.
165 J. Calbo, C. E. Weston, A. J. P. White, H. S. Rzepa, J. Contreras-García and M. J. Fuchter, *J. Am. Chem. Soc.*, 2017, **139**, 1261–1274.
166 J. Garcia-Amorós, S. Nonell and D. Velasco, *Chem. Commun.*, 2011, **47**, 4022.
167 J. Garcia-Amorós, S. Nonell and D. Velasco, *Chem. Commun.*, 2012, **48**, 3421.
168 J. Otsuki, K. Harada and K. Araki, *Chem. Lett.*, 1999, 269–270.
169 J. Otsuki and K. Narutaki, *Bull. Chem. Soc. Jpn.*, 2004, **77**, 1537–1544.
170 S. Venkataramani, U. Jana, M. Dommaschk, F. D. Sonnichsen, F. Tuczek and R. Herges, *Science*, 2011, **331**, 445–448.
171 N. A. Simeth, S. Crespi, M. Fagnoni and B. König, *J. Am. Chem. Soc.*, 2018, **140**, 2940–2946.
172 S. Crespi, N. A. Simeth, A. Bellisario, M. Fagnoni and B. König, *J. Phys. Chem. A*, 2019, **123**, 1814–1823.
173 N. A. Simeth, A. Bellisario, S. Crespi, M. Fagnoni and B. König, *J. Org. Chem.*, 2019, **84**, 6565–6575.
174 N. Jacob, L. Guillemard and J. Wencel-Delord, *Synthesis*, 2020, 574–580.
175 R. Travieso-Puente, S. Budzak, J. Chen, P. Stacko, J. T. B. H. Jastrzebski, D. Jacquemin and E. Otten, *J. Am. Chem. Soc.*, 2017, **139**, 3328–3331.
176 D. Kolarski, W. Szymanski and B. L. Feringa, *Org. Lett.*, 2017, **19**, 5090–5093.
177 D. Kolarski, A. Sugiyama, T. Rodat, A. Schulte, C. Peifer, K. Itami, T. Hirota, B. L. Feringa and W. Szymanski, *Org. Biomol. Chem.*, 2021, **19**, 2312–2321.
178 L. Čechová, J. Filo, M. Dračínský, C. Slavov, D. Sun, Z. Janeba, T. Slanina, J. Wachtveitl, E. Procházková and M. Cigáň, *Angew. Chem., Int. Ed.*, 2020, **59**, 15590–15594.
179 J. Garcia-Amorós, M. Díaz-Lobo, S. Nonell and D. Velasco, *Angew. Chem., Int. Ed.*, 2012, **51**, 12820–12823.
180 M. Schehr, C. Ianes, J. Weisner, L. Heintze, M. P. Müller, C. Pichlo, J. Charl, E. Brunstein, J. Ewert, M. Lehr, U. Baumann, D. Rauh, U. Knippschild, C. Peifer and R. Herges, *Photochem. Photobiol. Sci.*, 2019, **18**, 1398–1407.
181 T. Wendler, C. Schütt, C. Näther and R. Herges, *J. Org. Chem.*, 2012, **77**, 3284–3287.
182 J. Otsuki, K. Suwa, K. K. Sarker and C. Sinha, *J. Phys. Chem. A*, 2007, **111**, 1403–1409.
183 K. Rustler, P. Nitschke, S. Zahnbrecher, J. Zach, S. Crespi and B. König, *J. Org. Chem.*, 2020, **85**, 4079–4088.
184 C. Chu, L. Stricker, T. M. Kirse, M. Hayduk and B. J. Ravoo, *Chem. – Eur. J.*, 2019, **25**, 6131–6140.
185 L. Stricker, M. Böckmann, T. M. Kirse, N. L. Doltsinis and B. J. Ravoo, *Chem. – Eur. J.*, 2018, **24**, 8639–8647.
186 L. Stricker, E.-C. Fritz, M. Peterlechner, N. L. Doltsinis and B. J. Ravoo, *J. Am. Chem. Soc.*, 2016, **138**, 4547–4554.
187 C. E. Weston, R. D. Richardson, P. R. Haycock, A. J. P. White and M. J. Fuchter, *J. Am. Chem. Soc.*, 2014, **136**, 11878–11881.
188 S. Devi, M. Saraswat, S. Grewal and S. Venkataramani, *J. Org. Chem.*, 2018, **83**, 4307–4322.
189 P. Kumar, A. Srivastava, C. Sah, S. Devi and S. Venkataramani, *Chem. – Eur. J.*, 2019, **25**, 11924–11932.
190 P. R. Huddleston, V. V. Volkov and C. C. Perry, *Phys. Chem. Chem. Phys.*, 2019, **21**, 1344–1353.
191 C. Slavov, C. Yang, A. H. Heindl, H. A. Wegner, A. Dreuw and J. Wachtveitl, *Angew. Chem., Int. Ed.*, 2020, **59**, 380–387.
192 A. H. Heindl and H. A. Wegner, *Chem. – Eur. J.*, 2020, **26**, 13730–13737.
193 F. Aleotti, A. Nenov, L. Salvigni, M. Bonfanti, M. M. El-Tahawy, A. Giunchi, M. Gentile, C. Spallacci, A. Ventimiglia, G. Cirillo, L. Montali, S. Scurti, M. Garavelli and I. Conti, *J. Phys. Chem. A*, 2020, **124**, 9513–9523.
194 S. Kobayashi, H. Yokoyama and H. Kamei, *Chem. Phys. Lett.*, 1987, **138**, 333–338.
195 L. N. Lameijer, S. Budzak, N. A. Simeth, M. J. Hansen, B. L. Feringa, D. Jacquemin and W. Szymanski, *Angew. Chem., Int. Ed.*, 2020, **59**, 21663–21670.
196 C. Knie, M. Utecht, F. Zhao, H. Kulla, S. Kovalenko, A. M. Brouwer, P. Saalfrank, S. Hecht and D. Bléger, *Chem. – Eur. J.*, 2014, **20**, 16492–16501.

197 D. Bléger, J. Schwarz, A. M. Brouwer and S. Hecht, *J. Am. Chem. Soc.*, 2012, **134**, 20597–20600.
198 D. B. Konrad, G. Savasci, L. Allmendinger, D. Trauner, C. Ochsenfeld and A. M. Ali, *J. Am. Chem. Soc.*, 2020, **142**, 6538–6547.
199 S. Samanta, A. A. Beharry, O. Sadovski, T. M. McCormick, A. Babalhavaeji, V. Tropepe and G. A. Woolley, *J. Am. Chem. Soc.*, 2013, **135**, 9777–9784.
200 S. Samanta, T. M. McCormick, S. K. Schmidt, D. S. Seferos, G. A. Woolley, F. Renth, F. Temps and D. Trauner, *Chem. Commun.*, 2013, **49**, 10314.
201 O. Sadovski, A. A. Beharry, F. Zhang and G. A. Woolley, *Angew. Chem., Int. Ed.*, 2009, **48**, 1484–1486.
202 D. Martínez-López, A. Babalhavaeji, D. Sampedro and G. A. Woolley, *Beilstein J. Org. Chem.*, 2019, **15**, 3000–3008.
203 M. J. Hansen, M. M. Lerch, W. Szymanski and B. L. Feringa, *Angew. Chem., Int. Ed.*, 2016, **55**, 13514–13518.
204 D. B. Konrad, J. A. Frank and D. Trauner, *Chem. – Eur. J.*, 2016, **22**, 4364–4368.
205 D. Martínez-López, A. Babalhavaeji, D. Sampedro and G. A. Woolley, *Beilstein J. Org. Chem.*, 2019, **15**, 3000–3008.
206 C. Boulègue, M. Löweneck, C. Renner and L. Moroder, *ChemBioChem*, 2007, **8**, 591–594.
207 S. Zbaida, *Drug Metab. Rev.*, 1995, **27**, 497–516.
208 J. Dokić, M. Gothe, J. Wirth, M. V. Peters, J. Schwarz, S. Hecht and P. Saalfrank, *J. Phys. Chem. A*, 2009, **113**, 6763–6773.
209 S. Steinwand, T. Halbritter, D. Rastädter, J. M. Ortiz-Sánchez, I. Burghardt, A. Heckel and J. Wachtveitl, *Chem. – Eur. J.*, 2015, **21**, 15720–15731.
210 R. Siewertsen, H. Neumann, B. Buchheim-Stehn, R. Herges, C. Näther, F. Renth and F. Temps, *J. Am. Chem. Soc.*, 2009, **131**, 15594–15595.
211 P. Lentes, E. Stadler, F. Röhricht, A. Brahms, J. Gröbner, F. D. Sönnichsen, G. Gescheidt and R. Herges, *J. Am. Chem. Soc.*, 2019, **141**, 13592–13600.
212 R. Siewertsen, J. B. Schönborn, B. Hartke, F. Renth and F. Temps, *Phys. Chem. Chem. Phys.*, 2011, **13**, 1054–1063.
213 T. Tellkamp, J. Shen, Y. Okamoto and R. Herges, *Eur. J. Org. Chem.*, 2014, 5456–5461.
214 W. Moormann, D. Langbehn and R. Herges, *Synthesis*, 2017, 3471–3475.
215 J. B. Trads, K. Hüll, B. S. Matsuura, L. Laprell, T. Fehrentz, N. Görldt, K. A. Kozek, C. D. Weaver, N. Klöcker, D. M. Barber and D. Trauner, *Angew. Chem., Int. Ed.*, 2019, **58**, 15421–15428.
216 H. Sell, C. Näther and R. Herges, *Beilstein J. Org. Chem.*, 2013, **9**, 1–7.
217 M. Schehr, D. Hugenbusch, T. Moje, C. Näther and R. Herges, *Beilstein J. Org. Chem.*, 2018, **14**, 2799–2804.
218 W. Moormann, D. Langbehn and R. Herges, *Beilstein J. Org. Chem.*, 2019, **15**, 727–732.
219 P. Lentes, P. Frühwirt, H. Freißmuth, W. Moormann, F. Kruse, G. Gescheidt and R. Herges, *J. Org. Chem.*, 2021, **86**, 4355–4360.
220 C. Petermayer and H. Dube, *Acc. Chem. Res.*, 2018, **51**, 1153–1163.
221 R. Brode and G. M. Wyman, *J. Res. Natl. Bur. Stand.*, 1951, **47**, 170–178.
222 G. M. Wyman, *Chem. Rev.*, 1955, **55**, 625–657.
223 J. Pina, D. Sarmento, M. Accoto, P. L. Gentili, L. Vaccaro, A. Galvão and J. S. Seixas de Melo, *J. Phys. Chem. B*, 2017, **121**, 2308–2318.
224 S. Yamazaki, A. L. Sobolewski and W. Domcke, *Phys. Chem. Chem. Phys.*, 2011, **13**, 1618–1628.
225 I. Iwakura, A. Yabushita and T. Kobayashi, *Chem. Phys. Lett.*, 2010, **484**, 354–357.
226 C. Giuliano, L. Hess and J. Margerum, *J. Am. Chem. Soc.*, 1968, **90**, 587–594.
227 B. Koeppe and V. R. F. Schröder, *ChemPhotoChem*, 2019, **3**, 613–618.
228 D. Farka, M. Scharber, E. D. Głowacki and N. S. Sariciftci, *J. Phys. Chem. A*, 2015, **119**, 3563–3568.
229 D. Pinheiro, A. M. Galvão, M. Pineiro and J. S. S. de Melo, *J. Phys. Chem. B*, 2021, **125**, 4108–4119.
230 C.-Y. Huang, A. Bonasera, L. Hristov, Y. Garmshausen, B. M. Schmidt, D. Jacquemin and S. Hecht, *J. Am. Chem. Soc.*, 2017, **139**, 15205–15211.
231 L. A. Huber, P. Mayer and H. Dube, *ChemPhotoChem*, 2018, **2**, 458–464.
232 S. C. Dahlberg and C. B. Reinganum, *J. Chem. Phys.*, 1981, **75**, 2429–2431.
233 H. Kurata, S. Kim, K. Matsumoto, T. Kawase and M. Oda, *Chem. Lett.*, 2007, 386–387.
234 J. Z. Vlahakis, K. E. Maly and R. P. Lemieux, *J. Mater. Chem.*, 2001, **11**, 2459–2464.
235 G. Boice, B. O. Patrick, R. McDonald, C. Bohne and R. Hicks, *J. Org. Chem.*, 2014, **79**, 9196–9205.
236 D. Jacquemin, J. Preat, V. Wathelet, M. Fontaine and E. A. Perpète, *J. Am. Chem. Soc.*, 2006, **128**, 2072–2083.
237 J. Sühnel and K. Gustav, *J. Prakt. Chem.*, 1978, **320**, 917–921.
238 E. I. Stearns, *J. Opt. Soc. Am.*, 1942, **32**, 282.
239 R. Brode and G. M. Wyman, *J. Am. Chem. Soc.*, 1951, **73**, 1487–1493.
240 D. L. Ross, *Appl. Opt.*, 1971, **10**, 571–576.
241 B. Koeppe and F. Römpp, *Chem. – Eur. J.*, 2018, **24**, 14382–14386.
242 B. Koeppe, S. Rühl and F. Römpp, *ChemPhotoChem*, 2019, **3**, 71–74.
243 R. C. Pereira, M. Pineiro, A. M. Galvão and J. S. Seixas de Melo, *Dyes Pigm.*, 2018, **158**, 259–266.
244 S. Kitzig, M. Thilemann, T. Cordes and K. Rück-Braun, *ChemPhysChem*, 2016, **17**, 1252–1263.
245 C. Petermayer, S. Thumser, F. Kink, P. Mayer and H. Dube, *J. Am. Chem. Soc.*, 2017, **139**, 15060–15067.
246 X. Zhao and S. Yang, *J. Lumin.*, 2020, **220**, 116993.
247 B. Maerz, S. Wiedbrauk, S. Oesterling, E. Samoylova, A. Nenov, P. Mayer, R. de Vivie-Riedle, W. Zinth and H. Dube, *Chem. – Eur. J.*, 2014, **20**, 13984–13992.
248 S. Wiedbrauk and H. Dube, *Tetrahedron Lett.*, 2015, **56**, 4266–4274.
249 S. Wiedbrauk, B. Maerz, E. Samoylova, A. Reiner, F. Trommer, P. Mayer, W. Zinth and H. Dube, *J. Am. Chem. Soc.*, 2016, **138**, 12219–12227.

250 C. Petermayer and H. Dube, *J. Am. Chem. Soc.*, 2018, **140**, 13558–13561.
251 V. Smokal, O. Kharchenko, Y. Karabets, N. Iukhymenko, A. Kysil, O. Krupka and A. Kolendo, *Mol. Cryst. Liq. Cryst.*, 2018, **672**, 11–17.
252 M. W. H. Hoorens, M. Medved', A. D. Laurent, M. Di Donato, S. Fanetti, L. Slappendel, M. Hilbers, B. L. Feringa, W. Jan Buma and W. Szymanski, *Nat. Commun.*, 2019, **10**, 2390.
253 D. V. Berdnikova, *Beilstein J. Org. Chem.*, 2019, **15**, 2822–2829.
254 E. Carrascosa, C. Petermayer, M. S. Scholz, J. N. Bull, H. Dube and E. J. Bieske, *ChemPhysChem*, 2020, **21**, 680–685.
255 D. V. Berdnikova, *Chem. Commun.*, 2019, **55**, 8402–8405.
256 M. Ikegami and T. Arai, *Chem. Lett.*, 2005, 492–493.
257 W. Steinle and K. Rück-Braun, *Org. Lett.*, 2003, **5**, 141–144.
258 F. F. Graupner, T. T. Herzog, F. Rott, S. Oesterling, R. de Vivie-Riedle, T. Cordes and W. Zinth, *Chem. Phys.*, 2018, **515**, 614–621.
259 J. E. Zweig, T. A. Ko, J. Huang and T. R. Newhouse, *Tetrahedron*, 2019, **75**, 130466.
260 J. E. Zweig and T. R. Newhouse, *J. Am. Chem. Soc.*, 2017, **139**, 10956–10959.
261 A. Sailer, F. Ermer, Y. Kraus, F. H. Lutter, C. Donau, M. Bremerich, J. Ahlfeld and O. Thorn-Seshold, *ChemBioChem*, 2019, **20**, 1305–1314.
262 A. Sailer, F. Ermer, Y. Kraus, R. Bingham, F. H. Lutter, J. Ahlfeld and O. Thorn-Seshold, *Beilstein J. Org. Chem.*, 2020, **16**, 125–134.
263 M. Poutanen, Z. Ahmed, L. Rautkari, O. Ikkala and A. Priimagi, *ACS Macro Lett.*, 2018, **7**, 381–386.
264 M. Füllbeck, E. Michalsky, I. S. Jaeger, P. Henklein, H. Kuhn, K. Rück-Braun and R. Preissner, *Genome Inform.*, 2006, **17**, 141–151.
265 K. Hoffmann, M. Guentner, P. Mayer and H. Dube, *Org. Chem. Front.*, 2019, **6**, 1244–1252.
266 S. Wiedbrauk, T. Bartelmann, S. Thumser, P. Mayer and H. Dube, *Nat. Commun.*, 2018, **9**, 1456.
267 F. Kink, M. P. Collado, S. Wiedbrauk, P. Mayer and H. Dube, *Chem. – Eur. J.*, 2017, **23**, 6237–6243.
268 M. Guentner, E. Uhl, P. Mayer and H. Dube, *Chem. – Eur. J.*, 2016, **22**, 16433–16436.
269 G. Moncelsi, L. Escobar, H. Dube and P. Ballester, *Chem. – Asian J.*, 2018, **13**, 1632–1639.
270 L. A. Huber, K. Hoffmann, S. Thumser, N. Böcher, P. Mayer and H. Dube, *Angew. Chem., Int. Ed.*, 2017, **56**, 14536–14539.
271 E. Uhl, P. Mayer and H. Dube, *Angew. Chem., Int. Ed.*, 2020, **59**, 5730–5737.
272 K. Hoffmann, P. Mayer and H. Dube, *Org. Biomol. Chem.*, 2019, **17**, 1979–1983.
273 R. Wilcken, M. Schildhauer, F. Rott, L. A. Huber, M. Guentner, S. Thumser, K. Hoffmann, S. Oesterling, R. de Vivie-Riedle, E. Riedle and H. Dube, *J. Am. Chem. Soc.*, 2018, **140**, 5311–5318.
274 A. Gerwien, P. Mayer and H. Dube, *J. Am. Chem. Soc.*, 2018, **140**, 16442–16445.
275 M. Guentner, M. Schildhauer, S. Thumser, P. Mayer, D. Stephenson, P. J. Mayer and H. Dube, *Nat. Commun.*, 2015, **6**, 8406.
276 M. Schildhauer, F. Rott, S. Thumser, P. Mayer, R. de Vivie-Riedle and H. Dube, *ChemPhotoChem*, 2019, **3**, 365–371.
277 A. Gerwien, P. Mayer and H. Dube, *Nat. Commun.*, 2019, **10**, 4449.
278 C. Zwergel, F. Gaascht, S. Valente, M. Diederich, D. Bagrel and G. Kirsch, *Nat. Prod. Commun.*, 2012, **7**, 389–394.
279 A. V. Popova, S. P. Bondarenko and M. S. Frasinyuk, *Chem. Heterocycl. Compd.*, 2019, **55**, 285–299.
280 D. Rambabu, S. Srinivas, K. Manjulatha, S. Basavoju, M. V. B. Rao and M. Pal, *Mol. Cryst. Liq. Cryst.*, 2013, **577**, 83–94.
281 Y. Xue, Y. Dou, L. An, Y. Zheng, L. Zhang and Y. Liu, *RSC Adv.*, 2016, **6**, 7002–7010.
282 K. Muñoz-Becerra, N. Villegas-Escobar, C. Zúñiga-Loyola, D. Cortés-Arriagada and A. Toro-Labbé, *Mol. Phys.*, 2019, **117**, 1451–1458.
283 J. R. Pires, C. Saito, S. L. Gomes, A. M. Giesbrecht and A. T. Amaral, *J. Med. Chem.*, 2001, **44**, 3673–3681.
284 C. Espinosa-Bustos, D. Cortés-Arriagada, M. A. Soto-Arriaza, J. Robinson-Duggon, N. Pizarro, A. R. Cabrera, D. Fuentealba and C. O. Salas, *Photochem. Photobiol. Sci.*, 2017, **16**, 1268–1276.
285 N. Shanker, O. Dilek, K. Mukherjee, D. W. McGee and S. L. Bane, *J. Fluoresc.*, 2011, **21**, 2173–2184.
286 M. Li, S. Yang, W. Liang, X. Zhang and D. Qu, *Dyes Pigm.*, 2019, **166**, 239–244.
287 M. Medved', M. W. H. Hoorens, M. Di Donato, A. D. Laurent, J. Fan, M. Taddei, M. Hilbers, B. L. Feringa, W. J. Buma and W. Szymanski, *Chem. Sci.*, 2021, **12**, 4588–4598.
288 X. Su and I. Aprahamian, *Chem. Soc. Rev.*, 2014, **43**, 1963–1981.
289 L. A. Tatum, X. Su and I. Aprahamian, *Acc. Chem. Res.*, 2014, **47**, 2141–2149.
290 I. Aprahamian, *Chem. Commun.*, 2017, **53**, 6674–6684.
291 S. M. Landge and I. Aprahamian, *J. Am. Chem. Soc.*, 2009, **131**, 18269–18271.
292 S. M. Landge, E. Tkatchouk, D. Benitez, D. A. Lanfranchi, M. Elhabiri, W. A. Goddard and I. Aprahamian, *J. Am. Chem. Soc.*, 2011, **133**, 9812–9823.
293 X. Su and I. Aprahamian, *Org. Lett.*, 2011, **13**, 30–33.
294 X. Su, S. Voskian, R. P. Hughes and I. Aprahamian, *Angew. Chem., Int. Ed.*, 2013, **52**, 10734–10739.
295 M. J. Moran, M. Magrini, D. M. Walba and I. Aprahamian, *J. Am. Chem. Soc.*, 2018, **140**, 13623–13627.
296 M. L. Croteau, X. Su, D. E. Wilcox and I. Aprahamian, *ChemPlusChem*, 2014, **79**, 1214–1224.
297 X. Su and I. Aprahamian, *Org. Lett.*, 2013, **15**, 5952–5955.
298 J. T. Foy, D. Ray and I. Aprahamian, *Chem. Sci.*, 2015, **6**, 209–213.
299 J. D. Harris, M. J. Moran and I. Aprahamian, *Proc. Natl. Acad. Sci. U. S. A.*, 2018, **115**, 9414–9422.
300 B. Shao and I. Aprahamian, *ChemPhotoChem*, 2019, **3**, 361–364.
301 S. Pramanik and I. Aprahamian, *J. Am. Chem. Soc.*, 2016, **138**, 15142–15145.
302 B. Shao, N. Stankewitz, J. A. Morris, M. D. Liptak and I. Aprahamian, *Chem. Commun.*, 2019, **55**, 9551–9554.

303 L. A. Tatum, J. T. Foy and I. Aprahamian, *J. Am. Chem. Soc.*, 2014, **136**, 17438–17441.
304 I. Cvrtila, H. Fanlo-Virgós, G. Schaeffer, G. Monreal Santiago and S. Otto, *J. Am. Chem. Soc.*, 2017, **139**, 12459–12465.
305 B. Shao, M. Baroncini, H. Qian, L. Bussotti, M. Di Donato, A. Credi and I. Aprahamian, *J. Am. Chem. Soc.*, 2018, **140**, 12323–12327.
306 M. N. Chaur, D. Collado and J.-M. Lehn, *Chem. – Eur. J.*, 2011, **17**, 248–258.
307 P. Courtot, R. Pichon and J. Le Saint, *Tetrahedron Lett.*, 1976, **17**, 1181–1184.
308 H. Qian, S. Pramanik and I. Aprahamian, *J. Am. Chem. Soc.*, 2017, **139**, 9140–9143.
309 L.-Q. Zheng, S. Yang, J. Lan, L. Gyr, G. Goubert, H. Qian, I. Aprahamian and R. Zenobi, *J. Am. Chem. Soc.*, 2019, **141**, 17637–17645.
310 A. Ryabchun, Q. Li, F. Lancia, I. Aprahamian and N. Katsonis, *J. Am. Chem. Soc.*, 2019, **141**, 1196–1200.
311 B. Shao, H. Qian, Q. Li and I. Aprahamian, *J. Am. Chem. Soc.*, 2019, **141**, 8364–8371.
312 B. Mravec, J. Filo, K. Csicsai, V. Garaj, M. Kemka, A. Marini, M. Mantero, A. Bianco and M. Cigáň, *Phys. Chem. Chem. Phys.*, 2019, **21**, 24749–24757.
313 X. Guo, T. Mao, Z. Wang, P. Cheng, Y. Chen, S. Ma and Z. Zhang, *ACS Cent. Sci.*, 2020, **6**, 787–794.
314 B. Shao and I. Aprahamian, *ChemistryOpen*, 2020, **9**, 191–194.
315 Q. Li, H. Qian, B. Shao, R. P. Hughes and I. Aprahamian, *J. Am. Chem. Soc.*, 2018, **140**, 11829–11835.
316 A. Iagatti, B. Shao, A. Credi, B. Ventura, I. Aprahamian and M. Di Donato, *Beilstein J. Org. Chem.*, 2019, **15**, 2438–2446.
317 X. Guo, B. Shao, S. Zhou, I. Aprahamian and Z. Chen, *Chem. Sci.*, 2020, **11**, 3016–3021.
318 P. Gupta, T. Panda, S. Allu, S. Borah, A. Baishya, A. Gunnam, A. Nangia, P. Naumov and N. K. Nath, *Cryst. Growth Des.*, 2019, **19**, 3039–3044.
319 K. C. Hall, A. T. Franks, R. C. McAtee, M. S. Wang, V. I. Lu and K. J. Franz, *Photochem. Photobiol. Sci.*, 2017, **16**, 1604–1612.
320 G. Vantomme and J.-M. Lehn, *Angew. Chem., Int. Ed.*, 2013, **52**, 3940–3943.
321 S. Yang, D. Larsen, M. Pellegrini, S. Meier, D. F. Mierke, S. R. Beeren and I. Aprahamian, *Chem*, 2021, **7**, 2190–2200.
322 Y.-X. Yuan and Y.-S. Zheng, *ACS Appl. Mater. Interfaces*, 2019, **11**, 7303–7310.
323 Y. Yang, R. P. Hughes and I. Aprahamian, *J. Am. Chem. Soc.*, 2012, **134**, 15221–15224.
324 Y. Yang, R. P. Hughes and I. Aprahamian, *J. Am. Chem. Soc.*, 2014, **136**, 13190–13193.
325 H. Qian, Y.-Y. Wang, D.-S. Guo and I. Aprahamian, *J. Am. Chem. Soc.*, 2017, **139**, 1037–1040.
326 H. Qian, B. Shao and I. Aprahamian, *Tetrahedron*, 2017, **73**, 4901–4904.
327 M. Irie and M. Morimoto, *Photochemistry*, Royal Society of Chemistry, 2020, vol. 47, pp. 457–497.
328 M. Irie, Y. Yokoyama, M. Irie, Y. Yokoyama and M. Irie, *Chem. Rev.*, 2000, **100**, 1685–1716.
329 L. Kortekaas and W. R. Browne, *Chem. Soc. Rev.*, 2019, **48**, 3406–3424.
330 M. Irie, *Diarylethene Molecular Photoswitches*, Wiley-VCH Verlag GmbH & Co. KGaA, Weinheim, 2021.
331 M. Irie, T. Fukaminato, K. Matsuda and S. Kobatake, *Chem. Rev.*, 2014, **114**, 12174–12277.
332 T. Nakagawa, Y. Hasegawa and T. Kawai, *J. Phys. Chem. A*, 2008, **112**, 5096–5103.
333 C. Fleming, P. Remón, S. Li, N. A. Simeth, B. König, M. Grøtli and J. Andréasson, *Dyes Pigm.*, 2017, **137**, 410–420.
334 D. Wutz, C. Falenczyk, N. Kuzmanovic and B. König, *RSC Adv.*, 2015, **5**, 18075–18086.
335 C. Falenczyk, M. Schiedel, B. Karaman, T. Rumpf, N. Kuzmanovic, M. Grøtli, W. Sippl, M. Jung and B. König, *Chem. Sci.*, 2014, **5**, 4794–4799.
336 P. H.-M. Lee, C.-C. Ko, N. Zhu and V. W.-W. Yam, *J. Am. Chem. Soc.*, 2007, **129**, 6058–6059.
337 V. W.-W. Yam, C.-C. Ko and N. Zhu, *J. Am. Chem. Soc.*, 2004, **126**, 12734–12735.
338 N. A. Simeth, A. C. Kneuttinger, R. Sterner and B. König, *Chem. Sci.*, 2017, **8**, 6474–6483.
339 E. Saito, T. Ako, Y. Kobori and A. Tsuda, *RSC Adv.*, 2017, **7**, 2403–2406.
340 I. Colombier, S. Spagnoli, A. Corval, P. L. Baldeck, M. Giraud, A. Leaustic, P. Yu and M. Irie, *J. Chem. Phys.*, 2007, **126**, 011101.
341 E. C. Harvey, B. L. Feringa, J. G. Vos, W. R. Browne and M. T. Pryce, *Coord. Chem. Rev.*, 2015, **282–283**, 77–86.
342 N. M.-W. Wu, M. Ng, W. H. Lam, H.-L. Wong and V. W.-W. Yam, *J. Am. Chem. Soc.*, 2017, **139**, 15142–15150.
343 C. Zheng, C. Fan, S. Pu, B. Ben Chen and B. Ben Chen, *J. Mol. Struct.*, 2016, **1123**, 355–359.
344 X. Li, S. Pu, H. Li and G. Liu, *Dyes Pigm.*, 2014, **105**, 47–56.
345 R. Wang, S. Pu, G. Liu and S. Cui, *Beilstein J. Org. Chem.*, 2012, **8**, 1018–1026.
346 G. Liu, M. Liu, S. Pu, C. Fan and S. Cui, *Tetrahedron*, 2012, **68**, 2267–2275.
347 A. G. Lvov, M. Mörtel, A. V. Yadykov, F. W. Heinemann, V. Z. Shirinian and M. M. Khusniyarov, *Beilstein J. Org. Chem.*, 2019, **15**, 2428–2437.
348 L. Gundogdu, M. Kose, S. Takeuchi, Y. Yokoyama and E. Orhan, *J. Lumin.*, 2018, **203**, 568–575.
349 M. P. O'Hagan, J. Ramos-Soriano, S. Haldar, S. Sheikh, J. C. Morales, A. J. Mulholland and M. C. Galan, *Chem. Commun.*, 2020, **56**, 5186–5189.
350 S. Nakamura, S. Yokojima, K. Uchida, T. Tsujioka, A. Goldberg, A. Murakami, K. Shinoda, M. Mikami, T. Kobayashi, S. Kobatake, K. Matsuda and M. Irie, *J. Photochem. Photobiol., A*, 2008, **200**, 10–18.
351 S. Fukumoto, T. Nakashima and T. Kawai, *Angew. Chem., Int. Ed.*, 2011, **50**, 1565–1568.
352 R. Li, T. Nakashima, O. Galangau, S. Iijima, R. Kanazawa and T. Kawai, *Chem. – Asian J.*, 2015, **10**, 1725–1730.
353 R. Göstl, B. Kobin, L. Grubert, M. Pätzel and S. Hecht, *Chem. – Eur. J.*, 2012, **18**, 14282–14285.
354 K. Morimitsu, S. Kobatake and M. Irie, *Mol. Cryst. Liq. Cryst.*, 2005, **431**, 451–454.

355 T. Fukaminato, T. Hirose, T. Doi, M. Hazama, K. Matsuda and M. Irie, *J. Am. Chem. Soc.*, 2014, **136**, 17145–17154.
356 S. Fredrich, R. Göstl, M. Herder, L. Grubert and S. Hecht, *Angew. Chem., Int. Ed.*, 2016, **55**, 1208–1212.
357 M. Irie and K. Sayo, *J. Phys. Chem.*, 1992, **96**, 7671–7674.
358 K. Uno, M. L. Bossi, M. Irie, V. N. Belov and S. W. Hell, *J. Am. Chem. Soc.*, 2019, **141**, 16471–16478.
359 I. Hamdi, G. Buntinx, A. Perrier, O. Devos, N. Jaïdane, S. Delbaere, A. K. Tiwari, J. Dubois, M. Takeshita, Y. Wada and S. Aloïse, *Phys. Chem. Chem. Phys.*, 2016, **18**, 28091–28100.
360 S. Fredrich, T. Morack, M. Sliwa and S. Hecht, *Chem. – Eur. J.*, 2020, **26**, 7672–7677.
361 M. Irie and M. Morimoto, *Pure Appl. Chem.*, 2009, **81**, 1655–1665.
362 S. Kawai, T. Nakashima, K. Atsumi, T. Sakai, M. Harigai, Y. Imamoto, H. Kamikubo, M. Kataoka and T. Kawai, *Chem. Mater.*, 2007, **19**, 3479–3483.
363 M. Irie, T. Lifka, K. Uchida, S. Kobatake and Y. Shindo, *Chem. Commun.*, 1999, 747–750.
364 Y.-C. Jeong, D. G. Park, I. S. Lee, S. I. Yang and K.-H. Ahn, *J. Mater. Chem.*, 2009, **19**, 97–103.
365 Y.-C. Jeong, S. I. Yang, E. Kim and K.-H. Ahn, *Tetrahedron*, 2006, **62**, 5855–5861.
366 P. D. Patel, I. A. Mikhailov, K. D. Belfield and A. E. Masunov, *Int. J. Quantum Chem.*, 2009, **109**, 3711–3722.
367 M. Herder, B. M. Schmidt, L. Grubert, M. Pätzel, J. Schwarz and S. Hecht, *J. Am. Chem. Soc.*, 2015, **137**, 2738–2747.
368 Y.-C. Jeong, D. G. Park, E. Kim, K.-H. Ahn and S. I. Yang, *Chem. Commun.*, 2006, 1881.
369 J. J. D. de Jong, L. N. Lucas, R. Hania, A. Pugzlys, R. M. Kellogg, B. L. Feringa, K. Duppen and J. H. van Esch, *Eur. J. Org. Chem.*, 2003, 1887–1893.
370 D. Lachmann, A. Konieczny, M. Keller and B. König, *Org. Biomol. Chem.*, 2019, **17**, 2467–2478.
371 B. Roubinet, M. L. Bossi, P. Alt, M. Leutenegger, H. Shojaei, S. Schnorrenberg, S. Nizamov, M. Irie, V. N. Belov and S. W. Hell, *Angew. Chem., Int. Ed.*, 2016, **55**, 15429–15433.
372 T. Yamaguchi, K. Uchida and M. Irie, *J. Am. Chem. Soc.*, 1997, **119**, 6066–6071.
373 N. Ziebart, F. Schröder and K. Rück-Braun, *ChemPhotoChem*, 2019, **3**, 396–402.
374 M. Kathan, F. Eisenreich, C. Jurissek, A. Dallmann, J. Gurke and S. Hecht, *Nat. Chem.*, 2018, **10**, 1031–1036.
375 D. Wilson and N. R. Branda, *Angew. Chem., Int. Ed.*, 2012, **51**, 5431–5434.
376 J.-M. L. Alvaro Fernández-Acebes, A. Fernández-Acebes and J.-M. Lehn, *Chem. – Eur. J.*, 1999, **5**, 3285–3292.
377 F. Schweighöfer, L. Dworak, C. A. Hammer, H. Gustmann, M. Zastrow, K. Rück-Braun and J. Wachtveitl, *Sci. Rep.*, 2016, **6**, 28638.
378 S. Cobo, F. Lafolet, E. Saint-Aman, C. Philouze, C. Bucher, S. Silvi, A. Credi and G. Royal, *Chem. Commun.*, 2015, **51**, 13886–13889.
379 K. Klaue, Y. Garmshausen and S. Hecht, *Angew. Chem., Int. Ed.*, 2018, **57**, 1414–1417.
380 E. Lognon, M. Heitz, A. Bakkar, S. Cobo, F. Loiseau, E. Saint-Aman, G. Royal and M. Boggio-Pasqua, *ChemPhysChem*, 2020, **21**, 1571–1577.
381 K. Klaue, W. Han, P. Liesfeld, F. Berger, Y. Garmshausen and S. Hecht, *J. Am. Chem. Soc.*, 2020, **142**, 11857–11864.
382 B. Saima, N. Khan, Y. S. S. Al-Faiyz, R. Ludwig, W. Rehman, M. Habib-ur-Rehman, N. S. Sheikh and K. Ayub, *J. Mol. Graph. Model.*, 2019, **88**, 261–272.
383 R. H. Mitchell, T. R. Ward, Y. Chen, Y. Wang, S. A. Weerawarna, P. W. Dibble, M. J. Marsella, A. Almutairi and Z.-Q. Wang, *J. Am. Chem. Soc.*, 2003, **125**, 2974–2988.
384 P. Liesfeld, Y. Garmshausen, S. Budzak, J. Becker, A. Dallmann, D. Jacquemin and S. Hecht, *Angew. Chem., Int. Ed.*, 2020, **59**, 19352–19358.
385 M. Jacquet, L. M. Uriarte, F. Lafolet, M. Boggio-Pasqua, M. Sliwa, F. Loiseau, E. Saint-Aman, S. Cobo and G. Royal, *J. Phys. Chem. Lett.*, 2020, **11**, 2682–2688.
386 H.-W. Lee, S. G. Robinson, S. Bandyopadhyay, R. H. Mitchell and D. Sen, *J. Mol. Biol.*, 2007, **371**, 1163–1173.
387 A. Gonzalez, E. S. Kengmana, M. V. Fonseca and G. G. D. Han, *Mater. Today Adv.*, 2020, **6**, 100058.
388 M. Mansø, A. U. Petersen, Z. Wang, P. Erhart, M. B. Nielsen and K. Moth-Poulsen, *Nat. Commun.*, 2018, **9**, 1945.
389 M. Jevric, Z. Wang, A. U. Petersen, M. Mansø, C. J. Sumby, M. B. Nielsen and K. Moth-Poulsen, *Eur. J. Org. Chem.*, 2019, 2354–2361.
390 A. Dreos, Z. Wang, B. E. Tebikachew, K. Moth-Poulsen and J. Andréasson, *J. Phys. Chem. Lett.*, 2018, **9**, 6174–6178.
391 M. Bertram, F. Waidhas, M. Jevric, L. Fromm, C. Schuschke, M. Kastenmeier, A. Görling, K. Moth-Poulsen, O. Brummel and J. Libuda, *J. Chem. Phys.*, 2020, **152**, 044708.
392 O. Brummel, D. Besold, T. Döpper, Y. Wu, S. Bochmann, F. Lazzari, F. Waidhas, U. Bauer, P. Bachmann, C. Papp, H.-P. Steinrück, A. Görling, J. Libuda and J. Bachmann, *ChemSusChem*, 2016, **9**, 1424–1432.
393 O. Brummel, F. Waidhas, U. Bauer, Y. Wu, S. Bochmann, H.-P. Steinrück, C. Papp, J. Bachmann and J. Libuda, *J. Phys. Chem. Lett.*, 2017, **8**, 2819–2825.
394 U. Bauer, L. Fromm, C. Weiß, P. Bachmann, F. Späth, F. Düll, J. Steinhauer, W. Hieringer, A. Görling, A. Hirsch, H.-P. Steinrück and C. Papp, *J. Phys. Chem. C*, 2019, **123**, 7654–7664.
395 H. Hogeveen and H. C. Volger, *J. Am. Chem. Soc.*, 1967, **89**, 2486–2487.
396 W. G. Dauben and R. L. Cargill, *Tetrahedron*, 1961, **15**, 197–201.
397 B. E. Tebikachew, F. Edhborg, N. Kann, B. Albinsson and K. Moth-Poulsen, *Phys. Chem. Chem. Phys.*, 2018, **20**, 23195–23201.
398 A. Dreos, Z. Wang, J. Udmark, A. Ström, P. Erhart, K. Börjesson, M. B. Nielsen and K. Moth-Poulsen, *Adv. Energy Mater.*, 2018, **8**, 1703401.
399 C. Schuschke, C. Hohner, M. Jevric, A. Ugleholdt Petersen, Z. Wang, M. Schwarz, M. Kettner, F. Waidhas, L. Fromm, C. J. Sumby, A. Görling, O. Brummel, K. Moth-Poulsen and J. Libuda, *Nat. Commun.*, 2019, **10**, 2384.
400 M. Jevric, A. U. Petersen, M. Mansø, S. Kumar Singh, Z. Wang, A. Dreos, C. Sumby, M. B. Nielsen, K. Börjesson, P. Erhart and K. Moth-Poulsen, *Chem. – Eur. J.*, 2018, **24**, 12767–12772.

401 A. Lennartson, A. Roffey and K. Moth-Poulsen, *Tetrahedron Lett.*, 2015, **56**, 1457–1465.
402 A. U. Petersen, A. I. Hofmann, M. Fillols, M. Mansø, M. Jevric, Z. Wang, C. J. Sumby, C. Müller and K. Moth-Poulsen, *Adv. Sci.*, 2019, **6**, 1900367.
403 F. Waidhas, M. Jevric, L. Fromm, M. Bertram, A. Görling, K. Moth-Poulsen, O. Brummel and J. Libuda, *Nano Energy*, 2019, **63**, 103872.
404 M. D. Kilde, M. Mansø, N. Ree, A. U. Petersen, K. Moth-Poulsen, K. V. Mikkelsen and M. B. Nielsen, *Org. Biomol. Chem.*, 2019, **17**, 7735–7746.
405 M. Mansø, B. E. Tebikachew, K. Moth-Poulsen and M. B. Nielsen, *Org. Biomol. Chem.*, 2018, **16**, 5585–5590.
406 M. Mansø, M. D. Kilde, S. K. Singh, P. Erhart, K. Moth-Poulsen and M. B. Nielsen, *Phys. Chem. Chem. Phys.*, 2019, **21**, 3092–3097.
407 M. Quant, A. Hamrin, A. Lennartson, P. Erhart and K. Moth-Poulsen, *J. Phys. Chem. C*, 2019, **123**, 7081–7087.
408 N. A. Simeth, L.-M. M. Altmann, N. Wössner, E. Bauer, M. Jung and B. König, *J. Org. Chem.*, 2018, **83**, 7919–7927.
409 R. K. Weerasekara, H. Uekusa and C. V. Hettiarachchi, *Cryst. Growth Des.*, 2017, **17**, 3040–3047.
410 R. Matsushima and H. Sakaguchi, *J. Photochem. Photobiol., A*, 1997, **108**, 239–245.
411 K. Rustler, G. Maleeva, A. M. J. Gomila, P. Gorostiza, P. Bregestovski and B. König, *Chem. – Eur. J.*, 2020, **26**, 12722–12727.
412 F. Renth, R. Siewertsen and F. Temps, *Int. Rev. Phys. Chem.*, 2013, **32**, 1–38.
413 Y. Kohno, Y. Tamura and R. Matsushima, *J. Photochem. Photobiol., A*, 2009, **201**, 98–101.
414 M. Seibold, M. Handschuh, H. Port and H. C. Wolf, *J. Lumin.*, 1997, **72–74**, 454–456.
415 J. Andréasson, S. D. Straight, T. A. Moore, A. L. Moore and D. Gust, *J. Am. Chem. Soc.*, 2008, **130**, 11122–11128.
416 C. Slavov, C. Boumrifak, C. A. Hammer, P. Trojanowski, X. Chen, W. J. Lees, J. Wachtveitl and M. Braun, *Phys. Chem. Chem. Phys.*, 2016, **18**, 10289–10296.
417 X. Chen, N. I. Islamova, R. V. Robles and W. J. Lees, *Photochem. Photobiol. Sci.*, 2011, **10**, 1023–1029.
418 D. Wutz, D. Gluhacevic, A. Chakrabarti, K. Schmidtkunz, D. Robaa, F. Erdmann, C. Romier, W. Sippl, M. Jung and B. König, *Org. Biomol. Chem.*, 2017, **15**, 4882–4896.
419 M. Kose, E. Orhan, M. Köse and E. Orhan, *Turk. J. Chem.*, 2009, **33**, 579–588.
420 N. Sivasankaran and K. Palaninathan, *Polym. Degrad. Stab.*, 2013, **98**, 1852–1861.
421 E. N. Shepelenko, N. I. Makarova, V. A. Podshibyakin, K. S. Tikhomirova, A. D. Dubonosov, A. V. Metelitsa, V. A. Bren and V. I. Minkin, *Russ. J. Org. Chem.*, 2017, **53**, 366–370.
422 V. P. Rybalkin, N. I. Makarova, S. Y. Pluzhnikova, L. L. Popova, A. V. Metelitsa, V. A. Bren' and V. I. Minkina, *Russ. Chem. Bull.*, 2014, **63**, 1780–1784.
423 M. Vlajić, W. Unger, J. Bruns and K. Rueck-Braun, *Appl. Surf. Sci.*, 2019, **465**, 686–692.
424 A. Yassar, H. Jaafari, N. Rebière-Galy, M. Frigoli, C. Moustrou, A. Samat and R. Guglielmetti, *Eur. Phys. J. Appl. Phys.*, 2002, **18**, 3–8.
425 R. S. Becker and J. Michl, *J. Am. Chem. Soc.*, 1966, **88**, 5931–5933.
426 B. H. Strudwick, C. O'Bryen, H. J. Sanders, S. Woutersen and W. J. Buma, *Phys. Chem. Chem. Phys.*, 2019, **21**, 11689–11696.
427 S. V. Paramonov, V. Lokshin, H. Ihmels and O. A. Fedorova, *Photochem. Photobiol. Sci.*, 2011, **10**, 1279–1282.
428 A. Migani, P. L. Gentili, F. Negri, M. Olivucci, A. Romani, G. Favaro and R. S. Becker, *J. Phys. Chem. A*, 2005, **109**, 8684–8692.
429 S. Kumar, D. Hernandez, B. Hoa, Y. Lee, J. S. Yang and A. McCurdy, *Org. Lett.*, 2008, **10**, 3761–3764.
430 Y. Inagaki, Y. Kobayashi, K. Mutoh and J. Abe, *J. Am. Chem. Soc.*, 2017, **139**, 13429–13441.
431 C. M. Sousa, J. Berthet, S. Delbaere and P. J. Coelho, *Dyes Pigm.*, 2019, **169**, 118–124.
432 Y. Fang, Q. Meng, Z. Wang, G. Wang, H. Jiang, H. Zhao and Y. Wang, *J. Sol–Gel Sci. Technol.*, 2015, **73**, 293–298.
433 C. M. Sousa, J. Berthet, S. Delbaere, A. Polónia and P. J. Coelho, *J. Org. Chem.*, 2015, **80**, 12177–12181.
434 M. Zayat and D. Levy, *J. Mater. Chem.*, 2003, **13**, 727–730.
435 D. Avagliano, P. A. Sánchez-Murcia and L. González, *Phys. Chem. Chem. Phys.*, 2019, **21**, 8614–8618.
436 Y. Li, K. M.-C. Wong, A. Y.-Y. Tam, L. Wu and V. W.-W. Yam, *Chem. – Eur. J.*, 2010, **16**, 8690–8698.
437 C. Kaiser, T. Halbritter, A. Heckel and J. Wachtveitl, *ChemistrySelect*, 2017, **2**, 4111–4123.
438 L. Kortekaas, O. Ivashenko, J. T. van Herpt and W. R. Browne, *J. Am. Chem. Soc.*, 2016, **138**, 1301–1312.
439 L. Kortekaas, J. Chen, D. Jacquemin and W. R. Browne, *J. Phys. Chem. B*, 2018, **122**, 6423–6430.
440 J. T. C. Wojtyk, A. Wasey, N.-N. Xiao, P. M. Kazmaier, S. Hoz, C. Yu, R. P. Lemieux and E. Buncel, *J. Phys. Chem. A*, 2007, **111**, 2511–2516.
441 J. D. Steen, D. R. Duijnstee, A. S. Sardjan, J. Martinelli, L. Kortekaas, D. Jacquemin and W. R. Browne, *J. Phys. Chem. A*, 2021, **125**, 3355–3361.
442 R. Klajn, *Chem. Soc. Rev.*, 2014, **43**, 148–184.
443 C. L. Fleming, S. Li, M. Grøtli and J. Andréasson, *J. Am. Chem. Soc.*, 2018, **140**, 14069–14072.
444 F. Jonsson, T. Beke-Somfai, J. Andréasson and B. Nordén, *Langmuir*, 2013, **29**, 2099–2103.
445 T. Stafforst and D. Hilvert, *Chem. Commun.*, 2009, 287–288.
446 F. Liu and K. Morokuma, *J. Am. Chem. Soc.*, 2013, **135**, 10693–10702.
447 S. F. Bittmann, R. Dsouza, K. M. Siddiqui, S. A. Hayes, A. Rossos, G. Corthey, M. Kochman, V. I. Prokhorenko, R. S. Murphy, H. Schwoerer and R. J. D. Miller, *Phys. Chem. Chem. Phys.*, 2019, **21**, 18119–18127.
448 M. Hammarson, J. R. Nilsson, S. Li, T. Beke-Somfai and J. Andréasson, *J. Phys. Chem. B*, 2013, **117**, 13561–13571.
449 H. Görner, *Phys. Chem. Chem. Phys.*, 2001, **3**, 416–423.
450 C. Brieke and A. Heckel, *Chem. – Eur. J.*, 2013, **19**, 15726–15734.

451 S. Scarmagnani, Z. Walsh, C. Slater, N. Alhashimy, B. Paull, M. Macka and D. Diamond, *J. Mater. Chem.*, 2008, **18**, 5063.
452 M. Schnurbus, M. Kabat, E. Jarek, M. Krzan, P. Warszynski and B. Braunschweig, *Langmuir*, 2020, **36**, 6871–6879.
453 C. Berton, D. M. Busiello, S. Zamuner, E. Solari, R. Scopelliti, F. Fadaei-Tirani, K. Severin and C. Pezzato, *Chem. Sci.*, 2020, **11**, 8457–8468.
454 D. Avagliano, P. A. Sánchez-Murcia and L. González, *Chem. – Eur. J.*, 2020, **26**, 13039–13045.
455 M. J. Feeney and S. W. Thomas, *Macromolecules*, 2018, **51**, 8027–8037.
456 X. Xie, G. Mistlberger and E. Bakker, *J. Am. Chem. Soc.*, 2012, **134**, 16929–16932.
457 X. Wang, J. Hu, Y. Li, J. Jie, A. Xia, S. Zhu, Y. Wang and S. X.-A. Zhang, *J. Phys. Chem. C*, 2016, **120**, 598–605.
458 C. Özçoban, T. Halbritter, S. Steinwand, L.-M. Herzig, J. Kohl-Landgraf, N. Askari, F. Groher, B. Fürtig, C. Richter, H. Schwalbe, B. Suess, J. Wachtveitl and A. Heckel, *Org. Lett.*, 2015, **17**, 1517–1520.
459 M. Hammarson, J. R. Nilsson, S. Li, P. Lincoln and J. Andréasson, *Chem. – Eur. J.*, 2014, **20**, 15855–15862.
460 J. Kohl-Landgraf, M. Braun, C. Özçoban, D. P. N. Gonçalves, A. Heckel and J. Wachtveitl, *J. Am. Chem. Soc.*, 2012, **134**, 14070–14077.
461 J. Andersson, S. Li, P. Lincoln and J. Andréasson, *J. Am. Chem. Soc.*, 2008, **130**, 11836–11837.
462 J. R. Nilsson, S. Li, B. Önfelt and J. Andréasson, *Chem. Commun.*, 2011, **47**, 11020–11022.
463 Y. Shiraishi, M. Itoh and T. Hirai, *Phys. Chem. Chem. Phys.*, 2010, **12**, 13737–13745.
464 T. Halbritter, C. Kaiser, J. Wachtveitl and A. Heckel, *J. Org. Chem.*, 2017, **82**, 8040–8047.
465 D. Hu, Z. Tian, W. Wu, W. Wan and A. Li, *Microsc. Microanal.*, 2009, **15**, 840–841.
466 I. S. Park, Y.-S. Jung, K.-J. Lee and J.-M. Kim, *Chem. Commun.*, 2010, **46**, 2859–2861.
467 B. Seefeldt, R. Kasper, M. Beining, J. Mattay, J. Arden-Jacob, N. Kemnitzer, K. H. Drexhage, M. Heilemann and M. Sauer, *Photochem. Photobiol. Sci.*, 2010, **9**, 213–220.
468 D. Dulić, S. J. van der Molen, T. Kudernac, H. T. Jonkman, J. J. D. de Jong, T. N. Bowden, J. van Esch, B. L. Feringa and B. J. van Wees, *Phys. Rev. Lett.*, 2003, **91**, 207402.
469 S. Garg, H. Schwartz, M. Kozlowska, A. B. Kanj, K. Müller, W. Wenzel, U. Ruschewitz and L. Heinke, *Angew. Chem., Int. Ed.*, 2019, **58**, 1193–1197.
470 A. B. Kanj, A. Chandresh, A. Gerwien, S. Grosjean, S. Bräse, Y. Wang, H. Dube and L. Heinke, *Chem. Sci.*, 2020, **11**, 1404–1410.
471 S. K. Rastogi, Z. Zhao, M. B. Gildner, B. A. Shoulders, T. L. Velasquez, M. O. Blumenthal, L. Wang, X. Li, T. W. Hudnall, T. Betancourt, L. Du and W. J. Brittain, *Tetrahedron*, 2021, **80**, 131854.
472 F. Krohm, J. Kind, R. Savka, M. Alcaraz Janßen, D. Herold, H. Plenio, C. M. Thiele and A. Andrieu-Brunsen, *J. Mater. Chem. C*, 2016, **4**, 4067–4076.
473 Q. Zou, X. Li, J. Zhou, K. Bai and H. Ågren, *Dyes Pigm.*, 2014, **107**, 174–181.
474 S. Coleman, R. Byrne, S. Minkovska and D. Diamond, *Phys. Chem. Chem. Phys.*, 2009, **11**, 5608–5614.
475 L. Raboin, M. Matheron, J. Biteau, T. Gacoin and J.-P. Boilot, *J. Mater. Chem.*, 2008, **18**, 3242–3248.
476 R. Pardo, M. Zayat and D. Levy, *J. Mater. Chem.*, 2009, **19**, 6756–6760.
477 P. R. Sahoo and S. Kumar, *Sens. Actuators, B*, 2016, **226**, 548–552.
478 S. Helmy, F. A. Leibfarth, S. Oh, J. E. Poelma, C. J. Hawker and J. Read de Alaniz, *J. Am. Chem. Soc.*, 2014, **136**, 8169–8172.
479 A. D. Laurent, M. Medveď and D. Jacquemin, *ChemPhysChem*, 2016, **17**, 1846–1851.
480 D. M. Sanchez, U. Raucci, K. N. Ferreras and T. J. Martínez, *J. Phys. Chem. Lett.*, 2020, **11**, 7901–7907.
481 M. Ugandi and M. Roemelt, *J. Phys. Chem. A*, 2020, **124**, 7756–7767.
482 C. García-Iriepa, M. Marazzi and D. Sampedro, *ChemPhotoChem*, 2019, **3**, 866–873.
483 M. Di Donato, M. M. Lerch, A. Lapini, A. D. Laurent, A. Iagatti, L. Bussotti, S. P. Ihrig, M. Medved', D. Jacquemin, W. Szymański, W. J. Buma, P. Foggi and B. L. Feringa, *J. Am. Chem. Soc.*, 2017, **139**, 15596–15599.
484 M. M. Lerch, S. J. Wezenberg, W. Szymanski and B. L. Feringa, *J. Am. Chem. Soc.*, 2016, **138**, 6344–6347.
485 J. N. Bull, E. Carrascosa, N. Mallo, M. S. Scholz, G. da Silva, J. E. Beves and E. J. Bieske, *J. Phys. Chem. Lett.*, 2018, **9**, 665–671.
486 M. M. Lerch, M. Di Donato, A. D. Laurent, M. Medved', A. Iagatti, L. Bussotti, A. Lapini, W. J. Buma, P. Foggi, W. Szymański and B. L. Feringa, *Angew. Chem., Int. Ed.*, 2018, **57**, 8063–8068.
487 M. M. Lerch, M. Medved', A. Lapini, A. D. Laurent, A. Iagatti, L. Bussotti, W. Szymański, W. J. Buma, P. Foggi, M. Di Donato and B. L. Feringa, *J. Phys. Chem. A*, 2018, **122**, 955–964.
488 R. F. A. Gomes, J. A. S. Coelho and C. A. M. Afonso, *Chem. – Eur. J.*, 2018, **24**, 9170–9186.
489 N. Mallo, E. D. Foley, H. Iranmanesh, A. D. W. Kennedy, E. T. Luis, J. Ho, J. B. Harper and J. E. Beves, *Chem. Sci.*, 2018, **9**, 8242–8252.
490 Y. Duan, H. Zhao, C. Xiong, L. Mao, D. Wang and Y. Zheng, *Chin. J. Chem.*, 2021, **39**, 985–998.
491 M. M. Lerch, W. Szymański and B. L. Feringa, *Chem. Soc. Rev.*, 2018, **47**, 1910–1937.
492 J. R. Hemmer, S. O. Poelma, N. Treat, Z. A. Page, N. D. Dolinski, Y. J. Diaz, W. Tomlinson, K. D. Clark, J. P. Hooper, C. Hawker and J. Read de Alaniz, *J. Am. Chem. Soc.*, 2016, **138**, 13960–13966.
493 J. R. Hemmer, Z. A. Page, K. D. Clark, F. Stricker, N. D. Dolinski, C. J. Hawker and J. Read de Alaniz, *J. Am. Chem. Soc.*, 2018, **140**, 10425–10429.
494 M. M. Sroda, F. Stricker, J. A. Peterson, A. Bernal and J. Read de Alaniz, *Chem. – Eur. J.*, 2021, **27**, 4183–4190.
495 S. Helmy, S. Oh, F. A. Leibfarth, C. J. Hawker and J. Read de Alaniz, *J. Org. Chem.*, 2014, **79**, 11316–11329.

496 H. Zulfikri, M. A. J. Koenis, M. M. Lerch, M. Di Donato, W. Szymański, C. Filippi, B. L. Feringa and W. J. Buma, *J. Am. Chem. Soc.*, 2019, **141**, 7376–7384.
497 N. Mallo, P. T. Brown, H. Iranmanesh, T. S. C. MacDonald, M. J. Teusner, J. B. Harper, G. E. Ball and J. E. Beves, *Chem. Commun.*, 2016, **52**, 13576–13579.
498 B. F. Lui, N. T. Tierce, F. Tong, M. M. Sroda, H. Lu, J. Read de Alaniz and C. J. Bardeen, *Photochem. Photobiol. Sci.*, 2019, **18**, 1587–1595.
499 J. Alves, S. Wiedbrauk, C. Barner-Kowollik and J. P. Blinco, *ChemPhotoChem*, 2021, **5**, 1–6.
500 H. Zhao, D. Wang, Y. Fan, M. Ren, S. Dong and Y. Zheng, *Langmuir*, 2018, **34**, 15537–15543.
501 J. Lee, M. M. Sroda, Y. Kwon, S. El-Arid, S. Seshadri, L. F. Gockowski, E. W. Hawkes, M. T. Valentine and J. Read de Alaniz, *ACS Appl. Mater. Interfaces*, 2020, **12**, 54075–54082.
502 J. E. Yap, N. Mallo, D. S. Thomas, J. E. Beves and M. H. Stenzel, *Polym. Chem.*, 2019, **10**, 6515–6522.
503 J. Ahrens, T. Bian, T. Vexler and R. Klajn, *ChemPhotoChem*, 2017, **1**, 230–236.
504 N. Mallo, A. Tron, J. Andréasson, J. B. Harper, L. S. D. Jacob, N. D. McClenaghan, G. Jonusauskas and J. E. Beves, *ChemPhotoChem*, 2020, **4**, 407–412.
505 C. Zheng, Y. Yu, K. Shi, B. Zhu, H. Zhou, S. Zhang, J. Yang, L. Shi and C. Ran, 2020, Prepr. from bioRxiv, DOI: 10.1101/2020.10.04.325696.
506 R. Saha, A. Devaraj, S. Bhattacharyya, S. Das, E. Zangrando and P. S. Mukherjee, *J. Am. Chem. Soc.*, 2019, **141**, 8638–8645.
507 J. E. Yap, L. Zhang, J. T. Lovegrove, J. E. Beves and M. H. Stenzel, *Macromol. Rapid Commun.*, 2020, **41**, 2000236.
508 Q. Chen, Y. J. Diaz, M. C. Hawker, M. R. Martinez, Z. A. Page, S. Xiao-An Zhang, C. J. Hawker and J. Read de Alaniz, *Macromolecules*, 2019, **52**, 4370–4375.
509 S. H. Mostafavi, W. Li, K. D. Clark, F. Stricker, J. R. de Alaniz and C. J. Bardeen, *Macromolecules*, 2019, **52**, 6311–6317.
510 G. Sobczak, I. Misztalewska-Turkowicz and V. Sashuk, *J. Phys. Chem. C*, 2021, **125**, 5306–5314.
511 S. Singh, K. Friedel, M. Himmerlich, Y. Lei, G. Schlingloff and A. Schober, *ACS Macro Lett.*, 2015, **4**, 1273–1277.
512 Y.-D. Cai, T.-Y. Chen, X. Q. Chen and X. Bao, *Org. Lett.*, 2019, **21**, 7445–7449.
513 Y. Duan, H. Zhao, G. Xue, Z. Wang, C. Xiong, L. Mao, C. He, D. Wang and Y. Zheng, *Prepr. Res. Sq.*, 2020, DOI: 10.21203/RS.3.RS-43551/V1.
514 S. Seshadri, L. F. Gockowski, J. Lee, M. Sroda, M. E. Helgeson, J. Read de Alaniz and M. T. Valentine, *Nat. Commun.*, 2020, **11**, 2599.
515 H. Gotfredsen, M. D. Kilde, M. Santella, A. Kadziola and M. B. Nielsen, *Mol. Syst. Des. Eng.*, 2019, **4**, 199–205.
516 S. L. Broman and M. B. Nielsen, *Phys. Chem. Chem. Phys.*, 2014, **16**, 21172–21182.
517 N. Shahzad, R. U. Nisa and K. Ayub, *Struct. Chem.*, 2013, **24**, 2115–2126.
518 A. U. Petersen, M. Jevric, R. J. Mandle, E. J. Davis, S. J. Cowling, J. W. Goodby and M. B. Nielsen, *RSC Adv.*, 2015, **5**, 89731–89744.
519 H. Torres-Pierna, C. Roscini, A. Vlasceanu, S. L. Broman, M. Jevric, M. Cacciarini and M. B. Nielsen, *Dyes Pigm.*, 2017, **145**, 359–364.
520 A. Vlasceanu, M. Cacciarini and M. B. Nielsen, *Tetrahedron*, 2018, **74**, 6635–6646.
521 M. D. Kilde, R. Kristensen, G. Olsen, J. O. Jeppesen and M. B. Nielsen, *Eur. J. Org. Chem.*, 2019, 5532–5539.
522 M. Cacciarini, A. B. Skov, M. Jevric, A. S. Hansen, J. Elm, H. G. Kjaergaard, K. V. Mikkelsen and M. Brøndsted Nielsen, *Chem. – Eur. J.*, 2015, **21**, 7454–7461.
523 M. H. Hansen, J. Elm, S. T. Olsen, A. N. Gejl, F. E. Storm, B. N. Frandsen, A. B. Skov, M. B. Nielsen, H. G. Kjaergaard and K. V. Mikkelsen, *J. Phys. Chem. A*, 2016, **120**, 9782–9793.
524 A. Perrier, F. Maurel and D. Jacquemin, *Phys. Chem. Chem. Phys.*, 2011, **13**, 13791–13799.
525 A. S. Gertsen, S. T. Olsen, S. L. Broman, M. B. Nielsen and K. V. Mikkelsen, *J. Phys. Chem. C*, 2017, **121**, 195–201.
526 A. U. Petersen, S. L. Broman, S. T. Olsen, A. S. Hansen, L. Du, A. Kadziola, T. Hansen, H. G. Kjaergaard, K. V. Mikkelsen and M. Brøndsted Nielsen, *Chem. – Eur. J.*, 2015, **21**, 3968–3977.
527 A. G. Lvov and A. Bredihhin, *Org. Biomol. Chem.*, 2021, **19**, 4460–4468.
528 M. Å. Petersen, A. S. Andersson, K. Kilså and M. B. Nielsen, *Eur. J. Org. Chem.*, 2009, 1855–1858.
529 B. Cheng, J. Morstein, L. K. Ladefoged, J. B. Maesen, B. Schiøtt, S. Sinning and D. Trauner, *ACS Chem. Neurosci.*, 2020, **11**, 1231–1237.
530 R. M. Evans and D. J. Mangelsdorf, *Cell*, 2014, **157**, 255–266.
531 W. A. Velema, M. van der Toorn, W. Szymanski and B. L. Feringa, *J. Med. Chem.*, 2013, **56**, 4456–4464.
532 M. A. Brown and S. C. De Vito, *Crit. Rev. Environ. Sci. Technol.*, 1993, **23**, 249–324.
533 D. Mulatihan, T. Guo and Y. Zhao, *Photochem. Photobiol.*, 2020, **96**, 1163–1168.
534 C. Renner and L. Moroder, *ChemBioChem*, 2006, **7**, 868–878.
535 A. A. Beharry, L. Wong, V. Tropepe and G. A. Woolley, *Angew. Chem., Int. Ed.*, 2011, **50**, 1325–1327.
536 S. Samanta, A. Babalhavaeji, M. Dong and G. A. Woolley, *Angew. Chem., Int. Ed.*, 2013, **52**, 14127–14130.
537 M. Dong, A. Babalhavaeji, S. Samanta, A. A. Beharry and G. A. Woolley, *Acc. Chem. Res.*, 2015, **48**, 2662–2670.
538 J. Zielonka, J. Joseph, A. Sikora, M. Hardy, O. Ouari, J. Vasquez-Vivar, G. Cheng, M. Lopez and B. Kalyanaraman, *Chem. Rev.*, 2017, **117**, 10043–10120.
539 D. Kand, L. Pizarro, I. Angel, A. Avni, D. Friedmann-Morvinski and R. Weinstain, *Angew. Chem., Int. Ed.*, 2019, **58**, 4659–4663.
540 P. Mishra, B. Nayak and R. K. Dey, *Asian J. Pharm. Sci.*, 2016, **11**, 337–348.
541 N. J. Yang and M. J. Hinner, *Site-Specific Protein Labeling*, Humana Press, New York, 2015, pp. 29–53.
542 A. Keppler, C. Arrivoli, L. Sironi and J. Ellenberg, *Biotechniques*, 2006, **41**, 167–175.
543 D. E. Scott, A. R. Bayly, C. Abell and J. Skidmore, *Nat. Rev. Drug Discovery*, 2016, **15**, 533–550.

544 X. Xue, A. Lindstrom, H. Qu and Y. Li, *Wiley Interdiscip. Rev.: Nanomed. Nanobiotechnol.*, 2020, **12**, e1607.
545 N. Berdigaliyev and M. Aljofan, *Future Med. Chem.*, 2020, **12**, 939–947.
546 Z. Chen, S.-H. Yoo and J. S. Takahashi, *Annu. Rev. Pharmacol. Toxicol.*, 2018, **58**, 231–252.
547 M. R. Arkin, Y. Tang and J. A. Wells, *Chem. Biol.*, 2014, **21**, 1102–1114.
548 D. Bojadzic and P. Buchwald, *Curr. Top. Med. Chem.*, 2018, **18**, 674–699.
549 A. D. Bondarev, M. M. Attwood, J. Jonsson, V. N. Chubarev, V. V. Tarasov and H. B. Schiöth, *Expert Opin. Drug Discovery*, 2020, **15**, 1291–1307.
550 A.-M. Yu, Y. H. Choi and M.-J. Tu, *Pharmacol. Rev.*, 2020, **72**, 862–898.
551 T. P. Kogan, B. Dupre, K. M. Keller, I. L. Scott, H. Bui, R. V. Market, P. J. Beck, J. A. Voytus, B. M. Revelle and D. Scott, *J. Med. Chem.*, 1995, **38**, 4976–4984.
552 A. Bernardi and P. Cheshev, *Chem. – Eur. J.*, 2008, **14**, 7434–7441.
553 N. Jain, K. Tamura, G. Déjean, F. Van Petegem and H. Brumer, *ACS Chem. Biol.*, 2021, DOI: 10.1021/acschembio.1c00063.
554 J. K. Patra, G. Das, L. F. Fraceto, E. V. R. Campos, M. del, P. Rodriguez-Torres, L. S. Acosta-Torres, L. A. Diaz-Torres, R. Grillo, M. K. Swamy, S. Sharma, S. Habtemariam and H.-S. Shin, *J. Nanobiotechnol.*, 2018, **16**, 71.
555 C. Rousselle, P. Clair, J. Temsamani and J.-M. Scherrmann, *J. Drug Target*, 2002, **10**, 309–315.
556 F. Y. Aoki and K. E. Doucette, *Expert Opin. Pharmacother.*, 2001, **2**, 1671–1683.
557 R. Zhang, X. Qin, F. Kong, P. Chen and G. Pan, *Drug Delivery*, 2019, **26**, 328–342.
558 Y. Takeda, K. Samejima, K. Nagano, M. Watanabe, H. Sugeta and Y. Kyogoku, *Eur. J. Biochem.*, 1983, **130**, 383–389.
559 M. B. Smith and J. March, *March's Advanced Organic Chemistry*, 3rd edn, John Wiley & Sons, Inc., Hoboken, NJ, USA, 2006.
560 A. Mourot, T. Fehrentz, Y. Le Feuvre, C. M. Smith, C. Herold, D. Dalkara, F. Nagy, D. Trauner and R. H. Kramer, *Nat. Methods*, 2012, **9**, 396–402.
561 M. Schoenberger, A. Damijonaitis, Z. Zhang, D. Nagel and D. Trauner, *ACS Chem. Neurosci.*, 2014, **5**, 514–518.
562 D. E. Clapham, *Nature*, 2003, **426**, 517–524.
563 T. Fehrentz, F. M. E. Huber, N. Hartrampf, T. Bruegmann, J. A. Frank, N. H. F. Fine, D. Malan, J. G. Danzl, D. B. Tikhonov, M. Sumser, P. Sasse, D. J. Hodson, B. S. Zhorov, N. Klöcker and D. Trauner, *Nat. Chem. Biol.*, 2018, **14**, 764–767.
564 P. Leippe, N. Winter, M. P. Sumser and D. Trauner, *ACS Chem. Neurosci.*, 2018, **9**, 2886–2891.
565 J. Broichhagen, I. Jurastow, K. Iwan, W. Kummer and D. Trauner, *Angew. Chem., Int. Ed.*, 2014, **53**, 7657–7660.
566 K. Hüll, T. Benster, M. B. Manookin, D. Trauner, R. N. Van Gelder and L. Laprell, *Sci. Rep.*, 2019, **9**, 1–12.
567 M. R. Banghart, A. Mourot, D. L. Fortin, J. Z. Yao, R. H. Kramer and D. Trauner, *Angew. Chem., Int. Ed.*, 2009, **48**, 9097–9101.
568 D. D. Young and A. Deiters, *ChemBioChem*, 2008, **9**, 1225–1228.
569 X. Zhang, J. Zhang, Y.-L. Ying, H. Tian and Y.-T. Long, *Chem. Sci.*, 2014, **5**, 2642.
570 M. Hammarson, J. Andersson, S. Li, P. Lincoln and J. Andréasson, *Chem. Commun.*, 2010, **46**, 7130–7132.
571 A. Estévez-Torres and D. Baigl, *Soft Matter*, 2011, **7**, 6746–6756.
572 A. Venancio-Marques, A. Bergen, C. Rossi-Gendron, S. Rudiuk and D. Baigl, *ACS Nano*, 2014, **8**, 3654–3663.
573 A. Bergen, S. Rudiuk, M. Morel, T. Le Saux, H. Ihmels and D. Baigl, *Nano Lett.*, 2016, **16**, 773–780.
574 *The Tumour Microenvironment: Causes and Consequences of Hypoxia and Acidity*, ed. J. A. Goode and D. J. Chadwick, John Wiley & Sons, Ltd, Chichester, UK, 2001.
575 P. Montcourrier, P. H. Mangeat, C. Valembois, G. Salazar, A. Sahuquet, C. Duperray and H. Rochefort, *J. Cell Sci.*, 1994, **107**, 2381–2391.
576 T. L. I. Ihmels, *Materials Science of DNA Chemistry*, 1st edn, Jin JI. CRC Press, Boca Raton, 2011.
577 S. Özden, D. Atabey, S. Yıldız and H. Göker, *Bioorg. Med. Chem.*, 2005, **13**, 1587–1597.
578 W. D. Wilson, F. A. Tanious, D. Ding, A. Kumar, D. W. Boykin, P. Colson, C. Houssier and C. Bailly, *J. Am. Chem. Soc.*, 1998, **120**, 10310–10321.
579 K. C. Gross and P. G. Seybold, *Int. J. Quantum Chem.*, 2001, **85**, 569–579.
580 B. Heinrich, K. Bouazoune, M. Wojcik, U. Bakowsky and O. Vázquez, *Org. Biomol. Chem.*, 2019, **17**, 1827–1833.
581 C. Dohno, S. N. Uno and K. Nakatani, *J. Am. Chem. Soc.*, 2007, **129**, 11898–11899.
582 A. Mammana, G. T. Carroll, J. Areephong and B. L. Feringa, *J. Phys. Chem. B*, 2011, **115**, 11581–11587.
583 X. Wang, J. Huang, Y. Zhou, S. Yan, X. Weng, X. Wu, M. Deng and X. Zhou, *Angew. Chem., Int. Ed.*, 2010, **122**, 5433–5437.
584 X. Xing, X. Wang, L. Xu, Y. Tai, L. Dai, X. Zheng, W. Mao, X. Xu and X. Zhou, *Org. Biomol. Chem.*, 2011, **9**, 6639–6645.
585 M. P. O'Hagan, P. Peñalver, R. S. L. Gibson, J. C. Morales and M. C. Galan, *Chem. – Eur. J.*, 2020, **26**, 6224–6233.
586 I. Czerwinska and B. Juskowiak, *Int. J. Biol. Macromol.*, 2012, **51**, 576–582.
587 U. Al-Atar, R. Fernandes, B. Johnsen, D. Baillie and N. R. Branda, *J. Am. Chem. Soc.*, 2009, **131**, 15966–15967.
588 J. Spiegel, S. Adhikari and S. Balasubramanian, *Trends Chem.*, 2020, **2**, 123–136.
589 C. A. Zoto, M. G. Ucak-Astarlioglu and R. E. Connors, *J. Mol. Struct.*, 2016, **1105**, 396–402.
590 J. R. Franco, G. Cecchi, G. Priotto, M. Paone, A. Diarra, L. Grout, R. C. Mattioli and D. Argaw, *PLoS Negl. Trop. Dis*, 2017, **11**, e0005585.
591 M. P. Barrett, R. J. Burchmore, A. Stich, J. O. Lazzari, A. C. Frasch, J. J. Cazzulo and S. Krishna, *Lancet*, 2003, **362**, 1469–1480.
592 T. Kubař, M. Hanus, F. Ryjáček and P. Hobza, *Chem. – Eur. J.*, 2006, **12**, 280–290.
593 A. Basu and G. Suresh Kumar, *J. Agric. Food Chem.*, 2014, **62**, 317–326.

594 W. H. Ojala, C. R. Ojala and W. B. Gleason, *Antivir. Chem. Chemother.*, 1995, **6**, 25–33.

595 J. Morstein, R. Z. Hill, A. J. E. Novak, S. Feng, D. D. Norman, P. C. Donthamsetti, J. A. Frank, T. Harayama, B. M. Williams, A. L. Parrill, G. J. Tigyi, H. Riezman, E. Y. Isacoff, D. M. Bautista and D. Trauner, *Nat. Chem. Biol.*, 2019, **15**, 623–631.

596 T. Kamei, T. Fukaminato and N. Tamaoki, *Chem. Commun.*, 2012, **48**, 7625–7627.

597 D. M. Barber, S. A. Liu, K. Gottschling, M. Sumser, M. Hollmann and D. Trauner, *Chem. Sci.*, 2016, **8**, 611–615.

598 L. Turski, A. Huth, M. Sheardown, F. McDonald, R. Neuhaus, H. H. Schneider, U. Dirnagl, F. Wiegand, P. Jacobsen and E. Ottow, *Proc. Natl. Acad. Sci. U. S. A.*, 1998, **95**, 10960–10965.

599 L. Turski, H. H. Schneider, R. Neuhaus, F. McDonald, G. H. Jones, B. Löfberg, H. Schweinfurth, A. Huth, M. Krüger and E. Ottow, *Restor. Neurol. Neurosci.*, 2000, **17**, 45–59.

600 B. Reisinger, N. Kuzmanovic, P. Löffler, R. Merkl, B. König and R. Sterner, *Angew. Chem., Int. Ed.*, 2014, **53**, 595–598.

601 A. C. Kneuttinger, M. Winter, N. A. Simeth, K. Heyn, R. Merkl, B. König and R. Sterner, *ChemBioChem*, 2018, **19**, 1750–1757.

602 N. A. Simeth, T. Kinateder, C. Rajendran, J. Nazet, R. Merkl, R. Sterner, B. König and A. C. Kneuttinger, *Chem. – Eur. J.*, 2021, **27**, 2439–2451.

603 L. H. Jensen, A. Renodon-Corniere, I. Wessel, S. W. Langer, B. Søkilde, E. V. Carstensen, M. Sehested and P. B. Jensen, *Mol. Pharmacol.*, 2002, **61**, 1235–1243.

604 R. Göstl and S. Hecht, *Chem. – Eur. J.*, 2015, **21**, 4422–4427.

605 D. Sola, L. Rossi, G. P. C. Schianca, P. Maffioli, M. Bigliocca, R. Mella, F. Corlianò, G. P. Fra, E. Bartoli and G. Derosa, *Arch. Med. Sci.*, 2015, **4**, 840–848.

606 N. Seedher and M. Kanojia, *Pharm. Dev. Technol.*, 2009, **14**, 185–192.

607 Z. B. Mehta, N. R. Johnston, M. S. Nguyen-Tu, J. Broichhagen, P. Schultz, D. P. Larner, I. Leclerc, D. Trauner, G. A. Rutter and D. J. Hodson, *Sci. Rep.*, 2017, **7**, 1–11.

608 H. Mori, Y. Mori, S. Sugie, N. Yoshimi, M. Takahashi, H. Ni-i, H. Yamazaki, K. Toyoshi and G. M. Williams, *Cancer Res.*, 1986, **46**, 1654–1658.

609 D. Pal and S. Saha, *J. Adv. Pharm. Technol. Res*, 2012, **3**, 92.

610 W. Szymanski, M. E. Ourailidou, W. A. Velema, F. J. Dekker and B. L. Feringa, *Chem. – Eur. J.*, 2015, **21**, 16517–16524.

611 C. E. Weston, A. Krämer, F. Colin, Ö. Yildiz, M. G. J. Baud, F. J. Meyer-Almes and M. J. Fuchter, *ACS Infect. Dis.*, 2017, **3**, 152–161.

612 J. Zhang, Y. Zhang, F. Chen, W. Zhang and H. Zhao, *Phys. Chem. Chem. Phys.*, 2015, **17**, 12215–12221.

613 Z. Zhuo, Y. Yu, M. Wang, J. Li, Z. Zhang, J. Liu, X. Wu, A. Lu, G. Zhang and B. Zhang, *Int. J. Mol. Sci.*, 2017, **18**, 2142.

614 D. Steele, A. Kertsburg and G. A. Soukup, *Am. J. PharmacoGenom.*, 2003, **3**, 131–144.

615 R. Mogaki, K. Okuro and T. Aida, *Chem. Sci.*, 2015, **6**, 2802–2805.

616 Q. Wang, J. L. Mynar, M. Yoshida, E. Lee, M. Lee, K. Okuro, K. Kinbara and T. Aida, *Nature*, 2010, **463**, 339–343.

617 K. Okuro, K. Kinbara, K. Tsumoto, N. Ishii and T. Aida, *J. Am. Chem. Soc.*, 2009, **131**, 1626–1627.

618 R. Mogaki, K. Okuro and T. Aida, *J. Am. Chem. Soc.*, 2017, **139**, 10072–10078.

619 P. K. Hashim, K. Okuro, S. Sasaki, Y. Hoashi and T. Aida, *J. Am. Chem. Soc.*, 2015, **137**, 15608–15611.

620 H.-J. Böhm, A. Flohr and M. Stahl, *Drug Discovery Today Technol.*, 2004, **1**, 217–224.

621 Y. Hu, D. Stumpfe and J. Bajorath, *J. Med. Chem.*, 2017, **60**, 1238–1246.

622 N. N. Mafy, K. Matsuo, S. Hiruma, R. Uehara and N. Tamaoki, *J. Am. Chem. Soc.*, 2020, **142**, 1763–1767.

623 R. Ferreira, J. R. Nilsson, C. Solano, J. Andréasson and M. Grøtli, *Sci. Rep.*, 2015, **5**, 9769.

624 S. Pittolo, X. Gómez-Santacana, K. Eckelt, X. Rovira, J. Dalton, C. Goudet, J.-P. P. Pin, A. Llobet, J. Giraldo, A. Llebaria and P. Gorostiza, *Nat. Chem. Biol.*, 2014, **10**, 813–815.

625 C. W. Grathwol, N. Wössner, S. Behnisch-Cornwell, L. Schulig, L. Zhang, O. Einsle, M. Jung and A. Link, *ChemMedChem*, 2020, **15**, 1480–1489.

626 A. A. Blevins and G. J. Blanchard, *J. Phys. Chem. B*, 2004, **108**, 4962–4968.

627 W. R. Brode, J. H. Gould and G. M. Wyman, *J. Am. Chem. Soc.*, 1952, **74**, 4641–4646.

628 D. Lachmann, C. Studte, B. Männel, H. Hübner, P. Gmeiner and B. König, *Chem. – Eur. J.*, 2017, **23**, 13423–13434.

629 T. Yamaguchi and M. Irie, *Chem. Lett.*, 2004, 1398–1399.

630 O. Pieroni, A. Fissi, J. L. Houben and F. Ciardelli, *J. Am. Chem. Soc.*, 1985, **107**, 2990–2991.

631 H. Yamamoto, A. Nishida, T. Takimoto and A. Nagai, *J. Polym. Sci., Part A: Polym. Chem.*, 1990, **28**, 67–74.

632 A. Nojiri, N. Kumagai and M. Shibasaki, *Angew. Chem., Int. Ed.*, 2012, **51**, 2137–2141.

633 R. Zhang, Y.-J. Ji, L. Yang, Y. Zhang and G.-C. Kuang, *Phys. Chem. Chem. Phys.*, 2016, **18**, 9914–9917.

634 A. A. Beharry and G. A. Woolley, *Chem. Soc. Rev.*, 2011, **40**, 4422–4437.

635 E. Merlo, R. Freudenthal and A. Romano, *Neuroscience*, 2002, **112**, 161–172.

636 M. Ishikawa, T. Ohzono, T. Yamaguchi and Y. Norikane, *Sci. Rep.*, 2017, **7**, 3–8.

637 M. W. H. Hoorens, H. Fu, R. H. Duurkens, G. Trinco, V. Arkhipova, B. L. Feringa, G. J. Poelarends, D. J. Slotboom and W. Szymanski, *Adv. Ther*, 2018, **1**, 1800028.

638 P. Leippe and J. A. Frank, *Curr. Opin. Struct. Biol.*, 2019, **57**, 23–30.

639 L. Laprell, E. Repak, V. Franckevicius, F. Hartrampf, J. Terhag, M. Hollmann, M. Sumser, N. Rebola, D. A. DiGregorio and D. Trauner, *Nat. Commun.*, 2015, **6**, 8076.

640 O. Srinivas, N. Mitra, A. Surolia and N. Jayaraman, *Glycobiology*, 2005, **15**, 861–873.

641 O. Srinivas, N. Mitra, A. Surolia and N. Jayaraman, *J. Am. Chem. Soc.*, 2002, **124**, 2124–2125.

642 V. Chandrasekaran, K. Kolbe, F. Beiroth and T. K. Lindhorst, *Beilstein J. Org. Chem.*, 2013, **9**, 223–233.

643 K. Rustler, M. J. Mickert, J. Nazet, R. Merkl, H. H. Gorris and B. König, *Org. Biomol. Chem.*, 2018, **16**, 7430–7437.

644 N. Hartrampf, T. Seki, A. Baumann, P. Watson, N. A. Vepřek, B. E. Hetzler, A. Hoffmann-Röder, M. Tsuji and D. Trauner, *Chem. – Eur. J.*, 2020, **26**, 4476–4479.
645 G. P. Espino-Solis, *Rev. Vitae*, 2015, **22**, 9–11.
646 W. A. Velema, M. J. Hansen, M. M. Lerch, A. J. M. Driessen, W. Szymanski and B. L. Feringa, *Bioconjugate Chem.*, 2015, **26**, 2592–2597.
647 W. A. Velema, J. P. Van Der Berg, M. J. Hansen, W. Szymanski, A. J. M. Driessen and B. L. Feringa, *Nat. Chem.*, 2013, **5**, 924–928.
648 S. S. Tous, A. M. El Sayed, M. G. Abd El Mohsen, M. N. Agban and M. F. Boushra, *J. Drug Deliv. Sci. Technol.*, 2012, **22**, 341–346.
649 D. Martínez-López, M.-L. Yu, C. García-Iriepa, P. J. Campos, L. M. Frutos, J. A. Golen, S. Rasapalli and D. Sampedro, *J. Org. Chem.*, 2015, **80**, 3929–3939.
650 A. T. Ulijasz and R. D. Vierstra, *Curr. Opin. Plant Biol.*, 2011, **14**, 498–506.
651 E. Contreras-García, D. Martínez-López, C. A. Alonso, C. Lozano, C. Torres, M. A. Rodríguez, P. J. Campos and D. Sampedro, *Eur. J. Org. Chem.*, 2017, 4719–4725.
652 E. A. Specht, E. Braselmann and A. E. Palmer, *Annu. Rev. Physiol.*, 2017, **79**, 93–117.
653 P. Debie and S. Hernot, *Front. Pharmacol.*, 2019, **10**, 510.
654 Q. Hu, Y. Shi, X. Yang, J. Zhang, B. Li, X. Liao and X. Liu, *Sheng Wu Gong Cheng Xue Bao*, 2020, **36**, 1051–1059.
655 B. Roubinet, M. Weber, H. Shojaei, M. Bates, M. L. Bossi, V. N. Belov, M. Irie and S. W. Hell, *J. Am. Chem. Soc.*, 2017, **139**, 6611–6620.
656 M. Fernández-Suárez and A. Y. Ting, *Nat. Rev. Mol. Cell Biol.*, 2008, **9**, 929–943.
657 Y. Fu, H. H. Han, J. Zhang, X. P. He, B. L. Feringa and H. Tian, *J. Am. Chem. Soc.*, 2018, **140**, 8671–8674.
658 X. M. He and D. C. Carter, *Nature*, 1992, **358**, 209–215.
659 J. Ghuman, P. A. Zunszain, I. Petitpas, A. A. Bhattacharya, M. Otagiri and S. Curry, *J. Mol. Biol.*, 2005, **353**, 38–52.
660 F. Kratz, *J. Controlled Release*, 2008, **132**, 171–183.
661 X. Chai, H.-H. Han, A. C. Sedgwick, N. Li, Y. Zang, T. D. James, J. Zhang, X.-L. Hu, Y. Yu, Y. Li, Y. Wang, J. Li, X.-P. He and H. Tian, *J. Am. Chem. Soc.*, 2020, **142**, 18005–18013.
662 R. J. Mart and R. K. Allemann, *Chem. Commun.*, 2016, **52**, 12262–12277.
663 M. Stefani and C. M. Dobson, *J. Mol. Med.*, 2003, **81**, 678–699.
664 C. Z. Chung, K. Amikura and D. Söll, *Front. Bioeng. Biotechnol.*, 2020, **8**, 598577.
665 P. Arranz-Gibert, K. Vanderschuren and F. J. Isaacs, *Curr. Opin. Chem. Biol.*, 2018, **46**, 203–211.
666 J. W. Chin, *Annu. Rev. Biochem.*, 2014, **83**, 379–408.
667 A. R. Nödling, L. A. Spear, T. L. Williams, L. Y. P. Luk and Y.-H. Tsai, *Essays Biochem.*, 2019, **63**, 237–266.
668 A. A. John, C. P. Ramil, Y. Tian, G. Cheng and Q. Lin, *Org. Lett.*, 2015, **17**, 6258–6261.
669 J. Luo, S. Samanta, M. Convertino, N. V. Dokholyan and A. Deiters, *ChemBioChem*, 2018, **19**, 2178–2185.
670 M. Bose, D. Groff, J. Xie, E. Brustad and P. G. Schultz, *J. Am. Chem. Soc.*, 2006, **128**, 388–389.
671 A. C. Kneuttinger, K. Straub, P. Bittner, N. A. Simeth, A. Bruckmann, F. Busch, C. Rajendran, E. Hupfeld, V. H. Wysocki, D. Horinek, B. König, R. Merkl and R. Sterner, *Cell Chem. Biol.*, 2019, **26**, 1501–1514.
672 A. C. Kneuttinger, C. Rajendran, N. A. Simeth, A. Bruckmann, B. König and R. Sterner, *Biochemistry*, 2020, **59**, 2729–2742.
673 J. Lee, K. E. Schwieter, A. M. Watkins, D. S. Kim, H. Yu, K. J. Schwarz, J. Lim, J. Coronado, M. Byrom, E. V. Anslyn, A. D. Ellington, J. S. Moore and M. C. Jewett, *Nat. Commun.*, 2019, **10**, 5097.
674 T. Yanagisawa, M. Kuratani, E. Seki, N. Hino, K. Sakamoto and S. Yokoyama, *Cell Chem. Biol.*, 2019, **26**, 936–949.
675 C. Hoppmann, V. K. Lacey, G. V. Louie, J. Wei, J. P. Noel and L. Wang, *Angew. Chem., Int. Ed.*, 2014, **53**, 3932–3936.
676 C. Hoppmann, I. Maslennikov, S. Choe and L. Wang, *J. Am. Chem. Soc.*, 2015, **137**, 11218–11221.
677 D. M. M. Jaradat, *Amino Acids*, 2018, **50**, 39–68.
678 S. Chandrudu, P. Simerska and I. Toth, *Molecules*, 2013, **18**, 4373–4388.
679 A. G. Molina and Y. S. Sanghvi, *Curr. Protoc. Nucleic Acid Chem.*, 2019, **77**, e82.
680 R. Eritja, *Int. J. Pept. Res. Ther.*, 2007, **13**, 53–68.
681 R. F. Standaert and S. B. Park, *J. Org. Chem.*, 2006, **71**, 7952–7966.
682 L. D. DeLeve and N. Kaplowitz, *Pharmacol. Ther.*, 1991, **52**, 287–305.
683 A. Prestel and H. M. Möller, *Chem. Commun.*, 2016, **52**, 701–704.
684 L. Albert, A. Peñalver, N. Djokovic, L. Werel, M. Hoffarth, D. Ruzic, J. Xu, L. O. Essen, K. Nikolic, Y. Dou and O. Vázquez, *ChemBioChem*, 2019, **20**, 1417–1429.
685 F. Milletti, *Drug Discovery Today*, 2012, **17**, 850–860.
686 H. de Jong, K. M. Bonger and D. W. P. M. Löwik, *RSC Chem. Biol.*, 2020, **1**, 192–203.
687 I. V. Komarov and I. V. Bakanovych, *Chem. Heterocycl. Compd.*, 2020, **56**, 719–721.
688 L. Ulysse, J. Cubillos and J. Chmielewski, *J. Am. Chem. Soc.*, 1995, **117**, 8466–8467.
689 R. Behrendt, M. Schenk, H.-J. J. Musiol and L. Moroder, *J. Pept. Sci.*, 1999, **5**, 519–529.
690 A. D. Frankel and C. O. Pabo, *Cell*, 1988, **55**, 1189–1193.
691 S. Dissanayake, W. A. Denny, S. Gamage and V. Sarojini, *J. Controlled Release*, 2017, **250**, 62–76.
692 D. Birch, M. V. Christensen, D. Staerk, H. Franzyk and H. M. Nielsen, *Biochim. Biophys. Acta, Biomembr.*, 2017, **1859**, 2483–2494.
693 S. F. Hedegaard, M. S. Derbas, T. K. Lind, M. R. Kasimova, M. V. Christensen, M. H. Michaelsen, R. A. Campbell, L. Jorgensen, H. Franzyk, M. Cárdenas and H. M. Nielsen, *Sci. Rep.*, 2018, **8**, 6327.
694 T. Lougheed, V. Borisenko, T. Hennig, K. Rück-Braun and G. A. Woolley, *Org. Biomol. Chem.*, 2004, **2**, 2798–2801.
695 T. Schober, I. Wehl, S. Afonin, O. Babii, A. Iampolska, U. Schepers, I. V. Komarov and A. S. Ulrich, *ChemPhotoChem*, 2019, **3**, 384–391.

696 O. Babii, S. Afonin, T. Schober, L. V. Garmanchuk, L. I. Ostapchenko, V. Yurchenko, S. Zozulya, O. Tarasov, I. Pishel, A. S. Ulrich and I. V. Komarov, *Future Drug Discovery*, 2020, **2**, FDD28.
697 K. Okamoto, Y. Tomita, H. Yonezawa, T. Hirohata, R. Ogura and N. Izumiya, *Oncology*, 1984, **41**, 43–48.
698 O. Babii, S. Afonin, A. Y. Ishchenko, T. Schober, A. O. Negelia, G. M. Tolstanova, L. V. Garmanchuk, L. I. Ostapchenko, I. V. Komarov and A. S. Ulrich, *J. Med. Chem.*, 2018, **61**, 10793–10813.
699 O. Babii, S. Afonin, M. Berditsch, S. Reier, P. K. Mykhailiuk, V. S. Kubyshkin, T. Steinbrecher, A. S. Ulrich and I. V. Komarov, *Angew. Chem., Int. Ed.*, 2014, **53**, 3392–3395.
700 S. Afonin, O. Babii, A. Reuter, V. Middel, M. Takamiya, U. Strähle, I. V. Komarov and A. S. Ulrich, *Beilstein J. Org. Chem.*, 2020, **16**, 39–49.
701 O. Babii, S. Afonin, L. V. Garmanchuk, V. V. Nikulina, T. V. Nikolaienko, O. V. Storozhuk, D. V. Shelest, O. I. Dasyukevich, L. I. Ostapchenko, V. Iurchenko, S. Zozulya, A. S. Ulrich and I. V. Komarov, *Angew. Chem., Int. Ed.*, 2016, **128**, 5583–5586.
702 A. S. Lubbe, W. Szymanski and B. L. Feringa, *Chem. Soc. Rev.*, 2017, **46**, 1052–1079.
703 H. Nishioka, X. Liang, T. Kato and H. Asanuma, *Angew. Chem., Int. Ed.*, 2012, **51**, 1165–1168.
704 T. Goldau, K. Murayama, C. Brieke, H. Asanuma and A. Heckel, *Chem. – Eur. J.*, 2015, **21**, 17870–17876.
705 T. Goldau, K. Murayama, C. Brieke, S. Steinwand, P. Mondal, M. Biswas, I. Burghardt, J. Wachtveitl, H. Asanuma and A. Heckel, *Chem. – Eur. J.*, 2015, **21**, 2845–2854.
706 M. L. Hammill, G. Islam and J. P. Desaulniers, *ChemBioChem*, 2020, **21**, 2367–2372.
707 M. Singer and A. Jäschke, *J. Am. Chem. Soc.*, 2010, **132**, 8372–8377.
708 H. Cahová and A. Jäschke, *Angew. Chem., Int. Ed.*, 2013, **52**, 3186–3190.
709 H. Asanuma, K. Shirasuka, T. Yoshida, T. Takarada, X. Liang and M. Komiyama, *Chem. Lett.*, 2001, 108–109.
710 C. Beyer and H.-A. Wagenknecht, *J. Org. Chem.*, 2010, **75**, 2752–2755.
711 S. Barrois and H.-A. Wagenknecht, *Beilstein J. Org. Chem.*, 2012, **8**, 905–914.
712 C. Beyer and H.-A. Wagenknecht, *Synlett*, 2010, 1371–1376.
713 W. Szymański, J. M. Beierle, H. A. V. Kistemaker, W. A. Velema and B. L. Feringa, *Chem. Rev.*, 2013, **113**, 6114–6178.
714 Z. L. Pianowski, *Chemistry*, 2019, **25**, 5128–5144.
715 T. Arakawa, Y. Kita and S. N. Timasheff, *Biophys. Chem.*, 2007, **131**, 62–70.
716 J. Roche and C. A. Royer, *J. R. Soc., Interface*, 2018, **15**, 20180244.
717 P. L. Privalov, *Crit. Rev. Biochem. Mol. Biol.*, 1990, **25**, 281–306.
718 R. M. Daniel, M. Dines and H. H. Petach, *Biochem. J.*, 1996, **317**, 1–11.
719 D. R. Canchi and A. E. García, *Annu. Rev. Phys. Chem.*, 2013, **64**, 273–293.
720 M. Jackson and H. H. Mantsch, *Biochim. Biophys. Acta, Protein Struct. Mol. Enzymol.*, 1991, **1078**, 231–235.
721 K. Griebenow and A. M. Klibanov, *J. Am. Chem. Soc.*, 1996, **118**, 11695–11700.
722 G. T. Hermanson, *Bioconjugate Techniques*, 3rd edn, Academic Press, 2013.
723 O. Boutureira and G. J. L. Bernardes, *Chem. Rev.*, 2015, **115**, 2174–2195.
724 J. M. Chalker, G. J. L. Bernardes, Y. A. Lin and B. G. Davis, *Chem. – Asian J.*, 2009, **4**, 630–640.
725 S. T. Larda, D. Pichugin and R. S. Prosser, *Bioconjugate Chem.*, 2015, **26**, 2376–2383.
726 M. J. Matos, B. L. Oliveira, N. Martínez-Sáez, A. Guerreiro, P. M. S. D. Cal, J. Bertoldo, M. Maneiro, E. Perkins, J. Howard, M. J. Deery, J. M. Chalker, F. Corzana, G. Jiménez-Osés and G. J. L. Bernardes, *J. Am. Chem. Soc.*, 2018, **140**, 4004–4017.
727 D. G. Rawale, K. Thakur, S. R. Adusumalli and V. Rai, *Eur. J. Org. Chem.*, 2019, 6749–6763.
728 W. Szymański, B. Wu, C. Poloni, D. B. Janssen and B. L. Feringa, *Angew. Chem., Int. Ed.*, 2013, **52**, 2068–2072.
729 C. Poloni, W. Szymański, L. Hou, W. R. Browne and B. L. Feringa, *Chem. – Eur. J.*, 2014, **20**, 946–951.
730 Y. Zhang, K.-Y. Park, K. F. Suazo and M. D. Distefano, *Chem. Soc. Rev.*, 2018, **47**, 9106–9136.
731 M. Rashidian, J. K. Dozier and M. D. Distefano, *Bioconjugate Chem.*, 2013, **24**, 1277–1294.
732 J. A. Shadish and C. A. DeForest, *Matter*, 2020, **2**, 50–77.
733 M. Dal Peraro and F. G. van der Goot, *Nat. Rev. Microbiol.*, 2016, **14**, 77–92.
734 N. L. Mutter, J. Volarić, W. Szymanski, B. L. Feringa and G. Maglia, *J. Am. Chem. Soc.*, 2019, **141**, 14356–14363.
735 S. Loudwig and H. Bayley, *J. Am. Chem. Soc.*, 2006, **128**, 12404–12405.
736 G. Lukinavičius, G. Y. Mitronova, S. Schnorrenberg, A. N. Butkevich, H. Barthel, V. N. Belov and S. W. Hell, *Chem. Sci.*, 2018, **9**, 3324–3334.
737 L. Möckl, A. Müller, C. Bräuchle and T. K. Lindhorst, *Chem. Commun.*, 2016, **52**, 1254–1257.
738 V. V. Rostovtsev, L. G. Green, V. V. Fokin and K. B. Sharpless, *Angew. Chem., Int. Ed.*, 2002, **41**, 2596–2599.
739 T. Matsuzaki, Y. Tajika, N. Tserentsoodol, T. Suzuki, T. Aoki, H. Hagiwara and K. Takata, *Anat. Sci. Int.*, 2002, **77**, 85–93.
740 A. Kocer, A. Koçer, M. Walko, W. Meijberg and B. L. Feringa, *Science*, 2005, **309**, 755–758.
741 E. S. Haswell, R. Phillips and D. C. Rees, *Structure*, 2011, **19**, 1356–1369.
742 A. Anishkin, C.-S. Chiang and S. Sukharev, *J. Gen. Physiol.*, 2005, **125**, 155–170.
743 A. Koçer, M. Walko and B. L. Feringa, *Nat. Protoc.*, 2007, **2**, 1426–1437.
744 W. Szymanski, D. Yilmaz, A. Koçer and B. L. Feringa, *Acc. Chem. Res.*, 2013, **46**, 2910–2923.
745 H. A. Lester, M. E. Krouse, M. M. Nass, N. H. Wassermann and B. F. Erlanger, *J. Gen. Physiol.*, 1980, **75**, 207–232.
746 P. C. Donthamsetti, N. Winter, M. Schönberger, J. Levitz, C. Stanley, J. A. Javitch, E. Y. Isacoff and D. Trauner, *J. Am. Chem. Soc.*, 2017, **139**, 18522–18535.

747 L. Yue, M. Pawlowski, S. S. Dellal, A. Xie, F. Feng, T. S. Otis, K. S. Bruzik, H. Qian and D. R. Pepperberg, *Nat. Commun.*, 2012, **3**, 1095.
748 M. Volgraf, P. Gorostiza, R. Numano, R. H. Kramer, E. Y. Isacoff and D. Trauner, *Nat. Chem. Biol.*, 2006, **2**, 47–52.
749 C. Wyart, F. Del Bene, E. Warp, E. K. Scott, D. Trauner, H. Baier and E. Y. Isacoff, *Nature*, 2009, **461**, 407–410.
750 G. Kauwe and E. Y. Isacoff, *Proc. Natl. Acad. Sci. U. S. A.*, 2013, **110**, 9142–9147.
751 J. Levitz, C. Pantoja, B. Gaub, H. Janovjak, A. Reiner, A. Hoagland, D. Schoppik, B. Kane, P. Stawski, A. F. Schier, D. Trauner and E. Y. Isacoff, *Nat. Neurosci.*, 2013, **16**, 507–516.
752 G. Anderson, A. Noorian, G. Taylor, M. Anitha, D. Bernhard, S. Srinivasan and J. Greene, *Exp. Neurol.*, 2007, **207**, 4–12.
753 P. Gorostiza, M. Volgraf, R. Numano, S. Szobota, D. Trauner and E. Y. Isacoff, *Proc. Natl. Acad. Sci. U. S. A.*, 2007, **104**, 10865–10870.
754 I. Tochitsky, M. R. Banghart, A. Mourot, J. Z. Yao, B. Gaub, R. H. Kramer and D. Trauner, *Nat. Chem.*, 2012, **4**, 105–111.
755 A. Taly, P.-J. Corringer, D. Guedin, P. Lestage and J.-P. Changeux, *Nat. Rev. Drug Discovery*, 2009, **8**, 733–750.
756 C. Gotti, B. Balestra, M. Moretti, G. E. Rovati, L. Maggi, G. Rossoni, F. Berti, L. Villa, M. Pallavicini and F. Clementi, *Br. J. Pharmacol.*, 1998, **124**, 1197–1206.
757 M. R. Picciotto, M. J. Higley and Y. S. Mineur, *Neuron*, 2012, **76**, 116–129.
758 R. D. De Cuttoli, S. Mondoloni, F. Marti, D. Lemoine, C. Nguyen, J. Naudé, T. D'izarny-Gargas, S. Pons, U. Maskos, D. Trauner, R. H. Kramer, P. Faure and A. Mourot, *Elife*, 2018, **7**, 1–23.
759 M. Wegener, M. J. Hansen, A. J. M. Driessen, W. Szymanski and B. L. Feringa, *J. Am. Chem. Soc.*, 2017, **139**, 17979–17986.
760 M. Dong, A. Babalhavaeji, C. V. Collins, K. Jarrah, O. Sadovski, Q. Dai and G. A. Woolley, *J. Am. Chem. Soc.*, 2017, **139**, 13483–13486.
761 R. Prakash, O. Yizhar, B. Grewe, C. Ramakrishnan, N. Wang, I. Goshen, A. M. Packer, D. S. Peterka, R. Yuste, M. J. Schnitzer and K. Deisseroth, *Nat. Methods*, 2012, **9**, 1171–1179.
762 G. Bort, T. Gallavardin, D. Ogden and P. I. Dalko, *Angew. Chem., Int. Ed.*, 2013, **52**, 4526–4537.
763 M. Izquierdo-Serra, M. Gascón-Moya, J. J. Hirtz, S. Pittolo, K. E. Poskanzer, È. Ferrer, R. Alibés, F. Busqué, R. Yuste, J. Hernando and P. Gorostiza, *J. Am. Chem. Soc.*, 2014, **136**, 8693–8701.
764 M. Gascón-Moya, A. Pejoan, M. Izquierdo-Serra, S. Pittolo, G. Cabré, J. Hernando, R. Alibés, P. Gorostiza and F. Busqué, *J. Org. Chem.*, 2015, **80**, 9915–9925.
765 G. Cabré, A. Garrido-Charles, M. Moreno, M. Bosch, M. Porta-de-la-Riva, M. Krieg, M. Gascón-Moya, N. Camarero, R. Gelabert, J. M. Lluch, F. Busqué, J. Hernando, P. Gorostiza and R. Alibés, *Nat. Commun.*, 2019, **10**, 907.
766 S. Pujals, N. Feiner-Gracia, P. Delcanale, I. Voets and L. Albertazzi, *Nat. Rev. Chem.*, 2019, **3**, 68–84.
767 H. Li and J. C. Vaughan, *Chem. Rev.*, 2018, **118**, 9412–9454.
768 G. T. Dempsey, M. Bates, W. E. Kowtoniuk, D. R. Liu, R. Y. Tsien and X. Zhuang, *J. Am. Chem. Soc.*, 2009, **131**, 18192–18193.
769 M. Heilemann, S. van de Linde, M. Schüttpelz, R. Kasper, B. Seefeldt, A. Mukherjee, P. Tinnefeld and M. Sauer, *Angew. Chem., Int. Ed.*, 2008, **47**, 6172–6176.
770 J. B. Grimm, A. J. Sung, W. R. Legant, P. Hulamm, S. M. Matlosz, E. Betzig and L. D. Lavis, *ACS Chem. Biol.*, 2013, **8**, 1303–1310.
771 J. B. Grimm, A. K. Muthusamy, Y. Liang, T. A. Brown, W. C. Lemon, R. Patel, R. Lu, J. J. Macklin, P. J. Keller, N. Ji and L. D. Lavis, *Nat. Methods*, 2017, **14**, 987–994.
772 T. A. Klar, S. Jakobs, M. Dyba, A. Egner and S. W. Hell, *Proc. Natl. Acad. Sci. U. S. A.*, 2000, **97**, 8206–8210.
773 S. W. Hell, *Phys. Lett. A*, 2004, **326**, 140–145.
774 S. M. Polyakova, V. N. Belov, M. L. Bossi and S. W. Hell, *Eur. J. Org. Chem.*, 2011, 3301–3312.
775 R. Sharma, M. Singh and R. Sharma, *Spectrochim. Acta, Part A*, 2020, **231**, 117715.
776 Y. Shoji, A. Yagi, M. Horiuchi, M. Morimoto and M. Irie, *Isr. J. Chem.*, 2013, **53**, 303–311.
777 M. Takeshita and M. Irie, *Chem. Commun.*, 1997, 2265–2266.
778 M. Takeshita, N. Kato, S. Kawauchi, T. Imase, J. Watanabe and M. Irie, *J. Org. Chem.*, 1998, **63**, 9306–9313.
779 T. Hirose, K. Matsuda and M. Irie, *J. Org. Chem.*, 2006, **71**, 7499–7508.
780 T. Hirose, M. Irie and K. Matsuda, *Adv. Mater.*, 2008, **20**, 2137–2141.
781 N. Soh, K. Yoshida, H. Nakajima, K. Nakano, T. Imato, T. Fukaminato and M. Irie, *Chem. Commun.*, 2007, 5206–5208.
782 K. Uno, H. Niikura, M. Morimoto, Y. Ishibashi, H. Miyasaka and M. Irie, *J. Am. Chem. Soc.*, 2011, **133**, 13558–13564.
783 J. R. McCombs and S. C. Owen, *AAPS J.*, 2015, **17**, 339–351.
784 S. W. Hell, S. Jakobs and L. Kastrup, *Appl. Phys. A: Mater. Sci. Process.*, 2003, **77**, 859–860.
785 T. Fukaminato, T. Sasaki, T. Kawai, N. Tamai and M. Irie, *J. Am. Chem. Soc.*, 2004, **126**, 14843–14849.
786 M. Zhu and H. Zhou, *Org. Biomol. Chem.*, 2018, **16**, 8434–8445.
787 K. Fujimoto, M. Kajino, I. Sakaguchi and M. Inouye, *Chem. – Eur. J.*, 2012, **18**, 9834–9840.
788 A. V. Strizhak, O. Babii, S. Afonin, I. Bakanovich, T. Pantelejevs, W. Xu, E. Fowler, R. Eapen, K. Sharma, M. O. Platonov, V. V. Hurmach, L. Itzhaki, M. Hyvönen, A. S. Ulrich, D. R. Spring and I. V. Komarov, *Org. Biomol. Chem.*, 2020, **18**, 5359–5369.
789 G. M. Fahy, T. H. Lilley, H. Linsdell, M. S. J. Douglas and H. T. Meryman, *Cryobiology*, 1990, **27**, 247–268.
790 D. G. Flint, J. R. Kumita, O. S. Smart and G. A. Woolley, *Chem. Biol.*, 2002, **9**, 391–397.
791 P. Glock, J. Broichhagen, S. Kretschmer, P. Blumhardt, J. Mücksch, D. Trauner and P. Schwille, *Angew. Chem., Int. Ed.*, 2018, **57**, 2362–2366.
792 K. M. Blacklock, B. J. Yachnin, G. A. Woolley and S. D. Khare, *J. Am. Chem. Soc.*, 2018, **140**, 14–17.
793 J. R. Kumita, O. S. Smart and G. A. Woolley, *Proc. Natl. Acad. Sci. U. S. A.*, 2000, **97**, 3803–3808.

794 U. Kusebauch, S. A. Cadamuro, H.-J. Musiol, M. O. Lenz, J. Wachtveitl, L. Moroder and C. Renner, *Angew. Chem., Int. Ed.*, 2006, **45**, 7015–7018.
795 U. Kusebauch, S. A. Cadamuro, H.-J. Musiol, L. Moroder and C. Renner, *Chem. – Eur. J.*, 2007, **13**, 2966–2973.
796 G. C. Kim, J. H. Ahn, J. H. Oh, S. Nam, S. Hyun, J. Yu and Y. Lee, *Biomacromolecules*, 2018, **19**, 2863–2869.
797 V. Borisenko and G. A. Woolley, *J. Photochem. Photobiol., A*, 2005, **173**, 21–28.
798 A. M. Ali, M. W. Forbes and G. A. Woolley, *ChemBioChem*, 2015, **16**, 1757–1763.
799 N. Preußke, W. Moormann, K. Bamberg, M. Lipfert, R. Herges and F. D. Sönnichsen, *Org. Biomol. Chem.*, 2020, **18**, 2650–2660.
800 G. Cabré, A. Garrido-Charles, À. González-Lafont, W. Moormann, D. Langbehn, D. Egea, J. M. Lluch, R. Herges, R. Alibés, F. Busqué, P. Gorostiza and J. Hernando, *Org. Lett.*, 2019, **21**, 3780–3784.
801 R. Santucci, E. Laurenti, F. Sinibaldi and R. P. Ferrari, *Biochim. Biophys. Acta - Protein Struct. Mol. Enzymol*, 2002, **1596**, 225–233.
802 Z. Zhang, D. C. Burns, J. R. Kumita, O. S. Smart, G. A. Woolley, Z. Zhang, D. C. Burns, J. R. Kumita, O. S. Smart and G. A. Woolley, *Bioconjugate Chem.*, 2003, **14**, 824–829.
803 D. C. Burns, F. Zhang and G. A. Woolley, *Nat. Protoc.*, 2007, **2**, 251–258.
804 L. Nevola, A. Martín-Quirõs, K. Eckelt, N. Camarero, S. Tosi, A. Llobet, E. Giralt, P. Gorostiza, A. Martín-Quirós, K. Eckelt, N. Camarero, S. Tosi, A. Llobet, E. Giralt and P. Gorostiza, *Angew. Chem., Int. Ed.*, 2013, **52**, 7704–7708.
805 R. J. Mart, R. J. Errington, C. L. Watkins, S. C. Chappell, M. Wiltshire, A. T. Jones, P. J. Smith and R. K. Allemann, *Mol. BioSyst.*, 2013, **9**, 2597–2603.
806 P. Wysoczanski, R. J. Mart, E. J. Loveridge, C. Williams, S. B. M. Whittaker, M. P. Crump and R. K. Allemann, *J. Am. Chem. Soc.*, 2012, **134**, 7644–7647.
807 F. Zhang, K. A. Timm, K. M. Arndt and G. A. Woolley, *Angew. Chem., Int. Ed.*, 2010, **49**, 3943–3946.
808 R. S. Ritterson, K. M. Kuchenbecker, M. Michalik and T. Kortemme, *J. Am. Chem. Soc.*, 2013, **135**, 12516–12519.
809 S. Samanta and G. A. Woolley, *ChemBioChem*, 2011, **12**, 1712–1723.
810 J. L. Turnbull, B. R. Benlian, R. P. Golden and E. W. Miller, *J. Am. Chem. Soc.*, 2021, **143**, 6194–6201.
811 F. Zhang, O. Sadovski and G. A. Woolley, *ChemBioChem*, 2008, **9**, 2147–2154.
812 N. Yasuike, K. M. Blacklock, H. Lu, A. S. I. Jaikaran, S. McDonald, M. Uppalapati, S. D. Khare and G. A. Woolley, *ChemPhotoChem*, 2019, **3**, 431–440.
813 M. Dong, A. Babalhavaeji, M. J. Hansen, L. Kálmán and G. A. Woolley, *Chem. Commun.*, 2015, **51**, 12981–12984.
814 A. Müller, H. Kobarg, V. Chandrasekaran, J. Gronow, F. D. Sönnichsen and T. K. Lindhorst, *Chem. – Eur. J.*, 2015, **21**, 13723–13731.
815 A. Müller and T. K. Lindhorst, *Eur. J. Org. Chem.*, 2016, 1669–1672.